Control of fault geometry, interaction and mechanical stratigraphy on strain distribution in normal fault zones

IOAN ALEXANDRU LAPADAT

Department of Earth Sciences, Durham University

CONTROL OF FAULT GEOMETRY, INTERACTION AND MECHANICAL STRATIGRAPHY ON STRAIN DISTRIBUTION IN NORMAL FAULT ZONES

A thesis submitted to the Department of Earth Sciences at Durham University in partial fulfilment of the requirements for the Degree of Doctor of Philosophy

Ioan - Alexandru Lăpădat

December 2017

Page intentionally left blank

| Abstract |

It is known that the development and distribution of strain associated with normal faulting is influenced by the process of fault growth within mechanically layered and heterogeneous sedimentary rocks. Fault displacement is often partitioned between discontinuous throw on slip surfaces and zones of distributed strain, which in some cases can be the result of folding associated with normal faulting. The amount of ductile deformation can vary significantly along the strike of a normal fault array as a result of various processes, such as fault-tip propagation and fault interaction and linkage. In this study we investigate the influence of mechanical stratigraphy, fault geometry and fault mechanical interaction on the variability and distribution of ductile strain in the rock volume surrounding normal faults. We show that mechanical competence contrasts can control the manner in which strain is accommodated and, hence the overall patterns of secondary fault and fracture systems within normal fault-related folds. This can have consequences on the way in which disruption of an associated shale smear occurs, impacting the sealing properties of the fault zones. Also, we show that folding can be generated by different mechanisms that vary in importance in time and space along a normal fault array. Mechanical properties of the host rocks, together with the spatial configuration of the faults control the mechanical interaction between faults, exerting an influence on the variability of ductile strain within the volume of deformation surrounding normal faults. Specifically, conjugate normal faults that intersect within layers with low compressibility have geomechanical characteristics favourable for migration of stress concentrations near the upper fault tips which generate higher propagation/slip ratios and the development of lower amplitude folds, or no folding. The host rock lithology and the overlapping normal fault configuration at the time of interaction controls the three-dimensional relay ramp geometries and associated strains within relay ramps. Normal faults within mechanically competent rocks tend to develop relay ramps with tabular geometries, that have larger aspect ratios and smaller fault-parallel shear strains compared to those developed in mechanically incompetent rocks. Fault-normal shear strain within ramps can be the result of the development of asymmetric displacement gradients on the overlapping faults as a result of mechanical interaction between surface-breaking normal faults. The probability of a relay ramp bounded by surface-breaking normal faults to be completely breached depends not only on the accumulated ramp shear strains and the ratio between throw and separation of the bounding faults, but also on how the throw is partitioned between the interacting faults. Also, we argue that the style of breaching, dominantly through the upper part of the relay ramps, is influenced by the stress interaction between the overlapping faults and the Earth's free surface.

| Declaration |

No part of this thesis has previously been submitted for a degree at this or any other university. The work described in this thesis is entirely that of the author, except where reference is made to previously published or unpublished work.

| Acknowledgements |

I am very thankful for all the support received from my supervisors Jonny Imber, Ken McCaffrey, Graham Yielding, Jonathan Long, Richard Jones and David Iacopini. I would like to thank them for the valuable discussions, for their advices and the effort they put to go through the multiple versions of the manuscripts. I would especially like to thank Jonny for his incredible support, dedication, guidance and constant patience during all these years.

I am thankful to Badley Geoscience Ltd, Graham Yielding and Dave Quinn for inviting me at their office in Hundleby, for providing training and support for TrapTester. Also, I want to thank David Iacopini for receiving me at the Geology Department at the University of Aberdeen.

Also, I would like to thank professor Richard Hobbs for his help on seismic reflection modelling of fault deformation zones, a part of the research which was presented at the EGU Conference in Vienna (attached in the digital appendix of the thesis), which unfortunately I was not able to develop completely within the core chapters of the thesis.

I also want to thank Nicola de Paola and Stefan Nielsen for their feedback on my research progression and the discussions we had regarding normal fault-related deformation. I would also like to thank Mark Allen, Chris Jackson, Douglas Paton and Tom Manzocchi for providing very constructive reviews for parts of the work presented in this thesis.

I am thankful to the Geological Society of London for the Timothy Jefferson Field Research Grant (£ 1550.0) which allowed the fieldwork in Moab to be carried out. Alex Peace is thanked for his assistance in the field.

I appreciate all the effort from Gary, Dave and the finance team (Paula, Karen, Gail and Jill) for their IT and finance support whenever necessary.

Thanks to my friends and colleagues from Durham, that made the years spent here to be a great experience and made the time more bearable during the harder periods of my PhD. I am very grateful to Lamees for helping me with the printing and submission of this thesis when I was already away from Durham.

Also, I am particularly grateful to Csaba Krezsek, Zsolt Schleder and Gary Ingram, who inspired and motivated me to do a PhD in structural geology.

Finally, I want to thank my family, my sister, my mother and my late father for their support from the very beginning, without which I would have not been here.

| Table of contents |

Digital Appendix

| List of illustrations |

| Chapter 1 |

| Chapter 2 |

| Chapter 3 |

| Chapter 4 |

| Chapter 5 |

| Chapter 6 |

| Chapter 7 |

| Chapter 1 |

Introduction and aims of the thesis

1.1. Introduction

Normal faults form on a very wide range of scales (Walsh and Watterson, 1988; Kim and Sanderson, 2005) and in a variety of geological settings as a result of localized lateral extension of a volume of rock or by stretching and thinning of the entire crust (Anderson, 1951; Price and Cosgrove, 1990). Slip along normal faults can be associated with significant strain within the surrounding rock volume (Barnett et al., 1987) (***Figure 1.1***). Displacement is not always localized on a single main slip surface within the "fault core", but it can be partitioned between multiple slip surfaces within zones of distributed deformation (i.e. fracturing and small-scale faulting) in the "fault damage zone" (Caine et al., 1996). In some cases, ductile deformation, i.e. folding, can occur (Powell, 1875; Geikie, 1912; Walsh and Watterson, 1987; Long and Imber, 2010; Childs et al., 2016) (***Figure 1.1b***; ***Figure 1.2***; ***Figure 1.3***).

Previous research has shown that the development and distribution of strain is highly influenced by the fault growth processes within layered sedimentary rocks with variable mechanical properties (Powell, 1875; Peacock and Sanderson, 1992; Childs et al., 1996; Wilkins and Gross, 2002; Ferrill et al., 2005; Ferrill et al., 2007; Ferrill et al., 2008; Putz-Perrier and Sanderson, 2008; Putz-Perrier and Sanderson, 2011; Ferrill et al., 2012; Ferrill et al., 2017). Similarly, the amount of ductile deformation can vary significantly along the strike of a fault array as a result of the different deformation processes associated with the fault growth process, such as fault-tip propagation and fault interaction and linkage (***Figure 1.3***) (Long and Imber, 2010; Childs et al., 2016).

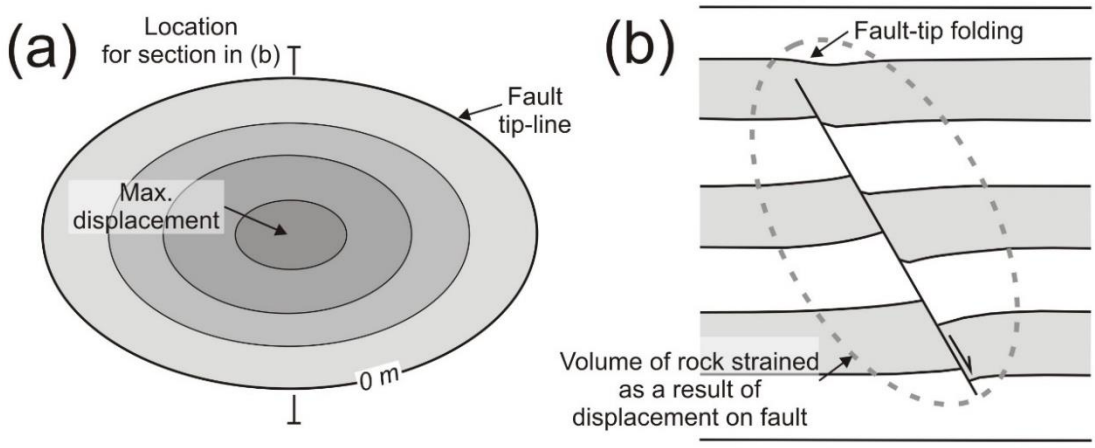

Figure 1.1 (a) *Schematic illustration of an idealized elliptical fault with contoured displacement (darker colours show larger displacements), viewed from a direction normal to the fault surface (modified from Barnett et al, 1987);* ***(b)*** *A cross-section normal to the fault surface illustrates that discontinuous displacement on the fault is accommodated within the surrounding volume of rock by ductile deformation (modified from Barnett et al., 1987).*

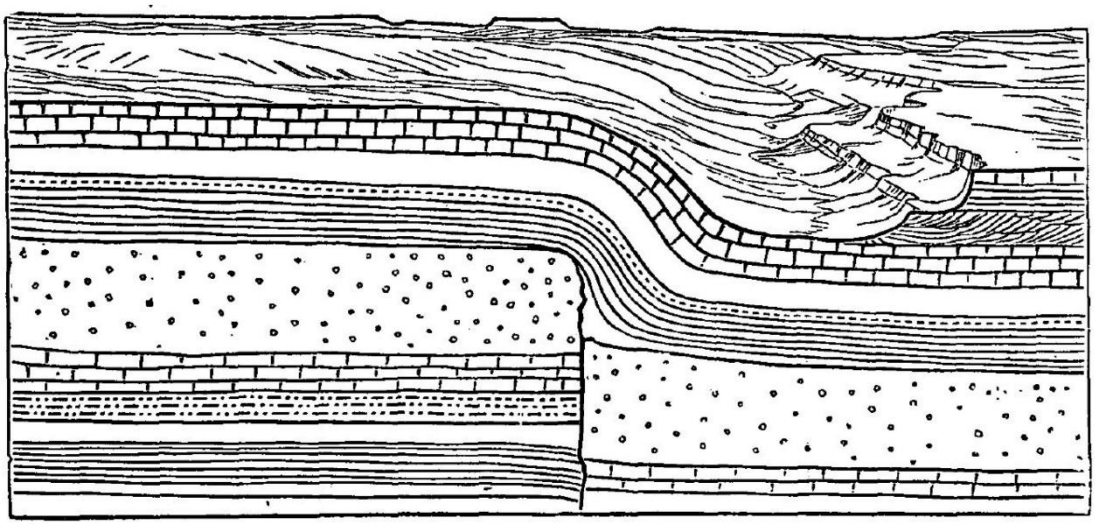

Figure 1.2 *Illustration from Powell (1875) showing that discontinuous displacement on a fault is replaced by continuous deformation (i.e. folding) within mechanically "more flexible" lithologies. His observations are one of the earliest to show the influence of the mechanical stratigraphy on the style of deformation (Ferrill et al., 2017).*

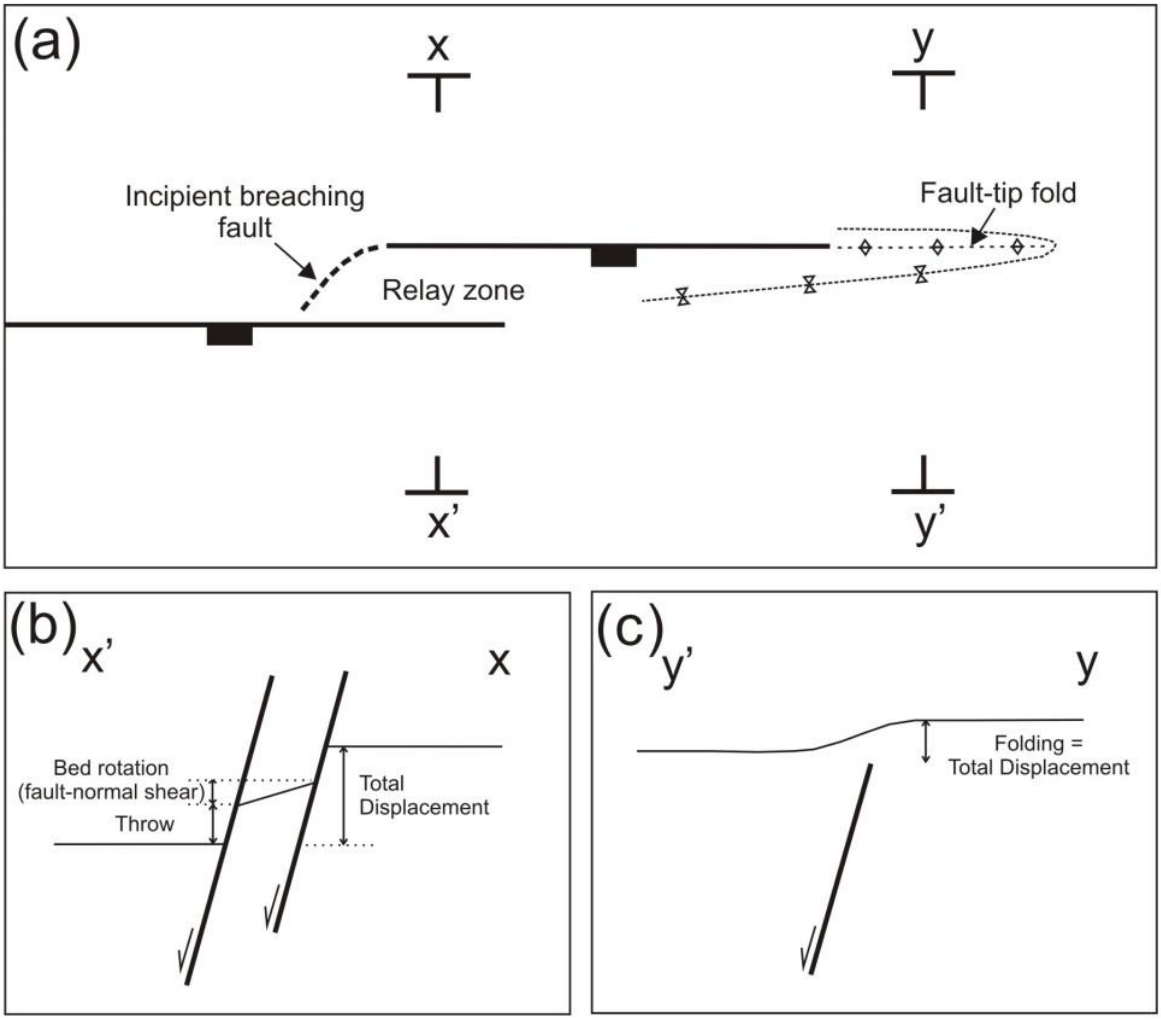

Figure 1.3 (a) *Schematic map-view illustration of two overlapping normal faults (bold black lines with box on downthrown side; modified from Long, 2011). Ductile deformation across the strike of the normal fault array can occur by different mechanisms, such as fault interaction and linkage within relay ramp - illustrated in the cross-section in* ***(b)*** *and fault-tip folding, as shown in the cross-section in* ***(c)***.

Because in normal faulting settings the maximum principal stress is almost perpendicular to horizontal bedding (Anderson, 1951), the deformation processes related with fault growth within a mechanically heterogeneous sequence depend principally on the geometry of the fault-tip line with respect to bedding and the sense of slip on the fault, i.e. mode of deformation (Walsh et al., 1999) (***Figure 1.4***).

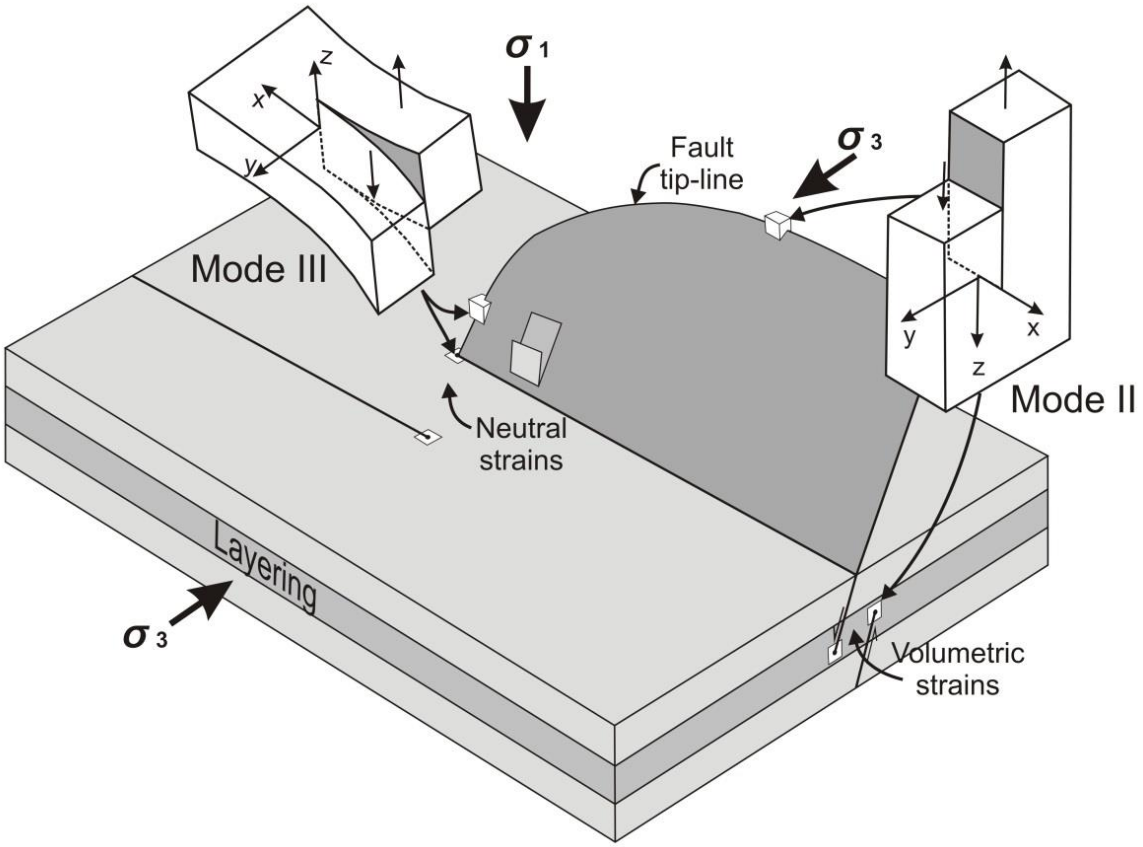

Figure 1.4 *Diagram showing the main modes of deformation associated with normal faults which cut through horizontal beds. The relationship between the sense of slip on fault relative to the tip-line geometry and layering attitude has important implications for the deformation types and associated strains within the surrounding volume. The white boxes represent small volumes of rock near the fault-tip subjected to a particular dominant mode of deformation (modified from Kanninen and Poppelar, 1985*).

For mode II type of deformation (or the edge dislocation mode), the slip is normal to the fault tip-line and the shear direction is in the plane of the fault, while mode III (or the screw dislocation mode) has the slip direction parallel to the fault tip-line and an anti-plane sense of shear (Kanninen and Poppelar, 1985; Pollard and Fletcher, 2005) (***Figure 1.4***). Near-fault-tip deformation associated with mode II dislocation requires a component of volume change by plastic deformation within the surrounding rock volume, whereas for mode III, volumetric strain changes are not necessarily required (Davis and Reynolds, 1996; Walsh et al., 1999) (***Figure 1.4***). Also, the near-tip stress distribution associated with

fracture dislocation of mode II and III are significantly different, determining different style of propagation and growth of the fault-tips (Willemse and Pollard, 2000; Pollard and Fletcher, 2005). Hence, the geometry of the fault-tip-lie and the slip direction relative to the fault tip-line and the layering can determine the development and preservation of complex volumes of deformation surrounding normal faults (Walsh et al., 1999) (***Figure 1.4*** *and* ***Figure 1.5***).

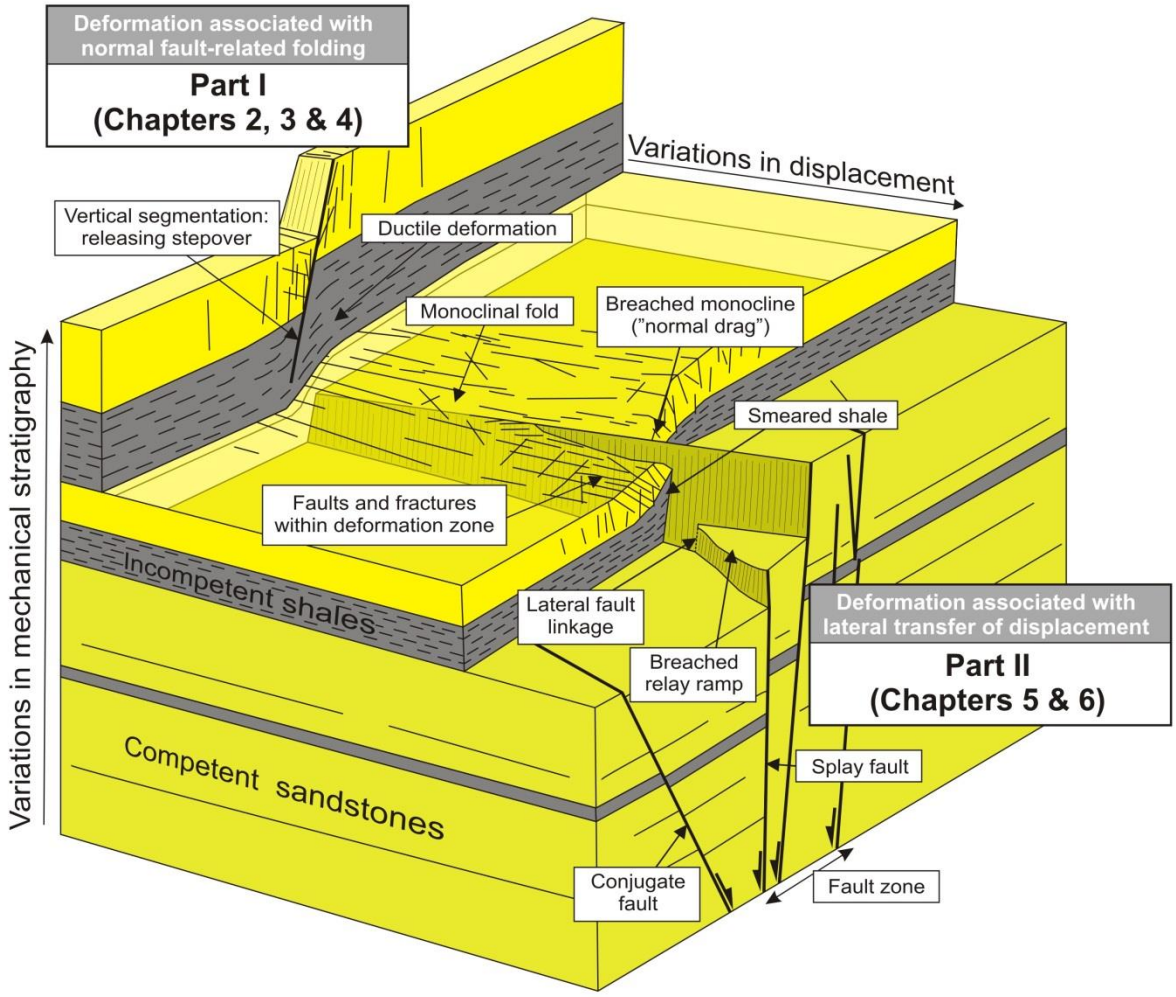

Figure 1.5 *Block-diagram illustrating some of the main deformation features associated with normal faulting within a heterogeneous sedimentary sequence with different mechanical properties, which are covered in this thesis. The first part of the thesis (Chapters 2, 3 and 4) discusses the variability of ductile deformation associated with normal fault-related folding. The second part (Chapters 5 and 6) covers the lateral linkage of normal faults and associated strain distribution within relay ramps.*

Fault segments develop very rarely as individual structures (at least at geologic time scale) and usually initiate and grow as part of a system or array of faults, which evolve with increasing strain (Peacock and Sanderson, 1991; Young et al., 2001; Walsh et al, 2003; Baudon and Cartwright, 2008). To date, geologists employ two end-member models to explain the growth of individual faults or fault arrays: the isolated fault model and the coherent fault growth model (Cartwright et al.,1995; Walsh et al, 2002; Walsh et al., 2003; Childs et al., 2017; Jackson et al., 2017) (***Figure 1.6***). The isolated fault growth model (***Figure 1.6a*** and ***1.6b***) assumes that fault segments or fault arrays grow from initial, randomly isolated segments, which are kinematically unrelated to each other. The isolated faults propagate and increase their length as they accrue displacement, interact and link incidentally. Because the faults grow in isolation and are kinematically unrelated, the displacement distribution is irregular, having a displacement deficit at the former boundaries or relay zones (***Figure 1.6b***). In the other model, the coherent fault growth model, the fault segments are part of a larger kinematically coherent structure. The segments can splay from a larger structure at depth, thus they can be hard-linked with the main fault structure or they can be physically unconnected in 3D (***Figure 1.6c*** and ***1.6d***) (Walsh et al., 2003). The kinematically coherent fault arrays show a displacement-distance distribution profile similar with a singular fault (***Figure 1.6e***).

Figure 1.6 – next page *Diagrams showing the two models which are employed to explain the formation of segmented normal fault arrays (from Walsh et al, 2003):* ***(a)*** *the isolated fault model and* ***(c)*** *and* ***(d)*** *the coherent fault model;* ***(b)*** *and* ***(e)*** *Fault displacement – distance plots for the two type of fault arrays (from Walsh et al., 2003). See text for detailed explanations.*

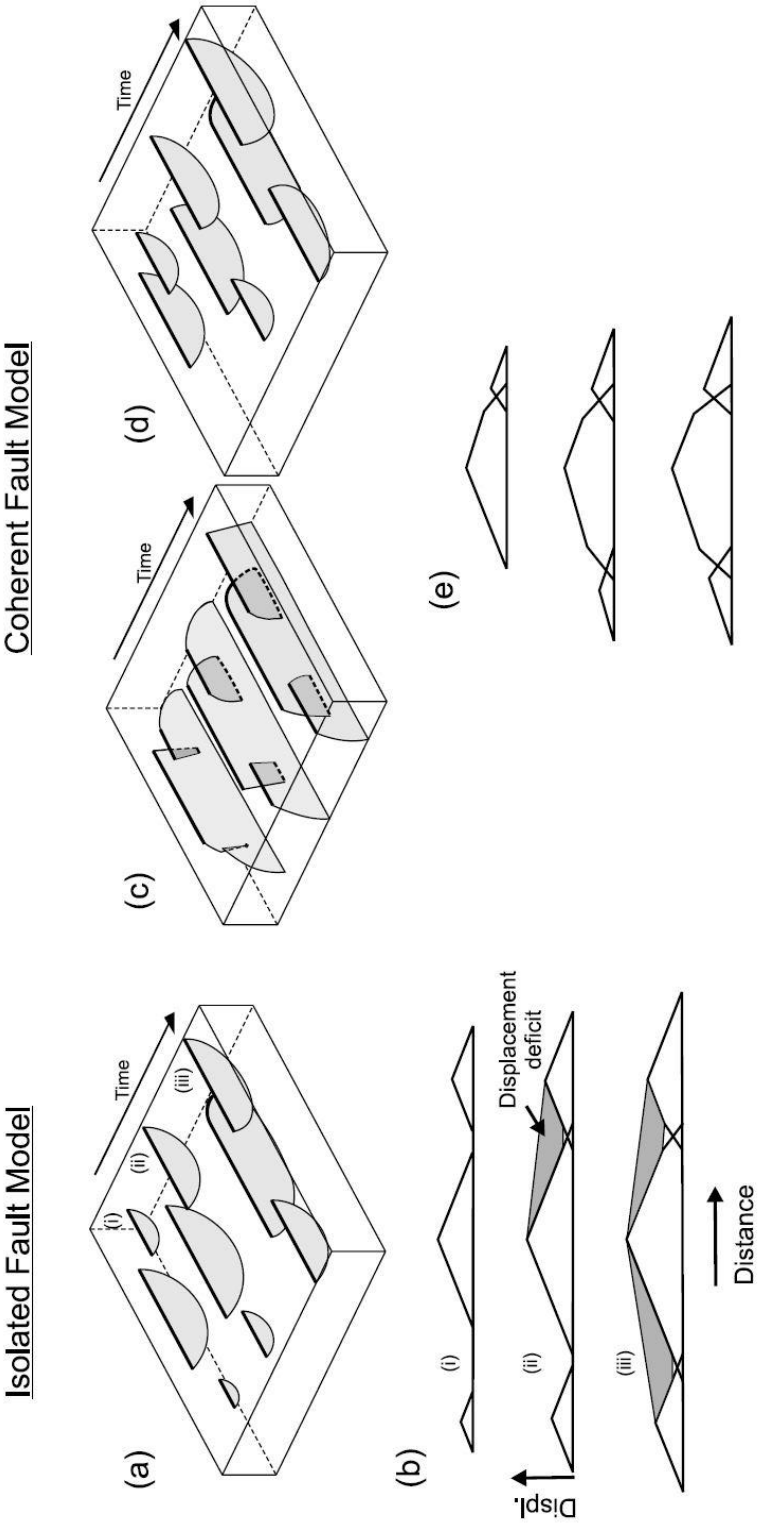
Isolated Fault Model
Coherent Fault Model
(a)
(b)
(c)
(d)
(e)
Time
(i)
(ii)
(iii)
Displacement deficit
Displ.
Distance

As the faults grow in size (Walsh and Watterson, 1987; Cartwright et al., 1995), the process of fault interaction and linkage (vertical or lateral) adds further complexities within the volume of strained rocks (***Figure 1.4*** and ***Figure 1.5***) (Crider and Pollard, 1998; Childs et al., 2009). Seismological evidence supported by mechanical models suggest that neighbouring fault segments interact through their slip-induced stress fields (Stein, 1999) (***Figure 1.7***), which can control preferential locations for slip and associated stress (and hence strain) localization (Crider and Pollard, 1998). Strains associated with lateral displacement transfer on normal faults are considered to be relatively simple because the ramps accommodate deformation predominantly in the direction parallel with the slip direction on the bounding faults (***Figure 1.3*** and ***1.4***) hence, the term "neutral" relay zones from Walsh et al., 1999. However, it has been shown that deformation within relay zones is very often non-plane strain, as a result of a shear strain component within the fault-normal direction which rotates the beds usually toward the hangingwall (Huggins et al., 1995; Walsh et al., 1996) (***Figure 1.3***). In particular, relay zones developed within mechanically heterogeneous sedimentary layers can display very complex three-dimensional strain distribution (Long and Imber, 2012). Fault nucleation and propagation and the breaching of relay zones (i.e. the physical linkage between the interacting normal faults) are dependent on the distribution and magnitude of the slip-induced perturbed stress fields around faults (Crider and Pollard, 1998; Gupta and Scholz, 2000). The degree of interaction is similarly dependent, beside the fault geometry and magnitude of slip by the mechanical properties of the rocks (Willemse, 1997).

Although, much progress on understanding the three-dimensional geometries and kinematics associated with normal faulting has been made in the last two decades through the use of 3D seismic reflection data (Walsh and Watterson, 1991; Cartwright and Husse, 2005; Baudon and Cartwright, 2008), there is still a need to integrate and better understand the different deformational behaviour of mechanically heterogeneous layers when interpreting and evaluating subsurface data (Richard et al., 2014; McGinnis et al., 2016). Additionally, through the analysis of ancient syn-sedimentary normal fault systems imaged by high resolution 3D seismic data, we can obtain critical insights into the complex geometries and the mechanical and kinematic behaviour of seismogenic normal faults.

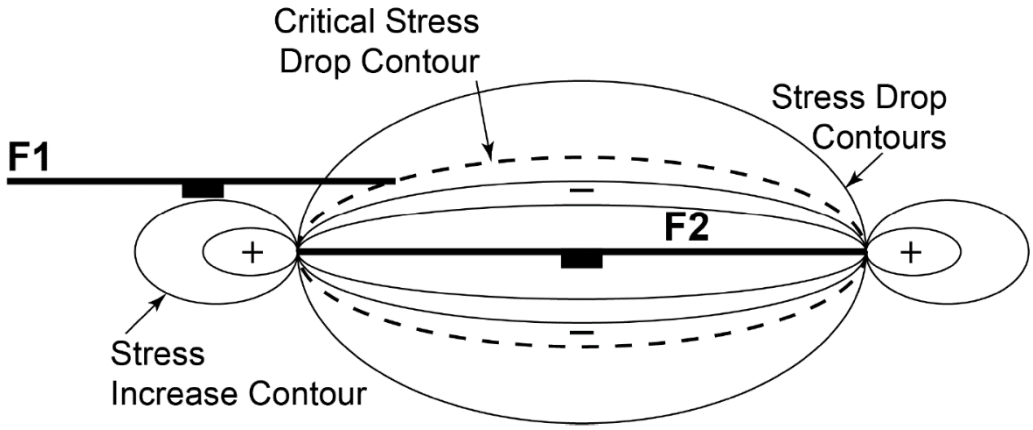

Figure 1.7 *Map-view of the distribution of elastic stress fields as a result of normal slip on fault F2 (from Gupta and Scholz, 2000). The stress drop zone surounding the fault and the stress increase in the vicinity of the tips will influences the evolution of the overlapping fault F1 and the localization and variability of strain / stress within the interacting region. Chapter 5 and 6 of the thesis cover aspects of the mechanical interaction between overlapping normal faults.*

1.2. Relevance of the research study

Normal faults can trap important volumes of hydrocarbons, especially within rifts and passive margin settings (Fraser et al., 2007; Roberts and Bally, 2012). Development of shale smears or dragging of sand layers and formation of "thief zones" (zones of fluid leakage) associated with normal fault-related folding (Davatzes and Aydin, 2005) or the evolution of fault linkage and development of fault lenses (Childs et al., 1995; Childs et al., 1996) can critically influence the cross-fault flow pathways and hence, the permeable properties of a fault zone (Hetshammer and Fossen,1998; Wibberley et al., 2008) (***Figure 1.8***). A good understanding of the variability and distribution of strain within the volume surrounding normal faults is essential for evaluating the trap integrity of normal fault-bounded structures.

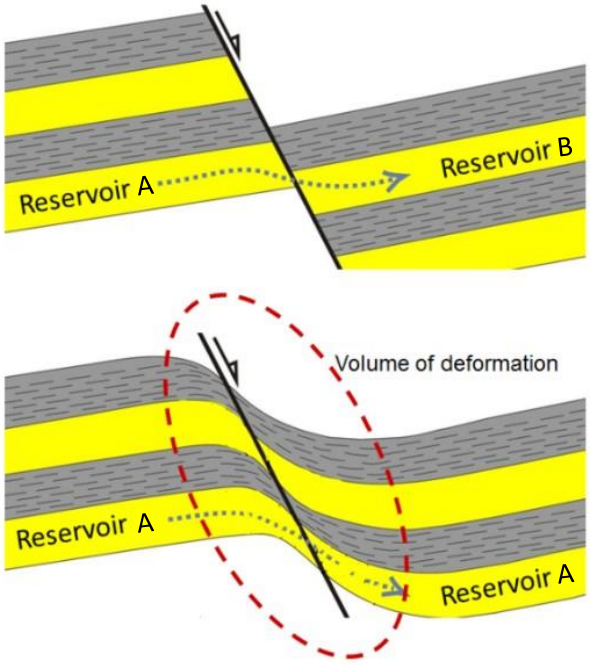

Figure 1.8 *Two schematic cross-sections of a normal faulted reservoir where the same amount of displacement is accommodated differently (discontinuous vs continuous), impacting the pathways of fluid migration across the fault (modified from Hesthammer and Fossen, 1998).*

Similarly, a better understanding of the processes and mechanisms that control the distribution of strain and stresses along normal fault segments can be important for the assessment of seismic hazards. Segmented seismogenic faults can display diverse and complex behaviours during seismic slip events. Depending on the amount of the accumulated strain energy and the geometry of the fault planes (e.g. segment length, distance between the stepping segments), seismic slip events can determine: (1) the individual rupture of fault segments (no immediate stress transfer between neighbouring segments occurs); (2) the consecutive rupture of segments (rapid stress transfer between segments); and (3) the continuous rupture of the faults segments. It is known that relay zones can act as barriers to rupture propagation or as rupture initiators along seismogenic normal faults (Zhang et al., 1999; Spina et al., 2008). Recent studies show that relay zones bounded by normal faults are less effective on stopping rupture propagation than relay zones associated with strike-slip or reverse-slip fault segments (Biasi and Wesnousky, 2016). Understanding better how normal faults interact and

how relays zones become breached can help mitigate some of the risks associated with rupture propagation during normal slip events.

1.3. Aims and objectives

The overall aim of the thesis is to investigate the influence of mechanical stratigraphy, fault geometry and fault mechanical interaction on the variability and distribution of ductile strain in the rock volume surrounding normal faults.

In our effort to investigate the variability of normal fault-related ductile deformation, we integrate empirical observations from well-calibrated high-quality seismic data and outcrop studies, with kinematic and mechanical models, and with previously published data and concepts.

The objectives of this thesis are:

1. To describe normal fault-related deformation from different geological settings and to test the hypothesis that mechanical properties of the host rocks and mechanical stratigraphy are a first order control on strain distribution within the normal fault volume.
2. To quantify the variations in fault displacement *vs* ductile deformation along normal fault zones in different lithologies.
3. To develop a conceptual model to explain the variable distribution of ductile deformation associated with normal fault-related folding and displacement transfer (i.e. relay ramps) in mechanically heterogeneous stratigraphic sequences.
4. To investigate the variability and limitations of relay breaching criteria such as critical ramp shear strains or throw / separation ratio.
5. To investigate the influence of the free surface on the breaching styles of relay ramps.
6. To investigate the process of mechanical fault interaction and its possible influence on the variability and distribution of strain within the rock volume containing normal faults arrays.

7. To explore the hypothesis that variable relay aspect ratios are controlled by lithology and by the interaction between overlapping normal faults.

1.4. Thesis Outline

The thesis comprises two main parts, each covering different deformation process associated with normal faulting and a third part in which I discuss the findings and the main conclusions of the research (***Figure 1.5***). In the first part of the thesis I discuss normal fault-related folding, as a result of mostly mode II type of deformation. Strains associated with transfer of displacement between segments, i.e. relay ramps, characteristic for a dominant mode III type of dislocation, are discussed in the second part of the thesis (***Figure 1.3*** and ***Figure 1.5***).

A comprehensive review of the literature and necessary background information is provided in each of the core chapters, which are conceived in the style of scientific papers. In particular, *Chapter 2* is a review study of the strain variability associated with normal fault-related folding in heterogeneous stratigraphic sequences.

Part I – Strain variability associated with normal fault-related folding

1.4.1. Chapter 2. Control of mechanical stratigraphy on distribution of strain within normal fault-related folds – a review

This chapter introduces key concepts of mechanical stratigraphy and the formation mechanisms of folds in extensional setting. The chapter summarises the current research on deformation associated with normal fault-related folds encountered within different mechanical stratigraphic and overburden stress conditions, from published work and our own observations. We describe the patterns of small and meso-scale faulting and fracturing which accommodate larger, seismic-scale ductile folding in relation with the mechanical properties of the layered stratigraphic sequence. We emphasize the

importance of mechanical competence contrast in controlling the manner in which strain is accommodated and, hence the overall patterns of secondary fault and fracture systems within normal fault-related folds.

1.4.2. Chapter 3. Variability and distribution of brittle strain accommodating hangingwall folding of a seismic-scale normal fault, Moab Fault, Utah

In this chapter we investigate the characteristics of small scale faulting and fracturing that accommodates larger, seismic-scale normal fault-related folding along the Moab fault, Utah. Four transects across the hangingwall normal drag folds are analysed. We show that the strain characteristics and deformation styles are highly controlled by the mechanical properties of the layered sandstone-shale sequence of the Cedar Mountain Formation.

1.4.3. Chapter 4. Occurrence and development of folding related to normal faulting within a mechanically heterogeneous sedimentary sequence: a case study from Inner Moray Firth, UK

In this chapter we use well-calibrated seismic reflection data to explore the control of fault geometry, lithology and fault interaction on the occurrence and the development of folds along a normal fault system. We exemplify how fault segmentation and associated ductile deformation are influenced by the heterogeneous mechanical properties of the stratigraphic sequence. We show that normal fault-related folds can be generated by different mechanisms that vary in importance in time and space along a single fault array. The occurrence of normal fault-related folds can also be explained by how normal faults interact mechanically. Specifically, the variability of extensional folding along the strike of a fault array can be explained by enhanced vertical propagation due to mechanical fault interaction between opposite-dipping normal faults.

Published: Lăpădat, A., Imber, J., Yielding, G., Iacopini, D., McCaffrey K. J. W., Long, J. J., Jones, R. R., 2016. Occurrence and development of folding related to normal faulting within a mechanically

heterogeneous sedimentary sequence: a case study from Inner Moray Firth, UK. In: Childs, C., Holdsworth, R. E., Jackson, C. A.-L., Manzocchi, T., Walsh, J. J., Yielding, G. (Eds) The Geometry and Growth of Normal Faults, Geological Society of London Special Publications 439.

Part II –Variability of strain within normal fault-bounded relay ramps

1.4.4. Chapter 5. Breaching of relay ramps bounded by surface-breaking normal faults

This chapter investigates the breaching of relay ramps associated with surface-breaking normal faults (***Figure 1.3a***). Empirical observations are integrated with kinematic and mechanical models to explain the differences in geometry, timing (relative to fault growth) and likelihood of relay ramp breaching along surface-breaking normal fault arrays. We show that the probability of full ramp breaching on surface-breaking normal faults depends not only on the accumulated ramp shear strains and the ratio between throw and separation of the bounding faults, but also on how the throw is partitioned between the faults. Mechanical models of surface breaking normal faults show asymmetric stress perturbations with larger shear stress drops within the hangingwalls (compared with the footwalls) which explains the variability in breaching strains and the preferential breaching location through the footwall side of the ramp.

To be submitted as: Lăpădat, A., Imber, J., Yielding, G., McCaffrey K. J. W., Jones, R. R., Long, J. J., Iacopini, D. (in prep). Breaching of relay ramps bounded by surface-breaking normal faults. Earth and Planetary Science Letters.

1.4.5. Chapter 6. Geological controls on the geometries and strain variability within relay ramps

In this chapter we investigate the variability of the three-dimensional geometries and strains within relay ramps. We show how the host rock lithology and the existing fault configuration at the time of interaction controls the three dimensional ramp geometries and associated strains within relay ramps.

Normal faults within mechanically competent rocks tend to develop relay ramps with tabular geometries, larger aspect ratios and smaller fault-parallel shear strains than the ones developed in incompetent rocks. We show that the fault-normal shear strain (***Figure 1.3b***) component within ramps is not necessarily the result of monoclinal folding during the underlapping stage of the faults, but also the result of the asymmetry of the displacement gradients on the overlapping faults. Mechanical models indicate asymmetrically larger shear stress drop zones within the hangingwall of surface-breaching normal faults, which can inhibit propagation of the front fault and result in the accumulation of larger displacement gradients on it, which will cause the ramp to twist and dip toward the hangingwall.

Part III – Discussion, conclusions and future work

1.4.6. Chapter 7. Discussion and future work

The chapter summarises the results of this research and discusses the potential implications of the findings, in the light of exploration activities for hydrocarbons and within the wider scientific research community. Also, we indicate some directions to develop future work.

| Chapter 2 |

Control of mechanical stratigraphy on distribution of strain within normal fault-related folds – a review

Abstract

This chapter provides some background information on mechanical stratigraphy and mechanisms for the development of folds associated with normal faults. We review the existing literature and present some of our own observations from outcrops and seismic reflection data to illustrate the spectrum of normal fault-related folds encountered within different mechanical stratigraphic and overburden settings. We describe the characteristics of small and meso-scale faulting and fracturing which accommodates larger, seismic-scale normal fault-related folding in relation with the mechanical properties of the layered stratigraphic sequence. We highlight the importance of mechanical competence contrast in controlling the manner in which strain is accommodated and, hence the overall patterns of secondary fault and fracture systems within normal fault-related folds. Understanding better the deformation processes associated with the large spectrum of folds adjacent to normal faults is important because of the influence they exert on the internal structure and permeability properties of the fault zones.

2.1. Introduction

A significant amount of work has been done on the deformation associated with compressional fault-related folds, much of which underlines the role of the mechanical behaviour of multi-layered sedimentary rocks in controlling the geometry of the folds and their associated strain patterns (Ramsay, 1974; Stearns, 1978; Cosgrove, 2015; Hughes and Shaw, 2015). Folds related to normal faults have also been widely described in the literature based on observations from outcrops, interpretation of seismic data, and analogue and numerical modeling (Withjack et al., 1991; Schlische, 1995; Corfield and Sharp, 2000; Sharp et al., 2000; Withjack and Callaway, 2000; Khalil and McClay, 2002; Johnson and Johnson, 2002; Ferrill et al., 2005; Fodor et al., 2005; Ferrill et al., 2007; Jackson et al., 2006; White and Crider, 2006; Schöpfer et al., 2007; Ole Kaven and Martel, 2007; Ferrill et al., 2012; Rotevatn and Jackson, 2013; Childs et al., 2016; Lăpădat et al., 2016). Folding is not always an integral part of the deformation process associated with extension and, unlike in the compressional regimes, is relatively rarely developed in association with normal faults (Childs et al., 2016). Because in normal fault regimes the maximum principal stress usually acts at a high angle to bedding (Anderson, 1951), the occurrence and development of folding is highly dependent on: (i) the *mechanical properties* of the rocks, which may influence, for example, fault tip propagation, and hence enhance the formation of fault-propagation folds (Ferrill et al., 2007; Ferrill and Morris, 2008) or shear distribution (Ferrill et al., 2005; Homberg et al., 2016); and (ii) the *geometry of the faults* (Rotevatn and Jackson, 2014; Lăpădat et al., 2016), which is similarly dependant on the mechanical properties of the host rocks (Peacock and Sanderson, 1992). Hence, ductile deformation associated with normal faults within the upper part of the crust can cover an entire spectrum from discrete faulting or localized shearing to large forced folds (Stearns, 1978). Recent review papers by Ferrill et al. (2016; 2017) synthesized the role played by the mechanical stratigraphy in controlling deformation characteristics related to normal faulting, such as fault nucleation, mode of failure, fault geometry (i.e. fault refraction), fault propagation/ arrest and associated fault-propagation folding and fault reactivation tendencies. Within their reviews (Ferrill et al., 2016; Ferrill et al., 2017), as in their previous research work (Ferrill et al., 2005; Ferrill et al.,

2007; Ferrill and Morris, 2008; Smart et al., 2009; Ferrill et al., 2011; Ferrill et al., 2012), the authors highlighted the importance of the mechanical properties of the rocks and the mechanical competence contrast in controlling the deformation patterns and distribution of strain within normal fault-propagation folds.

The aim of this chapter is to synthesise the spectrum of normal fault-related folds encountered within various mechanical stratigraphic and overburden conditions, from previously published work and the authors own observations on outcrops and seismic reflection data. We describe the patterns of small and meso-scale faulting and fracturing which accommodates larger, seismic-scale ductile folding in relation to the mechanical properties of the layered stratigraphic sequence. We emphasize the importance of mechanical competence contrasts in controlling the manner in which strain is accommodated and, hence the overall patterns of secondary fault and fracture systems within normal fault-related folds. Understanding better the deformation processes associated with the large spectrum of folds adjacent to normal faults is important because of the influence they exert on the internal structure and permeability proprieties of the fault zones. For example, shale smear, which is essential for entrapping hydrocarbons within faulted structures, is similar to folding, mainly a product of ductile deformation and its continuity is influenced by the distribution of secondary faults and fractures within the surrounding deformation zone (Childs et al., 2007). Therefore, a good understanding of the variability of strain and of the deformation mechanisms within a mechanically heterogeneous normal faulted sedimentary sequence is important for the evaluation of the capacity of faults to seal or transmit hydrocarbons (Yielding et al., 2012; Vrolijk et al., 2016).

The objectives of this chapter are three-fold: (i) to describe the deformation styles associated with normal fault-related folding and to analyse how strain characteristics and fold geometries vary with mechanical properties of the host stratigraphic section; and (ii) to develop a conceptual model for predicting small-scale deformation within seismic scale normal fault-related folds based on the variations in mechanical properties of the rocks at the time of deformation.

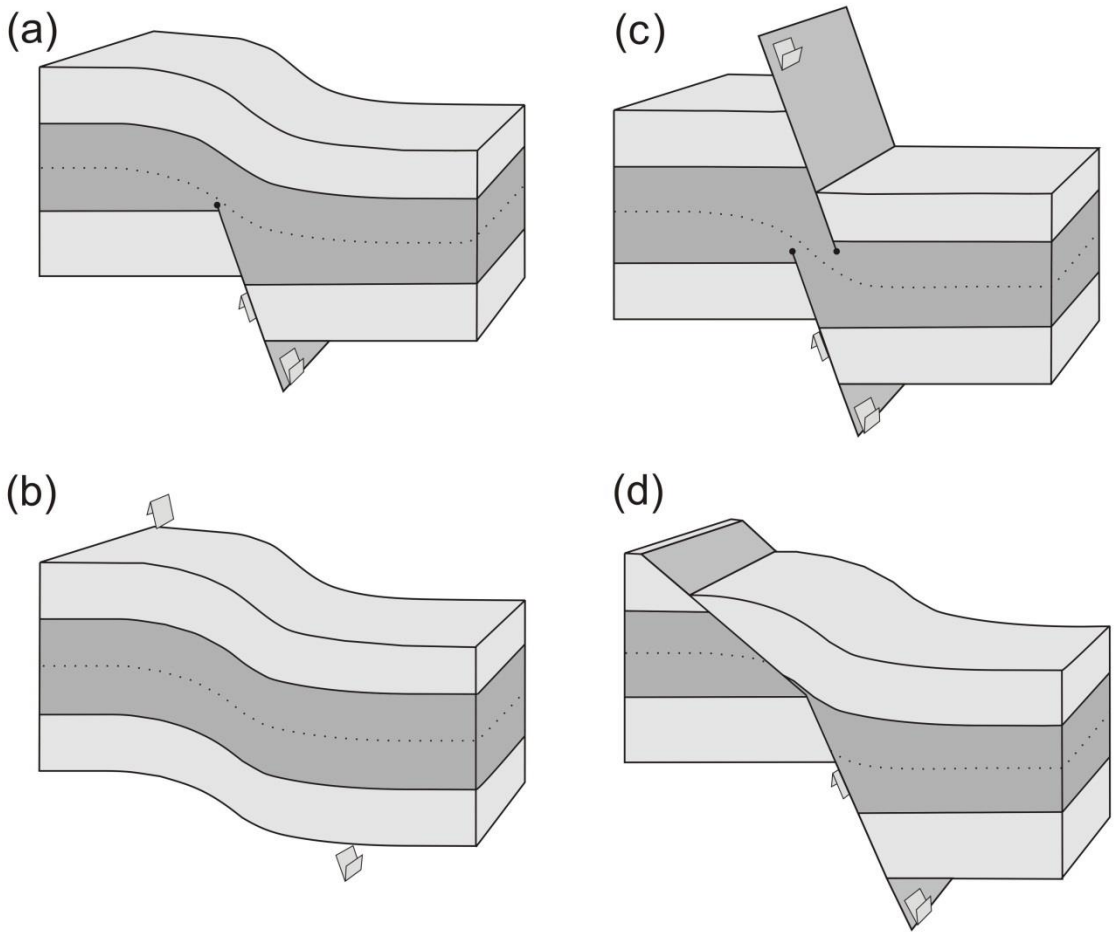

Figure 2.1 *Several mechanisms for generation of normal drag-like folds associated with extensional faults* ***(a)*** *Fault-propagation folding;* ***(b)*** *Fault-shear folding;* ***(c)*** *Formation of a releasing relay as a result of vertical fault segmentation and; (d) Fault-bend folding.*

2.2. Normal fault-related folding

In this thesis we focus on the spectrum of normal fault-related folds that are in general described as *normal drag folds*, hence we do not consider reverse drag folds or larger roll-over structures associated with displacement on listric fault planes (Ellis and McClay, 1988; Xiao and Suppe, 1992). We use the term "drag" in this paper simply to describe the geometry of the fold, i.e. fold with the limb dipping sub-parallel to the relative slip direction on the fault, without implying the responsible mechanism for its formation (Ferrill et al., 2012; Childs et al., 2016). Recent research studies have argued that normal drag folds are less the result of frictional resistance to slip (Grasemann et al.,

2005) - drag folds *in sensu stricto* (Twiss and Moores, 1992) - but are rather the consequence of the fault growth processes within mechanically heterogeneous sedimentary sequences, such as distributed shear deformation (Fossen and Hesthammer, 1998; Ferrill et al., 2005; Homberg et al., 2016) or fault-propagation folding (Walsh and Watterson, 1987; Ferrill et al., 2007; Ferrill et al., 2012) (***Figure 2.1a*** and ***2.1b***). Normal drag geometries can also develop as a result of translation of the hangingwall over a convex-toward-hangingwall bend in the fault plane, i.e. fault-bend folding (Ferrill et al., 2005; Lăpădat et al., 2016) (***Figure 2.1d***) or a combination of fault-propagation folding and fault-bend folding (Lăpădat et al., 2016 or see *Chapter 4*), or by folding between overlapping or underlapping, vertically or laterally segmented faults (Rykkelid and Fossen, 2002; Fodor et al., 2005; Childs et al., 2016) (***Figure 2.1c***).

Normal drag folds can occur on a wide range of scales and their geometries are relatively similar, irrespective of their genetic origin: the folds generally widen upward in a zone of distributed deformation adjacent to the main fault plane or above its upper tip, very often asymmetrically, with larger widths, i.e. fold wavelengths, within the hangingwall side (particularly in the case of fault-bend folding and fault-propagation folding). In the case of normal fault-propagation folds and fault-shear folds (***Figure 2.1a*** and ***2.1b***), the steep limb of the fold dips toward the hangingwall, with amplitude increasing generally with displacement until a certain threshold is reached, which usually depends on the lithology (Ferrill and Morris, 2008; Lăpădat et al., 2016). In some extreme cases the fold limb can reach the same dip as the fault.

Normal drag folds can account for a variable amount of the total fault displacement, which is accommodated, especially within the hangingwall, by rotation of the layers or seismic reflectors in a direction parallel to the sense of slip on the fault (***Figure 2.1; Figure 2.2a***) (Walsh et al., 1996; Long and Imber, 2010). This means that in some cases an important part of the throw on the fault (up to 90% in Gullfaks Field, offshore Norway; Hesthammer and Fossen, 1998) is accommodated by ductile deformation, which can have large implications, for example, when evaluating the communications of reservoir across a fault (***Figure 1.8*** and ***Figure 2.2***).

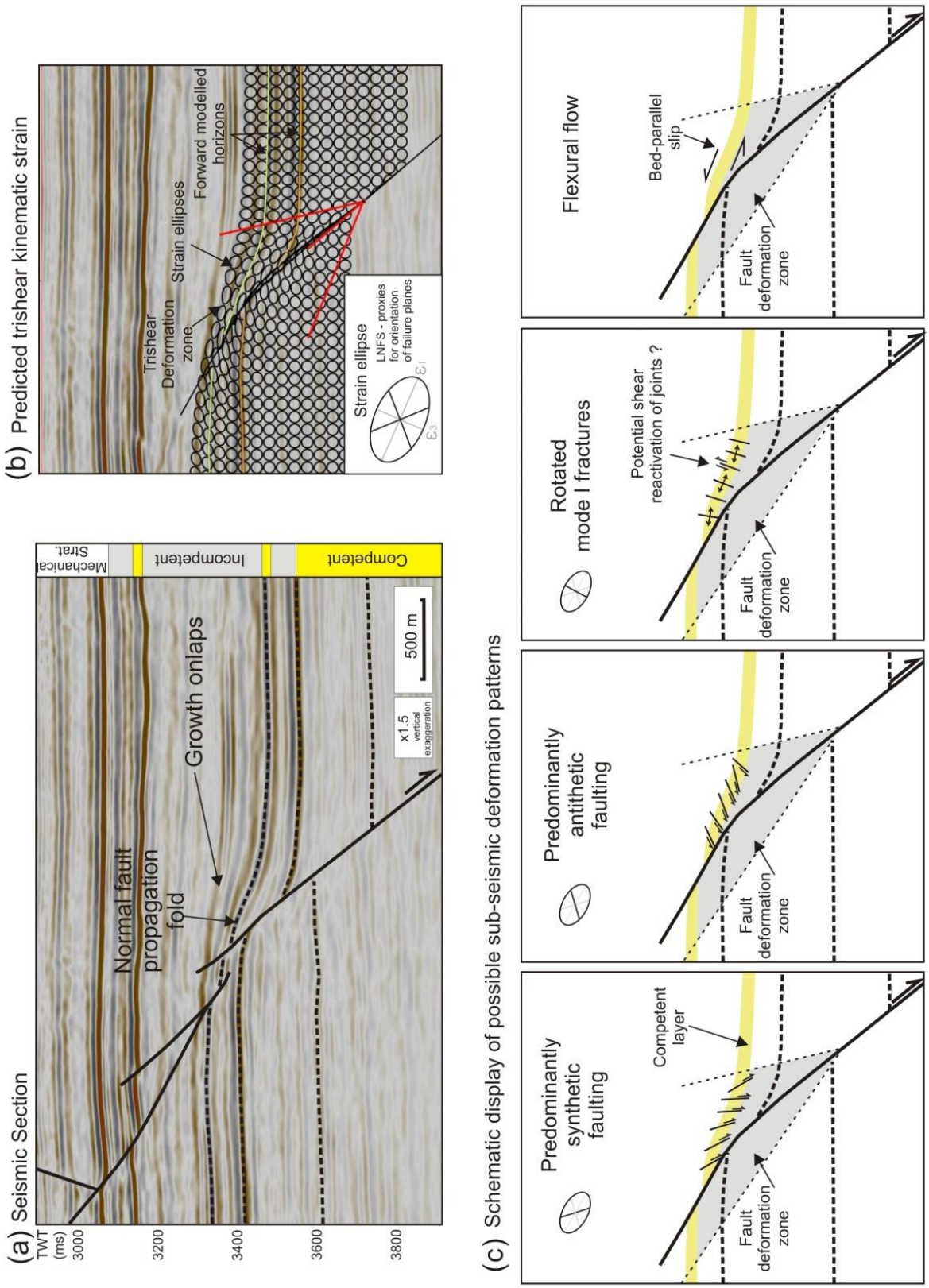
(a) Seismic Section
TWT (ms)
3000
3200
3400
3600
3800
Mechanical Strat.
Incompetent
Competent
Normal fault
propagation fold
Growth onlaps
500 m
x1.5 vertical exaggeration
(b) Predicted trishear kinematic strain
Trishear Deformation zone
Strain ellipses
Forward modelled horizons
Strain ellipse
LNFS - proxies for orientation of failure planes
(c) Schematic display of possible sub-seismic deformation patterns
Predominantly synthetic faulting
Competent layer
Fault deformation zone
Predominantly antithetic faulting
Rotated mode I fractures
Potential shear reactivation of joints ?
Flexural flow
Bed-parallel slip

***Figure 2.2*. – *previous page* (a)** *Seismic section of a normal fault-propagation fold from offshore NW Australia. The limb of the monoclinal fold dips toward the hangingwall and its growth is indicated by the onlapping seismic reflectors.* **(b)** *Kinematic models can predict the strain intensity within the folded structure, but do not consider the mechanical properties of the host rocks. Lines of no finite elongation (LNSF) can be used as proxies for the orientation of the fracture sytems (see 2c) which accommodates extensional strain within the folded beds (Allmendinger, 1999); The red lines delimit the trishear deformation zone within the hangingwall and fotwall;* **(c)** *A conceptual sketch with potential sub-seismic scale deformation structures which could accommodate larger seismic-scale folding. The flexure of the more competent layer can be accommodated by a combination of all these main mechanisms, however it is likely that one of them would predominate.*

Kinematic modeling techniques, in particular trishear modeling, are able to realistically reconstruct the geometry and the kinematic evolution of normal fault-propagation folds and to estimate the intensity and variability of strain within the deformation zone (Erslev, 1991; Allmendinger, 1998; Hardy and Allmendinger, 2011) (***Figure 2.2b***). The modelled strains are a good first estimation of the distribution and magnitude of strains within normal fault-related deformation zones and lines of no finite elongations can be used as proxies for potential orientation of secondary faults (Allmendinger, 1998; but see Imber et al., 2012) (***Figure 2.2b***). Secondary faults can also be predicted using the Mohr – Coulomb failure criterion, however information about the stress field is not contained within the kinematic trishear models. The estimations are purely geometrical and have no mechanical basis: they do not account for variations in the mechanical properties of the host rocks, which play an important role in the partitioning and distribution of strain (Gross, 1995; Schöpfer et al., 2007) or determine volumetric changes that are often seen to occur in real deformed rocks (Long and Imber, 2012).

In the following sections we review some of the key concepts associated with mechanical stratigraphy and then we describe examples of deformation associated with a spectrum of normal fault-related folds.

2.3. Mechanical stratigraphy

The amplitude (or magnitude) of folding is controlled not only by the amount of displacement on fault, but also by the *mechanical properties* of the host rocks at the time of deformation (Withjack and Callaway, 2000; Ferrill et al., 2007; Ferrill and Morris, 2008; Ferrill et al., 2012). The flexure of the beds adjacent to normal faults is usually associated with the presence of *mechanically weak* or *incompetent* lithologies, such as plastic shales or evaporites which are able to account for a large part of the strain by ductile deformation (Donath, 1970; Ferrill et al., 2017; ***Figure 2.3a***). The mechanical behaviour of the rocks is determined by their intrinsic properties, such as the mineralogical composition, porosity and texture (i.e. fabric anisotropy), which influence their capability to resist deformation (i.e. the relative *strength* or *stiffness* of the rocks) and their capability to undergo permanent strain (i.e. *ductility*) (Ferrill and Morris, 2008; Ferrill et al., 2017). *Incompetent rocks* (e.g. phyllosilicate rich lithologies and those with high porosity) are relatively weak and suffer permanent strains at smaller stress values (***Figure 2.3b****;* Ferrill et al., 2017). *Competent rocks* are defined as the ones that are relatively strong and require larger stresses to deform, i.e. quartz, feldspar or calcite-rich lithologies with low porosity (Ferrill et al., 2017). In their recent review papers, Ferrill et al. (2016, 2017) synthesized previous research which demonstrated the importance of rock mechanical properties in controlling nucleation of faults and fractures and their propagation (Wilkins and Gross, 2002; Ferrill et al., 2007; Roche et al., 2013), their geometry (Peacock and Sanderson, 1992; Schöpfer et al., 2007; Ferrill et al., 2009), modes of deformation (Ferrill et al., 2012), displacement gradients (Gudmundsson, 2004; Wibberley et al., 2008), distribution and partitioning of strain (Gross, 1995; Schöpfer et al., 2007) and fault zone architecture and properties (Aydin and Eyal, 2002; Davatzes and Aydin, 2005).

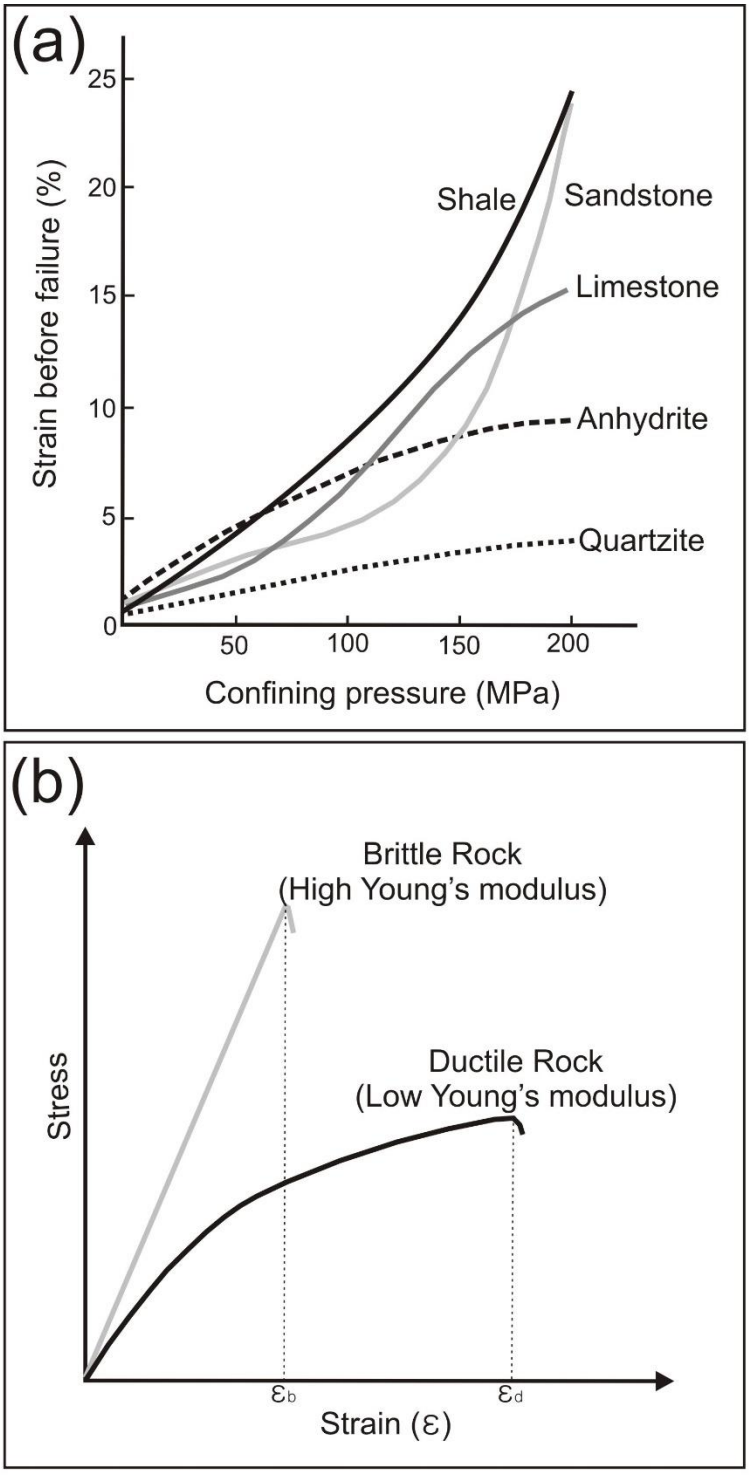

Figure 2.3 (a) *Ductility vs confining pressure for several common lithologies (from Ferrill et al., 2017; after Donath, 1970).* ***(b)*** *Schematic stress vs strain relation for a competent and a weak (ductile) rock (from Ferrill et al., 2017). The competent rocks accmmodates smaller strains prior to faulting (*ε_b*) than the weaker lithologies (*ε_d*).*

However, establishing the mechanical properties of individual layers is not sufficient enough to describe the deformational behaviour of sedimentary rocks because: (i) these rocks are generally arranged in a layered system, which can be characterized by beds with various mechanical parameters (e.g. Young's modulus or yield strength); (ii) layering involves an interface often with its own mechanical behaviour; and (iii) the thickness and distribution of beds with similar elastic properties define a larger stratigraphic unit which will have a mechanical behaviour of its own (Gross, 1995; Ferrill et al., 2008; Ferrill et al., 2017). Therefore, Ferrill et al. (2017) defined the mechanical stratigraphy based on three main parameters: (i) *the competence* of the rocks (related to the intrinsic properties of the rocks), as defined by elastic parameters such as *stiffness* or *Young's modulus*, and by *ductility*; (ii) *the competence contrast* between layers and the frictional behaviour of the mechanical boundaries; and (iii) *the thickness and distribution* of the competent/ incompetent rocks.

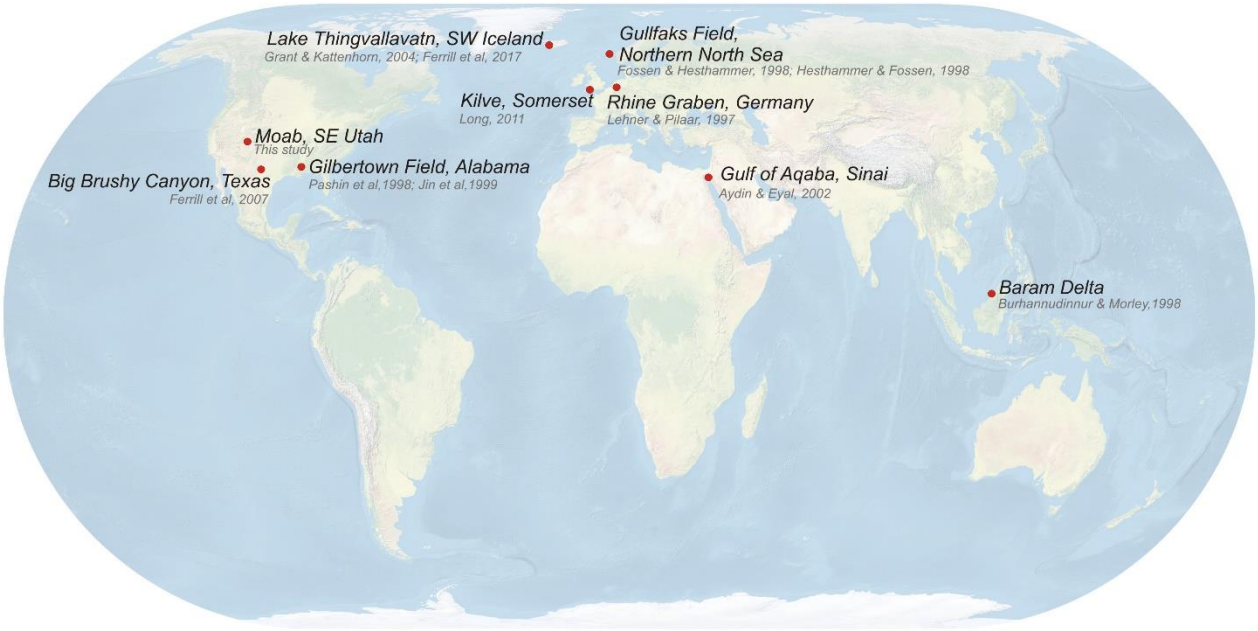

Figure 2.4 *Location map of the normal fault-related folds examples described in this chapter.*

In the next section, we will describe several examples of folds associated with normal faults from outcrops and seismic data sets from published literature and our own observations (***Figure 2.4***). We show how mechanisms of deformation and strain characteristics vary within different lithologies or mechanical stratigraphic units. These case studies are chosen in order to reflect a larger diversity of lithologies with heterogeneous mechanical properties.

2.4. Strain distribution within folds associated with normal faults - Case Studies

2.4.1. Normal fault-related folds developed within a predominantly incompetent stratigraphic sequence with low mechanical competency contrast

Gullfaks Field, northern North Sea (Fossen and Hesthammer, 1998; Hesthammer and Fossen, 1998)

The Gullfaks Field provides an abundance of data including well data with cores and well logs through fault zones, that makes it an excellent location to study the characteristics of small, sub-seismic scale deformation associated with large, seismic-scale normal faults. The structural characteristics of the field have been described in detail by several authors (Fossen and Hesthammer, 1998; Hesthammer and Fossen, 1998; Hesthammer and Fossen, 2001; Hesthammer et al., 2001). The Gullfaks Field structure is located on the western side of the Viking Graben in the northern North Sea and is characterized by a N-S striking normal fault system, parallel to the main rift axis, which compartmentalize the field into several blocks. A secondary trend of minor E-W oriented normal faults abuts onto this main fault system (Fossen and Hesthammer, 1998). The main fault blocks are highly rotated in a soft-domino style of deformation (Walsh and Watterson, 1991; Fossen and Hesthammer, 1998), with the main faults dipping as gently as 25-30°. Normal drag folds are developed within the footwall and hangingwall of these main N-S oriented faults, with significantly larger amplitudes and wavelengths within the hangingwall (***Figure 2.5a***) (Hesthammer and Fossen, 1998). Well data indicate that the beds within the fold limbs can reach a dip of 45° in the proximity

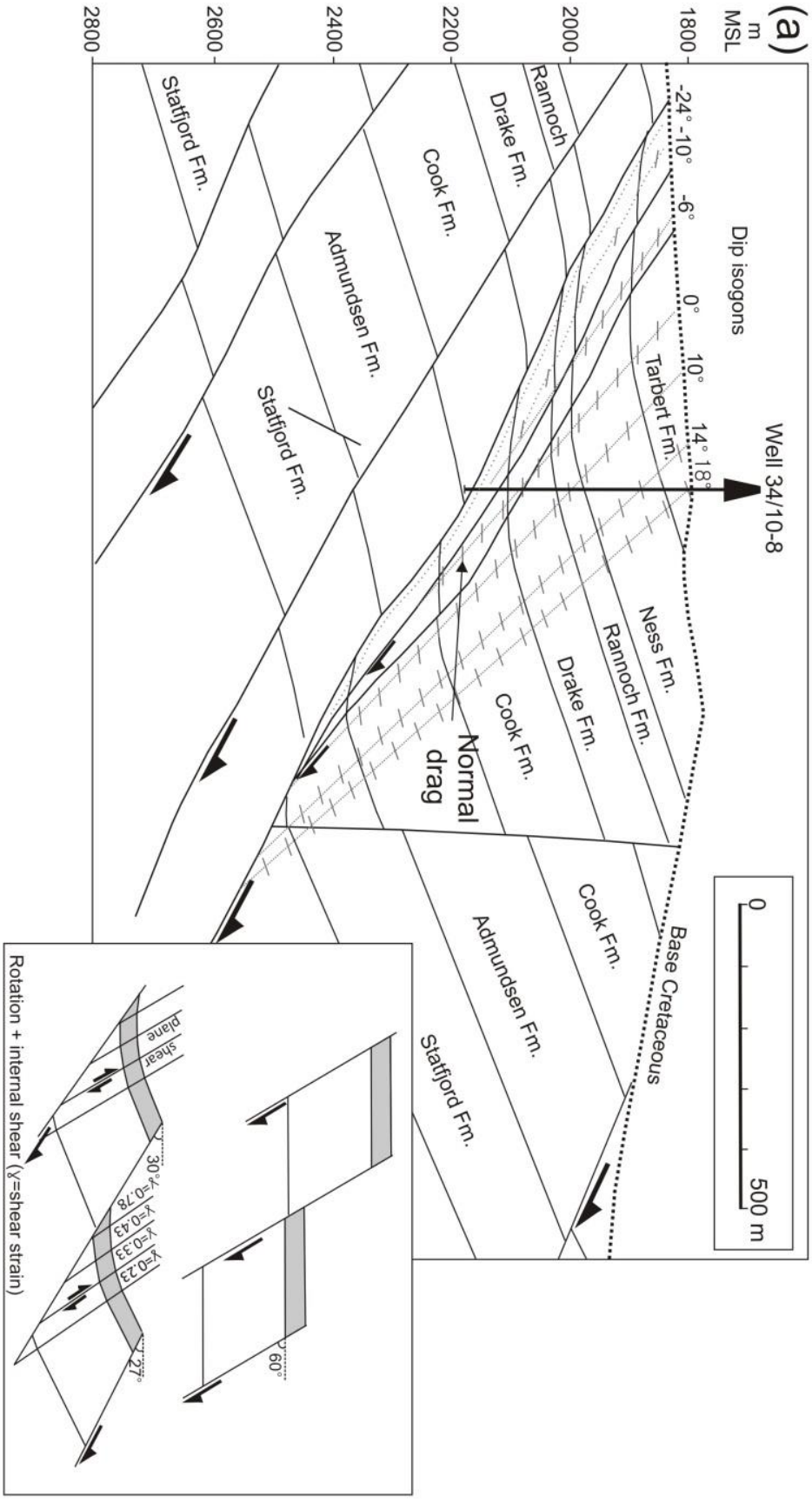
(a)
m
MSL
1800
2000
2200
2400
2600
2800
Dip isogons
-24°
-10°
-6°
0°
10°
14°
18°
Well 34/10-8
Tarbert Fm.
Rannoch
Drake Fm.
Cook Fm.
Admundsen Fm.
Statfjord Fm.
Ness Fm.
Rannoch Fm.
Drake Fm.
Cook Fm.
Admundsen Fm.
Statfjord Fm.
Normal drag
Base Cretaceous
0
500 m
Rotation + internal shear (γ=shear strain)
shear plane
30°
γ=0.78
γ=0.43
γ=0.33
γ=0.23
27°
60°

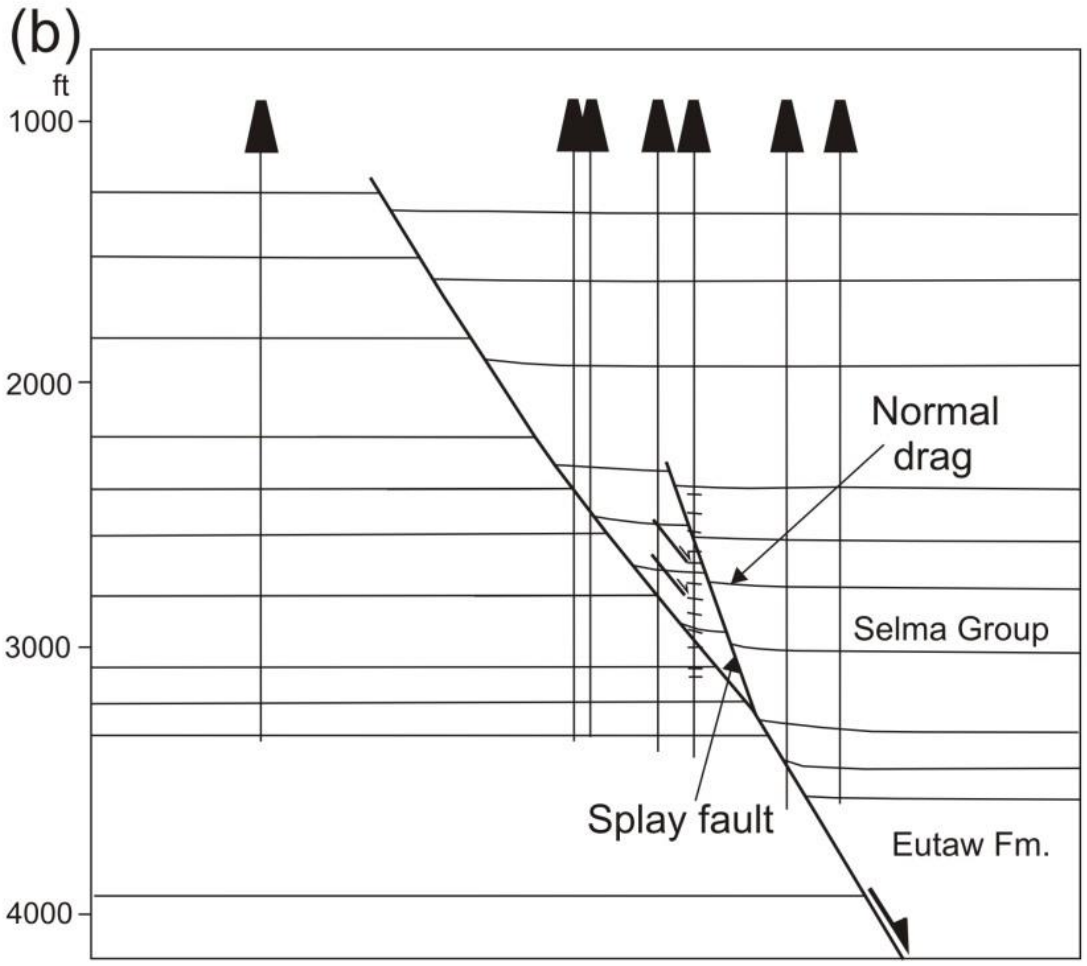

Figure 2.5 (a) – previous page *Section through a fault within the Gullfaks Field (modified from Hesthammer and Fossen, 1998). The section is constructed based on seismic and well data which indicate the presence of large scale normal drag folds within the hangingwall. Folding is accommodated mainly by secondary faults which are sub-parallel and synthetic with the main fault.* ***(b)*** *Section through the Gilbertown Field showing subtle normal drag folds within the hangingwall of an extensional fault. Well data indicates that secondary deformation within the hangingwall deformation zone is dominated by synthetic shear fractures and faults (modified from Jin et al, 2009).*

of the fault, and in some cases, they can accommodate more than 90% of the total displacement (Fossen and Hesthammer, 1998). The stratigraphic interval affected by normal drag folding consists of a heterogeneous deltaic sequence of interbedded sandstones, siltstones and shales of the Jurassic

Brent Group. Individual lithological formations within the Brent Group do not display significant down fault-dip variation of drag amplitude (Fossen and Hesthammer, 1998), hence it is reasonable to assume that the Brent Group sequence behaves as a large coherent mechanical unit. The Brent Group represents the uppermost part of the pre-faulting sequence, hence the sequence was close to the depositional surface and was most likely relatively unconsolidated at the time of deformation (Hesthammer and Fossen, 1998). Therefore, we assume a relatively small mechanical contrast between the sand and shale beds within the Brent Group, which explains the relatively homogeneous style of deformation within this interval. The deformation is characterized by strain-dependent grain reorganization within the less consolidated Brent Group (Fossen and Hesthammer, 1998). The normal drag folding is accommodated at different scales by granular flow (i.e. ductile deformation), deformation bands which are sub-parallel to the main faults and secondary synthetic faults which splay upward from the major fault within the likely more competent and more consolidated sandstones of the underlying Statfjord Formation (Hesthammer and Fossen, 1998; Hesthammer and Fossen, 2001). Since there seems no correlation between drag fold amplitude and amount of displacement, it is suggested that the folding occurred prior to faulting as a "process zone" ahead of a propagating tip (Hesthammer and Fossen, 1998). However, because the normal drag folding seems to occur primarily within the faulted domino-blocks which suffered significant rotation (ca. 30-40°), it is very likely that folding developed also as a result of internal block deformation associated with the progressive rotation of the fault blocks, which may have continued after the breaching of the monocline (***Figure 2.5a***).

Gilbertown Field, Alabama (Pashin et al., 1998; Jin et al., 1999; Jin et al., 2009)

The Gilbertown Field (Alabama, USA) is located on the northern rim of the Gulf Coast basin and produces oil from a normal-faulted structural trap within the Upper Cretaceous Eutaw glauconitic sandstone formation and Selma chalk (Jin et al, 1999). The structural characterization and production geology of the field has been discussed in detail by Pashin et al. (1998), Jin et al. (1999) and Jin et al. (2009). The Selma Group comprises a ~400 m thick homogenous sequence of chalk and marl which thickens within the graben area of the Gilbertown Field fault system, indicating its

syn-faulting deposition. The normal faults display a shallower dip within the chalk formation (ca 45°) than at depth (ca 60°), a possible consequence of compaction or fault refraction (change in dip) as the fault passes from one lithology to the next (***Figure 2.1d***). Well data indicates that the Selma chalk is productive within the hangingwall side, in the proximity of the main faults, where it is intensely fractured (Jin et al., 1999). Dipmeter and fracture identification logs together with structural area-balance modelling indicate that the faults are characterized by pronounced normal drag folds within the hangingwall with beds reaching ca 40° in dip in the immediate proximity of the fault (Jin et al., 2009) (***Figure 2.5b***). Meanwhile the footwall side shows little or no evidence of normal drag folding (***Figure 2.5b***). All the oil from Selma chalk is produced from the fractured and faulted area within the drag zone (Jin et al., 1999). Well data indicate that most of the secondary, sub-seismic scale faults within the hangingwall are synthetic and sub-parallel to the main fault (***Figure 2.5b***). This suggests that folding in the hangingwall is mainly accommodated by a synthetic simple shear type of deformation, similar to the Gullfaks example. It is also very possible that the convex toward the hangingwall bend in the fault plane influences the localization and intensity of fracturing within the hangingwall.

Outcrop examples of faulted shale-sandstone sequences

Figure 2.6 shows the main deformation patterns associated with displacement on similar, syn-sedimentary normal faults within an interbedded shale-sandstone sequence from outcrops. ***Figure 2.6a*** shows the style of deformation related to seismic-scale normal faulting within an interbedded sequence of moderately to less consolidated deltaic sandstones and shales, from Frechen coal mine, Germany (Weber et al., 1978). This was the location where the concept of shale smear has been developed for explaining the sealing behaviour of faults which juxtapose porous-permeable lithologies (Weber et al., 1978; Lehner and Pilaar, 1997). We can observe that the smearing of the shale is associated with normal drag folding of the layers (***Figure 2.6a***). The faults from Gullfaks are also thought to develop a similar impermeable seal membrane by ductile shale smearing (Yielding et al., 1999). In the outcrop example from ***Figure 2.6a***, we observe that the thickness of the smeared shale or the sands entrained within the fault zone varies substantially as it is faulted primarily by

small faults which are synthetic and sub-parallel to the main fault (primary Riedel structures as described by Lehner and Pilaar, 1997). The flexure and thinning of the beds in the proximity of the faults is accommodated mainly by the secondary faults which are synthetic to the main fault. Lehner and Pilaar (1997) observed that these synthetic faults are usually associated with a conjugate pair (secondary Riedel structures), which are antithetic to the main fault, but that the synthetic faults predominate at least in the early phase of deformation. The predominance of synthetic faults has been widely observed within poorly consolidated sandstone and shales, which are characterized by a low mechanical competence contrast, as it is the case for the faults outcropping in the Baram Delta Province from Brunei in ***Figure 2.6b*** and described by Burhannudinnur and Morley (1997).In all these cases previously described, the normal drag-like folds develop within a mechanically incompetent lithological sequence, with low mechanical contrast between the dominant lithological units. In all cases deformation occurred at low confining pressures, close to the free surface. The folding of the beds and smearing of the shale is accommodated by secondary faults and shear fractures which are dominantly synthetic and sub-parallel to the main fault.

Figure 2.6 – next page (a) *Sketch of main deformation structures associated with a syn-sedimentary normal fault within an interbedded and moderately consolidated sandstone-shale sequence from the Frechen coal mine, Germany (modified after Weber et al., 1978). No scale provided, but the faults from Frechen mine can reach throws of up to 100 m. The shear zone incorporates smeared shale from the adjacent beds which display normal drag folds especially within the hangingwall;* ***(b)*** *Dragging of a shale bed in the footwall of a fault in poorly consolidated shales and sandstones in the Baram Delta Province, Brunei (after Burhannudinnur and Morley, 1997). The localized shearing can be the result of intense strain within a relay zone.*

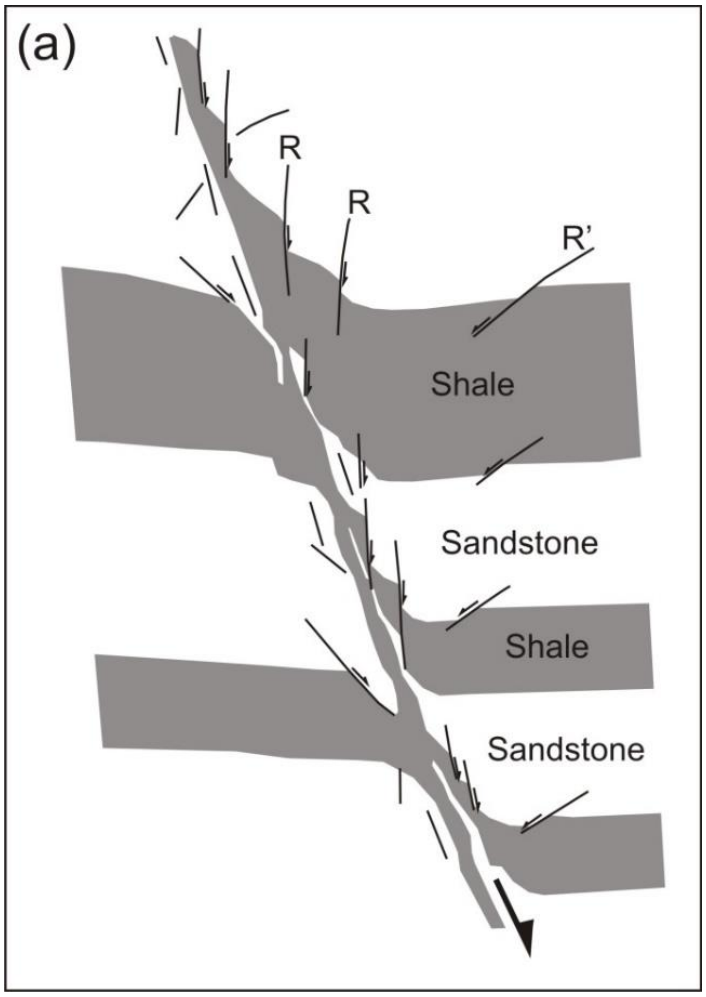
(a)
R
R
R'
Shale
Sandstone
Shale
Sandstone

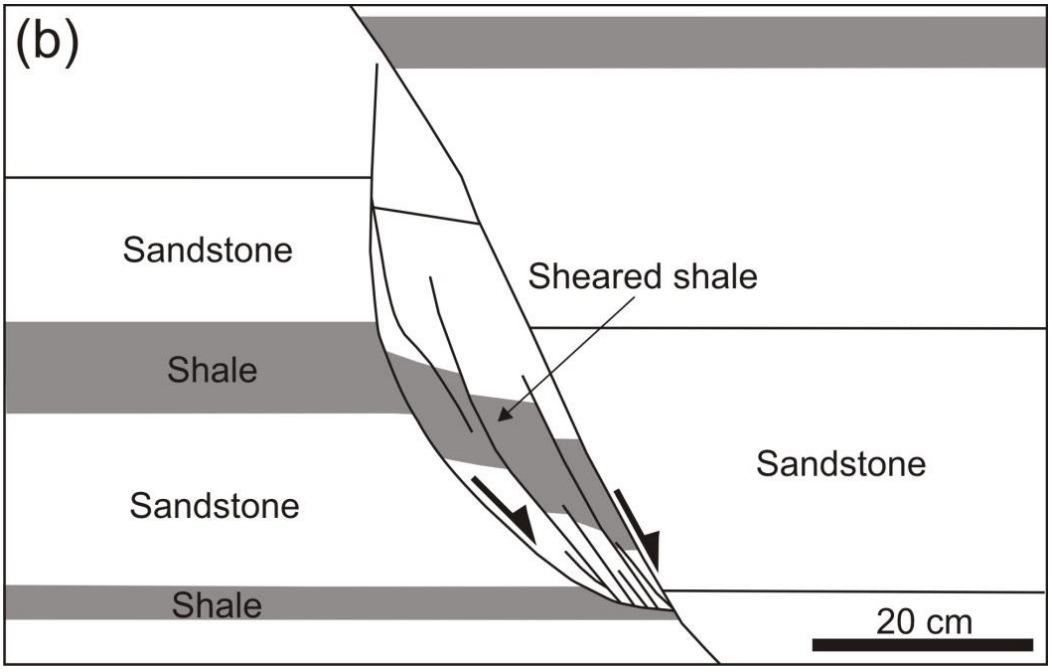
(b)
Sandstone
Sheared shale
Shale
Sandstone
Sandstone
Shale
20 cm

2.4.2. Normal fault-related folds developed within predominantly competent lithologies with low mechanical competency contrast

Lake Thingvallavatn, SW Iceland (Grant and Kattenhorn, 2004; Ferrill et al., 2017)

The normal faults at Lake Thingvallavatn, in the SW part of the Icelandic volcanic rift zone, develop steep, vertical/sub-vertical fault dips at the surface and are characterized by mixed mode displacements, with a significant component of opening (Gudmundsson, 1988; Grant and Kattenhorn, 2004). The deformed sequence consists of homogeneous basalt flows, but at depth it is possible that the lavas are interbedded with mechanically weaker fluvial sediments (Ferrill et al, 2017). The surface breaking faults/ fractures are associated in some cases with relatively gently dipping monoclinal folds (Grant and Kattenhorn, 2004; Ferrill et al., 2017) (***Figure 2.7a***). The monoclines developed as a result of propagation toward the surface of deeper located normal faults (Grant and Kattenhorn, 2004). The dip of the monocline limbs varies between 4-16° and the fold width is relatively narrow, from 10-20 m to 150 m (Grant and Kattenhorn, 2004). Therefore, the folding is most likely to be below the resolution of conventional reflection seismic data. The monoclines are breached by large, en-echelon tension fractures, located in clusters predominantly at the crest of the monocline (Grant and Kattenhorn, 2004) (***Figure 2.7b***). Some of the faults and fractures exploit pre-existing columnar joints within the basalts. With increasing displacement, the fractures increase in width and length, link and become reactivated in shear. The deformation accommodating the rotation of the monoclinal fold is concentrated within the crest of the fold, where open fractures developed as a result of outer arc extension, corresponding with a tangential longitudinal strain model (***Figure 2.7b***). It is expected that mechanically strong and stiff layers, such as the basalts, will fail in tension at low confining pressure, while weaker lithologies, such as the sands and shales from the previous examples, will fail in shear (Schöpfer et al., 2007). But we can observe that not only is the type of failure different, but also the distribution of strain. The normal fault-related folds in basalts are accommodated by tensile fractures located mainly at the crest of the fold, which are rotated with continuous flexure of the surface beds and some of them reactivated in shear in a direction antithetic to the main fault.

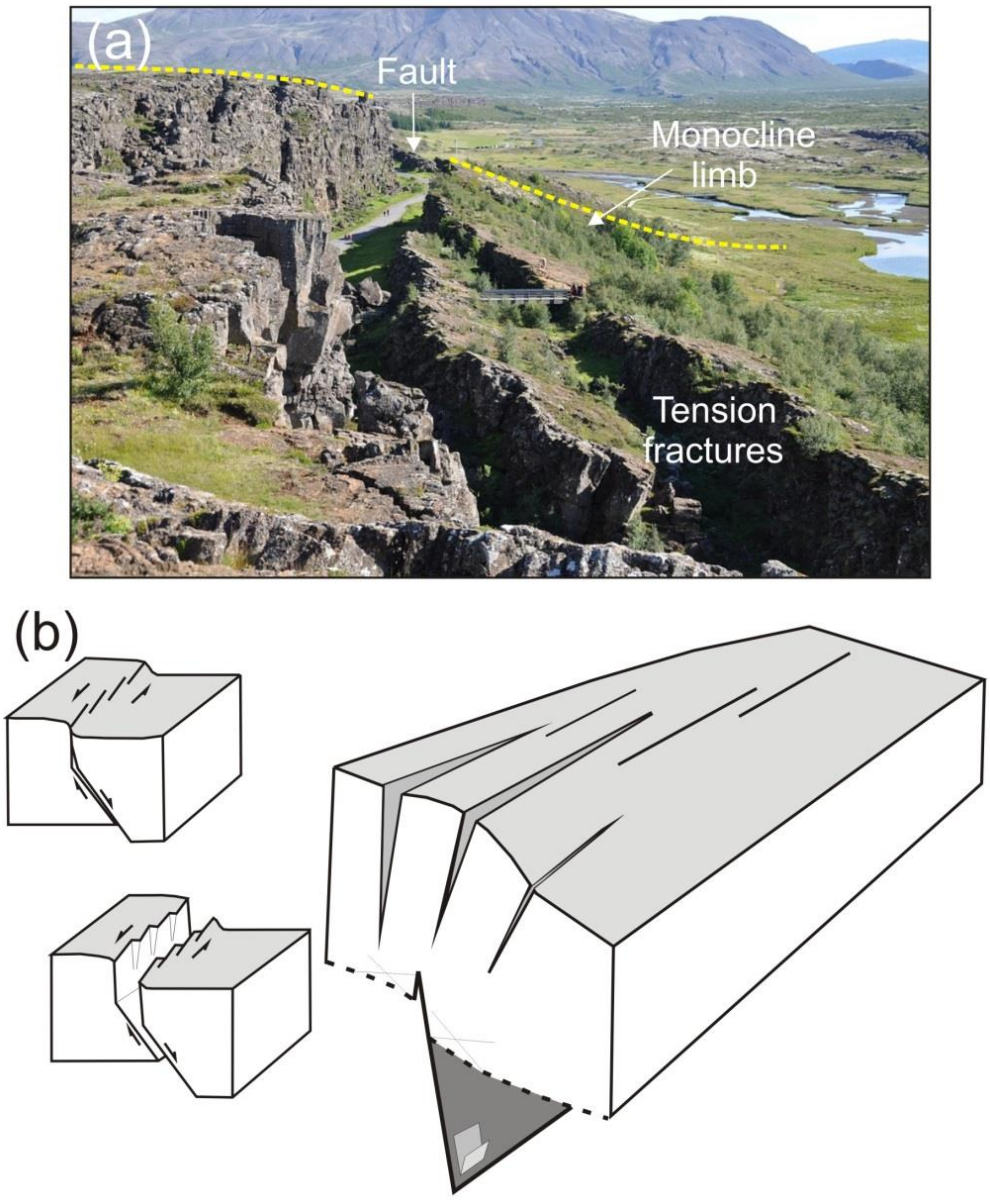

Figure 2.7 (a) *Monoclinal fold associated with normal faults within basalts from Lake Thingvallavatn, SW Iceland (photo from https://pixabay.com/en/iceland-pingvellir-268144/).* ***(b)*** *Model for the formation of the monoclines and related fractures in basalts (modified from Grant and Kattenhorn, 2004). A component of oblique slip on the buried faults determines formation of en-echelon tensile fractures above the crest of the monocline fold. The fracture characteristics correspond to a tangential longitudinal strain folding (Ramsay, 1967). With increasing strain, the steep fractures link with the buried fault resulting in breaching of the monocline.*

2.4.3. Normal fault-related folding within mechanical units with high competency contrast

Kilve, Somerset (Long, 2011)

Normal faults cut through an interbedded limestone shale sequence of Lower Jurassic age which crops out on the shoreface and coastal cliffs at Kilve and Lilstock, Somerset, south of the Bristol Channel (Long, 2011). The faults are associated with the Mesozoic development of the Bristol Channel Basin (Peacock and Sanderson, 1999) and post-date the deposition of the Liassic limestone-shale layers. The brittle deformation of the limestone beds indicates that the rocks, especially the limestones, were consolidated at the time of deformation. The competent limestone layers have a thickness ranging from several centimetres to 1 m and the weaker shale from several centimetres to 5 m (Long, 2011). The ratio of mechanically competent to incompetent rocks of the overall thickness is about 1/5 (Putz-Perrier and Sanderson, 2008). The strong mechanical contrast between the layers controls how strain is distributed within the deformation zone surrounding normal faults (Putz-Perrier, 2008; Long, 2011). Folding of the carbonate layers is observed in the vicinity of the upper tip-lines, where thicker ductile shale inhibited the propagation of the faults (***Figure 2.8***). The flexure of the beds is accommodated by ductile flow within the shale, which thins significantly toward the fault and by tensile fracturing in the stiffer limestone layer. The aperture of the veins increases with increasing displacement on the underlying fault (***Figure 2.8b***). Most of the strain within the folded carbonate layers is accommodated within the immediate proximity of the fault (Putz-Perrier and Sanderson, 2008). Increasing flexure of the carbonate layer determines reactivation in shear of the veins, mostly in a direction antithetic to the main fault (***Figure 2.8a***), similar to the structures developed within the monoclinal folds from Lake Thingvallavatn.

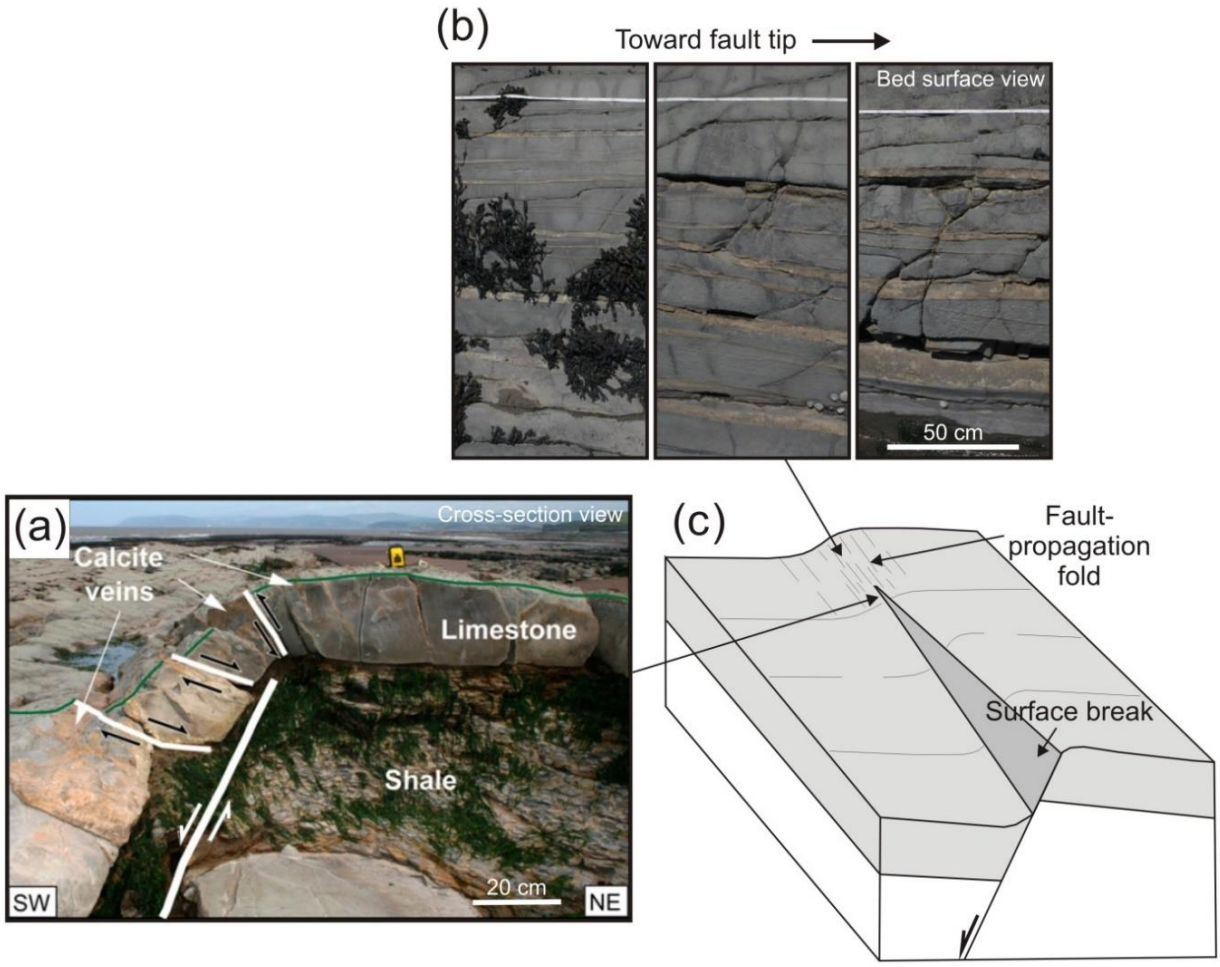

Figure 2.8 (a) *Folding of a limestone layer at the tip of a fault from Lilstock, Somerset (from Long and Imber, 2011). The strain within the limestone layer is accommodated by veins, which are reactivated in antithetic shear as a result of continuous ductile flow within the underlying shale.* ***(b)*** *The aperture of the veins increases toward the fault tip (from Long, 2011).* ***(c)*** *Location of the deformation documented by Long (2011) and Long and Imber (2011) on a diagram showing a monoclinal fold near the tip-line of a normal fault (modified from Walsh and Watterson, 1987).*

Moab Fault, Utah

Moab Fault is part of an extensional fault system associated with salt-related deformation within the Paradox Basin of SE Utah (Doelling, 1988). The fault is more than 40 km long and has a maximum throw of approximately 1000 m (Foxford et al., 1998). Folds adjacent to the Moab fault are well developed in the hangingwall, where the Upper Jurassic, shale-dominated Morrison Formation and

Lower Cretaceous fluvial sandstones, conglomerates and shales of the Cedar Mountain Formation crop out. The beds dip toward the hangingwall and the folds have an amplitude of ca. 70 m and a wavelength usually larger than 200 m. The folds are interpreted to be fault-propagation folds, the upward propagation of the faults being inhibited by the ca 100 m thick smectite-rich shaly interval of Brushy Basin Member, part of the Morrison Formation (Davatzes and Aydin, 2005). The Brushy Basin shales are observed to be sheared and smeared toward the main fault, accommodating the flexure of the beds by ductile deformation (Davatzes and Aydin, 2005).

Several transects across the fault have been realized to document the character and distribution of secondary faulting and fracturing within the Cedar Mountain competent sandstones and conglomerates (for details see *Chapter 3*). The exposures from Waterfall Canyon (***Figure 2.9a***) show some of the characteristic deformation structures observed within the folded sandstones and conglomerates of the Cedar Mountain Formation along the Moab Fault. In this location the total throw is about 270 m (Davatzes and Aydin, 2005) and the fold amplitude is about 80 m measured at the level of Cedar Mountain Formation sandstone layer. We observed that the intensity of the small-scale deformation increases toward the main fault and extends about 200 m into the hangingwall. The strain is accommodated by shear fractures and joints, most of which are antithetic with respect to the main fault. Elsewhere along the fault (in the Blue Hills area and in Bartlett Canyon – for details see *Chapter 3*) antithetic deformation bands are observed to cross-cut their conjugate pairs, which are synthetic to the main fault. The vast majority of the faults or shear fractures have relatively small displacement (several cm) and die out within the underlying mudstones, where deformation is accommodated by plastic flow of the shales (***Figure 2.9g*** and ***2.9e***). The deformation styles indicate that the silica-rich sandstones and conglomerates were well consolidated at the time of deformation, at a burial depth which is believed to have been around 2000 m (Garden et al., 2001). The high mechanical competence contrast between the quartz-rich sandstones and the plastic shales is indicated by the shale fabric which shows flow patterns within the opened fractures formed within the sandstones (***Figure 2.9d***). Bed - parallel slip seems to be localized and influenced by the irregular, channelized geometries of the sandstones and conglomerates.

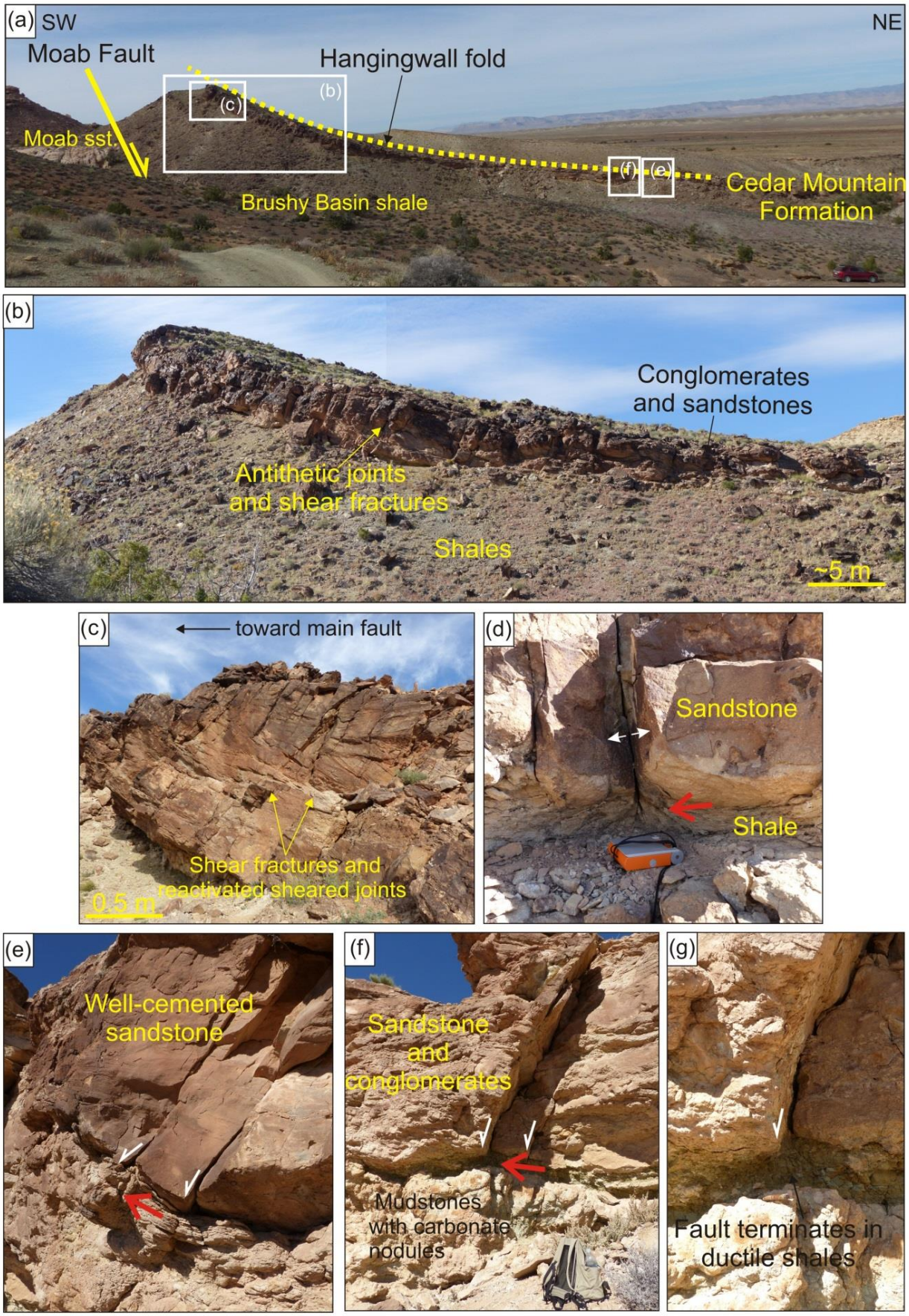
(a)
SW
NE
Moab Fault
Hangingwall fold
(b)
(c)
(f)
(e)
Moab sst.
Brushy Basin shale
Cedar Mountain Formation
(b)
Conglomerates and sandstones
Antithetic joints and shear fractures
Shales
~5 m
(c)
toward main fault
Shear fractures and reactivated sheared joints
0.5 m
(d)
Sandstone
Shale
(e)
Well-cemented sandstone
(f)
Sandstone and conglomerates
Mudstones with carbonate nodules
(g)
Fault terminates in ductile shales

Figure 2.9 – previous page *Deformation structures within the Cedar Mountain Formation within the hangingwall fold of Moab Fault exposed along the Waterfall Canyon. The primary structures within the fold are shear fractures (**b**, **c**, **d**, **e**, **f**, **g**) and joints (**c**, **d**). The high mechanical competence contrast at the time of deformation between the sandstones, conglomerates and shales is indicated by the fabric of the shales, which show flowing within the opened fractures formed within the sandstones **(d)**. The majority of the faults within the competent sandstones and conglomerates terminate in the ductile mudstones, which are deformed plastically (red arrows).*

Slip on irregular bed interfaces favours localized stress concentration, which can result in compressional reactivation of pre-existing joints and shear fractures and localized developing of fracturing coeval with flexural-slip deformation (Cooke and Pollard, 1997) (for details see *Chapter 3*). Hence, deformation in the hangingwall of Moab Fault is highly partitioned by the contrasting mechanical properties of the well-cemented quarzitic-rich sandstone and conglomerate beds of the Cedar Mountain Formation and the interlayered shale beds from the same formation and the smectite-rich shales of Brushy Basin Member.

Big Brushy Canyon, Sierra del Carmen, Texas (Ferrill et al., 2007)

The geometry and the strain characteristics of the Big Brushy Canyon monocline have been discussed in detail by Ferrill et al. (2007). This short synthesis is based on their detailed observations and interpretations. The monocline fold is associated with displacement along a seismic-scale normal fault cutting through a Cretaceous carbonate-dominated sequence. A 36 m thick shale interval of the Del Rio Clay separates the massive Santa Elena limestone from the overlying Buda Formation, which consists of interbedded limestone and shales. At the investigated location, the fault has a maximum displacement of 75 m within the massive Santa Elena Limestone, which dies out upward within the Del Rio Clay. The large vertical displacement gradients are accommodated by intense shearing and thinning of the Del Rio Clay and by folding of the overlying Buda limestone

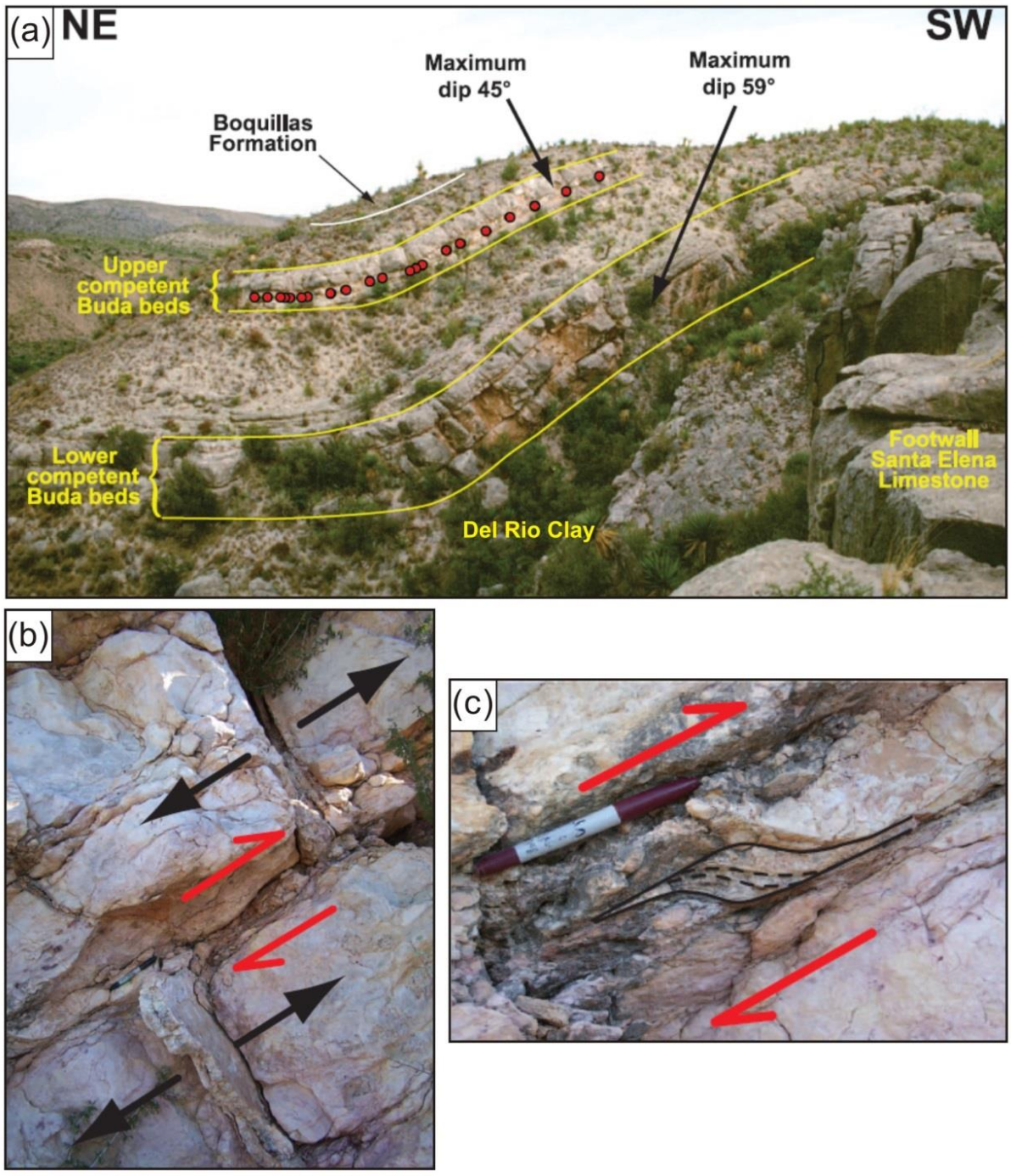

Figure 2.10 (a) *Monoclinal fold associated with a normal fault from the Big Brushy Canyon, Texas (from Ferrill et al, 2007 and Smart et al, 2010).* ***(b)*** *and* ***(c)*** *Folding of the Buda Limestone is accommodated by tensile fractures filled with calcite cement and bed-parallel shear planes which offsets the pre-existing veins (from Ferrill et al., 2007; Smart et al., 2010).*

(***Figure 2.10***). The shale thins progressively with increasing bed dip and is especially thin in the proximity of the footwall edge of the Santa Elena limestone, where it is only about 1 m thick. The limbs of the monoclinal fold reach a dip of 20 to 59°, and the fold has a maximum observed amplitude of ca. 33m. The folding is accommodated within the competent layers of the Buda limestone by tensile fractures, which are oriented parallel to the fault strike / fold axis strike and sub-perpendicular to bedding interface. Offset of calcite-filled veins along bed surfaces indicates a significant component of bed-parallel slip (average shear strain between 0.15 -0.2), consistently distributed along the main bed interfaces (***Figure 2.10b*** and ***2.10c***). These observations are supported by mechanical models which indicate that extension of layered materials causes initiation of tensile fractures and slip on the layer interfaces located above a buried normal fault tip (Cooke and Pollard, 1997). In the case of the monoclinal fold from Big Brushy Canyon, the bed-parallel slip occurs along thin (cm thick) shale intervals between the carbonate beds of the Buda Limestone. These well-defined, planar layer boundaries with high mechanical competence contrast are favourable features for accommodating flexural slip. The increase in fold amplitude favours activation of these mechanically weak layers as slip surfaces, which cut through and offset the veins (Smart et al., 2011). The component of shear-strain parallel to bedding results in less intense brittle deformation within the competent Buda limestone, with no evidence of reactivation in shear of pre-existing tensile fracture (as in the fold example from Kilve) and less development of new secondary fractures and fault zones with increasing fold amplitude (as in the case of Moab fault-related folds).

2.5. Control of mechanical stratigraphy on strain variability

2.5.1. The influence of mechanical competence contrast on strain geometry

Observations of normal fault-related folds developed within various mechanical stratigraphic settings show that the characteristics of strain are highly dependent on the mechanical properties of the layers and the mechanical competence contrast between them. High mechanical competence contrast favours strain partitioning and a style of secondary deformation within the competent beds

which is predominantly antithetic to the main fault, while the incompetent layers deform by plastic flow. If the competent units are layered and have geometrically planar bed boundaries and high mechanical competence contrast, folding is accommodated by a large component of layer-parallel shear strain, which inhibits shear reactivation of precursory tensile fractures. If bed interfaces have irregular geometries (e.g. down-cutting sandstone channels), the slip on these surfaces will generate localized stress concentrations, which can result in localized fracturing/ faulting or reactivation of pre-existing joints. Where mechanical competence contrast is low the strain is influenced by the overall strength of the layers. In cases where we have homogeneous thick, strong layers, folding is accommodated by tangential longitudinal strain (Ramsay, 1967) with fractures localized at the crest of the fold. If the layers are predominantly weak, unconsolidated sediments, the strain within folds is characterized by synthetic simple shear deformation. These observations are supported by analogue modelling results, which show that viscosity contrast is a main controlling factor on the deformation patterns within the normal fault-related folds (***Figure 2.11***) (Withjack and Callaway, 2000). The presence of a thick viscous layer decouples the deformation in the hangingwall and folding is accommodated in the overlying layers by distributed secondary faulting antithetic to the main fault. Also, we observe that the folds formed in materials with strong mechanical competence contrast develop a wider zone of deformation and broader monocline wavelengths (***Figure 2.11b***), than the narrower folds developed in materials with low competence contrast (***Figure 2.11a***). The geometries of the folds are explained by the characteristic strain patterns within the folded competent layers. Large wavelength monoclines accommodate the folding of the layers predominantly by antithetic secondary faulting. This type of deformation associated with rotation of the bed increases the component of pure shear strain, which generates an increase in lengthening in the horizontal direction. This contrasts with the narrower monoclinal folds developed in homogeneous weak lithologies and characterized by a simple shear strain geometry that resulted from the predominance of secondary faults which are synthetic and sub-parallel to the main fault.

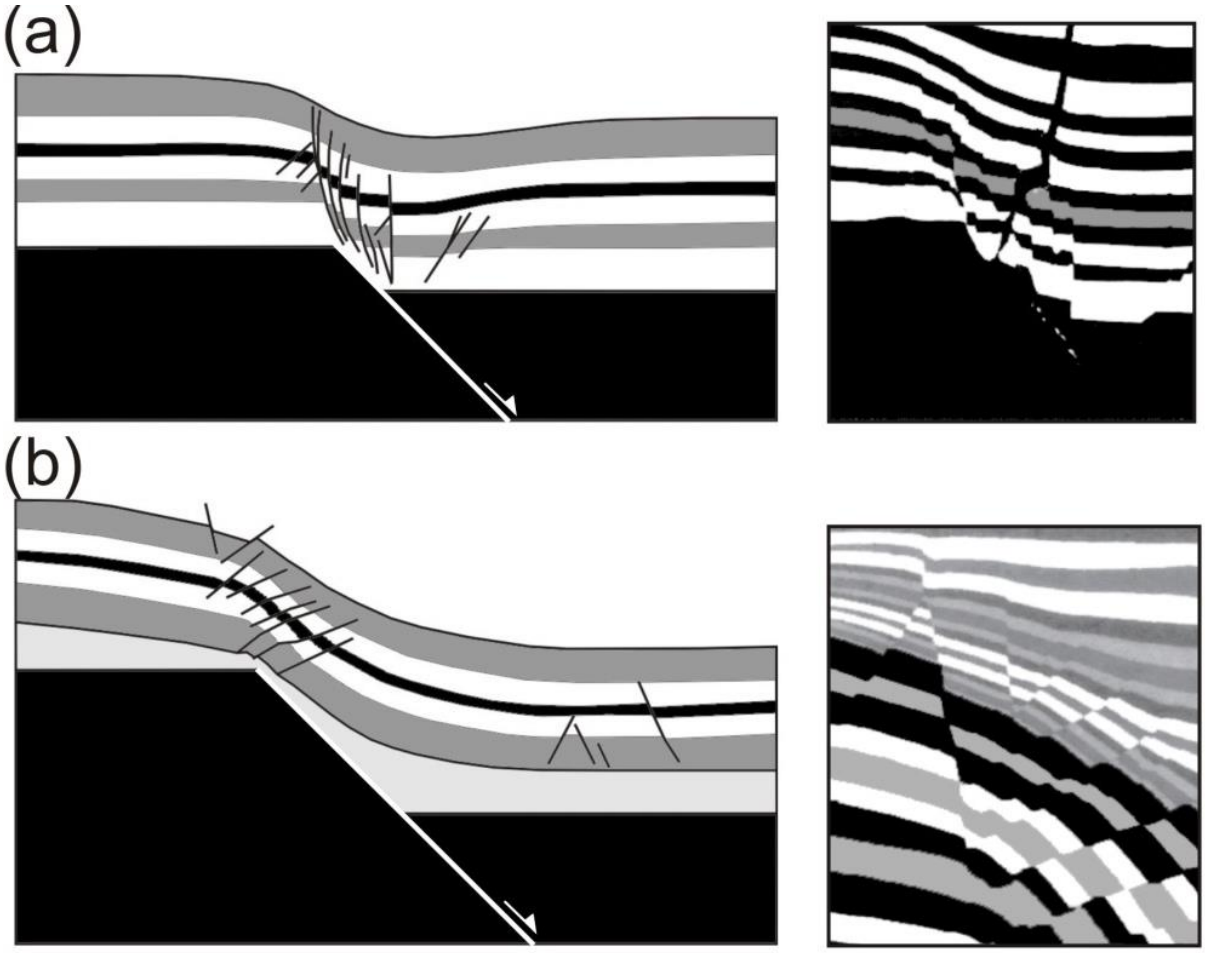

Figure 2.11 *Analogue models of normal fault-propagation folds in wet clay* ***(a)*** *and wet clay and silicone putty* ***(b)*** *(modified from Withjack and Callaway, 2000). The deformation structures accommodating the folding of the clay layer vary significantly for the two cases displayed here (insets in the right-hand side represent a detail view of the models). Although fault displacement is different for the two illustrated models, that does not influence the fold wavelength geometry (which defines the width of the deformation zone) and the deformation style. The weak silicone layer accommodates the displacement on the main fault by ductile flow and decouples the deformation in the overlying clay layer from the main fault. Flexure of the clay layer is accommodated by a series of small antithetic faults, which progressively rotate to shallower dips as the monoclinal limb dip increases. In the model shown in (a), the deformation structures are represented by steeply dipping synthetic normal faults which are hard-linked with the basement fault.*

Many of the secondary antithetic faults developed in the competent layers within the hangingwall fold limbs of the Moab fault display very low dip angles (<30˚) (***Figure 2.12b***) and some of them are almost sub-horizontal (***Figure 2.12b***, for details see *Chapter 3*). A problem with these shallow dipping normal faults is that the component of normal stress acting on the faults would become too large relative to the shear stress, thus inhibiting the normal fault slip (Morris et al., 1996). One likely possibility is that the faults were active in the early stage of folding and have been passively rotated as the limb of the fold became steeper, with the antithetic faults becoming inactive. However, evidence of cross-cutting relationships between the conjugate fault pairs, and steeper bed dips in the hangingwall than the footwall beds of these antithetic faults, corroborated with wider and more intense deformation zone within the hangingwall (***Figure 2.12a***), suggests that the faults were active and contributed to the overall rotation of the fold limb. Previous research work highlighted the importance of the mechanical competence contrast in contributing to the rotation and refraction of the principal stress axes within layered lithologies (Bradshaw and Zoback, 1988). Treagus (1973) showed that the angle of rotation of the principal stress axes in normal fault regime increases with increasing viscosity contrast between layers, with higher rotations in the weaker, ductile layers. That results in shear surfaces which in plastic, overpressured shales can become parallel to bedding (Bradshaw and Zoback, 1988). In a layered sandstone-shale sequence with high mechanical competence contrast which is subjected to normal faulting and folding, the ductile flow within the weak shales induces a component of bed-parallel shearing toward the hinge of the monocline fold (***Figure 2.12b***). Added to the vertical maximum principal stress, this component of bed-parallel shear stress will generate a local (in this case anti-clockwise) rotation of the principal stress axes (Price and Cosgrove, 1990). Therefore, the reorientation of the principal stress, during flexural flow folding, is more favourable for slip conditions on antithetic secondary faults, and less so for their synthetic conjugate pair (***Figure 2.12b***).

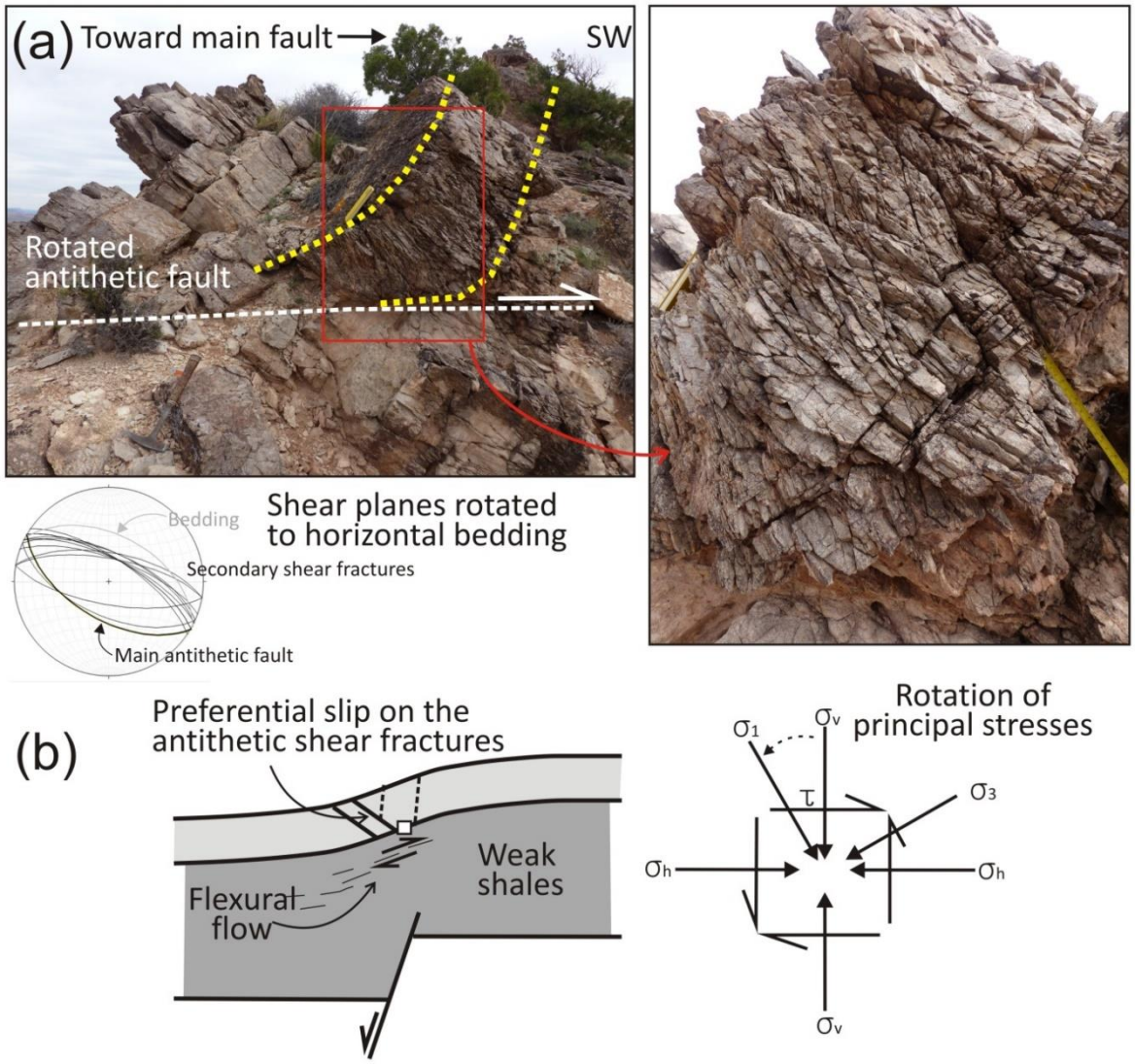

Figure 2.12 (a) *Antithetic shear fractures and normal faults dominate as secondary structures in the hangingwall fold of the Moab Fault. The antithetic fault shown here is almost horizontal and displays strong deformation within its steeper hangingwall;* ***(b)*** *Ductility contrast between the competent Cedar Mountain sandstones and the smectite-rich shales of the Brushy Basin Formation induces a component of shear stress parallel to layering which cause the rotation of the principal stresses. The reorientation of the maximum principal stress favour slip on the rotated, shallower dipping antithetic normal faults.*

2.5.2 Normal fault-propagation folding vs fault dip segmentation

Observations from outcrops and analogue models show that the presence of weak, incompetent lithologies enhances the formation of folds ahead of propagating fault tips (Ferrill et al., 2007; Withjack et al., 1990). Hence, the maximum amplitude that a fold can reach is influenced by the thickness and ductility of the incompetent layer, and also by the thickness and strength of the competent layers (Withjack and Callaway, 2000). For the normal fault-related fold examples with high mechanical competence contrast presented above, the competent layers are subordinate within a predominantly incompetent stratigraphy. The competent/incompetent layer thickness ratio varies from 1/5 in the Jurassic carbonate-shale layer sequence from Somerset to 1/30 for the sandstone-shale sequence from Moab (if we include the shaly overburden at the time of deformation). If the thickness of the competent layer increases, its flexural rigidity is expected to increase, hence the amplitude of the fold is expected to decrease. Because of the contrasting mechanical properties strain partitioning is still expected to occur, however the strain partitioning develops in a substantially different way. ***Figure 2.13*** shows a vertically segmented normal fault within a mechanically heterogeneous sedimentary sequence from Gulf of Aqaba, in Sinai, which was described by Aydin and Eyal (2002). They observed that propagation of the main fault is inhibited by the incompetent shales of the Ora Formation, and another overstepping segment develops in the hangingwall, leading to intense smearing of the shale within this extensional dip relay zone. Some folding and associated fold-related structures are observed within the overlying carbonates layers.

In ***Figure 2.14*** we plot the thickness of the competent layers *vs* thickness of the incompetent layers for several normal fault zones within mechanically heterogeneous stratigraphic sequences from previously published data. We observe that releasing vertical oversteps tend to develop in stratigraphic sequences where the ratio of competent to incompetent layers is 1 or larger than 1, while dominant fault-propagation folding occurs for consistently smaller values (around 0.2). This seems very reasonable, if we consider that in the case of fault-propagation folding the deformation of the competent layer is controlled by the deformation of the dominant incompetent layers and in the case of vertical segmentation the situation is vice-versa (Davatzes and Aydin, 2005).

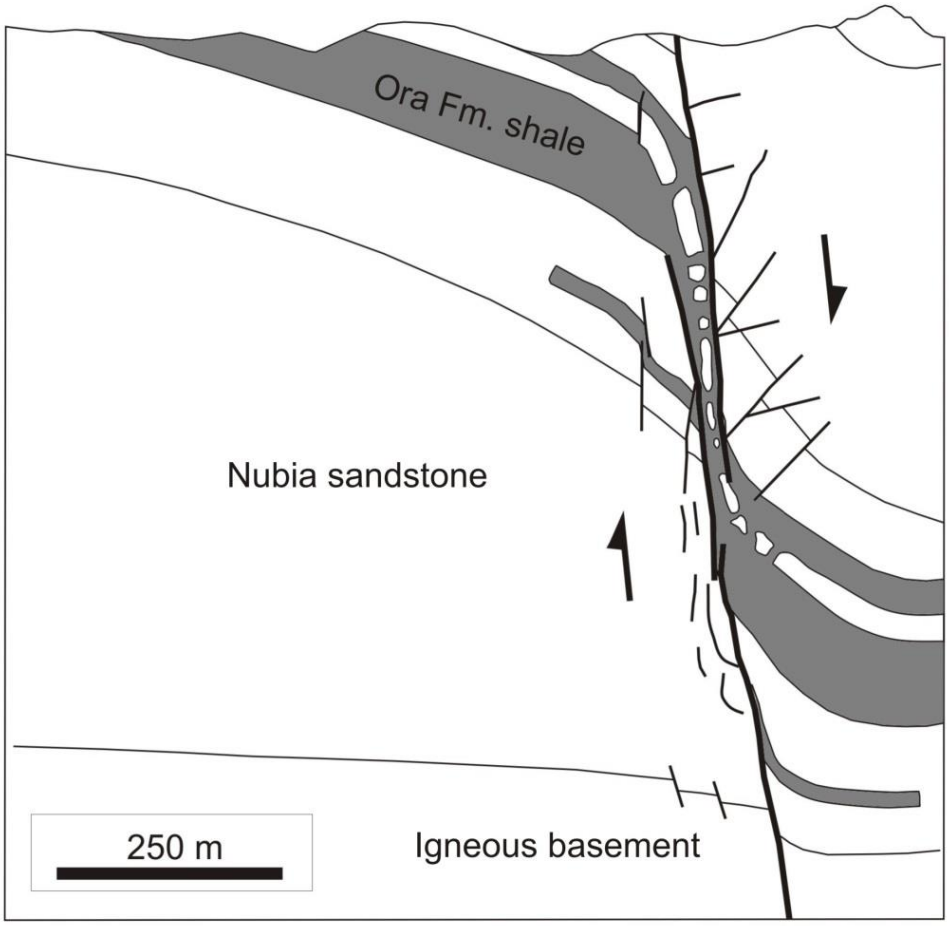

***Figure 2.13**. Fault deformation zone within an interbedded sedimentary sequence from Gulf of Aqaba, Sinai (from Aydin and Eyal, 2002). The presence of a weak and relatively thick shale layer decouples the deformation from the underlying fault and enhances the formation of a vertically segmented fault trace. Formation of a releasing overstep is favoured because the overlying competent carbonates are too thick in respect to the thickness of the shale to be simply folded. In this case the deformation of the incompetent unit is compliant with the deformation in the competent layers. However, we can observe that a thinner carbonate layer within the shale unit is highly folded and broken by boudinage. In this case the deformation of the competent layer is compliant with the one in shale.*

Mechanical experiments show that flexure of a thick competent layer above an underlying fault produces increased stress concentration in the syncline hinge of the monoclinal fold (***Figure 2.15a***) (Couples et al., 1999). This stress concentration would favour localized formation of fractures that

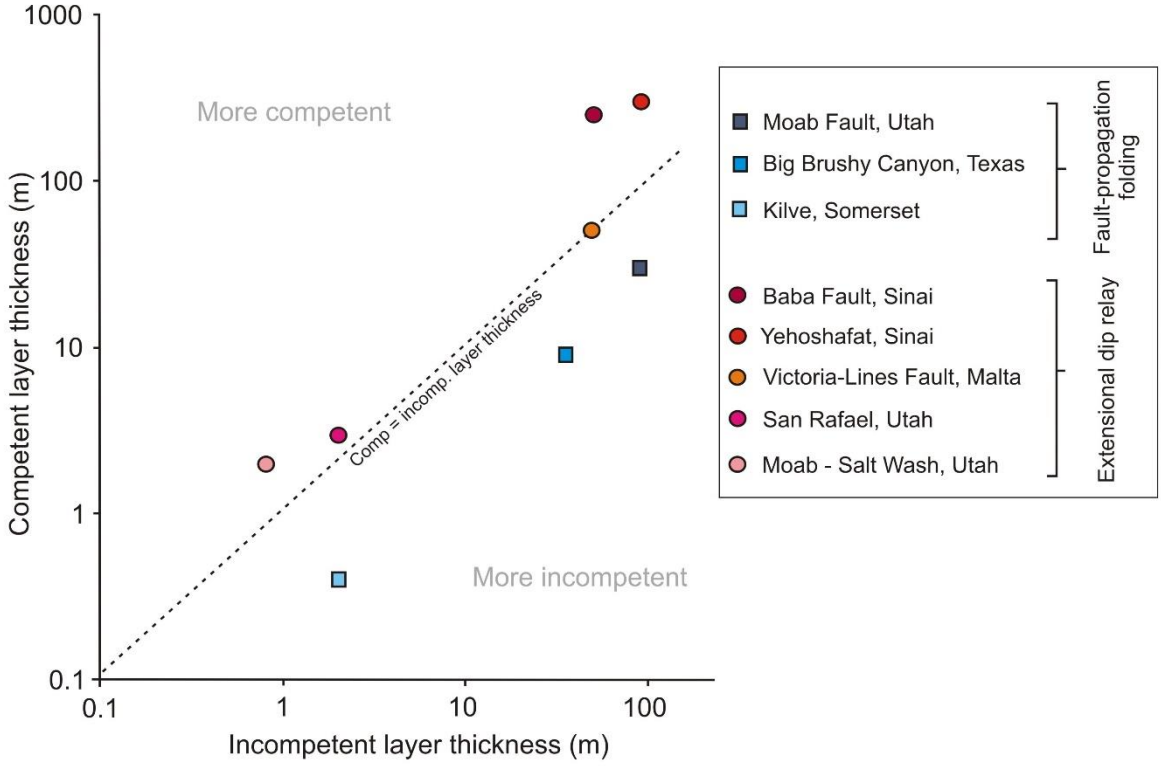

Figure 2.14 *Diagram showing the variation in thickness of competent and incompetent layers for some examples of fault-propagation folds and fault dip extensional stepovers from published literature (data from Ferrill et al., 2007; Faerseth et al., 2006; Aydin and Eyal, 2002; Rykkelid et al., 2002; Davatzes and Aydin, 2005; Long, 2011).*

can lead to the development of an overstepping upper vertical segment. In the situation where the same thickness is subdivided into several competent beds, the bending is accommodated by flexural-slip between the layer planes and stress concentrations are significantly reduced (***Figure 2.15b***).

The published data synthesized in this chapter, provide examples that illustrate the critical role that the mechanical properties of the layered rocks, their thicknesses distribution and the mechanical competence contrast between layers exert on controlling the development of normal fault-related structures, such as folds or extensional dip relays, or on the variability of the strain within the folds. Hence, if we understand better the distribution of strain associated with normal fault-related deformation in relation with the mechanical stratigraphic conditions, we can potentially better explain the variability of the internal structure and sealing capabilities of normal fault zones.

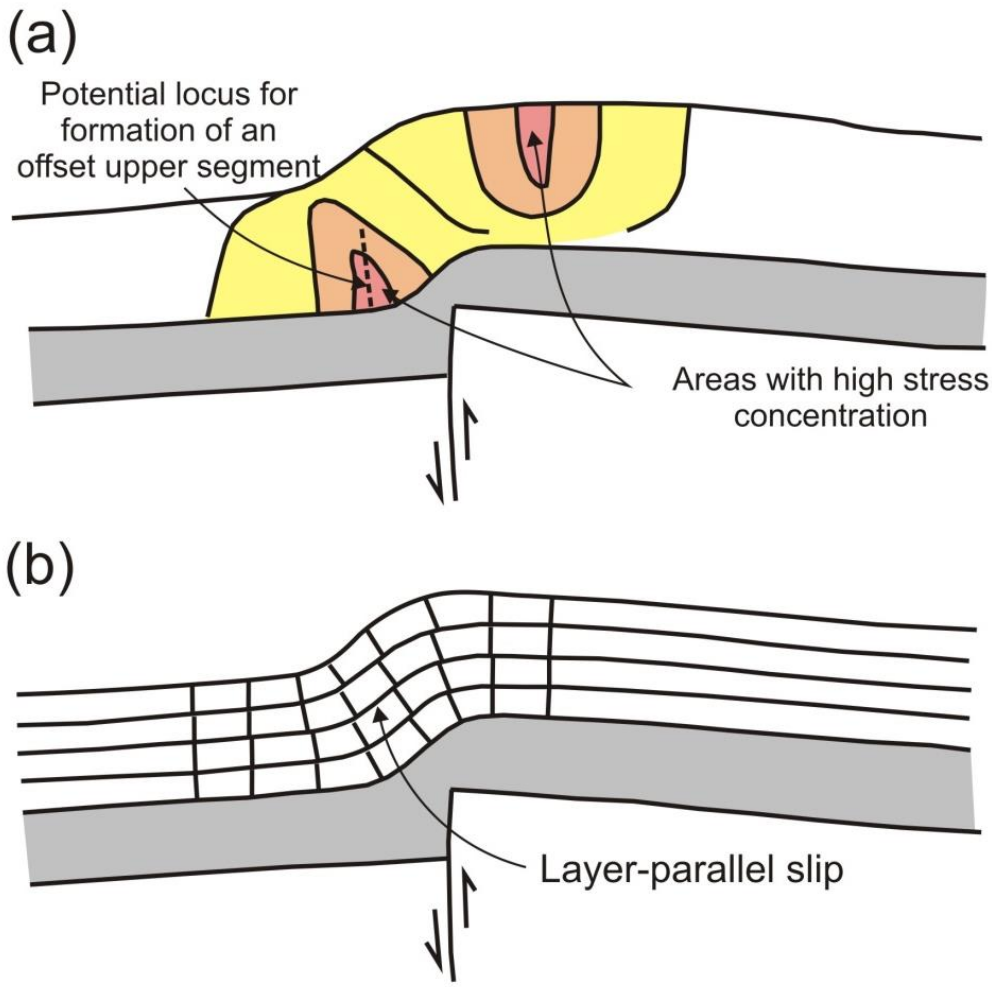

Figure 2.15 *Forced folding experiments of a single limestone layer* ***(a)*** *and a multi-layer limestone package* ***(b)*** *due to displacement on assembly located underneath (modified from Couples et al, 1998). Note the high stress in the lower area of the monoclinal hinge syncline for the single layer experiment in* ***(a)****, favourable for nucleation of fractures and faults, which may develop in a releasing overstep with the fault located below. Meanwhile, the thin, multi-layered limestones accommodate folding by layer-parallel slip which helps decrease and inhibits the stress localization in the monocline syncline.*

2.6. Conclusions

Our review highlighted the importance of mechanical stratigraphy in controlling the distribution of strain associated with normal fault-related folding.

The folds developed within sedimentary sequences with *low mechanical competence contrast* are defined by:

(i) no or minimum strain partitioning between the interbedded lithologies;

(ii) deformation which is accommodated by secondary faults and shear fractures, dominantly synthetic and sub-parallel to the main fault;

(iii) development of synthetic secondary faults, as a result of an increased coupling between the deformation within the fold and the main fault, as demonstrated by analogue modelling;

The normal fault-related folds developed within sedimentary sequences with *high mechanical competence contrast* are defined by:

(i) highly partitioned strain distribution between the weak shale layers, which deform by ductile flow and the mechanically competent layers which deform in a brittle manner;

(ii) the incompetent shales deform by plastic flow, and as the displacement and folding increases, they thin progressively;

(iii) the brittle deformation within the competent layers is accommodated by tensile fractures or shear fractures, depending on the overburden pressure at the time of deformation;

(iv) with increasing flexure of the beds, the tensile fractures are reactivated in shear, which is usually in a direction antithetic to the main fault and antithetic shear fractures are predominant and cross-cut less developed synthetic secondary shear fractures;

(v) high mechanical competence contrast favours slip parallel to bedding and pre-existing bed geometries play an important role in controlling the localization or continuity of bed-parallel slip surfaces; irregular channel-like bed geometries are characterized by

localized bed-parallel slip, and induced fracturing or reactivation of pre-existing structures as a result of shearing on geometrically irregular bed surfaces;

(vi) if the thickness of the competent layer increases, the folding amplitude decreases and a releasing fault dip segmentation is likely to develop.

| Chapter 3 |

Hangingwall deformation within a seismic-scale normal fault-related fold: a case study from Moab Fault, Utah

Abstract

The strain patterns associated with folding under compressional or extensional faulting stress conditions are highly influenced by the mechanical layering of the sedimentary rocks. Here we investigate the characteristics of small scale faulting and fracturing which accommodates large, seismic-scale normal fault-related folding along the Moab fault, Utah. In the four analysed transects across hangingwall "normal drag"-like folds we observed that the mechanical properties and the bed geometries of the fluvial sandstone-shale sequence of the Cedar Mountain Formation influence the deformation styles and the strain characteristics within the fold. The extensional strain within the hangingwall fold limb is accommodated, depending on the lithologies and local stress conditions, by shear fractures, deformation bands, bed-parallel slip surfaces, and by bed-perpendicular and sub-horizontal tensile fractures. Most of the secondary faults are antithetic with respect to the main fault. These dominantly antithetic faults display a combination of dip-slip and strike-slip displacement on two distinct sets of faults to accommodate along strike variation in the fold amplitude. Bed-parallel slip surfaces occur along the interfaces between competent sandstone beds or within less consolidated lithologies. The irregular geometry of the channelized sandstone beds can determine the "locking" of the slip, causing possible reactivation of pre-existing structures. Also, the development of sub-horizontal tensile fracture networks in the proximity of the brittle faults suggests that faulting contributes to the generation of overpressure and hydrofracturing within confined shale layers. This study highlights the influence that the mechanical stratigraphy and the local heterogeneities in the lithology have on the variability and complexity of deformation associated with normal fault-related folding.

3.1. Introduction

The examples of normal fault-related folds described in the previous chapter (*Chapter 2*) suggest that the strain patterns associated with folding are highly dependent on the mechanical stratigraphy and the confining pressure conditions at the time of deformation. The Moab fault, in SE Utah, provides an exceptional location to study the characteristics of secondary deformation in relation to large-scale normal fault-related folding within a mechanically heterogeneous stratigraphic sequence (Foxford et al., 1996). Much of the previous research has focused on the general structural characteristics of the Moab fault zone (Foxford et al, 1996; Foxford et al, 1998), placing a particular emphasis on the small-scale deformation associated with cataclasis or grain reorganization within the porous and permeable sandstones outcropping especially within the footwall of the Moab fault (Fossen et al, 2005; Schueller et al, 2013). Other papers have described the overall fault zone structure and its implications for the sealing capacity of normal faults (Foxford et al., 1998; Davatzes and Aydin, 2005). Relatively few studies have been focused on a more detailed characterization of the brittle strains associated with normal drag folding developed along the north-western segments of the Moab fault (Berg and Skar, 2005). The folded layers consist of highly heterogeneous fluvial deposits comprising channelized sandstones and conglomerates with different degrees of cementation, and interbedded with overbank siltstones and mudstones. From *Chapter 2,* we might expect these sedimentary layers to display evidence that their mechanical properties played an important role in controlling the deformation mechanisms and strain variability within these hangingwall folds.

The aim of this study is to analyse how macroscopically ductile strain – specifically, "normal drag folding" - is accommodated within a mechanically heterogeneous sandstone-shale sequence surrounding a well-exposed, seismic-scale normal fault array. Specifically, we investigate the variability of strain distribution and deformation mechanisms in relation to the mechanical properties of the layered stratigraphy and in relation to the geometry of the fault. The permeability properties of a normal fault zone are directly influenced by the characteristics and distribution of secondary deformation related to the process of faulting within heterogeneous sedimentary layers (Davatzes and Aydin, 2005; Childs et al., 2007). Understanding the relationship between the mechanical stratigraphic

conditions and the strain variability within normal fault-related folds is important for understanding the sub-seismic scale structure of normal fault zones and their ability to enhance or impede cross-fault fluid flow.

3.2. Geological setting

The Moab fault is part of an extensional fault system associated with salt-related deformation within the Paradox Basin of SE Utah (Doelling, 1988). The fault is oriented NW-SE along the continuity of the Moab-Spanish Valley salt wall (Doelling, 2001) and experienced several episodes of activity related to salt movements (Doelling, 2001). The deformation episode that affected the study area is probably associated to the Laramide compression and uplift event during Late Cretaceous-Early Tertiary times which triggered salt migration and extensional faulting of the overburden (Foxford et al., 1996; Trudgill, 2011). The Moab fault has a length of more than 40 km and a maximum throw of approximately 1000 m in the vicinity of the town of Moab (Utah), offsetting clastic sediments from Pennsylvanian to Cretaceous age (Foxford et al., 1998) (***Figure 3.1***). The fault displacement decreases northwest-ward within the Blue Hills and Tenmile Wash area, where the main fault splays out into several segments and where the throw on the fault transfers laterally into monoclinal folds (***Figure 3.1*** and ***Figure 3.2***). As the throw increases south-eastward, the monocline is breached giving rise to normal drag-like folds within the hangingwall of the fault, where Upper Jurassic shale-dominated Morrison Formation and Lower Cretaceous fluvial sediments of the Cedar Mountain Formation crop out (***Figure 3.1***). The folds have limbs dipping sub-parallel to the relative slip direction on the fault, with the largest dips locally around 60° in the immediate proximity of the main fault trace. The fold limbs dip generally in a NE direction with variable wavelengths, usually up to several hundreds of meters, before reaching the regional dip which is about 5°, in a direction toward the Courthouse rim syncline axis (***Figure 3.1***). The folds are interpreted to be normal fault-propagation folds, with the upward propagation of the faults being inhibited by the shales within the Brushy Basin Member, of the Morrison Formation (Davatzes and Aydin, 2005). The Brushy Basin shales are observed to be sheared

and smeared toward the main fault, accommodating the flexure of the beds by ductile deformation (Davatzes and Aydin, 2005). In the next section we describe in more detail the stratigraphy within the study area.

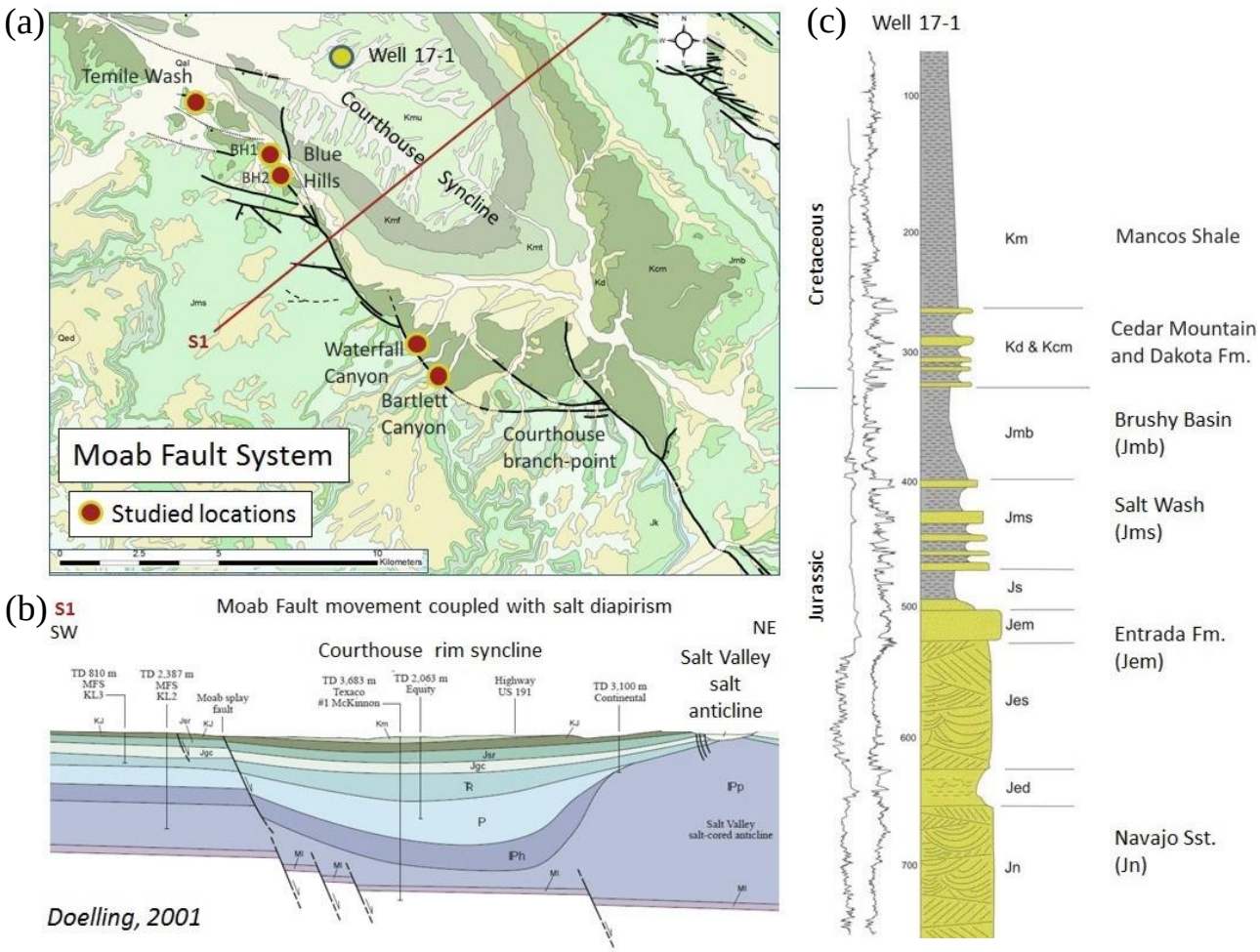

Figure 3.1 (a) *Geological map of the area comprising the north-western splay segments of the Moab fault with the locations of the studied outcrops (map from Utah Geological Survey).* ***(b)*** *Regional section across the Moab fault the Courthouse syncline and the Salt Valley anticline (from Doelling, 2001).* ***(c)*** *Well within the Courthouse syncline (see location in (a)) showing the litho-stratigraphy within the study area (Data from Utah Geological Survey).*

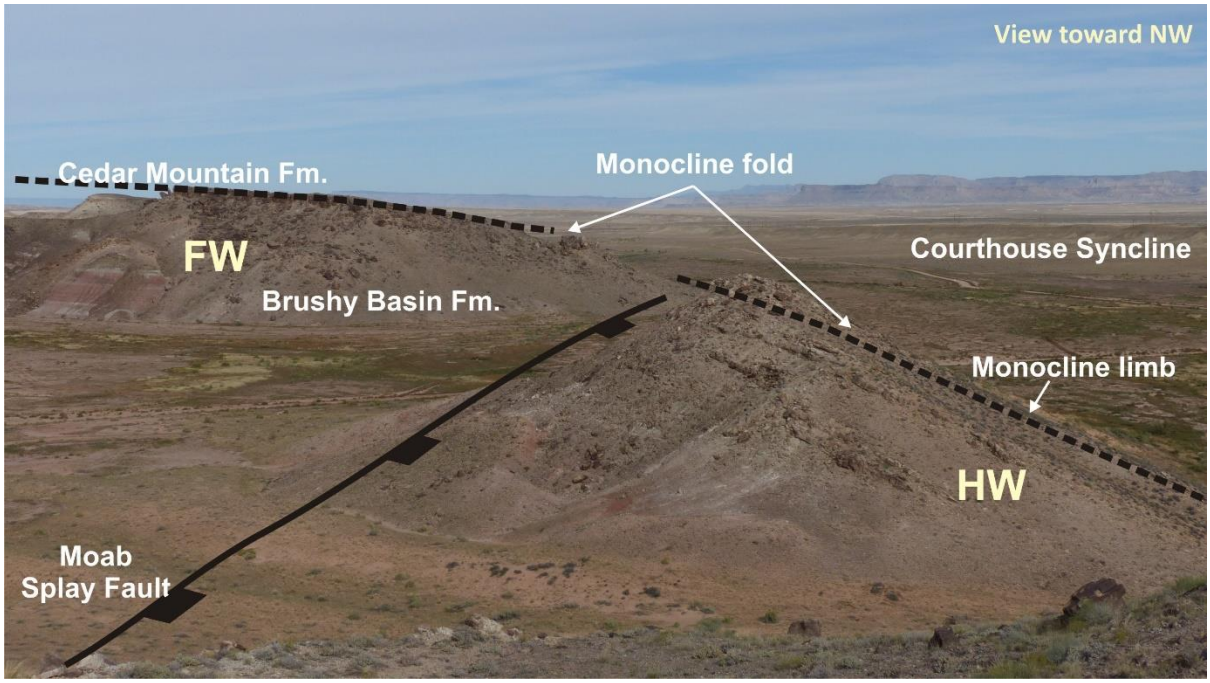

Figure 3.2 *Monoclinal fold at the NW tip of the Moab fault segment in the Blue Hills area (view toward NW). The beds in the footwall side of the fault dip very gently toward N-NE while in the hangingwall side the monoclinal fold limb dips more steeply toward NE. The height of the hill in the foreground (the hangingwall side) is more than 30 m above the elevation of the surrounding flat area. The hill in the background (the footwall) is over 50 m above the surrounding elevation.*

3.3. Stratigraphic framework

The Moab fault offsets a thick sequence comprising Carboniferous to Cretaceous sediments. Our study focuses on the north-western part of the Moab fault array where the throw decreases to less than 300 m and where, at the topographic level, the fault juxtaposes lithological formations of the Upper Jurassic to Cretaceous interval. Hence, in this short stratigraphic description we present only the formations which crop out in the analysed area that are the subject of this study. Along the north-western segment traces, the fault juxtaposes lithologies with contrasting mechanical properties. Within the footwall of the Moab fault the stratigraphy encompasses quartz-rich aeolian sandstones of the Late Jurassic Navajo (ca 50 m thick) and Entrada Formation (ca 150 m thick) (***Figure 3.1c***), which comprise three main members: Dewey Bridge, Slickrock and Moab (Foxford et al., 1996). This homogeneous quartz-arenite sandstone-dominated sequence, with a very high net-to-gross ratio can be

defined as a mechanically competent unit. The sandstones are covered by a shale-dominated interbedded sequence of shale and sandstones comprising the Late Jurassic Morrison Formation, the Cedar Mountain Formation (Lower Cretaceous), the Dakota Formation and the Mancos Shale (Cretaceous), which crop out in the hangingwall of the fault (***Figure 3.1***). The mechanical properties of this shale dominated heterogeneous sequence are very different from the underlying aeolian sandstones, which is reflected in the contrasting deformation styles within the footwall and the hangingwall side of the fault (Berg and Skar, 2005). Our analysis focuses on the deformation characteristics within the folded Cedar Mountain Fm. The Cedar Mountain Formation comprises approximately 5 m thick fluvial channels of sandstones and conglomerates with chert pebbles, interbedded within overbank siltstones and mudstones layers that in some places contain carbonate nodules. The Cedar Mountain Formation overlies the Brushy Basin Member which consists of ca. 100 m thick shale-dominated sedimentary rocks with shales that are rich in swelling clays (e.g. smectite) that cause this unit to behave as an incompetent layer (Davatzes and Aydin, 2005). This shale interval is thought to be responsible for impeding the propagation of the fault segments. The shales are observed to be sheared and smeared toward the main fault, accommodating the flexure of the beds by plastic deformation (Davatzes and Aydin, 2005). The underlying Salt Wash Member, part of the same Morrison Formation comprises interbedded mudstones, siltstones and sandstones. Overall, in the hangingwall sections from the study area, the stratigraphy is very heterogeneous, with fluvial channel sandstones and conglomerates alternating with interbeds of shales of the Cedar Mountain Formation. The mechanical heterogeneity of this sedimentary sequence is complicated also by the fact that the sandstone or the conglomerate layers suffered diagenetic processes which caused different degrees of cementation, variably distributed within the same lithological unit. Hence, cementation plays an important role in controlling the mechanical behaviour of the lithological units during faulting and the characteristic deformation processes that occur (Davatzes and Aydin, 2005) (***Figure 3.3***). The main lithologies and the characteristic deformation styles are illustrated in ***Figure 3.4***. Some of the silica-rich sandstones are very well cemented and are characterized by brittle shear fractures and tensile fractures filled with quartz and calcite mineralization. Less cemented sandstones are characterized by deformation bands and tensile fractures, which seem to post-date the cataclastic deformation.

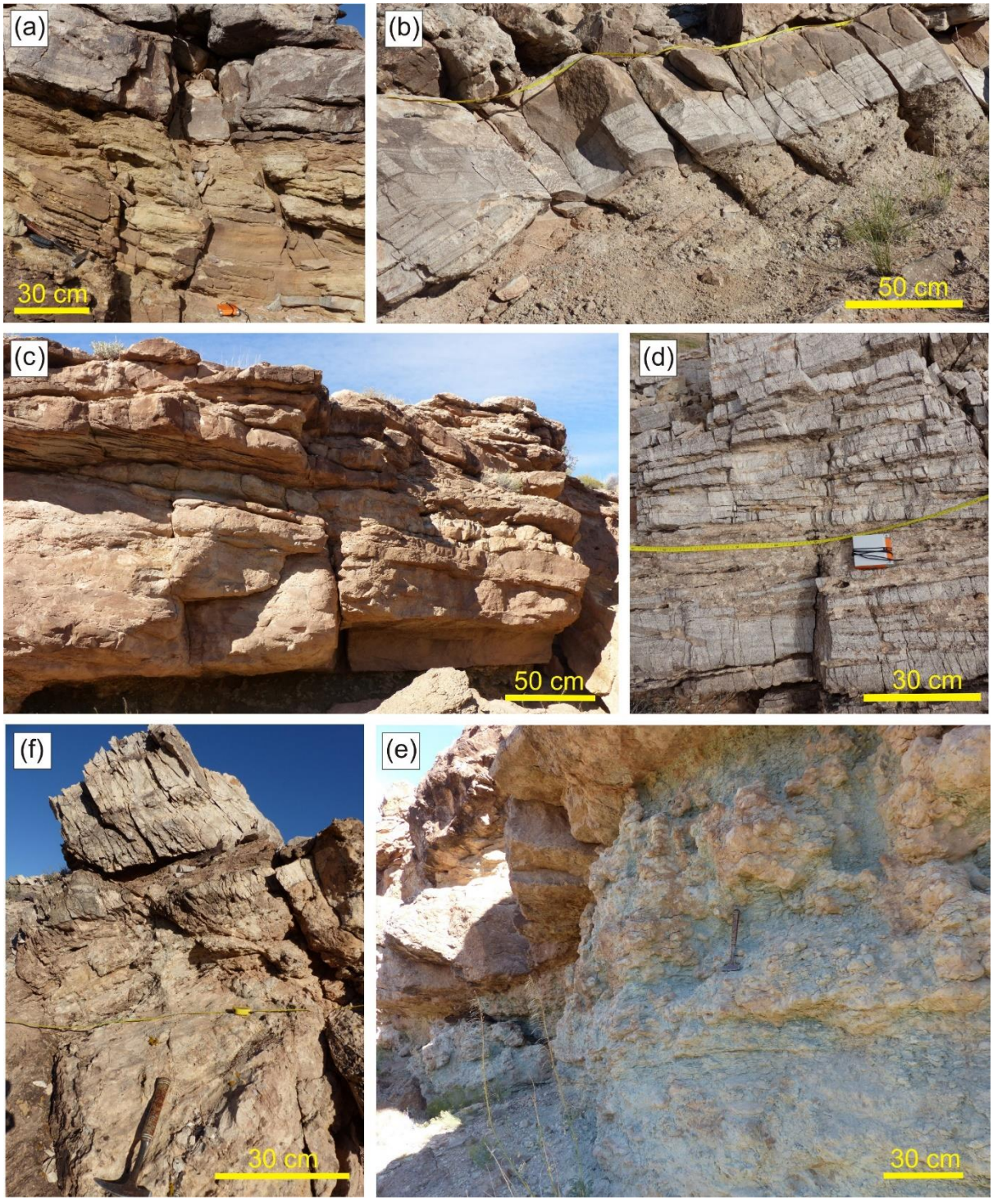
(a)
30 cm
(b)
50 cm
(c)
50 cm
(d)
30 cm
(f)
30 cm
(e)
30 cm

Figure 3.3 - previous page *Main lithologies within the Cedar Mountain Formation which control the style of deformation:* ***(a)*** *highly cemented silica-rich sandstones (top) and thin cross-bedded micro-conglomerates;* ***(b)*** *well cemented conglomerates overlying less consolidated conglomerates;* ***(c)*** *medium consolidated, massive conglomerates and sandstone beds (bottom) overlaid by thin (dm) layers of sandstones and conglomerates;* ***(d)*** *thin bedded (cm), highly cemented quartzitic sandstones and conglomerates;* ***(e)*** *deformation within interbedded highly cemented silica-rich sandstone layers with less cemented sandstone is very heterogeneous: brittle fractures within the highly cemented sandstones on top continue into deformation bands within the less cemented sandstones at the base;* ***(f)*** *grey-green silty mudstone with carbonate nodules (separating the main two conglomerate-sandstone units).*

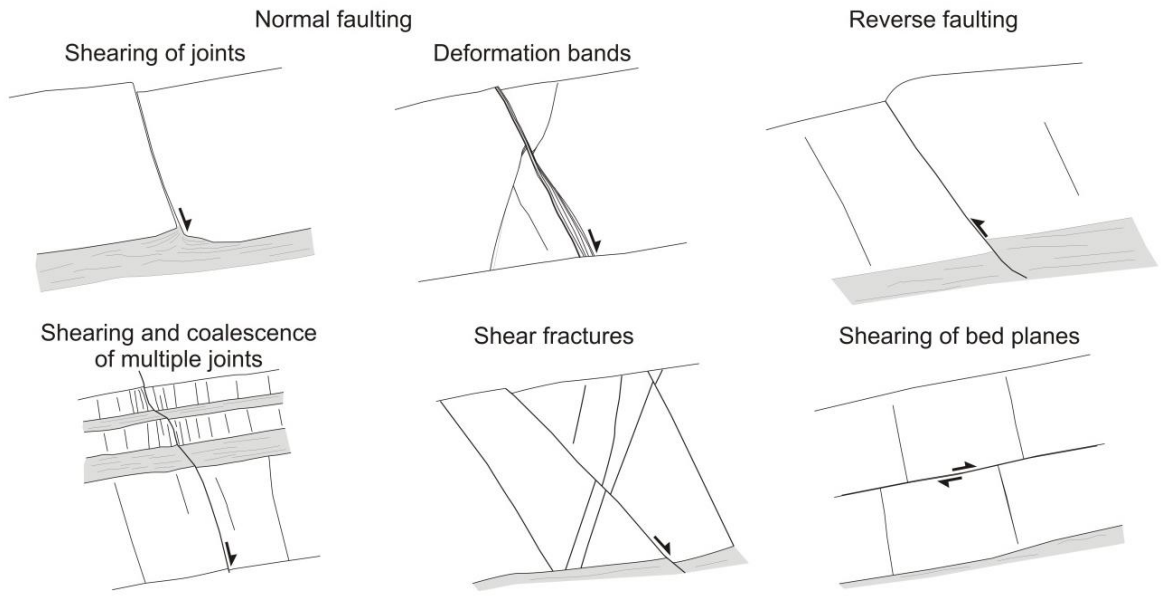

Figure 3.4 *Main deformation structures observed within all the studied localities within the folded layers of Cedar Mountain sandstones and conglomerates. The type of deformation is highly dependent on the lithology of the host rocks.*

The deformation styles indicate that the sandstones and conglomerates have been well consolidated at the time of deformation, at a burial depth which is believed to have been around 2000 m (Garden et al., 2001; Davatzes and Aydin, 2005). However, ductile deformation of the shales and shale flow patterns into the tensile fractures developed within the brittle competent layers indicate a large mechanical competence contrast between the shales and the sandstones - conglomerates layers (as discussed in *Chapter 2*).

3.4. Methods

Field data were collected on transects orientated approximately orthogonal to the fault zone within the hangingwall normal drag folds along the Moab fault. The transects are located along the north-west-trending splay segments of the main fault, north-west from the Courthouse branch-point (***Figure 3.1a***), across the Bartlett segment (in Bartlett Canyon and Waterfall Canyon) and in the previously little-studied Blue Hills segment area (***Figure 3.1a***). In the Blue Hills area, Cedar Mountain Formation, Brushy Basin and Salt Wash Members of the Morrison Formation crop out within both the footwall and hangingwall side of the fault. Here, displacement on the Moab Fault is partitioned onto several smaller splays that pass NW-ward into a continuous monocline. We documented the variability and distribution of secondary faulting and fracturing within the folded competent beds (sandstones and conglomerates) of the Cedar Mountain Formation. We used GPS-located mapping and collected structural data along key sandstone horizons within Cedar Mountain comprising orientation, frequency, displacement and geometries of joints, shear fractures and deformation bands on the multiple transects to estimate the strain distribution at different points across the monocline and hanging wall drag fold. Here, we investigate the relationship between the spatial variation of brittle finite strain within the folded layers, fault geometry and fault throw.

3.5. Analysis of deformation patterns in the hangingwall fold of Moab fault

3.5.1. Blue Hills sections

The Blue Hills area covers the NW part of the Moab fault, where several ENE-WSW oriented segments splay from the main fault on the footwall side possibly transferring displacement onto the E-W oriented Tenmile Graben (Foxford et al., 1996) (***Figure 3.1a***). Displacement on the main fault decreases gradually toward the NW, and normal-drag like folds developed in the hangingwall become fault-related monoclines (Foxford et al., 1996) towards the NW. We analysed the distribution of brittle deformation along two transects within the hangingwall fold limb developed along the north-western tip of the main Moab fault segment in the Blue Hills area (***Figure 3.1a***)., about 38 km NW of the town of Moab. The two transects are located across two hills which are capped by the mechanical competent and resistant to erosion Cedar Mountain sandstones formation (***Figure 3.2***). The transects are about 80 m long each and 250 m distance away from each other, separated by a saddle or an erosional gap (***Figure 3.5***).

The geomorphology of the two hills reflects the bedding of the Cedar Mountain sandstones. The NE facing hill slopes are bed dip slopes which have slightly different attitudes within the two locations. The hangingwall fold exposed within the northern hill (BH 1) is characterized by steeper bed dips with an average dip of about 40° and a dip direction toward NE (***Figure 3.5***). The bedding within the southern hill (BH 2) has shallower average dips (about 20°) and an overall dip direction toward E-NE, rotated slightly clockwise relative to the bed attitude within the northern hills (***Figure 3.5***).

Figure 3.5 – next page *View toward SE of the two outcrops from the Blue Hills area described in this study, the northern hill (BH1) and the southern one (BH 2). The beds dip toward NE for the BH1 location and to the ENE for BH2. Fractures within the two locations have similar orientations, the faults from BH1 have two distinct trends NW-SE and NE-SW compared to faults mapped in BH2 which have a E-W orientation*

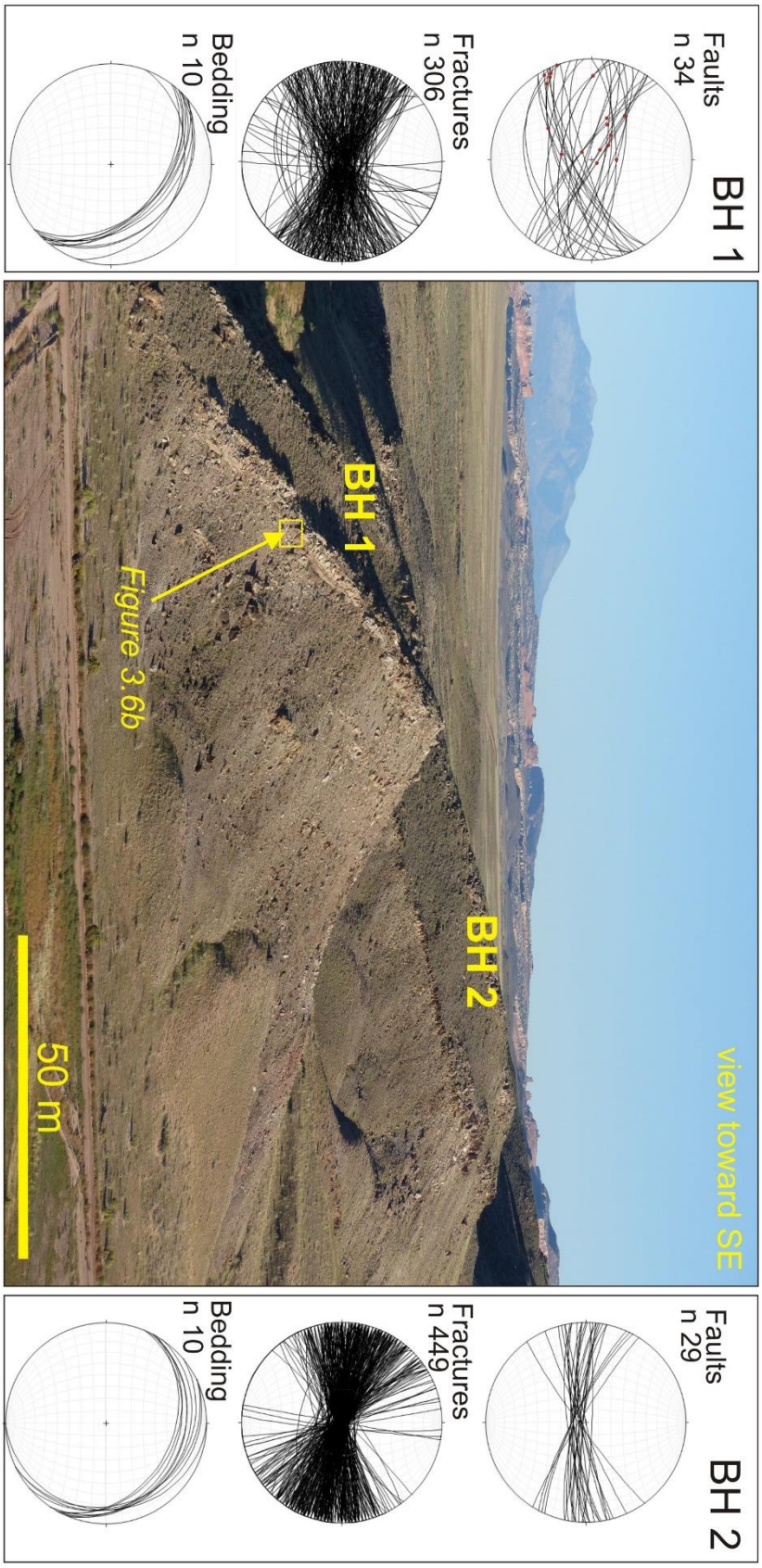
BH 1
Faults
n 34
Fractures
n 306
Bedding
n 10
BH 1
BH 2
Figure 3.6b
50 m
view toward SE
BH 2
Faults
n 29
Fractures
n 449
Bedding
n 10

The style of deformation is very similar at both localities. Brittle strain is accommodated by deformation bands within the softer, more porous sandstones and tensile fractures which post-date the deformation bands. Shear fractures or shearing of pre-existing tensile fractures are also very common. Most of the secondary fractures and faults are antithetic with respect to the main fault (***Figure 3.6***). Conjugate pairs of deformation bands show that antithetic structures cross-cut their opposite dipping pair, which are synthetic to the main fault. An illustrative example of secondary faults in this heterogeneous sequence of sandstones and conglomerates with different degrees of cementation and mudstones is shown in ***Figure 3.7***. The fracture density is relatively constant (5-10 / m) along the transect, however the density of the bed-confined fractures increases within the very well cemented sandstones adjacent to secondary faults (>20-30 / m). Most of the fractures are oriented at a high angle relative to bedding and are predominantly antithetic with respect to the main fault. The measured displacement on the observed secondary faults varies from 0.30 centimeters to 6.50 meters. The main fault illustrated in ***Figure 3.7*** has a vertical component of displacement of 1.15 m, but including the dextral strike-slip component, has a total displacement of 6.50 m.

Two main structural trends can be observed based on the orientation of the secondary faults mapped on the northern transect BH1 (***Figure 3.5***). One trend is oriented NW-SE, sub-parallel to the main fault. Kinematic indicators show for this fault set a dominant component of normal dip slip, with some minor oblique slip components (***Figures 3.5, 3.6*** and ***3.7***). The faults are both antithetic and synthetic in respect to the main fault, but the antithetic ones predominate. The other trend of secondary faults is oriented obliquely about 065 NE, forming a dihedral angle of ca. 50° with the NW-SE oriented fault set. The faults of the NE-SW set are antithetic in respect to the main fault and are characterized by a significant component of dextral strike slip, as the example shown in ***Figure 3.7b***. On the southern hill (BH2) the trend of the faults is slightly different, indicating the predominance of the faults and fracture sets oriented mainly E-W (***Figure 3.5***). The other trend which is sub-parallel with the main fault might be under-represented because of the orientation of the transect which becomes gradually sub-parallel with the orientation of the main fault. In this locality we have no indications of any oblique slip on the observed faults. The difference in the geometry of the beds (in orientation and dip),

the kinematic indicators on the faults and the gap in between the two folded structures indicate the possible presence of a fault linkage zone with an abandoned splay in the hangingwall of the Moab fault trending north-ward (which is not mapped on the USGS 1:24000) (***Figure 3.8***). It is reasonable to assume an increase in fold amplitude SE of BH1, considering an overall increase in total fault displacement toward SE (Davatzes and Aydin, 2005) (***Figure 3.8***). Also, in the case of a potential segment linkage zone, an increase in the fold amplitude is expected as a result of bed rotation between the interacting segments (Childs et al., 2016). Kinematic analysis of the secondary faults suggests that the fault trend parallel to the Moab fault (the NW-SE set) accommodates the main horizontal component of extension of the hangingwall fold limb. The dextral oblique slip component on the NE-SW oriented normal faults is required to accommodate the horizontal component of extension on the underlying main fault and the lateral variations in fold amplitude along its axis (i.e. non-cylindricity of the fold geometry) (***Figure 3.8***). Hence, the elongation of the beds within the fold limb in the fault-normal and fault-parallel direction is favorably accommodated by a combination of dip-slip and strike-slip displacement on two distinct sets of secondary faults (***Figure 3.6*** and ***3.8***).

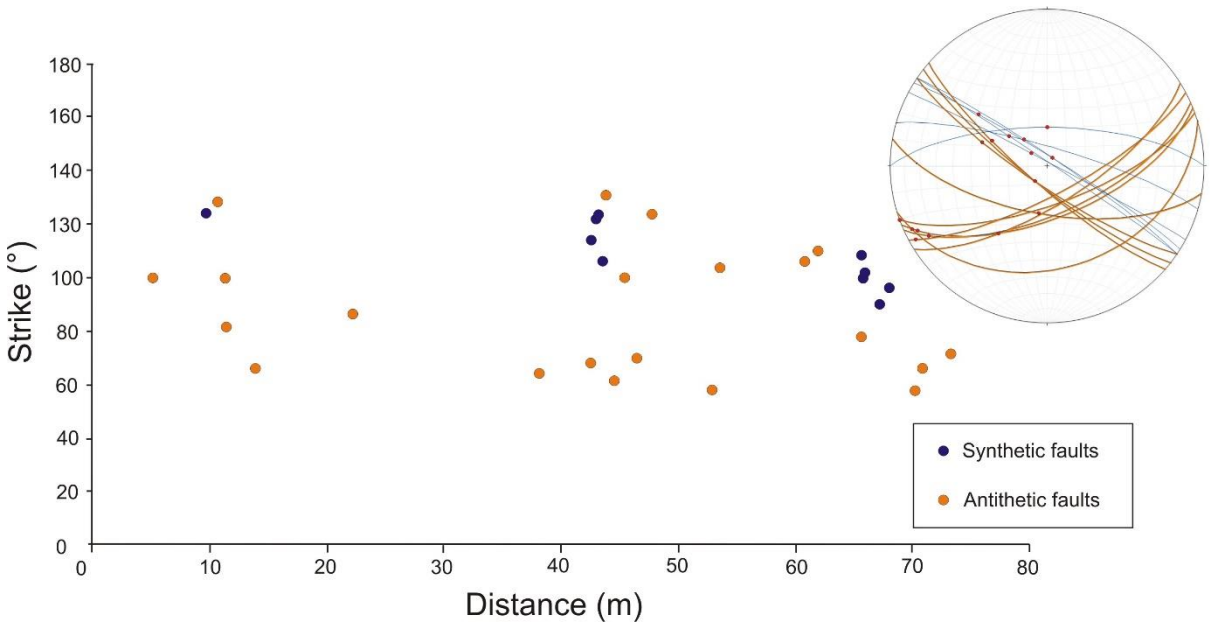

Figure 3.6 *Distribution of secondary faults vs fault strike along the BH1 transects. The faults oriented NW-SE (parallel to the master fault) are predominantly dip-slip, while those oriented NE-SW are characterized by a component of dextral slip*

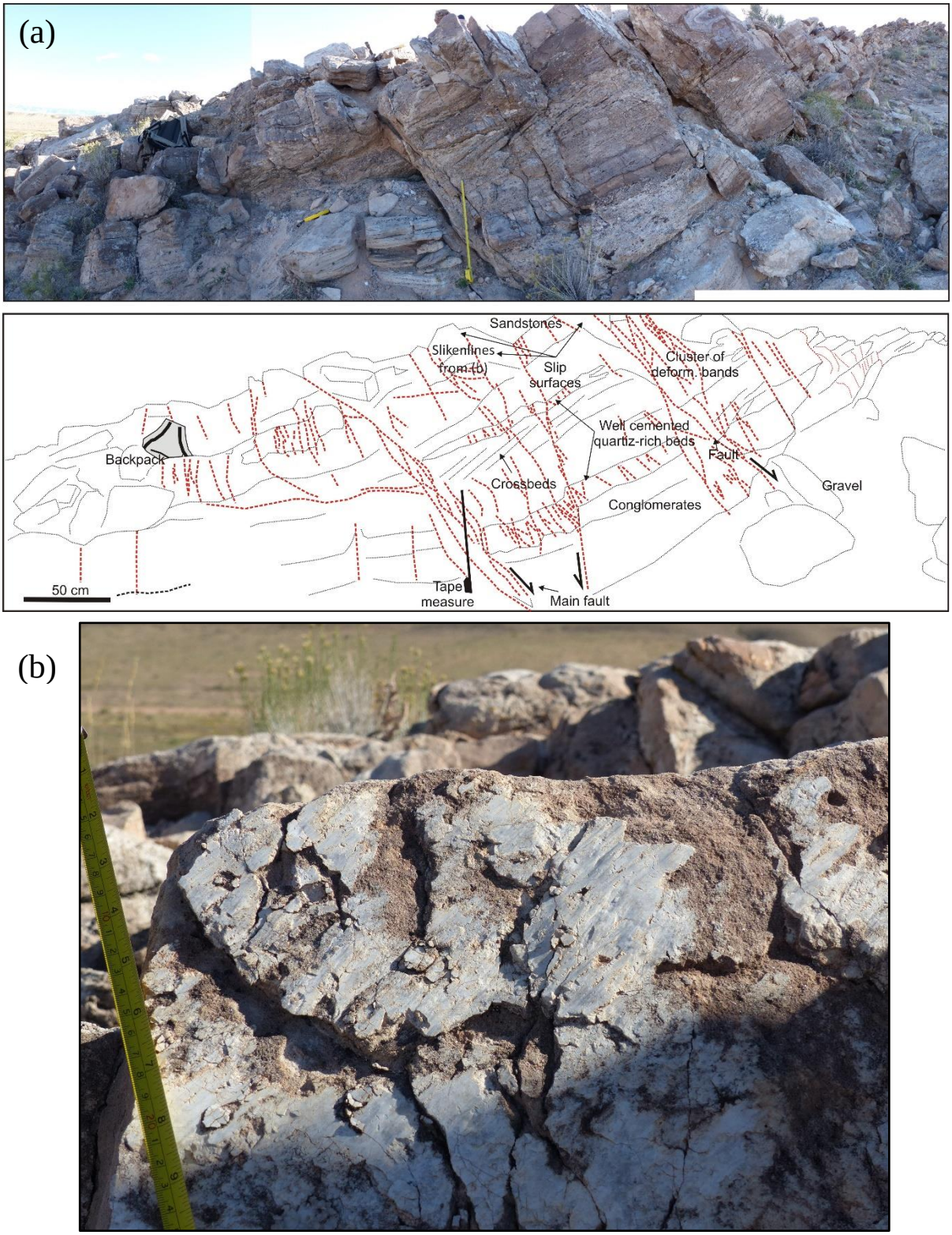

Figure 3.7 (a) *Example of secondary faults within the fold limb, which are all dominantly antithetic to the main fault. These faults are oriented NE-SW, dip toward SE and have kinematic indicators that show a component of dextral strike slip, toward SW such as the striated surface from* ***(b)****.*

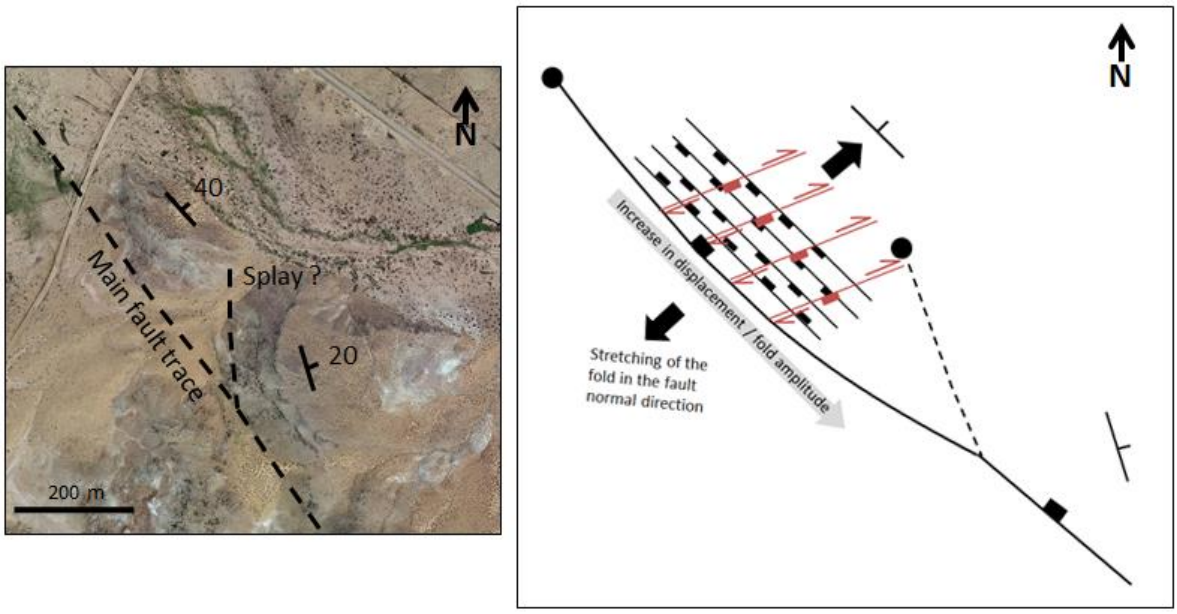

Figure 3.8 *Structural model which predicts an abandoned hangingwall splay between the two studied outcrops within the Blue Hills area. Kinematic analysis of the secondary faults suggests that the Moab fault parallel trend (the NW-SE set) accommodates the main horizontal component of extension of the fold limb, while the NE-SW antithetic dextral slip faults accommodates a component of elongation in the SE direction, probably generated by the non-cylindricity of the fold geometry. This happens because of an increase in displacement and fold amplitude toward SE.*

3.5.2. Bartlett Canyon section

Within the Bartlett Canyon section of the Moab fault the throw increases to about 275 m (Davatzes and Aydin, 2005). Here, the fault juxtaposes Cedar Mountain Formation and Brushy Basin Member mudstones in the hangingwall against the Late Jurassic Entrada Formation sandstones within the footwall (***Figure 3.9***). The hangingwall normal drag fold that crops out in the Bartlett Canyon has an amplitude of ca. 70 m and displays steeper bed dips than the folds developed within the Blue Hills area. The larger fold dips are most likely to be the result of an increase in displacement and better preservation conditions of the folds when juxtaposed along the competent and more resistant to erosion Jurassic aeolian sandstones.

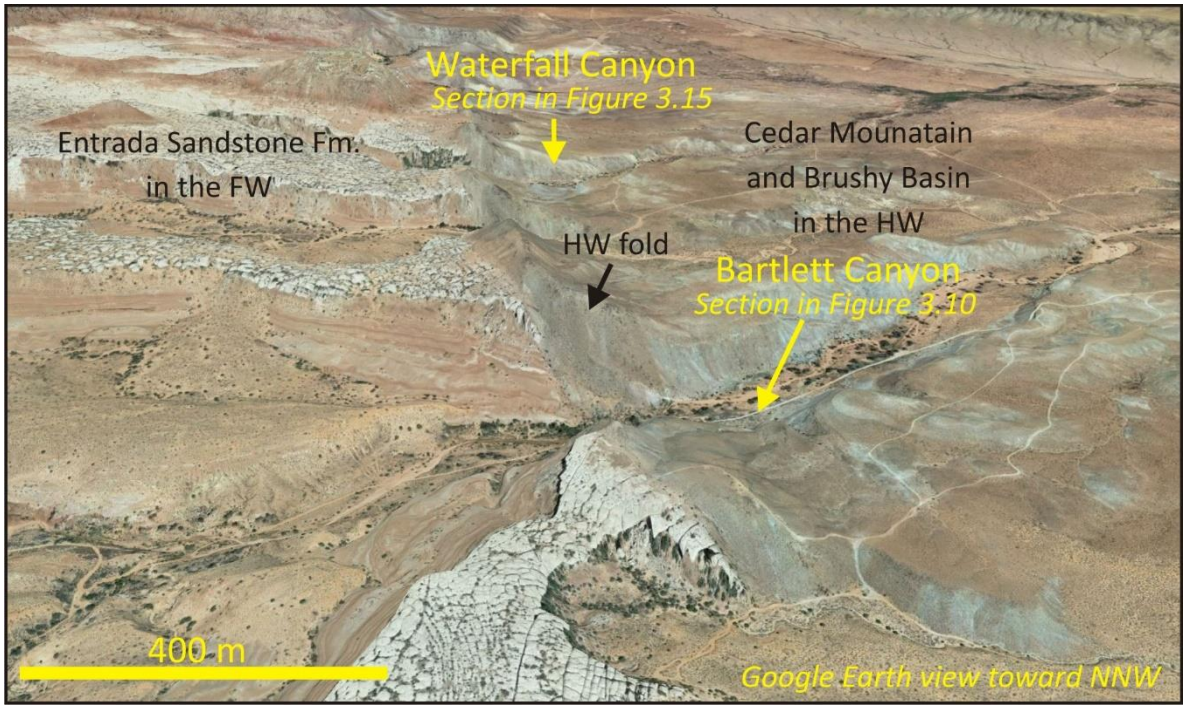

Figure 3.9 *Google Earth view of the Bartlett segment of the Moab Fault, showing the locations of the profiles along two of the canyons that cut almost orthogonal to the strike of the main fault.*

The beds can reach dips of ca. 60° in the proximity of the main fault, accommodating 2/3 of the total fold amplitude in less than 50 m distance from the fault, after which the bedding dips gradually decrease and approach the regional dip about 200 m away from the main fault (***Figure 3.10***). We separated the folded section into three main zones (dip domains) based on the dominant bed dips observed. These dip domains are characterized by distinctive secondary deformation patterns (***Figure 3.10***). Deformation decreases in intensity from the dip domains A to C, where C represents the outer zone of the hangingwall fold limb. Close to the main fault, within the dip domain A, the competent beds of the Cedar Mountain Formation have dips generally greater than 40° and they are highly fractured or brecciated. In the immediate proximity to the main fault (5-10 m), the secondary faults within the fold are synthetic to the master fault (dip to the NE). However, most of the secondary faults within this section of the hangingwall fold are antithetic to the main fault (dip toward SW) and display at the present day very low dip angles (<30˚), with some being almost sub-horizontal (***Figure 3.10***).

Depending on the host-rock lithology, these faults encompass deformation bands organized in parallel or conjugate sets (***Figure 3.11a***), or shear fractures (***Figure 3.11b***), or a combination of these two, when crossing sandstones with different degrees of cementation ((***Figure 3.11a*** and ***3.11b***). Very often, the conjugate fault pairs show that the antithetic faults cross-cut their synthetic counterpart. Steeper bed dips in the hangingwall compared to the footwall of the secondary antithetic faults, associated with wider and more intense deformation zones within the hangingwall (***Figure 3.11***), indicates that these faults were not passively rotated and contributed to the overall rotation of the fold limb.

In the previous chapter, we discussed that slip on these shallow dipping antithetic normal faults is expected to be inhibited, since the normal stress acting on these faults is likely larger than the shear stress (Morris et al., 1996). However, layer interfaces commonly show evidence for bed-parallel slip, which suggest that during folding many of the bed boundaries reactivate as shear planes (***Figure 3.12***). In the dip domain A, slickenlines parallel to bedding indicate a sense of shear motion toward the anticlinal fold axis.

This component of bed-parallel shear toward the hinge of the monocline fold (***Figure 2.12b***) is expected to generate a rotation of the principal stress axes (Price and Cosgrove, 1990) which would favor in this case slip on the antithetic normal faults at lower angles then the ones normally predicted by Mohr-Coulomb theory. Within the fold dip domain B, antithetic shear fractures still predominate. Kinematic indicators show that bed-parallel slip surfaces (bed interfaces or sub-horizontal slip planes within finer and less consolidated lithologies) have a sense of slip toward the hangingwall syncline (toward NE). Some of the bed-parallel shear fractures reactivate in shear (i.e. invert) pre-existing fractures (***Figure 3.13c***) or develop localized low angle thrust faults (***Figure 3.13b***). As observed in ***Figure 3.13***, many of the bed boundaries within these channelized systems are non-planar and show down-cutting geometries which can interfere with the slip surfaces within or in between adjacent lithological units (***Figure 3.14***). This interference causes localized stress concentrations in the proximity of the bed asperities, such as down-cutting channels, which generates the development of fractures and faults or reactivation in shear of pre-existing fractures (***Figure 3.14b***).

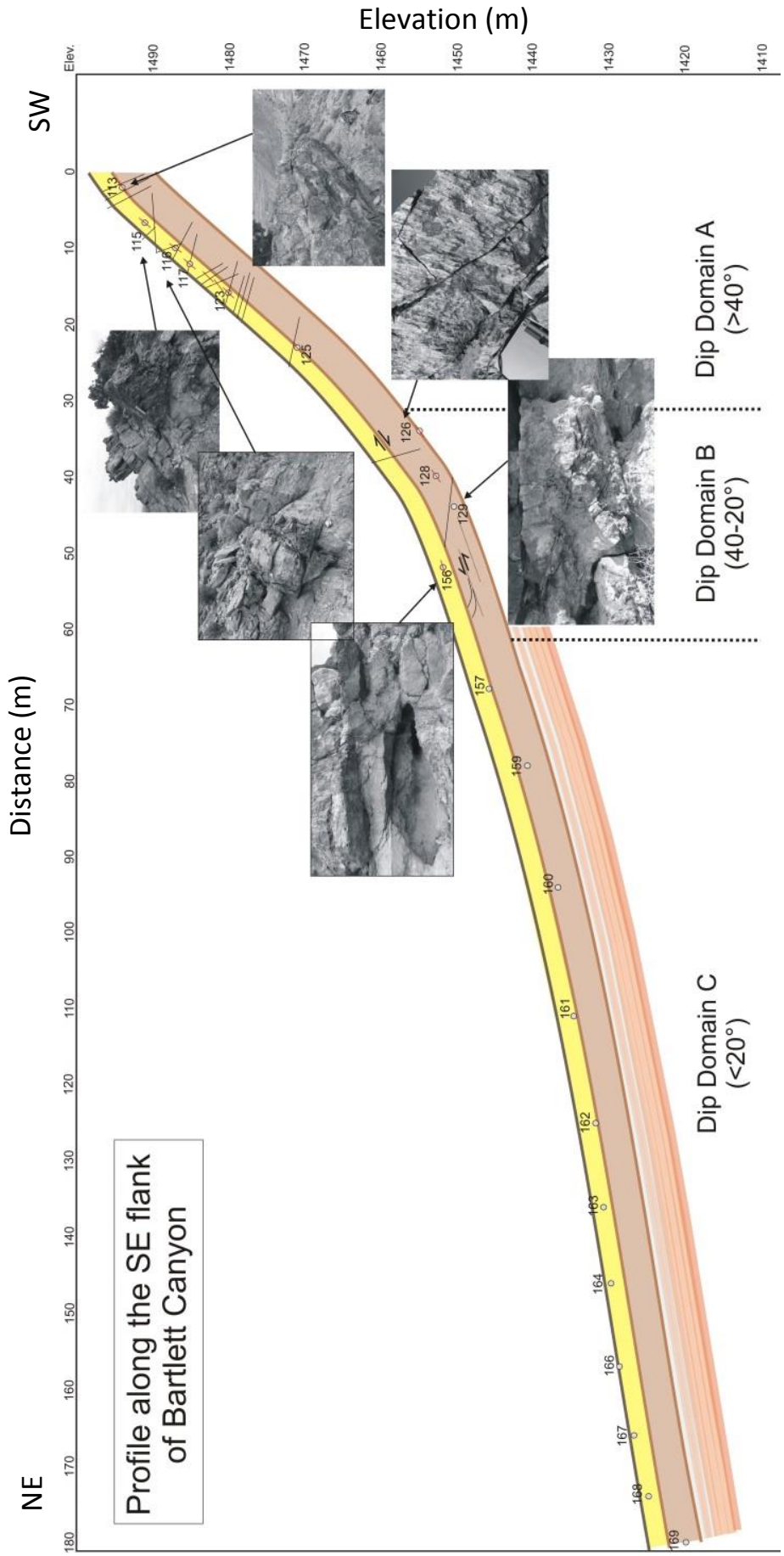
Elevation (m)
Elev.
1490
1480
1470
1460
1450
1440
1430
1420
1410
SW
NE
Distance (m)
0
10
20
30
40
50
60
70
80
90
100
110
120
130
140
150
160
170
180
Dip Domain A
(>40°)
Dip Domain B
(40-20°)
Dip Domain C
(<20°)
Profile along the SE flank
of Bartlett Canyon

Figure 3.10 - previous page *Section along the hangingwall fold from the Bartlett Canyon with some of the main deformation structures observed within the defined fold dip domains (details described in the text).*

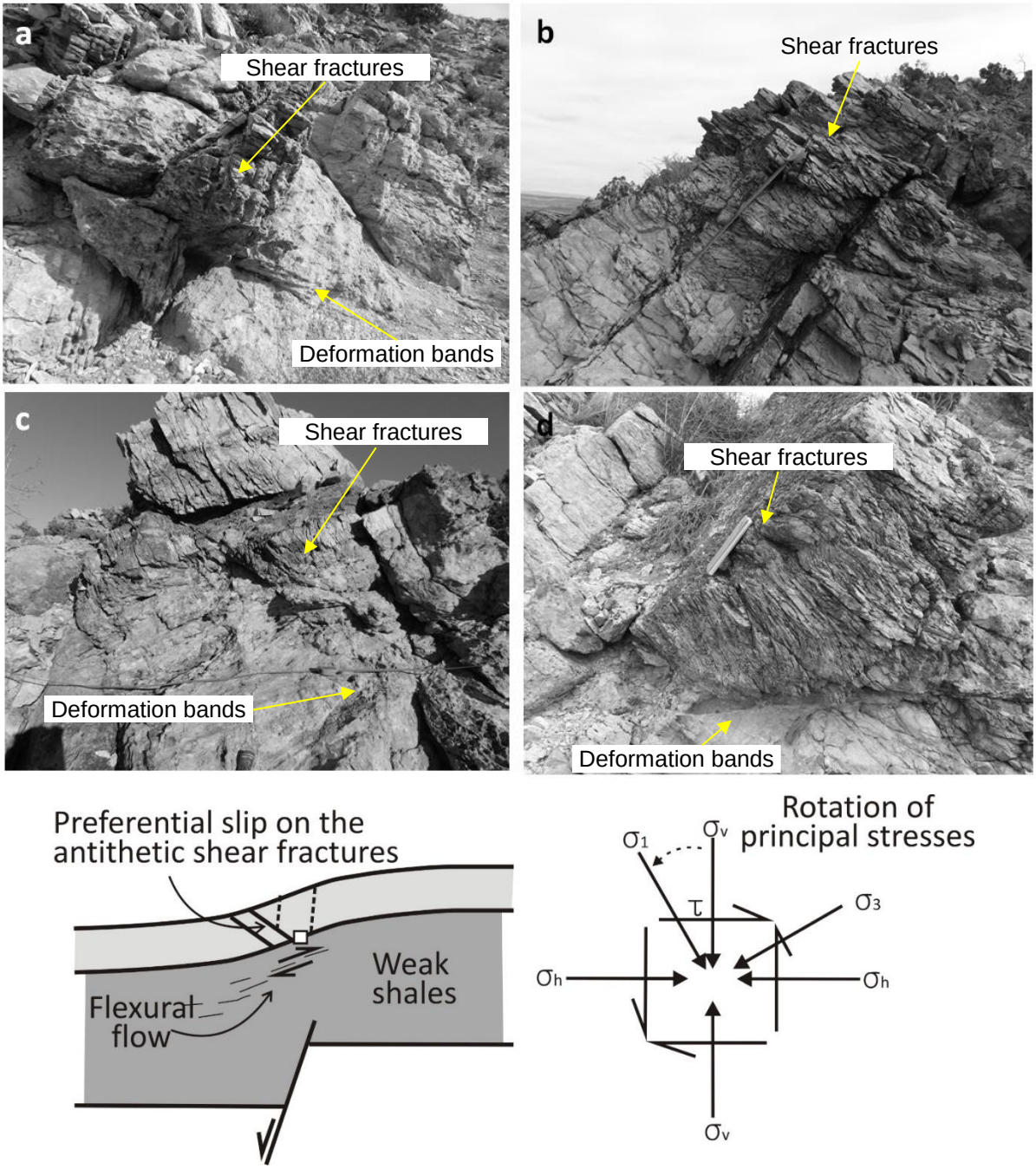

Figure 3.11 *Antithetic shear fractures and normal faults dominate as secondary structures within the folds. The antithetic fault shown here are highly rotated and are almost horizontal. Note the intense deformation within the hangingwall of these faults. Slip on the interfaces of the beds with similar*

mechanical competency and the ductility contrast between the competent layers and the weaker shales induces a component of shear stress parallel to layering which causes the rotation of the principal stresses. The reorientation of the maximum principal stress favours slip on the rotated, shallower dipping antithetic normal faults.

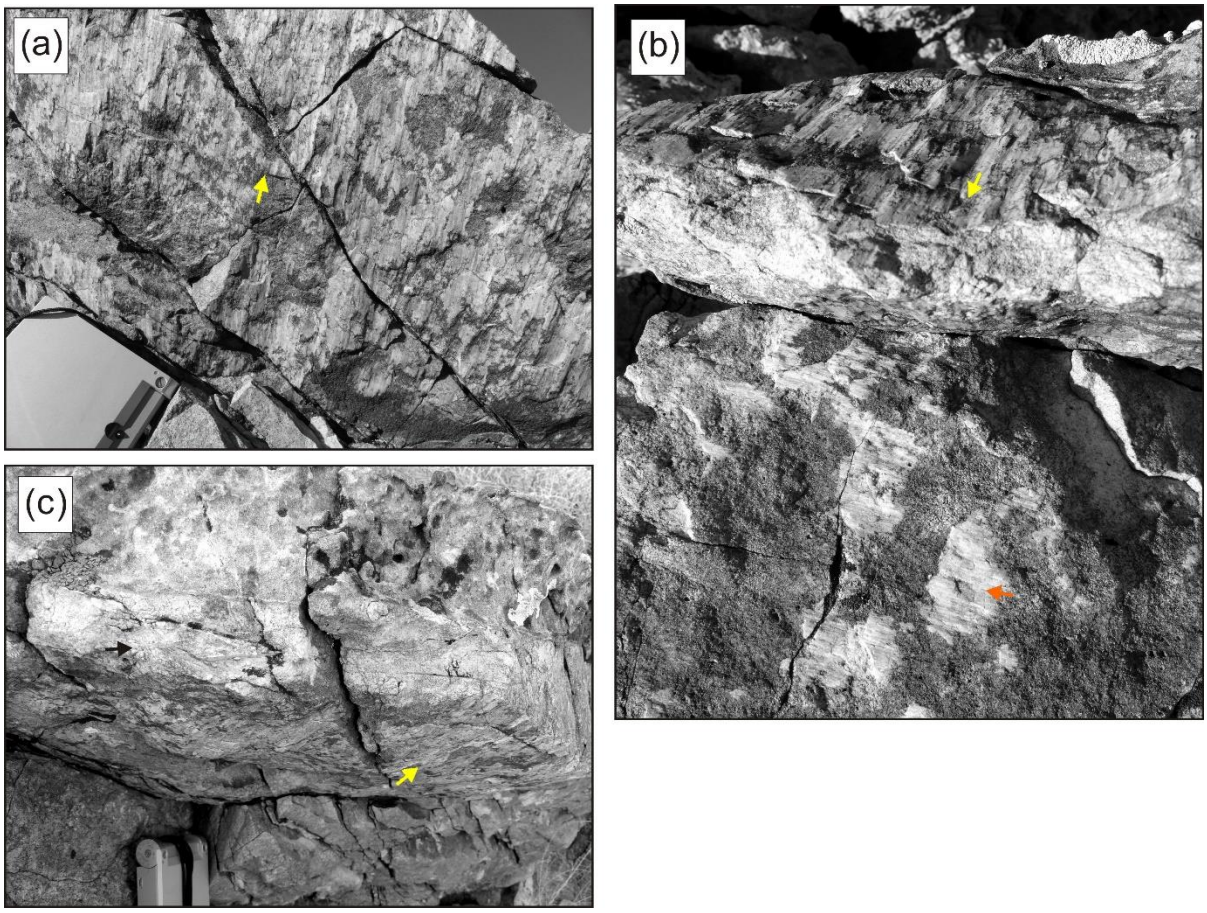

Figure 3.12 *Slip surfaces with kinematic indicators observed on bedding planes. Slickenlines indicate up-dip slip toward the fold anticline axis* ***(a, b, c)****. Compass (~8 cm) for scale;* ***(b)*** *Some of the bed-parallel slip surfaces (yellow arrow) post-date strike-slip movement (orange arrow) on fractures which cut through beds.*

Figure 3.13 (next page) *Section of the fold within the dip domain B which shows sub-horizontal slip surfaces that are evidence for local thrusting and reactivation in compression of pre-existing shear and tensile fractures. Hammer (33 cm) for scale.*

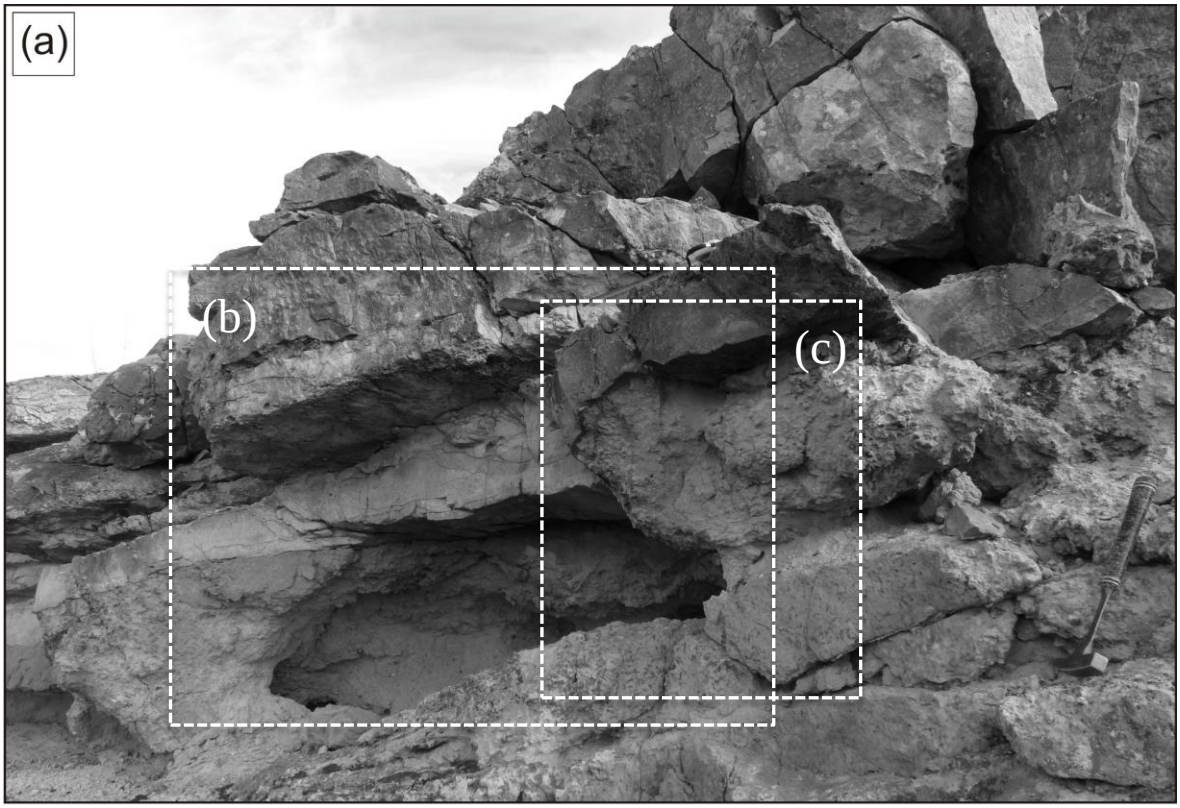
(a)
(b)
(c)


(b)

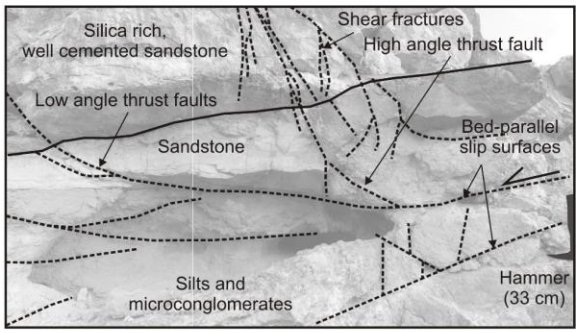
Silica rich,
well cemented sandstone
Shear fractures
High angle thrust fault
Low angle thrust faults
Sandstone
Bed-parallel
slip surfaces
Silts and
microconglomerates
Hammer
(33 cm)

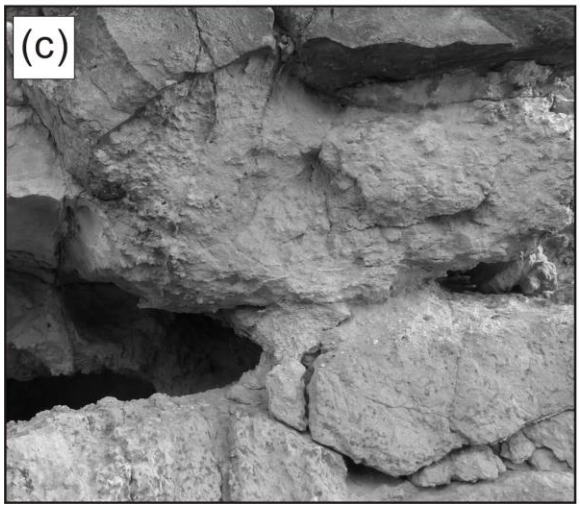
(c)

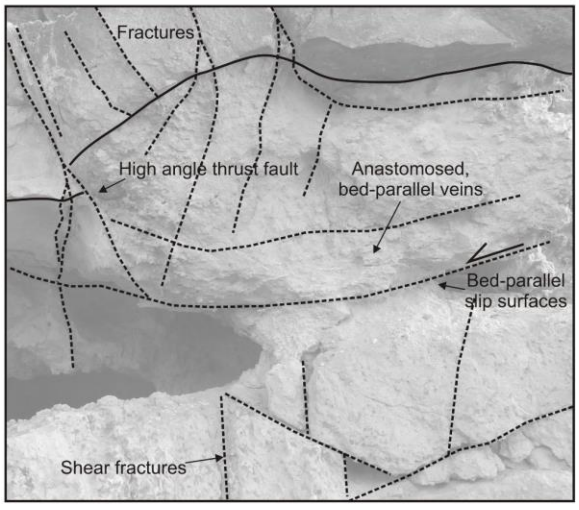
Fractures
High angle thrust fault
Anastomosed,
bed-parallel veins
Bed-parallel
slip surfaces
Shear fractures

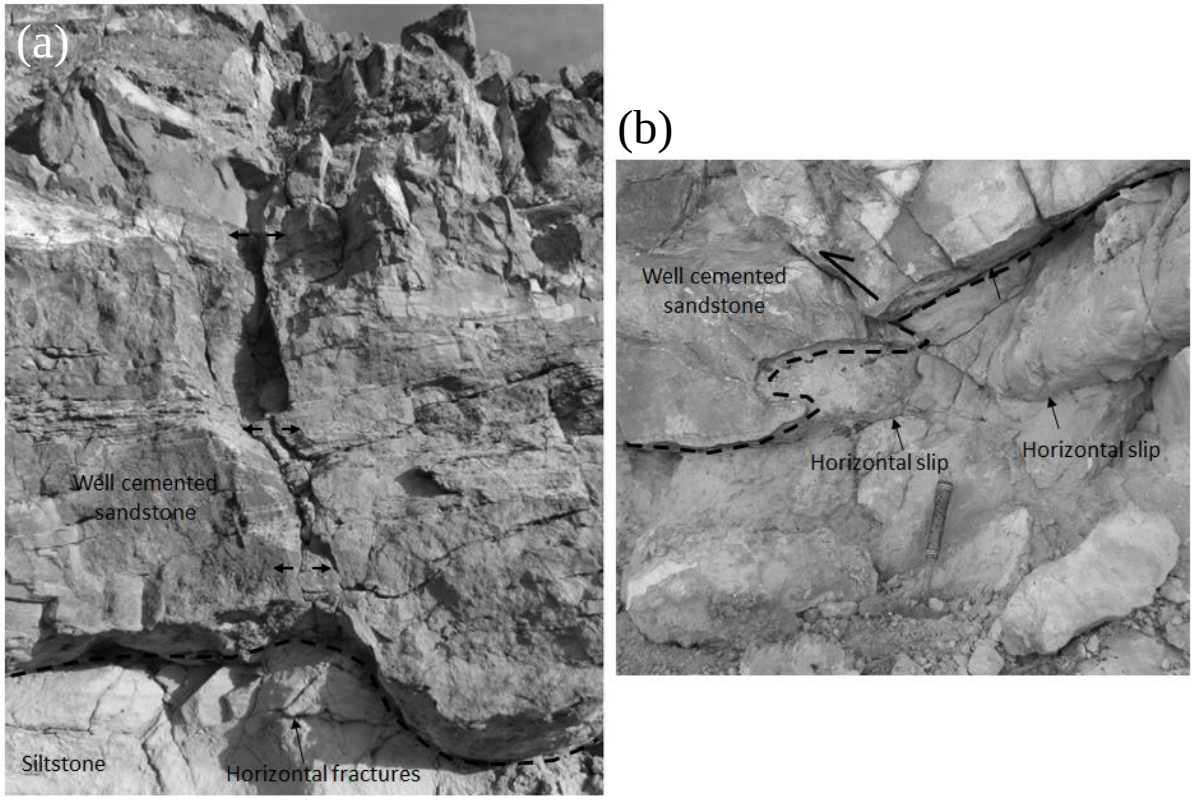

Figure 3.14 (a) *Localized formation of tensile fractures is enhanced by the stress concentrations developed adjacent to irregular bed geometries, such as these down-cutting channel sandstones;* ***(b)*** *Folding by flexural slip of layers with irregular geometries can determine compressional reactivation of pre-existing joints and shear fractures adjacent to these depositional asperities.*

3.5.3. Waterfall Canyon section

The Waterfall Canyon is located along the Bartlett segment of the Moab fault, about 1300 m NW from the Bartlett Canyon (***Figure 3.1 and Figure 3.9***). Here, the fault has a throw of ca. 270 m (Davatzes and Aydin, 2005) and juxtaposes the same aeolian Jurassic sandstone units within the footwall and shale-dominated Upper Jurassic - Cretaceous deposits within the hangingwall. The amplitude of the hangingwall fold is about 80 m and has a wavelength larger than 200 m. Some key observations on the deformation characteristics have been made in the previous chapter (*Chapter 2*). Brittle strain is accommodated within the competent sandstone and conglomerate beds by shear fractures and tensile fractures (***Figure 3.15***).

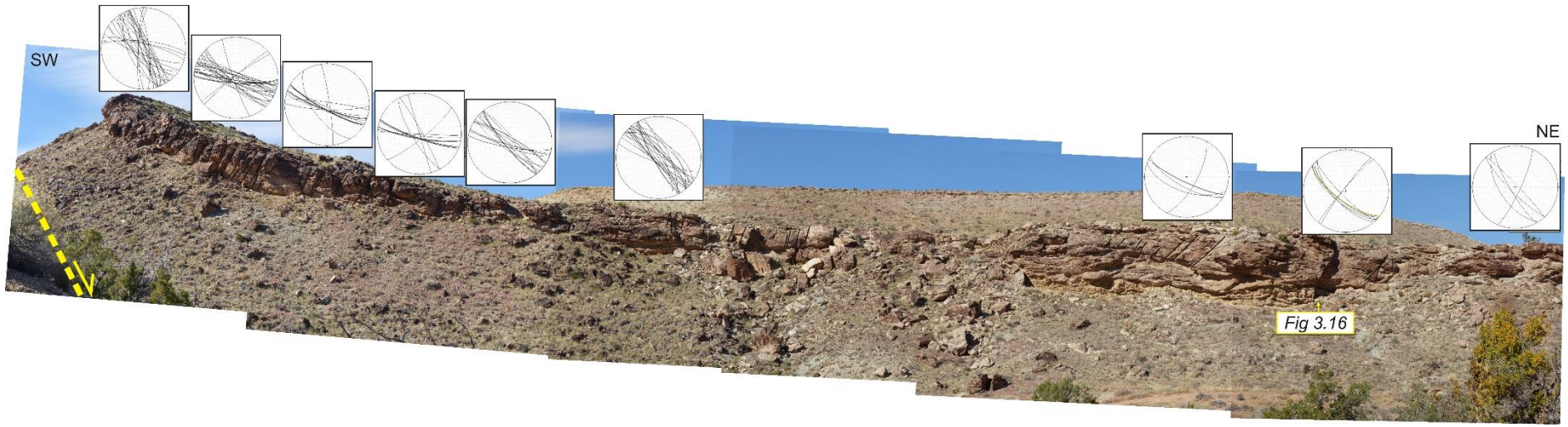

Figure 3.15 *Composite section of the Waterfall Canyon transect with stereonets showing the orientation of the main fracture sets which accommodate the brittle strain within the hangingwall fold. The majority of the shear fractures, faults and joints are oriented parallel to the main fault (NW-SE) and are antithetic with respect to it.*

Some of the tensile fractures show reactivation in shear and are antithetic with respect to the main fault, similar to the relationships observed at the Blue Hills and Bartlett Canyon localities. Conglomerates and sandstone layers overlie blue-green mudstones rich in carbonate nodules which is part of the Cedar Mountain Formation. Hence, we have inferred a high mechanical competence contrast between the quartz-rich sandstones and the underlying mudstones, which is illustrated by the shale fabric which shows flow patterns within the opened fractures formed within the sandstones (shown in previous chapter in ***Figure 2.9d***). The faults and the shear fractures within the brittle, competent layers have relatively small displacements of several centimeters that die out within the underlying mudstones, where deformation was accommodated by plastic flow. Within this weaker layer of mudstones, we observed zones of intense tensile fracturing. The veins have apertures between 0.05 and 1 cm, filled with calcite mineralization. The veins are arranged in an anastomosed network of horizontal, sub-horizontal and inclined, planar and curving opening mode structures (***Figure 3.16b*** and ***3.16c***). The calcite mineralization displays a fibrous texture and the growth direction of the calcite cement is approximately vertical, no matter what the orientation of the veins (***Figure 3.16b*** and ***3.16c***). There is no evidence of shearing to indicate that these structures accommodate flexural slip within these weaker shale layers. Importantly, veining only seems to be present in the vicinity of faults that cut the overlying brittle conglomerate and sandstone layers. In other locations along the transect, where there is no faulting within the overlying competent beds, there is no veining in the mudstones. Hence, we hypothesize that the formation within the shale layer of this network of calcite-filled sub-horizontal tensile fractures was related to the process of faulting within the overlying competent conglomerate-sandstone beds. It seems likely that faulting in the normal fault regime, where the maximum principal stress, σ_1, is vertical, was accompanied by circulation and redistribution of fluids, indicated by the presence of calcite and quartz mineralization. Also, it seems likely that the interbedded mudstones are confined between layers with low porosity and have a relative high pore fluid content (above hydrostatic), which is suggested by the flow fabric of the deformed shales (***Figure 2.9d*** and ***2.9e***). We suggest that as the fault suffers a sudden decrease in shear stress and slip

occurs, fluid is expelled into the underlying, relatively low permeability and probably already overpressured, bed-confined shale layer.

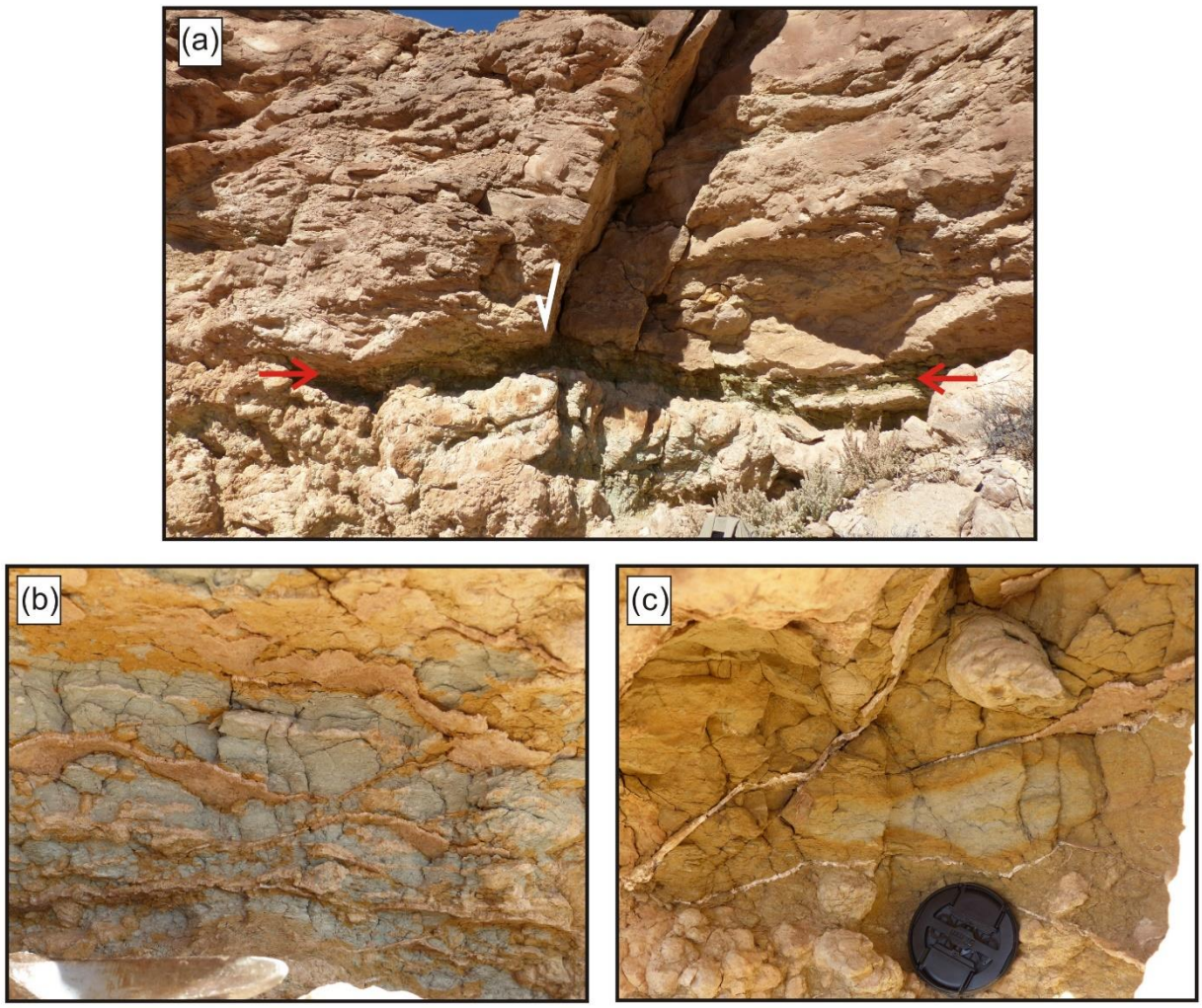

Figure 3.16 (a) *Brittle faults within the competent layers terminate into an underlying incompetent shale bed (red arrows).* ***(b)*** *Intense anastomosed fractures with* ***(c)*** *horizontal, sub-horizontal and inclined, calcite-filled veins are developed within this shale bed. The veining seems to occur only when faulting in the overlying brittle layers is present.*

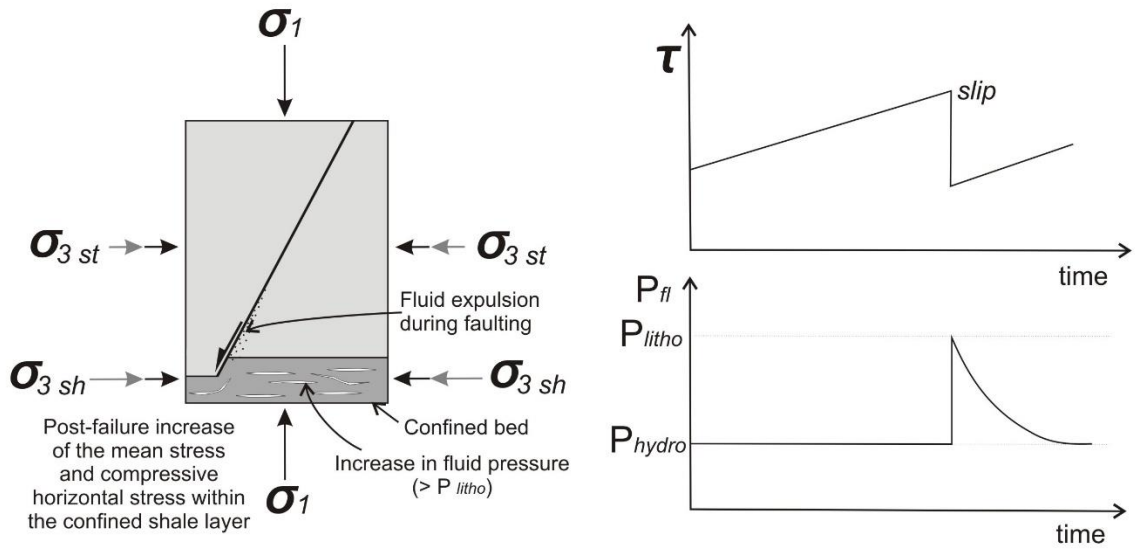

Figure 3.17 *Conceptual model for the formation of sub-horizontal fractures within a confined shale layer in association with adjacent faulting within a brittle, competent layer. Faulting in the normal fault regime (σ1 vertical) is accompanied by circulation and redistribution of fluids (indicated by calcite and quartz mineralization). As the fault suffers a sudden decrease in shear stress, fluids are expelled into the underlying, relatively low permeability, and probably already overpressured, bed confined shale layer. While σ1 is assumed to remain constant before and after failure, the minimum horizontal stress (σ3) and the mean stress increase immediately after faulting. The post-failure increase in the minimum horizontal compressive stress (grey arrows) depends on the elastic properties of the rocks (e.g. Poisson's ratio and Young's modulus), which results in larger horizontal compressive stress within the incompetent shale layer. This, coupled with fluid expulsion results in a rapid increase in fluid pressure within the confined shale beds. When fluid pressure overcomes the lithostatic pressure horizontal fractures develop. Right-hand side diagrams modified from Sibson (2000).*

While σ_1 is assumed to remain constant before and after failure, the minimum horizontal stress (σ_3) and the mean stress increase immediately after faulting (***Figure 3.17***). The post-failure increase in the minimum horizontal compressive stress (grey arrows in ***Figure 3.17***) would depend on the elastic properties of the rocks (e.g. Poisson's ratio and Young's modulus), and would in this case, results in larger horizontal compressive stress within the incompetent shale layer. Coupled with fluid expulsion within the same bed-confined layer, this results in a rapid increase in fluid pressure. If the fluid

pressure overcomes the lithostatic pressure, horizontal fractures may develop. Hence, there is a local rotation of the principal stress axes within the shale layer, with σ_1 changing from sub-vertical to sub-horizontal, and the minimum compressive stress, σ_3, which is expected to be oriented sub-horizontal in a NE-SW direction becomes sub-vertical.

3.6. Concluding remarks

We described the characteristics of small-scale faulting and fracturing which accommodates larger, seismic-scale normal fault-related folding along the Moab fault, Utah. In the four investigated transects across the normal drag folds, we observed that the strain characteristics and deformation styles are highly controlled by the mechanical properties of the layered sandstone-shale sequence of the Cedar Mountain Formation.

The brittle strain is accommodated by shear fractures, deformation bands and joints, most of which are antithetic with respect to the main fault, as previously observed by Berg and Skar (2005). The antithetic faults are highly rotated, some of them to almost sub-horizontal dips. Wider and more intense deformation zones within the hangingwall and associated steeper bed dips in the hangingwall (***Figure 3.11***) indicates that the faults were not passively rotated and contributed to the overall rotation of the fold limb.

Folding of the layers is accommodated also by slip between the bed interfaces (i.e. flexural slip). Bed-parallel slip is localized and influenced by the irregular, channelized geometries of the sandstones and conglomerates. Slip on irregular bed planes enhanced localized stress concentration, which generated reactivation in compression of pre-existing joints and shear fractures and localized developing of fracturing coeval with flexural-slip deformation.

Extensional strain within the hangingwall fold limb is accommodated by a combination of dip-slip and strike-slip displacement on two distinct sets of secondary faults, to account for the along strike

variation in the fold geometry (e.g. fold amplitude), which is primarily controlled by the evolution of the underlying fault segments.

Deformation in the hangingwall of Moab Fault is highly partitioned by the contrasting mechanical properties of the competent sandstone and conglomerate beds and the interlayered shale beds. Faulting and fracturing with mineralization indicates the presence of mineralized fluids at the time of deformation. The presence of a sub-horizontal network of fractures within the shale interval in the proximity of brittle faults within the overlying competent layers suggests that the two types of deformation structures are closely linked, with brittle faulting contributing to the generation of overpressure and hydrofracturing within the underlying shale layers.

Acknowledgments

I would like to thank the Geological Society of London for the Timothy Jefferson Field Research Grant which allowed the fieldwork in Moab to be carried out. Alex Peace is thanked for his assistance in the field.

| Chapter 4 |

Occurrence and development of folding related to normal faulting within a mechanically heterogeneous sedimentary sequence: a case study from Inner Moray Firth, UK

Abstract

Folds associated with normal faults are potential hydrocarbon traps and may impact the connectivity of faulted reservoirs. Well-calibrated seismic reflection data that image a normal fault system from the Inner Moray Firth basin, offshore Scotland, show that folding was preferentially localized within the mechanically incompetent Lower-Middle Jurassic pre-rift interval, comprising interbedded shales and sandstones, and within Upper Jurassic syn-rift shales. Upward propagation of fault tips was initially inhibited by these weak lithologies, generating fault propagation folds with amplitudes of ~50 m. Folds were also generated, or amplified, by translation of the hangingwall over curved, convex-upward fault planes. These fault bends resulted from vertical fault segmentation and linkage within mechanically incompetent layers. The relative contributions of fault propagation and fault-bend folding to the final fold amplitude may vary significantly along the strike of a single fault array. In areas where opposite-dipping, conjugate normal faults intersect, the displacement maxima are skewed upwards towards the base of the syn-rift sequence (i.e. the free surface at the time of fault initiation) and significant fault propagation folding did not occur. These observations can be explained by high compressive stresses generated in the vicinity of conjugate fault intersections, which result in asymmetric displacement distributions, skewed toward the upper tip, with high throw gradients enhancing upward fault propagation. Our observations suggest that mechanical interaction between faults, in addition to mechanical stratigraphy, is a key influence on the occurrence of normal fault-related folding, and controls kinematic parameters such as fault propagation/slip ratios and displacement rates.

4.1. Introduction

Folding related to normal faulting is mainly the result of fault propagation and linkage at different stages of the growth of normal faults (Withjack et al., 1990; Schlische, 1995; Janecke et al., 1998; Corfield and Sharp, 2000; Sharp et al., 2000; Ferrill et al., 2005; White and Crider, 2006; Jackson et al., 2006; Ferrill et al., 2007; Ferrill et al., 2012; Tvedt et al., 2013; Tavani and Granado, 2015). The main mechanisms generating fault-related folds in extensional domains are: (i) flexural deformation around vertical and lateral tips of propagating blind faults (fault-propagation folding) (Walsh and Watterson, 1987; Ferrill et al, 2005); (ii) folding between overlapping / underlapping, vertically or laterally segmented faults (Rykkelid and Fossen, 2002; Rotevatn and Jackson, 2014; Childs et al., 2016); (iii) translation of the hangingwall over a bend in a fault plane (Groshong, 1989; Xiao and Suppe, 1992; Rotevatn and Jackson, 2014); (iv) distributed shear deformation (Fossen and Hesthammer, 1998; Ferrill et al., 2005); and (v) frictional drag (Davis and Reynolds, 1984). Mechanical properties of the host rocks exert a primary influence on normal fault geometry and development of extensional folds (Ferrill et al., 2007; Ferrill and Morris, 2008; Tvedt et al., 2013). With the help of analogue, numerical and kinematic models (Groshong, 1989; Whitjack et al., 1990; Dula, 1991; Saltzer and Pollard, 1992; Hardy and McClay, 1999; Johnson and Johnson, 2002; Jin and Groshong, 2006), researchers have shown that changes in fault dip, strain rate and thickness of the incompetent layer also control the development of extensional fault-related folds. For example, thick incompetent layers will tend to inhibit fault propagation and promote formation of fault-tip monoclines (Withjack and Callaway, 2000).

Nevertheless, models are constrained by imposed boundary conditions and are usually designed to test a single mechanism. Growth of the faults is a dynamic process in which fault geometry, slip-related stress perturbations and strain rates can vary in both space and time (Cowie, 1998; Gupta and Scholz, 2000) and, as a consequence, different processes might be responsible for the generation of folds during the evolution of a normal fault system. Numerical models, supported by seismological evidence, indicate that faults develop and interact within heterogeneous stress fields resulting from regional tectonic stress and local stress perturbations (Cowie, 1998; Gupta and Scholz, 2000). This

heterogeneity induces local variations in fault slip, fault propagation and strain rates (Willemse et al., 1996; Crider and Pollard, 1998; Gupta et al., 1998; Gupta and Scholz, 2000; Willemse and Pollard, 2000; White and Crider, 2006), key parameters in controlling the development of extensional monoclines (Withjack and Callaway, 2000; Hardy and Allmendinger, 2011). We still know relatively little about the possible influence of heterogeneous stress distributions on the development of fault-related folding (White and Crider, 2006), and have yet to explain the variable occurrence and development of extensional folding along single fault arrays.

In this study we use 2- and 3D seismic reflection data from the Inner Moray Firth basin, offshore Scotland, to investigate the influence of host-rock lithology, fault geometry and fault interaction on the development of normal fault-related folds. First, we describe the three-dimensional geometries of the faults and folds using 3D seismic data. We map the fault throw distributions, and describe variations in the thicknesses and geometries of the syn-rift seismic sequences, to interpret the spatial and temporal (i.e. kinematic) evolution of the faults and folds. Next, we augment these observations with interpretations of faults and folds from regional 2D seismic lines, to investigate the relationship between fold growth, fault propagation and fault interaction across the basin. We show that: (i) normal fault-related folds can be generated by different mechanisms that vary in importance in time and space along a single fault array; (ii) the heterogeneous mechanical properties of the host rocks control the fault segmentation and associated ductile deformation; and (iii) the occurrence and development of normal fault-related folds is influenced not only by mechanical stratigraphy and fault plane geometry, but also by mechanical interaction between the faults themselves. Specifically, the variability of extensional folding along the strike of a fault array can be explained by the enhanced vertical propagation due to mechanical fault interaction between opposite-dipping normal faults.

4.2. Geological setting

4.2.1. Regional tectonic framework

The studied fault system is located in the Inner Moray Firth (IMF) basin (***Figure 4.1***). The basin is characterized by NE-SW striking normal faults that accommodated a Late Jurassic -Early Cretaceous extensional episode which resulted in the opening of the North Sea rift system (Ziegler, 1990; Thomson and Underhill, 1993; Davies et al., 2001). Some authors proposed a transtensional opening of the IMF basin (Roberts et al., 1990). We have no evidence for fault oblique displacement, but previous studies considered that faults in the area of interest are dominated by dip-slip displacement (Underhill, 1991; Davies et al., 2001; Long and Imber, 2010) and that any strike-slip movement was associated mainly with Great Glen Fault (to the northwest of the present study-area) and post-dated Mesozoic rifting (Underhill, 1991). Regional, Late Cretaceous post-rift subsidence and sedimentation were followed by Cenozoic uplift and reactivation of some of the faults. These faults show very mild post-Cretaceous reactivation, as indicated by small-scale folding of the Base Cretaceous horizon (H7 on ***Figure 4.1b***), but there is no evidence of large inversion structures affecting the geometries of the pre-inversion folds.

Figure 4.1 - next page (a) *Schematic structural map of Inner Moray Firth (IMF) basin (modified from Long and Imber, 2010). (**b).** Regional 2D seismic section across IMF, showing the main interpreted horizons and faults. **c.** TWT structural map of pre-rift horizon H1 (Top Triassic). The letters represent the names of the analysed normal faults from the 3D seismic data. The red rectangle delineates the detailed area of analysis. The yellow stippled lines mark the transvere fold hinges separating the depocenters associated with faults A and B.*

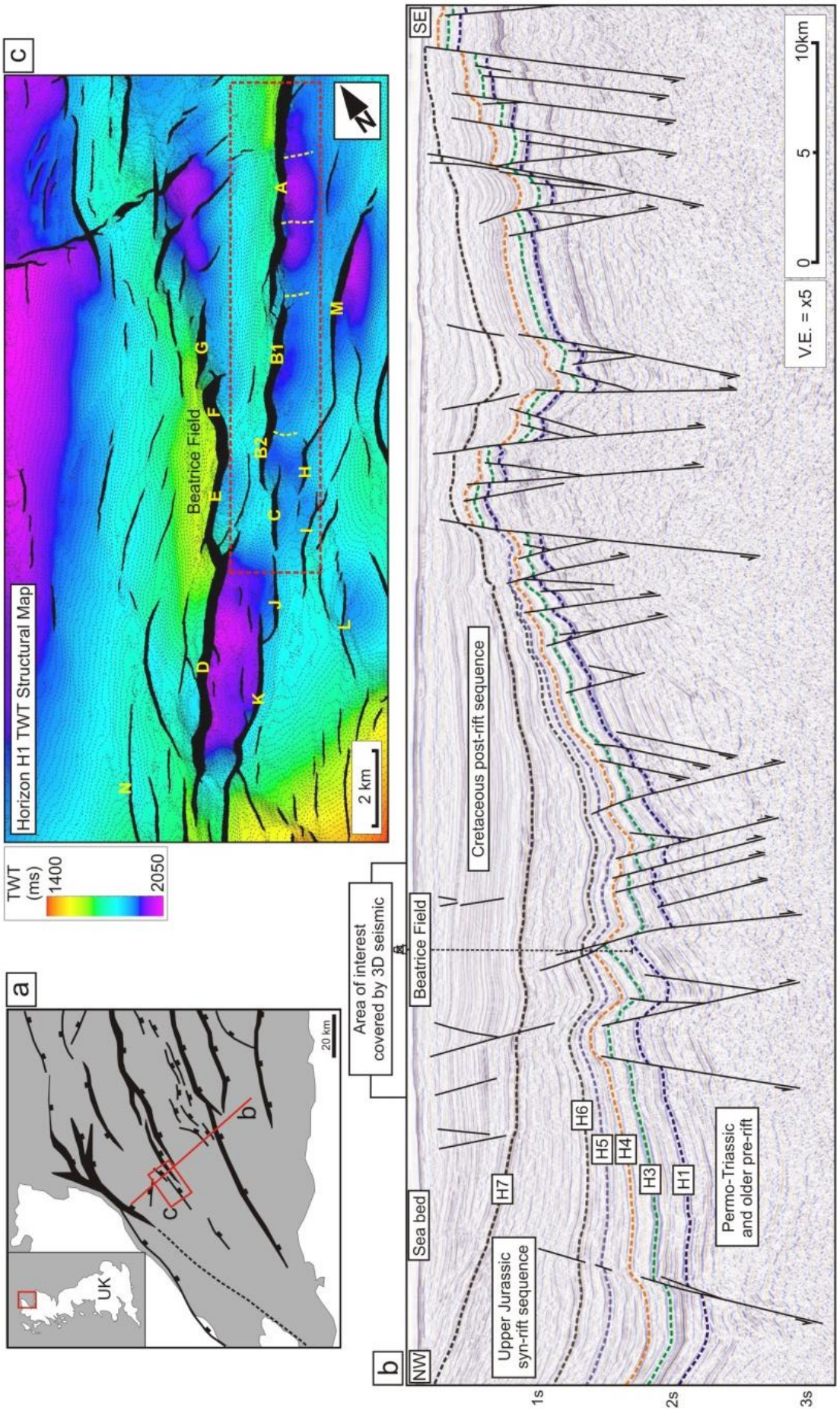
a
UK
20 km
b
c
Area of interest covered by 3D seismic
A
A'
NW
SE
Sea bed
Beatrice Field
Cretaceous post-rift sequence
Upper Jurassic syn-rift sequence
Permo-Triassic and older pre-rift
H1
H3
H4
H5
H6
H7
1s
2s
3s
V.E. = x5
0
5
10km
c
Horizon H1 TWT Structural Map
Beatrice Field
TWT (ms)
1400
2050
2 km
N
A
B1
B2
C
D
E
F
G
H
J
K
L
M

4.2.2. Stratigraphic framework and mechanical stratigraphy

The stratigraphy of the IMF can be divided into pre-, syn- and post-rift tectono-stratigraphic sequences (***Figure 4.1*** *and* ***4.2***). Our study investigates deformation within the upper part of the Triassic to Early - Middle Jurassic, pre-rift succession (pre-H3 horizons), and within the Late Jurassic, syn-rift succession (H3-H7) (***Figure 4.2***). We used information from nearby wells and published literature (Stevens, 1991) to infer the presence of three main mechanical units, based on stratigraphic variations in the net-to-gross ratio (***Figure 4.2***).

Horizon H1, which follows a strong and regionally continuous seismic reflection, corresponds to the top of the mechanical unit 1 (MU 1). Well data indicate that H1 follows the top of the pre-rift, Triassic alluvial plain sandstones of the Lossiehead Formation (> 100 m thick; ***Figure 4.2***). These strata overlie the Permian to Permo-Triassic Hopeman, Bosies Bank and Rotliegend formations, all of which are dominated by sandstone lithologies. In turn, the Permian deposits unconformably succeed the Devonian Old Red Sandstone (Goldsmith et al., 2003; Glennie et al., 2003). Based on the high net-to-gross of the Lossiehead Formation and underlying strata, we infer that MU 1 is likely to be mechanically "competent", here defined as being susceptible to deformation by seismic-scale faulting.

The upper part of the pre-rift sequence (H1-H3 interval; ***Figure 4.2***) comprises a ~300 m thick succession of interbedded sandstones and shales with a net-to-gross ratio of 38%, which we define as mechanical unit 2 (MU 2). We infer that the alternation of competent sandstones and less competent shale layers is likely to favour layer-parallel slip (Watterson et al., 1998). At the time of rifting, these Lower-Middle Jurassic sediments may have not been completely lithified, and were probably characterised by a reduced strength contrast between the sandstones and weaker shale layers. However, results of discrete element method modelling have shown that deformation can be partitioned between layers with small strength contrast at low confining pressure conditions (Schöpfer et al., 2007), with faults initiating in the slightly more competent sandstone layers. We hypothesise that thicker and relatively stiffer sandstone intervals within the MU 2, such as the 50-60 m thick "H" and "I" reservoir sandstones of the Beatrice Field (Stevens, 1991), may favour fault nucleation and

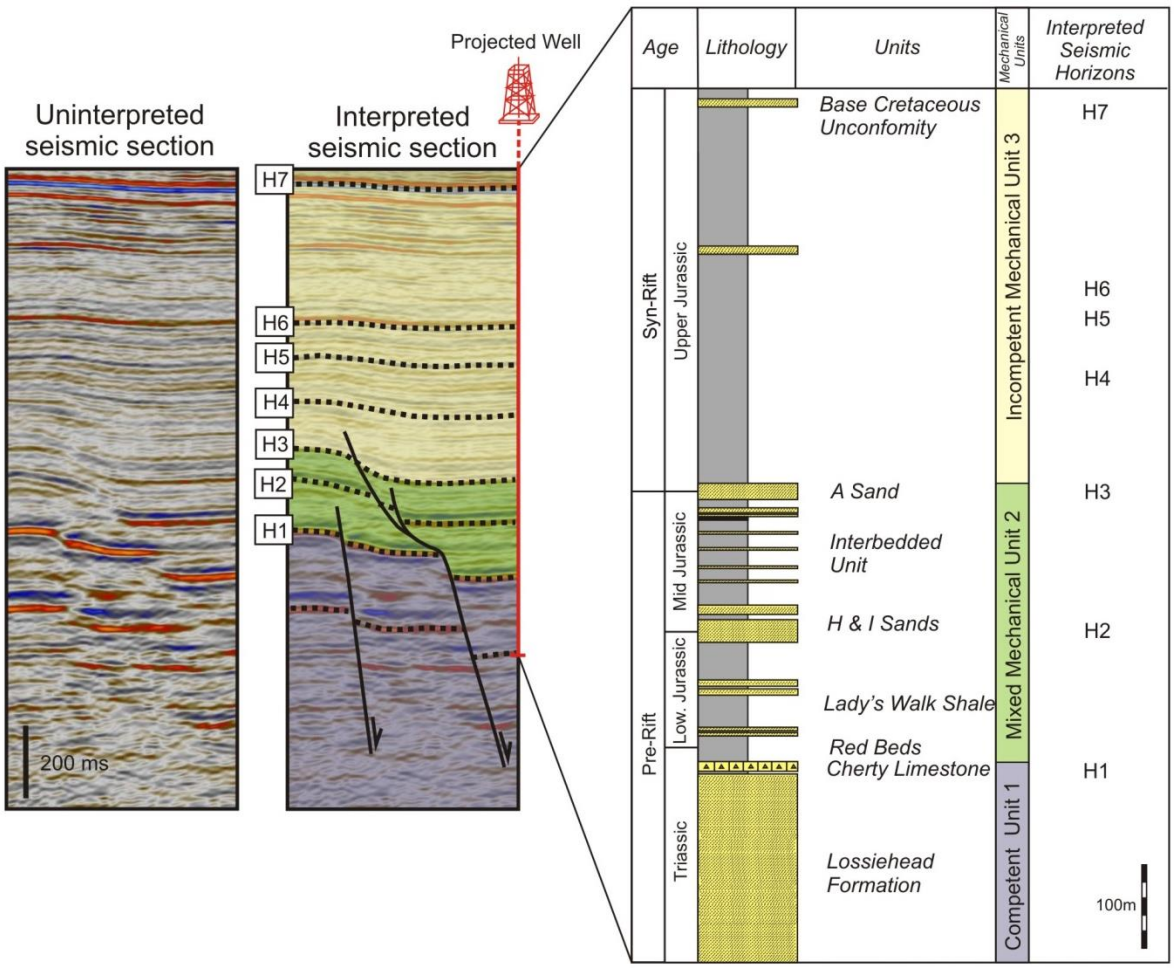

Figure 4.2 *Uninterpreted and interpreted seismic section (with x2 vertical exaggeration) from the studied 3D volume. The mapped horizons and the main mechanical stratigraphic units are shown in the interpreted version. Lithological formations were separated into three mechanical stratigraphic units based on the net-to-gross ratios obtained from the Beatrice Field well data.*

propagation (see Section *4.4.2.*), whilst the intervening shale intervals (e.g. Lady's Walk Shale) may inhibit fault propagation (***Figure 4.2***). This overall arrangement is likely to promote vertical segmentation of faults.

The syn-rift sequence (H3-H7 mapped horizons) thickens toward the main faults and is dominated by Upper Jurassic shales, which we define as mechanical unit 3 (MU 3). This succession is likely to be mechanically "incompetent", here defined as being susceptible to distributed (i.e. ductile) deformation. Hangingwall reflectors within several hundreds of metres of the mapped faults clearly

dip toward the graben (synthetic layer dips *sensu* Ferrill et al., 2005), with hangingwall syncline depocentres shifted away from the fault. Previously, these folds have been interpreted as the result of differential compaction of the shale-dominated syn-rift sequence (MU 3) overlying the older and more rigid pre-rift, footwall formations (MU 1 and 2) (Thomson and Underhill, 1993). While we do not exclude the possibility that some folds are the result of compaction, we show below that the analysed hangingwall folds display structural patterns that cannot be attributed to compaction, and that compaction effects are secondary with respect to other mechanisms.

4.3. Dataset and methods

4.3.1. Seismic and well data

The dataset used in this study comprises a 3D reflection seismic survey acquired over the Beatrice Field (Linsley et al., 1980; Stevens, 1991) and several regional 2D seismic lines that are orientated NW-SE, orthogonal to the main structure of the Inner Moray Firth Basin (***Figure 4.4***). The 3D time-migrated seismic data covers an area of 11 x 22 km, and has a crossline and inline spacing of 12.5 m. The dominant frequency for the interval of interest is between 30-40 Hz, with velocities ranging between 2500-3500 m/s (***Figure 4.3a***), resulting in a vertical seismic resolution of 15-30 m. Velocity data from the Beatrice wells indicates a consistently increasing velocity with depth, with no significant lateral or vertical velocity variations (***Figure 4.3a***). There are no significant variations in geometry between time and depth data, just a relatively uniform expansion by a factor of 1.55 on the depth profiles (***Figure 4.3b***). As a result, we used the two-way-time data to measure parameters such as fault throw and the amplitude of the hangingwall folds. However, when we analysed attributes such as fault dip, the fault surfaces have been converted to depth in order to show the realistic geometries of the faults. Eight seismic horizons were mapped in total (seven in detail: H1-H7) within the pre-rift and syn-rift stratigraphic intervals, with Beatrice Field wells providing information on the associated lithological formations. The study focusses on the segmented, SE-dipping ABC fault array (see box in ***Figure 4.1c***), supplemented by examples from other fault systems to highlight salient points.

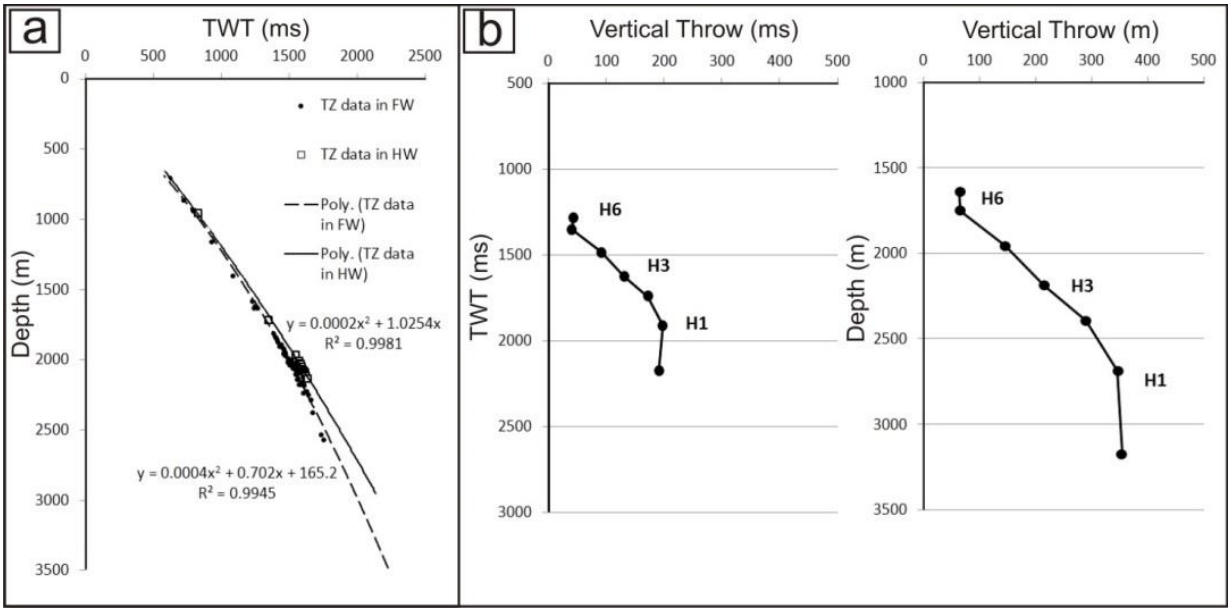

Figure 4.3 (a) *Time-depth (T-Z) curves from the Beatrice Field wells showing different velocity gradients for wells which penetrated the footwall or the hangingwall sections of the faults. For depth conversion, we used the T-Z relationship derived from the wells which penetrated the thicker syn-faulting sequences deposited within fault-controlled depocenters because we are interested in quantifying deformation located mainly within the hangingwalls of the faults. This younger, syn-faulting section is characterized by slightly lower velocities compared with the older pre-rift sequence in the footwall.* ***(b)*** *Comparison of throw distribution in time (ms) with throw distribution in depth (m). The pattern of throw distribution is very similar, but the throw-depth plot shows a vertical expansion of ~1.55.*

4.3.2. Methods

We used several methods to analyse the distribution and growth of the faults and folds:

(i) *Throw-distance (T-x) profiles* and *throw-depth (T-z) profiles* enabled us to investigate the lateral and vertical variations in discontinuous fault throw and continuous deformation (folding), and to analyse the lateral and vertical linkage of faults (Walsh and Watterson, 1991; Childs et al., 1996; Mansfield and Cartwright, 1996; Hongxing and Anderson, 2007; Long and Imber, 2010; Tvedt et al., 2013; Jackson and Rotevatn, 2013; Rotevatn and Jackson, 2014). For T-x profiles, fault throw was measured perpendicular to the strike of the fault every 125 m (every 10th inline), with more dense sampling points near the fault tip or where the fault complexity required it;

(ii) *Isochore thickness maps* and *expansion indices* were used to analyse the timing of faulting and folding (Tvedt et al., 2013; Jackson and Rotevatn, 2013) and to constrain the position of the upper tip-line at the time of deformation. The expansion index (Thorsen, 1963) is defined by the ratio between the maximum thickness of a chosen syn-rift interval in the hangingwall of a fault (adjacent to the fault surface, or within the synclinal depocentre) and the thickness of the equivalent interval in the footwall;

(iii) *Fault surface analysis* provided insights into the relations between fault geometry and linkage style, expressed by parameters such as fault dip, fault cylindricity and throw variation (Ziesch et al., 2015), and distribution of ductile deformation. Cylindricity measures the deviation of a fault surface from a best-fit planar surface (Ferrill et al., 1999; Jones et al., 2009; Ziesch et al., 2015);

(iv) *Seismic trace and coherency attributes* (a combination of instantaneous phase, tensor, discontinuity and semblance attributes) (Chopra and Marfurt, 2007) were used in some cases to enhance the visibility of deformational patterns at the limit of seismic resolution within the hangingwall folds (Iacopini and Butler, 2011), or to highlight the fold geometry (dip, dip-azimuth) and stratal onlaps onto fold limbs.

4.4. Observations of normal faults and fault-related folds from 3D seismic data

4.4.1. Geometric characteristics of the studied faults and fault-related folds

At H1 (Top Triassic) level, the studied fault system comprises three left-stepping normal fault segments named A, B and C. These are separated by two relay zones. The relay ramp between faults A and B is at an early stage of breaching (***Figure 4.1c***). At the base syn-rift level (H3), the relay ramps are completely breached by the footwall faults, forming a continuous fault trace. Bends in the fault trace are associated with minor, hangingwall splay faults (***Figure 4.4a***). This downward bifurcation, (with intact or partially breached relay ramps at depth, and breached relay ramps at shallower levels), seems to be a common feature in our area of study (see *Section 4.4.2.*).

The seismic sequence between the H3 and H7 horizons thickens toward the analysed faults, consistent with their syn-sedimentary nature. The ABC fault array is part of a larger NE-SW striking normal fault system that dips SE, along with the faults bounding the Beatrice Field structure, here named D, E, F and G. These two major fault systems are linked within the syn-rift sequence (on horizons H6-H7) by smaller segments (segments b and c) that splay upward from the main faults (***Figure 4.4b*** and ***4.4c***). The upper tip-lines of fault C and the SW continuation of fault B (named B2) are buried within the H3-H5 interval, and are overlain by parallel seismic reflections. These observations indicate that the faults become inactive during the later syn-rift stage, when linkage of the AB fault with the D fault occurred. Faults B2 and C are located within a larger syn-rift transfer zone comprising the synthetic dipping D and E faults, but also the opposite (NW) dipping faults H, I and J (***Figure 4.4a***), with which B2 and C form a conjugate normal fault pair (***Figure 4.4d***).

At H1 level, we observe that the deepest structural levels lie immediately adjacent to the fault trace (***Figure 4.1c***), whilst at H3 (base syn-rift) and H6 (intra-syn-rift) levels, the depocentres are shifted further into the hangingwall, with increasing distance from the fault on progressively younger syn-rift horizons (***Figure 4.4a*** and ***4.4b***). At H3 level, the faults are bordered on the hangingwall side by monoclinal folds with limbs that dip in the same direction as the fault (***Figure 4.4a*** and ***4.4c***). However, not all the faults are associated with folds at horizon H3 level: faults B2 and C appear to have depocentres adjacent to the fault trace (***Figure 4.4a*** and ***4.4d***). Hence, an intriguing question is why do some faults display hangingwall folds and depocentres that are shifted into the hangingwall, whilst others in the same array lack folds and are characterized by depocentres adjacent to the fault trace? The fact that the folds are developed within the *pre-rift* sequence, and that their location does not necessarily correspond with the major depocentres suggests that the generating process cannot be entirely attributed to differential compaction (cf. Thomson and Underhill, 1993).

Seismic attribute analysis using the instantaneous phase attribute (Chopra and Marfurt, 2007) shows that folds associated with the B2 fault are associated with clear, antithetic-dipping axial planes that separate the upward-widening monocline from the hangingwall synclines *(**Figure 4.5a*** and ***4.5b***). This fold does *not* display vertical axial planes and thinner hangingwall dipping limbs, which are

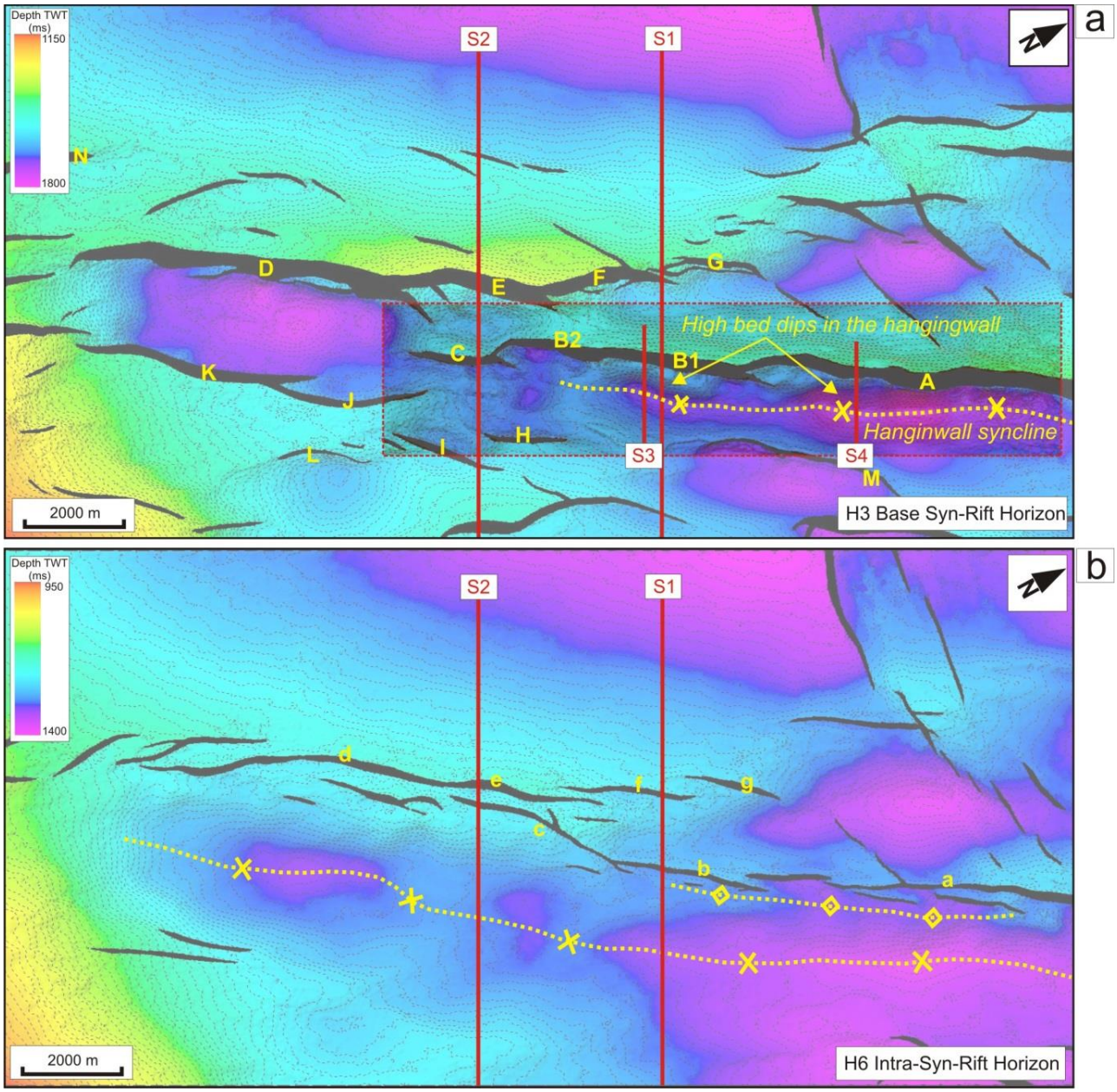

Figure 4.4 (a) *TWT structural map of horizon H3 (top pre-rift and top mechanical unit 2); the letters represent the names of the analysed normal faults from the 3D seismic data. The red rectangle borders the A, B and C faults which are analysed in detail. The traces of the faults A and B are bordered by longitudinal folds on the hangingwall side. The steepest reflector dips occur on the fold limb adjacent to the fault traces and are consistently down towards the basin.* ***(b)*** *TWT structural map of horizon H6 (intra syn-rift). Note the basinward migration of the hinge line of the hangingwall syncline and the decrease in the density of the faults compared with the fault density within the pre-rift sequence (see Figure 4.1c or 4.4a).* ***(c)*** *and* ***(d)*** *interpreted seismic profiles orthogonal to the studied faults. Location in Figure 4a and b (see text for detailed description).*

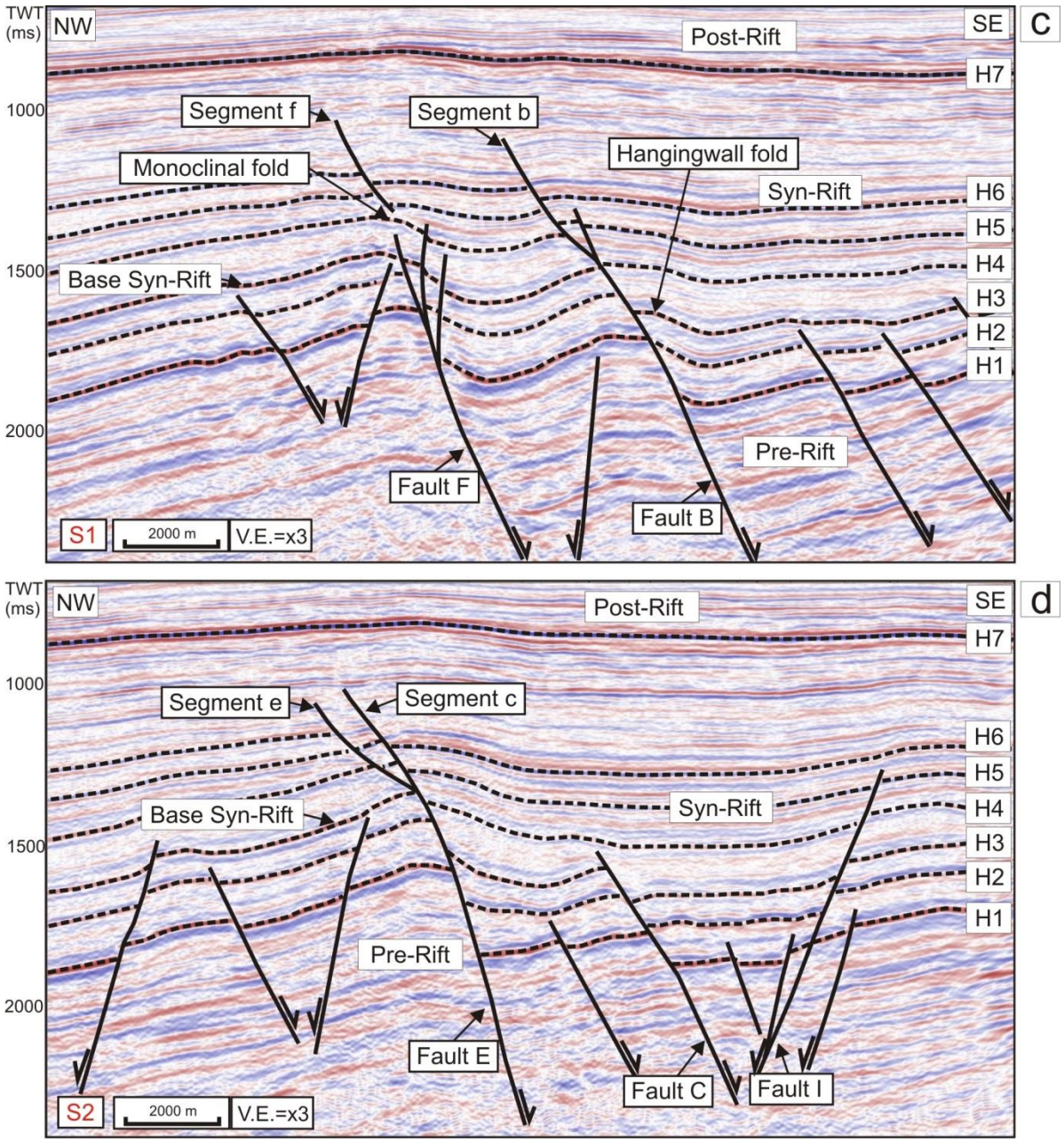

Figure 4.4 (c) *and* ***(d)*** *Interpreted seismic profiles orthogonal to the studied faults. Location in* ***Figure 4.4a*** *and* ***b*** *(see text for detailed description).*

characteristic for compaction folds in the hangingwalls of normal faults (Skuce, 1996). The instantaneous phase attribute also highlights seismic reflections within the syn-rift sequence that onlap onto the steep limb of the monocline. These onlaps are an indication of the fold growth, rather than the effect of compaction. Furthermore, a combined tensor-semblance-discontinuity attribute (Henderson et al., 2012) indicates the presence of secondary faults (steeply dipping normal faults or even small reverse faults) associated with the monocline that, presumably, accommodated folding (***Figure 4.5c***). These secondary faults resemble structures of normal fault-propagation folds modelled in clay (Withjack, et al., 1990), and described in other rift settings which exhibit extensional fault-propagation folds, e.g. Suez Rift, NW Egypt (Sharp et al., 2000; Khalil and McClay, 2002). Fault dips are commonly observed to be gentler within the syn-rift and late pre-rift sequences (mechanical units 3 and 2) compared with the early pre-rift sequence (MU 1) (e.g. see segments b, e and f in ***Figure 4.4c*** and ***4.4d***; and the fault dip attribute map in ***Figure 4.9b***). The change in fault dip therefore corresponds to the change in lithology from the mechanically competent Triassic sandstones (H1 and below), to the Lower-Middle Jurassic interbedded shale-sandstone succession (H1-H3) and Upper Jurassic shales (H3-H7). The overall effect is to generate pronounced convex upward fault geometries (***Figure 4.4c*** and ***4.4d***) but, because the upward transition to gentler fault dips occurs within the *pre-rift* interval, differential compaction should be secondary in respect to other factors. We can explain the difference in dips by the variation in shear failure angles within rocks that have different mechanical properties (Mandl, 1988), with higher angle faults developed within the mechanically competent Triassic sandstones (MU 1). These observations have important consequences for understanding the vertical segmentation of faults across the different mechanical units, a point we return to in the following section.

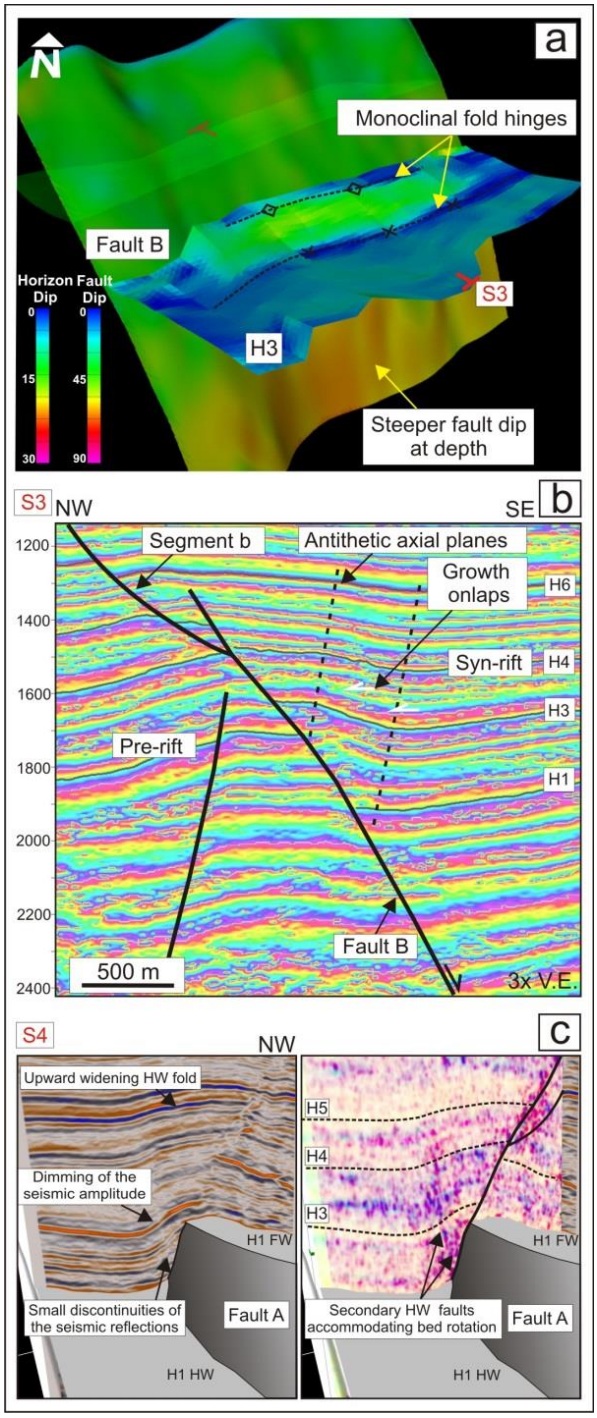

Figure 4.5 (a) *3D view of the breached monocline along Fault B;* ***(b)*** *Section (S3) displaying the instantaneous phase attribute and showing the breached monoclines associated with Fault B. The instantaneous phase attribute enhances visualization of the reflector configuration, and highlights the onlap of reflectors onto the limb of the monoclinal fold.* ***(c)*** *Hangingwall fold associated with Fault A (location in Figure 4.4a) with combined tensor-semblance-discontinuity attribute volume (right) that enhances visualization of secondary faults within the hangingwall of Fault A.*

4.4.2. Spatial and stratigraphic variations in fault throw and fold amplitude

Figure 4.6 is a T-x profile showing the variation in throw (i.e. the discontinuous component of vertical displacement) along the strike of faults A, B and C. We observe a systematic decrease in throw towards the SW, with the largest throws within the pre-rift sequence (H1 level) reaching 300 ms (~450 m) along fault A and decreasing to a maximum of ~100 ms (~155m) along fault C. Note that fault A continues beyond the NE limit of the 3D seismic volume. The profiles for faults A and B display distinct throw minima that correlate with undulations in the fault trace, fault surface corrugations and the locations of transverse hangingwall folds (***Figure 4.1c***, ***Figure 4.6*** *and* ***Figure 4.9a***). These observations suggest that at H1 level, fault A comprises at least three linked fault segments and fault B comprises two linked segments (B1 and B2 in ***Figure 4.1c***). We propose that faults A and B formed through the coalescence of multiple fault segments and that "corrugation zones" mark the locations of former segment boundaries (***Figure 4.6*** *and* ***Figure 4.9a***).

The syn-sedimentary nature of the faults is reflected by a systematic, upward decrease in throw within the syn-rift interval (H3-H7) (***Figures 4.6*** *and* ***4.7***), and by the horizontal pattern of the throw contours projected onto the fault surface (***Figure 4.8***) (Childs et al, 2003). Some of the throw-depth (T-z) profiles display an upward decrease in throw within the *pre-rift* interval (between H1 and H2-H3 for profiles P2-P6; ***Figure 4.7***) as a consequence of folding. ***Figure 4.6*** shows that the amplitude of folding (measured on H3) approximately compensates for decreases in throw, and varies significantly along the strike of the fault. Folds are not observed adjacent to faults B2 and C, which display throw maxima at H3 level, i.e. at the top of the pre-rift interval (profiles P7-P9, ***Figure 4.7*** and ***Figure 4.8***). Another observation that can be made from the T-z profiles is that within the syn-faulting interval, the throw values for H6 and H5 markers are very similar (***Figure 4.7***), which indicates either that the ~40-50 ms (60-80 m) displacement post-dated deposition of H5-H6, or that the ratio of fault throw rate to sedimentation rate may have decreased during this interval.

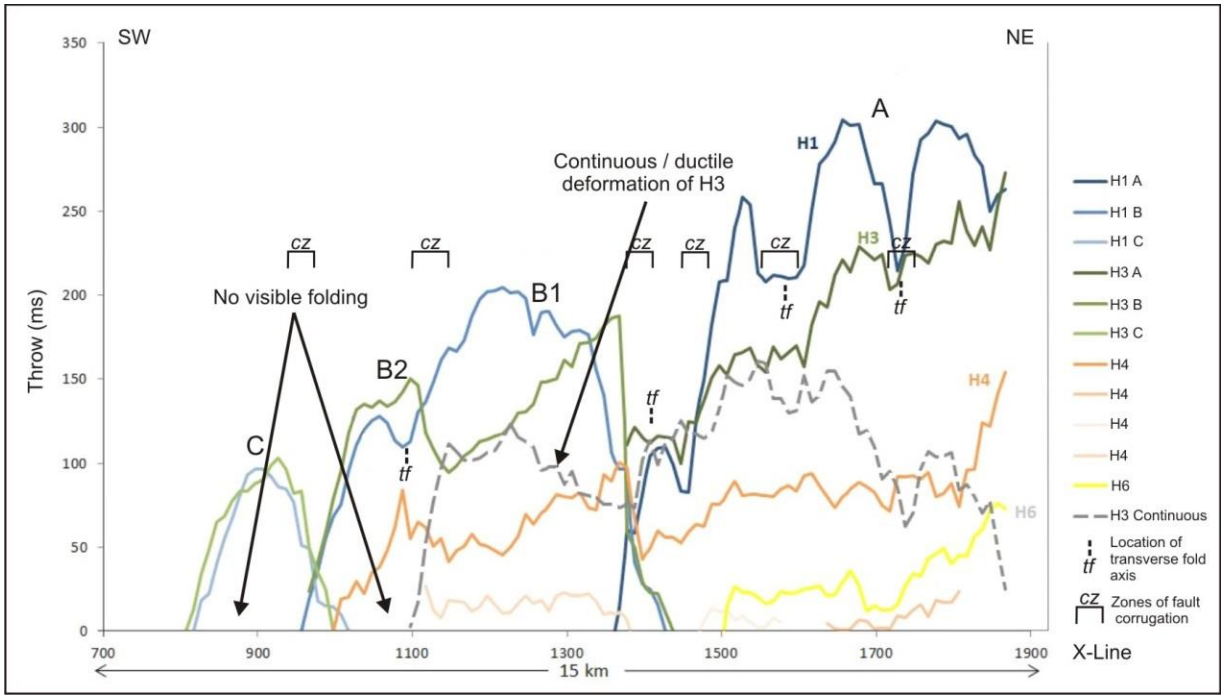

Figure 4.6 *Throw-distance profiles for the 3 analysed fault segments A, B and C (located in Figure 4a). The throw decreases systematically from NE (right) to SW (left), and from the pre-rift (H1) to syn-rift horizons (H3-H6 horizons). The component of ductile deformation (folding) on the H3 horizon was measured separately (stippled line).*

Previous studies have shown that bends in a fault plane, such as those described in the previous section, can result from vertical fault segmentation and linkage within an incompetent mechanical unit (Childs et al, 1995). Fault L (***Figure 4.1c***, ***Figure 4.2*** and ***Figure 4.10***) provides a clear example of vertical segmentation across contrasting mechanical units. ***Figure 4.2*** and ***Figure 4.10c*** show there is a marked upward decrease in the dip of fault L, which corresponds to the lithological boundary between the mechanically competent Triassic sandstones of MU 1 and the interbedded, Early-Middle Jurassic succession of MU 2. This change in dip coincides with a throw minimum that separates two distinct throw maxima within MU 1 and the Middle Jurassic H and I Sands (H2) within MU 2 (***Figure 2*** and ***Figure 4.10 b***). Based on these observations, we infer that the upper, en-echelon segments La, Lb and Lc (***Figure 4.10***) probably nucleated within the Middle Jurassic H and I sands, and linked with the deeper L1 and L2 segments within the underlying, incompetent Lady's Walk Shale formation.

This vertical linkage generated a convex upward fault geometry, with a pronounced bend developed in the linkage zone (***Figure 4.2***), expressed by the gentle fault dips and displacement minima (Childs et al, 1996). The fault bend geometry is controlled by the spatial position of the upper segments (e.g. La, Lb and Lc) relative to the location of the deeper main faults (e.g. L1 and L2). Essentially, the fault bend (or fault ramp) is controlled by the separation distance between the vertically segmented normal faults, with the widest ramp corresponding to the largest segment separation. As a consequence, the locations of the bends in the fault plane can be variable along strike of the fault array and explains the observed geometries of the analysed faults (***Figures 4.9*** and ***Figure 4.10***). The changes in fault dip correspond, in some cases, with downward-bifurcation of fault segments, in which relay ramps are breached at shallower levels but remain intact at depth (***Figure 4.10***). These fault patterns, which are similar to the geometry of the faults A and B, are unusual for coherent fault models that describe fault growth by upward-bifurcation (Walsh et al, 2003), suggesting again vertical linkage (Marchal et al., 2003; Jackson and Rotevatn, 2013; Rotevatn and Jackson, 2014) by downward propagation of segments that nucleated within the shallower Jurassic sequence.

The relationship between vertical segmentation and folding is illustrated in ***Figure 4.4c*** and 4.***4d***. Here, we observe that segments b, e and f dip gently within the syn-rift section and that the linkage with the deeper main faults varies along strike. Close to its lateral tip (where the displacement is small), fault F is not hard-linked to the overlying segment f. Instead, the two faults are separated by a monocline that overlies the upper tip line of fault F (***Figure 4.4a***, ***4.4b*** and ***4.4c***). Analogue models indicate that discontinuities within layering (analogous to the heterogeneities in mechanical properties of the MU2 and MU3) tend to promote breaching of the monocline by downward propagation of a fault that nucleates at shallow depths above the footwall of the main, underlying fault, and which are not initially hard-linked to the main fault (Bonini et al., 2015).

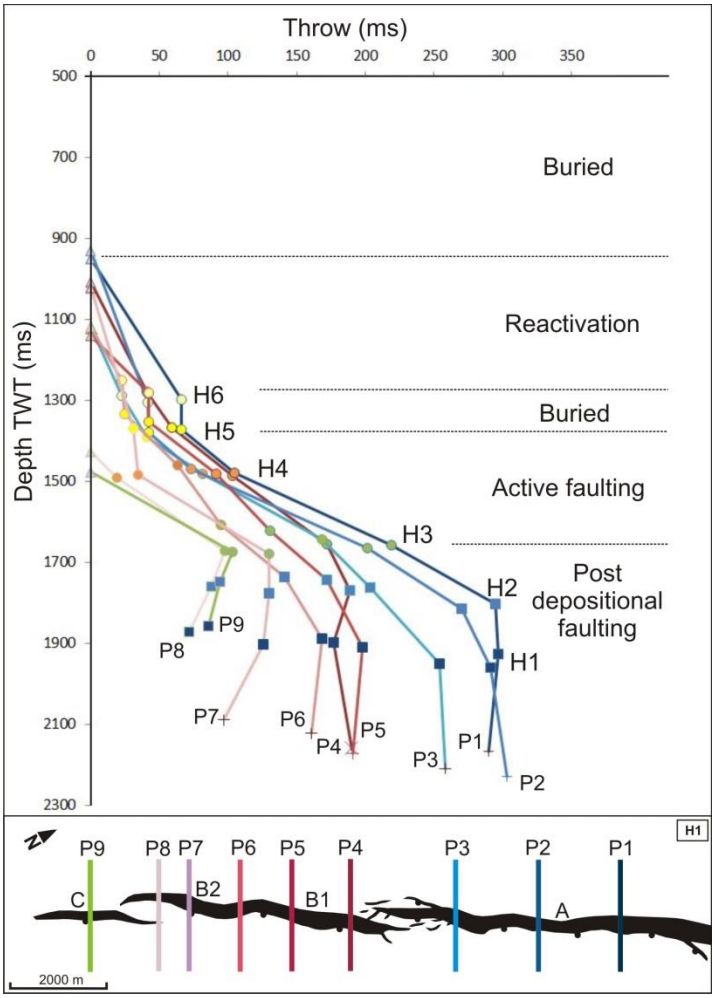

Figure 4.7 *Throw-depth (ms) plots for 9 profiles across the studied faults. The maximum throw is located within the pre-rift section (pre-H3) but varies along the strike of the fault array. The SW part of the B segment and C segment (P7-P9) are characterised by throw maxima at the base syn-rift level (H3). For the other profiles, the lower throw values at base syn-rift are the result of folding.*

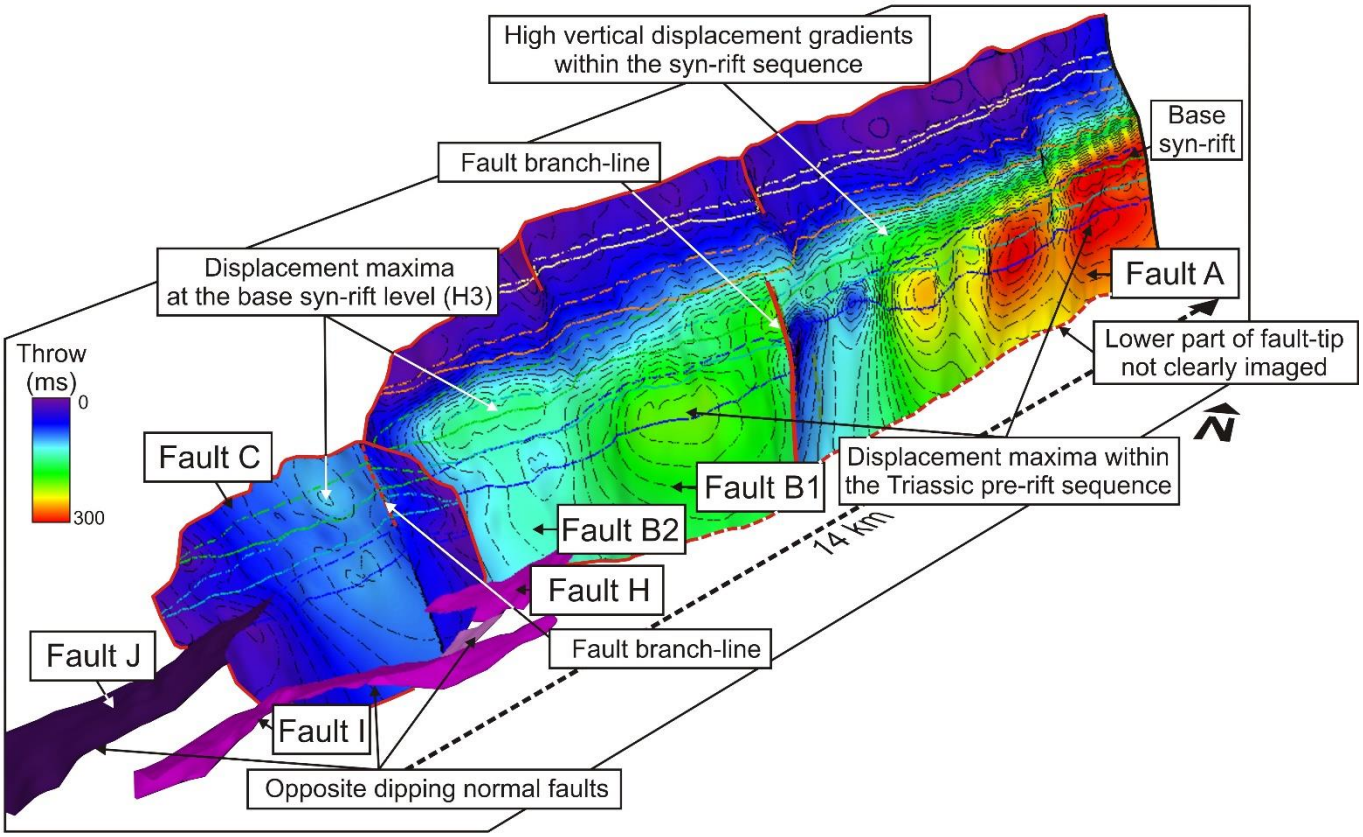

Figure 4.8 *Throw distribution on the A, B and C faults, with horizon cut-offs projected onto the fault surface (continuous line for hangingwall cut-offs and discontinuous line for footwall cut-offs). Note that the maximum displacement is located within the pre-rift sequence for the A and B1 faults. For faults B2 and C, the maximum displacement is shifted upwards towards the base syn-rift.*

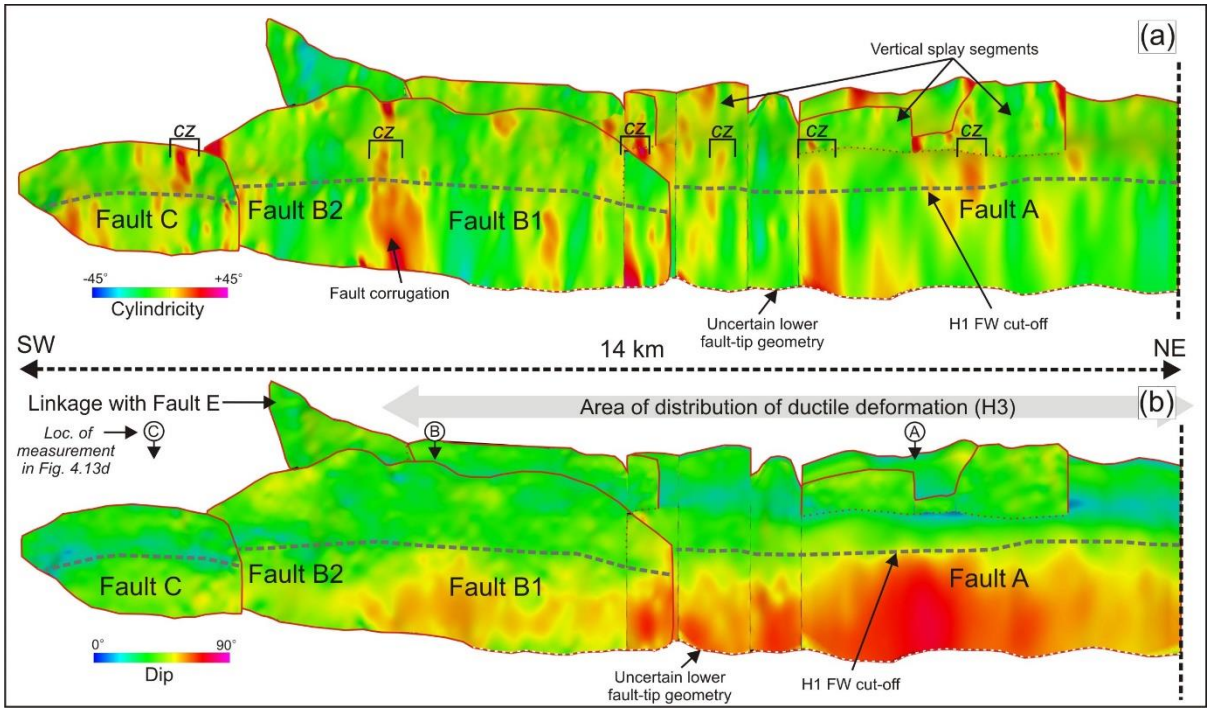

Figure 4.9 *Strike projections of the analysed fault surfaces displaying:* ***(a)*** *Fault cylindricity attribute indicating possible zones of lateral corrugation (cz); The cylindricity attribute calculates the average deviation relative to the best fit surface plane (in Move);* ***(b)*** *Fault dip – note the sharp decrease in fault dip above horizon H1. This change in dip corresponds with a change in lithology, from the Triassic sandstone (mechanical unit 1) to Jurassic shale-sandstone interbedded sequence (mechanical unit 2; see Figure 4.2).*

Figure 4.10 – next page (a) *3D diagram showing segmentation of Fault L (location in Figure 4.1c and 4.5a) and the main interpreted horizon surfaces adjacent to the fault. Fault-related deformation is characterised by the high bed dips associated with the uppermost surface (H3) in the vicinity of the fault trace Lc and above the adjacent blind segments.* ***(b)*** *Strike projection of Fault L contoured for throw.* ***(c)*** *Strike projection of Fault L contoured for dip.*

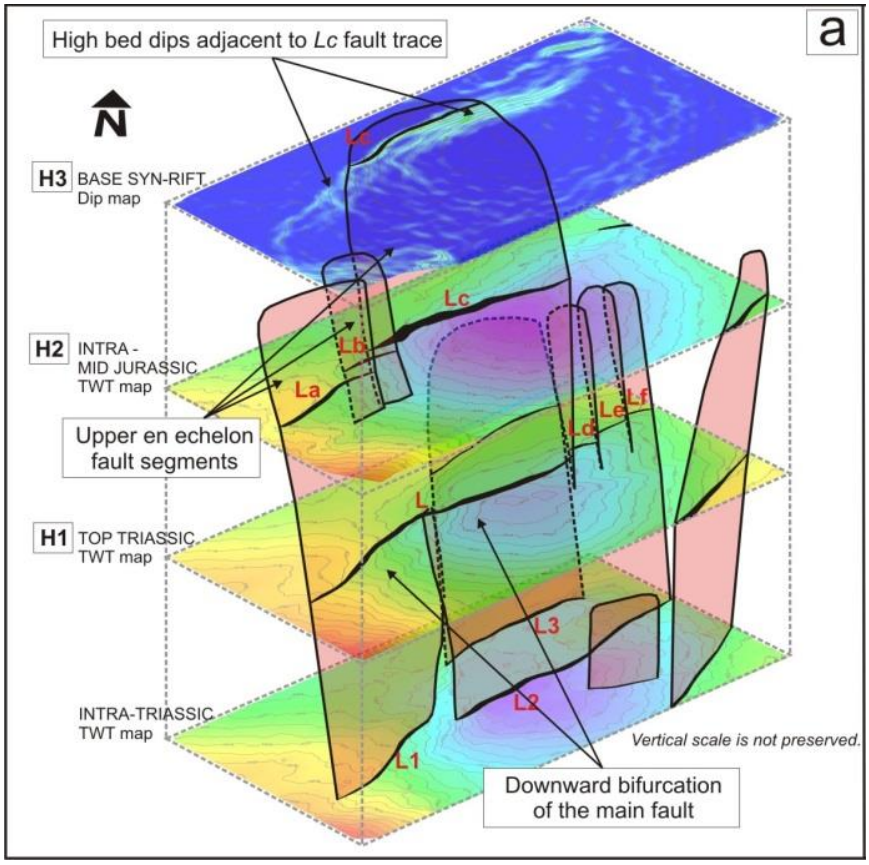
a
High bed dips adjacent to Lc fault trace
N
H3 BASE SYN-RIFT Dip map
H2 INTRA - MID JURASSIC TWT map
H1 TOP TRIASSIC TWT map
INTRA-TRIASSIC TWT map
Upper en echelon fault segments
Downward bifurcation of the main fault
Vertical scale is not preserved.
La
Lb
Lc
Ld
Le
Lf
L
L1
L2
L3

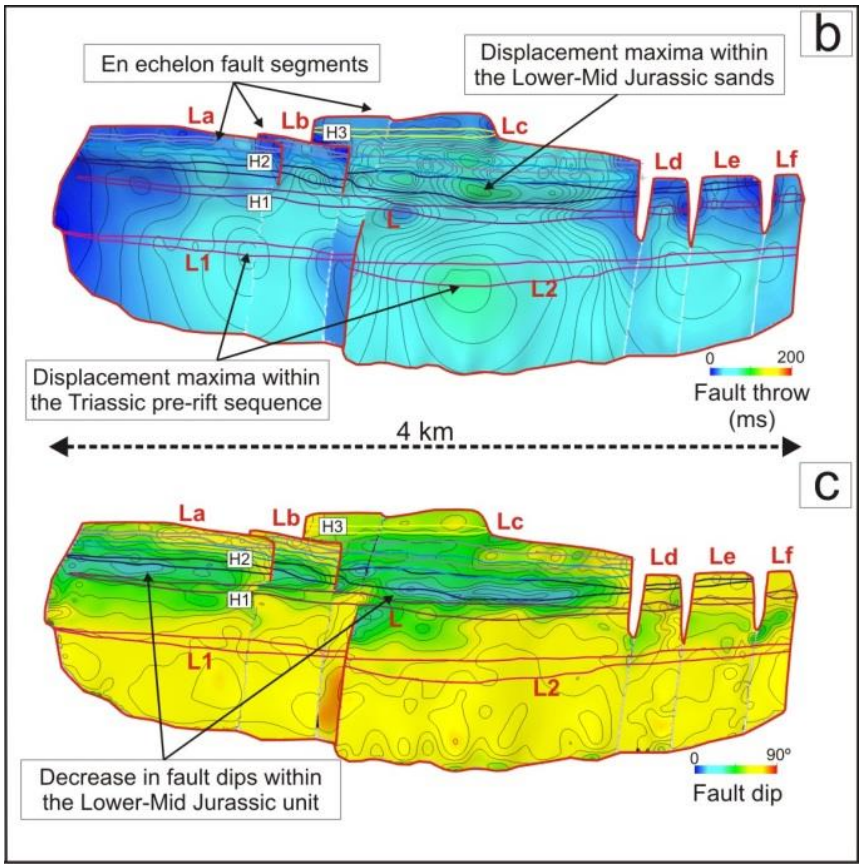
b
En echelon fault segments
Displacement maxima within the Lower-Mid Jurassic sands
Displacement maxima within the Triassic pre-rift sequence
H3
H2
H1
La
Lb
Lc
Ld
Le
Lf
L
L1
L2
0
200
Fault throw (ms)
4 km
c
0
90°
Fault dip
Decrease in fault dips within the Lower-Mid Jurassic unit

A similar situation is indicated by high reflector dips observed above other fault arrays within the 3D seismic volume. For example, horizon H3 displays high reflector dips above the tip lines of segments La, Lb and Lc (***Figure 4.10a***, H3 horizon dip map). This observation is consistent with folding ahead of the propagating tip of the "L" segments (Ferrill et al., 2007; Long and Imber, 2010). With increasing displacement, we suggest that the monocline (expressed by high reflector dips at H3 level), is likely to be breached completely and subsequent translation of the hangingwall across the convex upwards fault plane will increase the amplitude of the initial fault propagation fold, possibly completely overprinting it. The final amplitude of the fold will therefore vary along strike as a function of the initial amplitude of fault propagation-fold, the amount of throw, and the geometry of the fault bend.

4.4.3. Summary of key observations and inferences

Mechanical unit 1 is characterised by steeply dipping faults that accommodated localized displacement with little evidence for associated folding. Fault dips are gentler within MU 2 and 3, reflecting the lower shear failure angles associated with these mechanically less competent units, and vertical linkage zones with the main faults. Fault propagation folds overlie the upper and lateral tip lines of faults within MU2 and 3, and we infer that the competence contrast between MU 1 and the overlying strata promoted vertical segmentation and linkage of faults. Contrary to a previous study, several observations suggest that differential compaction is unlikely to have been the primary mechanism responsible for fold generation. We now investigate the fold growth in more detail.

4.4.4. Folding mechanisms

Fault-propagation folding

Isochore thickness maps provide insights not only into the growth of the faults but also on the early growth and development of the fault related folds. ***Figure 4.11*** shows the stratigraphic thickness of

the early syn-rift interval (H3-H4). Hangingwall syncline depocentres are observed along the strike of faults A and B. ***Figure 4.11b*** is a graph of the stratigraphic thickness of the H3-H4 interval measured along strike of the fault in the footwall, in the hangingwall and within the hangingwall syncline. We observe that the maximum recorded thickness is located predominantly within the syncline depocentres. Similar thicknesses in the footwall and in the proximal part of the hangingwall along parts of A and B suggests that, at the time the H3-H4 sequence was deposited, parts of these faults were blind and overlain by a gentle monocline, with growth strata onlapping the monocline limb (***Figure 4.11b*** and ***Figure 4.10***). At this stage, the amplitude of the monocline reached ~ 40 ms (50-60 m), indicated by the difference in the real stratigraphic thicknesses of the syn-faulting deposits in the syncline and in the proximal part of the hangingwall, with the condition that this latter thickness is similar to the stratigraphic thickness in the footwall (***Figure 4.11b***). We suggest that vertical propagation of faults A and B was inhibited within the ductile, shale-dominated Early-Middle Jurassic sediments, most likely within the Lady's Walk Shale Formation, considering that horizon H2 is also folded. Other faults from the study area that exhibit vertical segmentation (e.g. faults L, N) display lateral offsets or dip linkage (and associated bends in the fault plane) within the same stratigraphical level.

The formation of a fault propagation fold is controlled by the relative position of the upper tip-line of the faults with respect to the mechanical stratigraphy, in our case, by the presence of MU 2. Our observations show that the elevation of the vertical tip-line was very variable along the strike of the fault ABC, hence a question arises: why in some places was the upper tip line buried beneath the free surface (developing a fault propagation-fold) whilst in other places, for example along the conjugate fault pairs B2-H and C-I, did the fault breach the depositional surface shortly after the onset of rifting? We do not have any evidence from wells, or from the analysis of the seismic facies, of any significant lateral changes in lithology or a decrease in thickness of MU 2, which together could enhance upward propagation of the faults and early surface breaching. Expansion indices (Thorsen, 1963) show constantly higher values for faults C and B2 for the H3-H4 interval, compared with segment B1 and parts of A (***Figure 4.11c***).

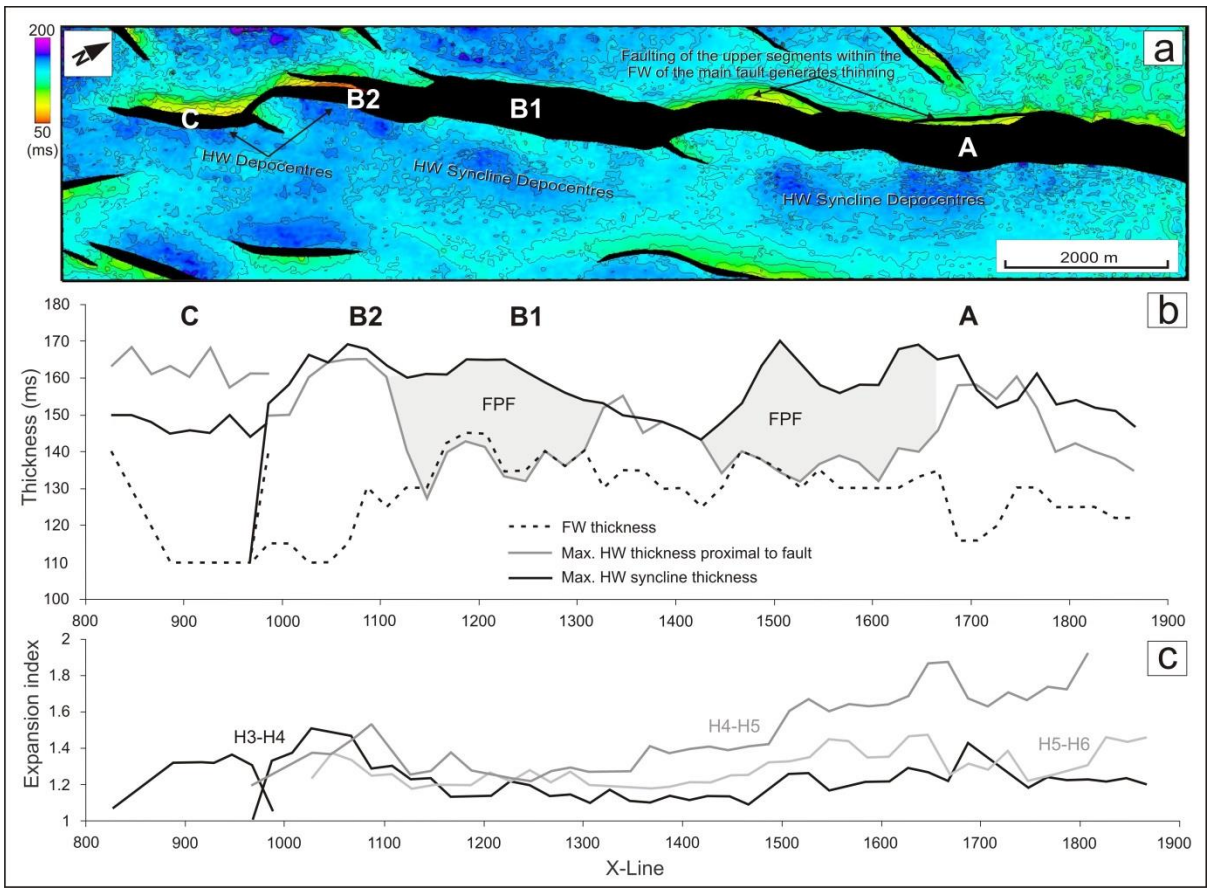

Figure 4.11 (a) *Isochore thickness map of the H3-H4 early syn-rift sequence.* ***(b)*** *Graph with the thickness of the H3-H4 growth sequence measured in the immediate vicinity of the fault trace, in the footwall (dashed red line), in the hangingwall (light black line) and in the hangingwall syncline (bold black line). The fault propagation folds (FPF) are identified where maximum thicknesses are recorded within the hangingwall syncline, and the thicknesses of syn-rift strata within the footwall and proximal part of the hangingwall are similar.* ***(c)*** *Expansion indices measured along strike of the faults.*

These high expansion indices can be an indicator of the high displacement rates on these two faults during deposition H3-H4, which is consistent with their early breaching of the surface. We propose a mechanical explanation for these observations in the *Discussion* section.

Fault-bend folding

The present-day fold amplitudes on horizon H3 are very variable (stippled line on the T-x profile, ***Figure 4.6***), and larger than the amplitudes inferred to be solely the result of initial fault propagation folding (***Figure 4.11***). ***Figure 4.9b*** shows that the lateral distribution of folds correlates well with the extent of regions characterised by upward decreases in dip of the ABC fault plane. We observe that the fold amplitude is largest where there is a more pronounced change in the fault dip with depth (adjacent to faults A and B1) (***Figure 4.6***). The increase in the fold amplitude of H3 also seems to correlate with increasing displacement of the H1 horizon (***Figure 4.6***). At shallower levels, ***Figure 4.4b*** and ***4.4c*** show that the H6 horizon developed a broad anticline flanked by a depocentre immediately adjacent to the trace of fault b, and another broad, distal synclinal depocentre parallel with the fault trace. This morphology is similar to the hangingwall geometries developed above ramp-flat-ramp normal faults (McClay and Scott, 1991; Rotevatn and Jackson, 2014). We will come back to discuss the relation between fault-bend and fold amplitude in the following sections.

4.5. Analysis of normal faults and fault-related folds from a regional (basin-wide) dataset

4.5.1. 2D geometry of faults and fault-related folds

To obtain a more representative sample of the extensional fault-related folds from the IMF basin, we analysed a further 57 cross-sections from the regional 2D seismic dataset in addition to measurements of the 18 faults interpreted from the 3D survey. Examples of the analysed extensional folds are illustrated in ***Figure 4.12***. Most of the faults terminate within the syn-rift sequence and are associated with monoclinal folds above their upper tip points (***Figure 4.12a*** and ***4.12b***). Some of the monoclines are breached by their associated faults, resulting in normal drag-like fold geometries within the hangingwall (***Figure 4.12e***). The following key observations suggest that the analysed monoclines originated as fault propagation folds: (i) the folds display an upward widening geometry; (ii) there is a qualitative relationship between the amplitude of the monoclines (breached or unbreached) and the amount of throw recorded within the pre-rift sequence; and (iii) in some, but not all cases, reflectors

within the syn-rift sequence onlap onto the fold limbs (***Figure 4.12a***, ***4.12b*** and ***4.12c***). Where stratal onlaps are absent, seismic reflectors within the syn-rift sequence have a sub-parallel to slightly divergent pattern away from the fault, with minor differences in thickness between the hangingwall and footwall strata. This observation can be explained by the relatively high sedimentation rates (150-400 m/Myr) in this part of the basin (Davies et al, 2001), which exceeded the relatively low fault displacement rates (Nicol et al, 1997). This interpretation is consistent with the relatively low expansion indices for the H3-H4 interval, compared to the younger analysed intervals (***Figure 4.11c***). Consistent with our interpretations of the 3D seismic data, breaching of fault propagation folds occurs either by upward propagation of the main faults from below, or by downward propagation of shallower fault segments that nucleate within the syn-rift sequence (i.e. MU 3), typically within the footwall domain of the monocline (***Figure 4.12c***, ***4.12e*** and ***4.12f***). In the latter case, *v*ertical linkage with the deeper faults may give rise to irregular fault traces.

In summary, our observations and inferences based on the basin-wide, 2D seismic dataset corroborate our initial conclusions based on detailed analysis of the (spatially restricted) 3D seismic dataset, providing confidence in the general applicability of our results. We now undertake a quantitative analysis of fold growth and breaching using the combined results from both datasets.

4.5.2. Quantitative analysis of fold growth and breaching

Our observations show that conjugate faults (e.g. faults B2, C and H, I) tend to breach the depositional surface soon after the onset of rifting. We therefore sub-divide the data into two categories based on the fault geometry. "Simple" normal faults are those *not* associated with a conjugate pair, whilst "conjugate" normal faults are those that interact (and may share a sub-horizontal branch-line) with opposite-dipping faults (***Figure 4.12*** and ***Figure 4.13***). Conjugate normal faults may display a cross-sectional V-style geometry if throw is similar on both faults and a Y shape, if displacement is larger on one fault than the other (Nicol et al, 1995). The amplitudes of breached and intact monoclines were measured for two horizons, H3 and H4. Although the data are relatively scattered, we observe that

conjugate faults tend to have smaller associated fold amplitudes compared with simple faults (***Figure 4.13a*** and ***4.13b***). For example, only 8% of the analysed simple normal faults have no associated folding on horizon H3, compared to 41% of the conjugate faults (***Figure 4.13a***). 51% of the simple normal faults in our sample are associated with folds that accommodate more than half of the total throw (i.e. ratio of fold amplitude/total throw > 0.5; ***Figure 4.13a***), compared with only 8% of the conjugate faults.

Figure 4.13 also shows that fold amplitudes vary from 0% to 100% as a proportion of the total displacement (fault throw + fold amplitude) on the two interpreted horizons: H3 (top MU 2) and H4 (intra MU 3). By comparing the ratio of fold amplitude to the total throw on each horizon, we are able to explore the influence of the two different mechanical units on the magnitude of ductile deformation. The extensional fold amplitudes measured for horizon H4 are typically larger than the fold amplitudes of horizon H3 (***Figure 4.13a*** *and* ***4.13b***). The largest amplitude recorded for an intact monocline (fold amplitude/total throw = 1) for H4 is 120 ms compared with 50 ms for H3. Larger amplitude values observed for breached monoclines (fold amplitude/total throw < 1) can be explained by increased bed rotation within relay zones (e.g. between vertically segmented faults) and/or by movement of the hangingwall across a bend in the fault surface, which we discuss, below.

Fault-propagation fold geometries (in terms of monocline amplitude and wavelength) can be described by kinematic parameters such as propagation to slip ratio (P/S) and apical angle, which together define the trishear zone of deformation located above propagating blind faults (Hardy and Allmendinger, 2011). P/S ratio, the main controlling factor on the amplitude of the fold, represents the propagation of the fault with respect to the displacement accrued, and is influenced by the mechanical properties of the rocks and the effective confining pressure (Cardozo et al., 2003). Incompetent lithologies tend to inhibit fault propagation by accommodating larger amounts of strain before failure, while more competent layers are characterized by localized brittle shear fractures. The larger fold amplitudes observed on horizon H4 compared to those associated with H3 are consistent with lower P/S ratios associated with propagation of the fault through the shale-dominated H3-H4 interval. This interval, which is part of the syn-rift, mechanical unit 3, has a higher proportion of incompetent shale

layers (>90 %) than MU 2 (62%). This observation suggests that fault propagation rates, as a proportion of fault displacement rate, vary according to the ratio of incompetent versus competent lithologies, given that the bulk thickness of the two stratigraphic intervals is similar. The relatively early breaching of the interbedded MU 2 – despite its likely propensity to deform by layer-parallel slip – is consistent with the models of Bonini et al. (2015), which indicate breaching of the monocline by downward propagation of a fault that nucleates at shallow depths above the footwall of the main fault.

As previously shown, vertical linkage may generate a bend in the fault plane that, with increasing displacement, will promote further fold growth as a result of hangingwall translation over the convex upward fault plane. ***Figure 4.13d*** shows a series of vectors, plotted in fold amplitude *vs*. total throw space, that illustrate the growth of fault-bend folds on horizon H3 within the 3D seismic survey area. The left-hand point on each vector corresponds to the amplitude of the precursor fault propagation fold (zero in some cases). The right-hand point on each vector corresponds to the final fold amplitude (at the cessation of fault movement) resulting from fault propagation *and* fault-bend folding. According to Groshong (1989), the relationship between fault throw and the amplitude of a fault-bend fold depends primarily on the bend geometry, which is given by the change in fault dip. The maximum throw on the faults presented in ***Figure 4.13d*** is similar to the thickness of MU 2, hence we assume a linear relationship between fault throw and fault-bend folding, since horizon H3 (top of MU2) is not completely displaced over the fault bend. In this situation, steeper gradients (e.g. vectors A and B) correspond with more pronounced bends in the fault surface, while lower gradients (e.g. vector C) are characteristic of more planar faults, which lack or have smaller associated folds (***Figure 4.13d*** and ***Figure 4.9***). These observations suggest that the final fold amplitude is the result of both fault propagation and fault-bend folding processes, and that the relative importance of each mechanism may vary significantly along the strike of a single fault array.

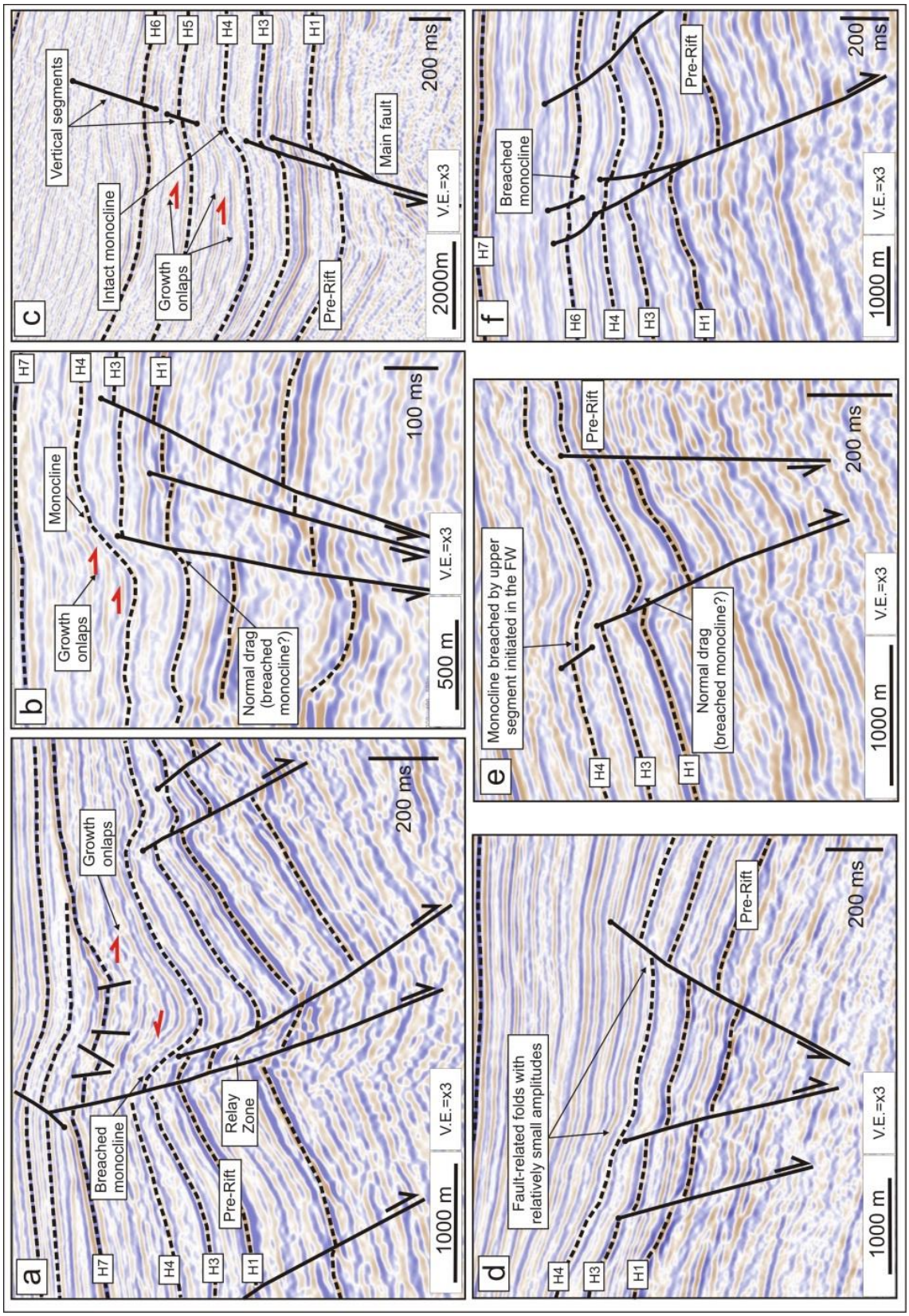

Figure 4.12 *Examples of fault-propagation folds associated with different sets of "simple" and "conjugate" normal faults, interpreted from regional 2D seismic profiles across the IMF (see text for explanations).*

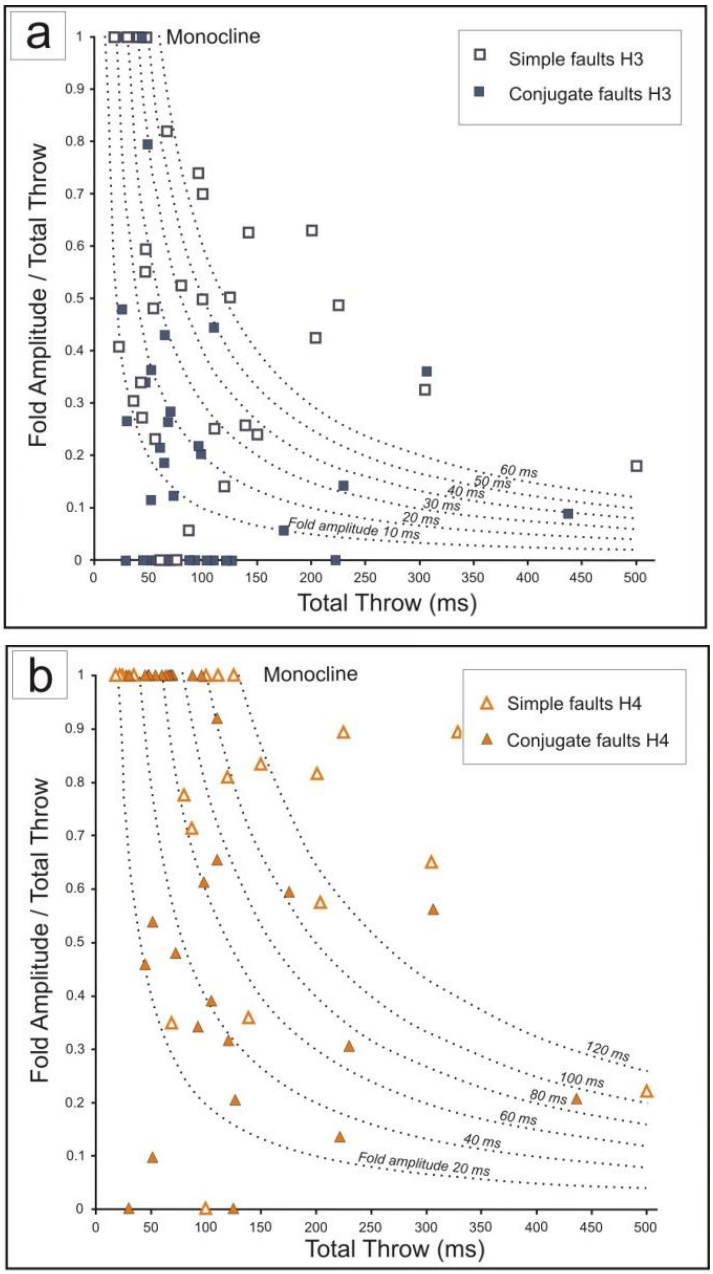

Figure 4.13 (a) *Ratio of fold amplitude to total throw vs. total throw for horizon H3 (part of mechanical unit 2) measured on both 2D and 3D seismic data on two types of faults, simple normal faults and conjugate normal faults.* ***(b)*** *Ratio of fold amplitude to total throw vs. total throw for horizon H4 (part of mechanical unit 3).* *See continuation on the next page.*

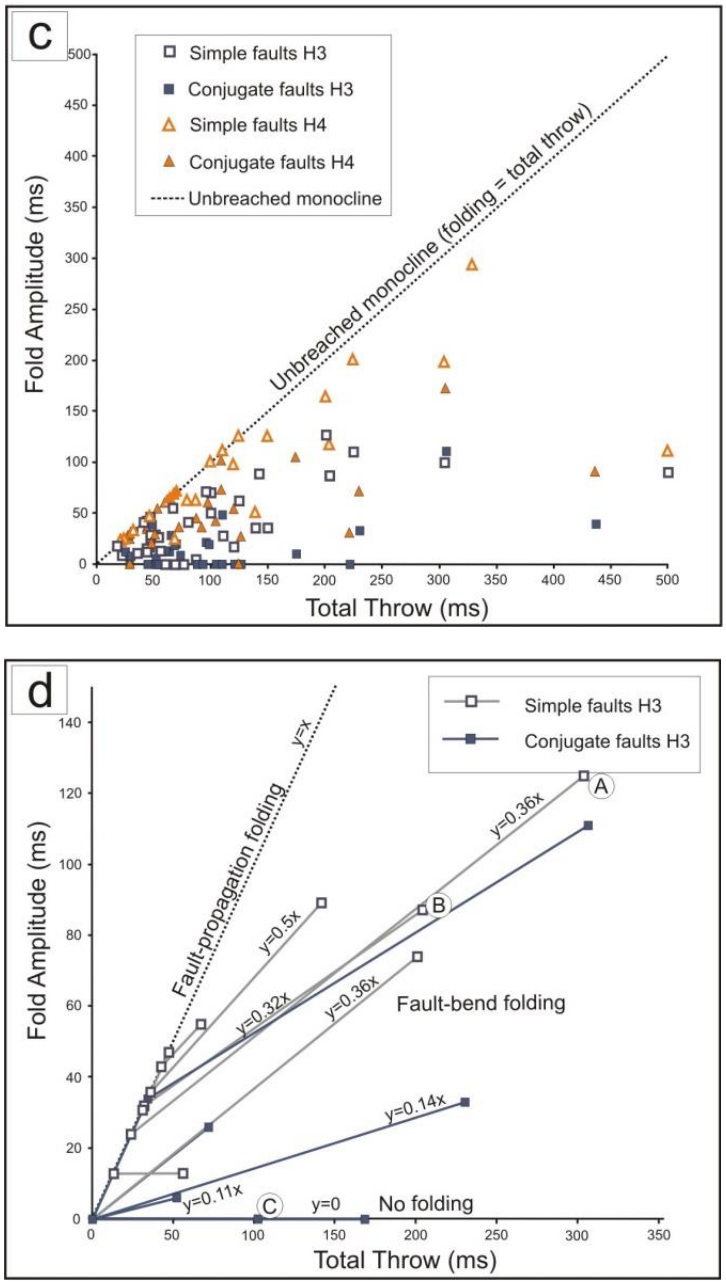

Figure 4.13 (c) *Fold amplitude vs. total throw measured for the two horizons, H3 and H4.* ***(d)*** *Fold amplitude vs. total throw for horizon H3 measured on faults from the 3D seismic data set only. A, B, C are measurement localities for the faults displayed in Figure 4.9. The vectors show possible evolution of folding with increasing fault throw (see text for explanation). Fault-propagation folds are characterized by vectors with a gradient of 1.0 (folding = throw), while fault-bend folds are characterized by vectors with gradients from 0.11 to 0.5. The gradients correlate with the change in fault dip within mechanical unit 2 with higher gradients reflecting a larger change in fault dip (see Figure 4.9).*

4.6. Discussion: mechanical interaction between faults and implications for fault propagation and fold development

Geomechanical models indicate that faults interact with the elastic stress fields of neighbouring segments, resulting in asymmetric displacement distributions and preferential locations of slip and/or fault propagation (Willemse et al., 1996; Crider and Pollard, 1998; Maerten et al., 1999). Maerten et al. (1999) used boundary element models to analyse the displacement distribution for Y-shape conjugate normal faults within a homogeneous elastic medium, whilst Young (2001) used finite element models to investigate the slip distribution for V-shape conjugate normal faults within a heterogeneous elastic medium (***Figure 4.14***). Their results showed that conjugate faults are characterized by asymmetric vertical displacement gradients, supporting previous observations from seismic data (Nicol et al, 1995). They postulated that the asymmetry is unlikely to be the result of nucleation of faults on different layers, but rather is the effect of mechanical interaction between the opposite dipping segments. The models showed that conjugate normal faults display asymmetric displacement distributions that vary with distance between the conjugate segments and the mechanical properties of the material (Young, 2001). ***Figure 4.14c*** shows how the Poisson's ratio of the layer containing the fault intersection (i.e. the branch line) influences the fault displacement distribution. The threshold of volumetric strain is lower for less compressible rocks (higher Poisson's ratio) resulting in high horizontal compressive stresses within the fault intersection region. In this case, the mechanical models predict an upward shift of the locus of maximum displacement towards the upper fault tip. This skewed displacement distribution, with higher displacement gradients near the upper tip, implies a greater tendency for preferential upward fault propagation. Specifically, previous studies have shown that the spatial energy release rate, which is a measure of the energy required for a fracture to propagate, is directly proportional to displacement and displacement gradients (Aydin and Schultz, 1990; Willemse and Pollard, 2000).

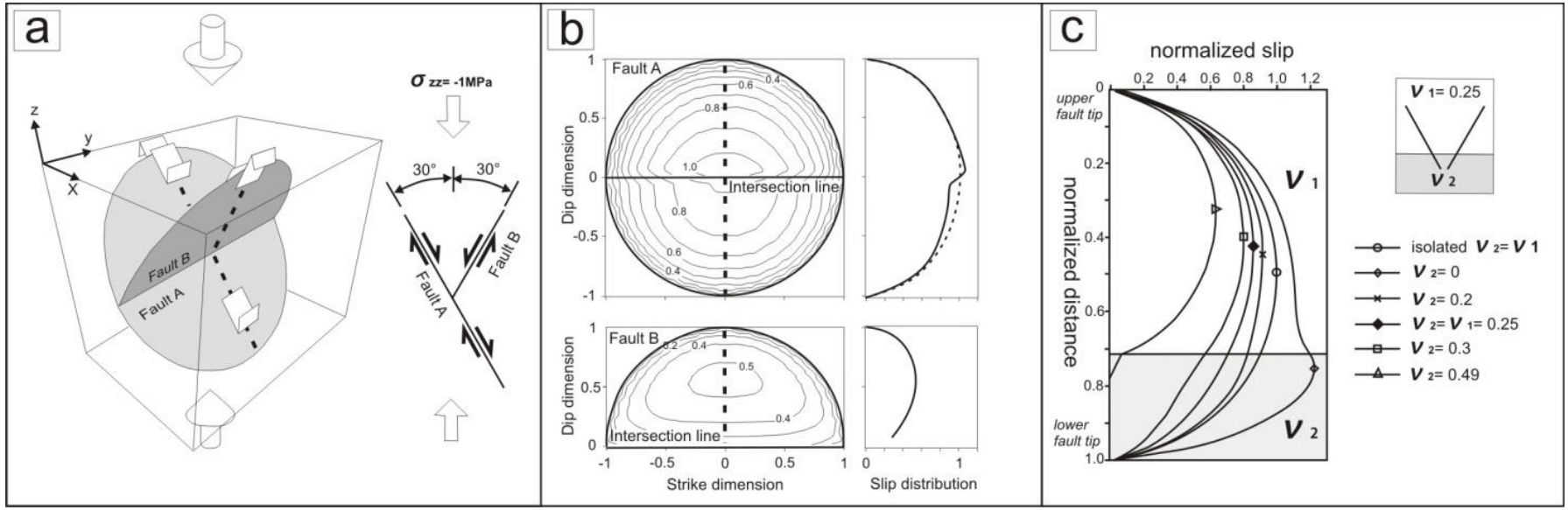

Figure 4.14 (a) *Configuration of the elastic boundary element model for conjugate normal faults with a "Y"-type geometry within a homogeneous whole elastic space, from Maerten et al (1999).* ***(b)*** *Results of the modelled displacement distribution (Maerten, 1999).* ***(c)*** *Calculated displacement distributions for conjugate normal faults with a "V"-type geometry located within a heterogeneous elastic material, derived from finite element method modelling (Young, 2001). Note the asymmetric slip distribution, skewed towards the upper fault tip, for models in which the fault intersection lies within a layer that has a higher Poisson's ratio than the surrounding material (i.e. $v_2 > v_1$).*

The displacement analysis of simple and conjugate normal faults from the IMF basin shows that the displacement maxima for conjugate normal faults is shifted upwards in the stratigraphic section, to within mechanical unit 2 (***Figure 4.7*** and ***4.8***). In contrast, simple normal faults tend to have displacement maxima within MU 1 (e.g. ***Figure 4.6***). The smaller fold amplitude to total throw ratios associated with conjugate faults (***Figure 4.13***) can therefore be explained by high, upward fault propagation rates due to mechanical interaction between the opposite dipping faults. As a consequence, conjugate normal faults that intersect within layers with low compressibility display geomechanical characteristics favourable for migration of stress concentrations near the upper fault tips. These stress perturbations enhance upward propagation of the fault, generating higher P/S ratios and result in the early breaching of the free surface, and the development of low amplitude extensional folds, or no folding at all. Nevertheless, because some of the conjugate pairs may have formed as a result of incidental intersection of opposite dipping faults (Nicol et al., 1995), it is possible that the faults initially developed as isolated simple normal faults, without mechanical interaction with other faults, at an incipient stage in their evolution. As a consequence, some conjugate faults, typically displaying Y type geometries, may exhibit symmetrical displacement distributions and associated fault propagation folding that is similar to simple normal faults. Further analysis of these faults is required to test this hypothesis.

Figure 4.15 *Schematic model summarising the mechanisms responsible for generating spatial and temporal variability in normal fault-related folding within IMF. The heterogeneous sedimentary unit favours fault restriction, segmentation and development of fault-propagation folds (1, 2). Linkage of the main deeper fault with the upper en-echelon segments can generate convex-upward fault geometries and further development of fault-bend folding (3) (modified from Lacazette, 2001). The bend in the fault plane (and the associated folding) is localized and depends on the lateral separation between the upper segments and the main fault. Conjugate faults tend to breach early the depositional surface without developing significant folds ahead of the propagating upper tip (4).*

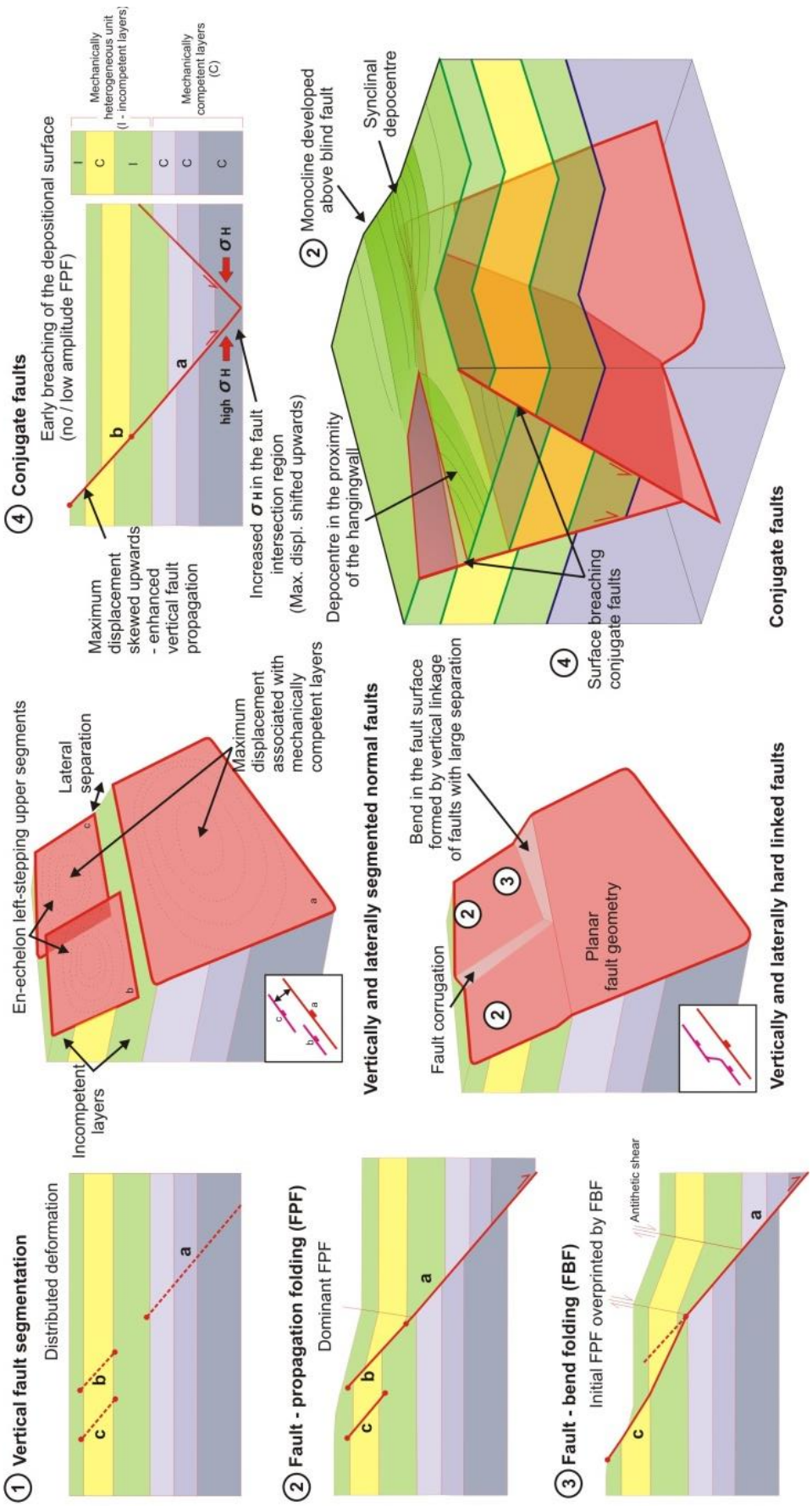
① Vertical fault segmentation
Distributed deformation
② Fault - propagation folding (FPF)
Dominant FPF
③ Fault - bend folding (FBF)
Initial FPF overprinted by FBF
Antithetic shear
En-echelon left-stepping upper segments
Lateral separation
Maximum displacement associated with mechanically competent layers
Incompetent layers
Vertically and laterally segmented normal faults
Bend in the fault surface formed by vertical linkage of faults with large separation
Fault corrugation
Planar fault geometry
Vertically and laterally hard linked faults
④ Conjugate faults
Early breaching of the depositional surface (no / low amplitude FPF)
Mechanically heterogeneous unit (I - incompetent layers)
Mechanically competent layers (C)
Maximum displacement skewed upwards - enhanced vertical fault propagation
Increased σH in the fault intersection region (Max. displ. shifted upwards)
high σH
σH
② Monocline developed above blind fault
Synclinal depocentre
Depocentre in the proximity of the hangingwall
④ Surface breaching conjugate faults
Conjugate faults

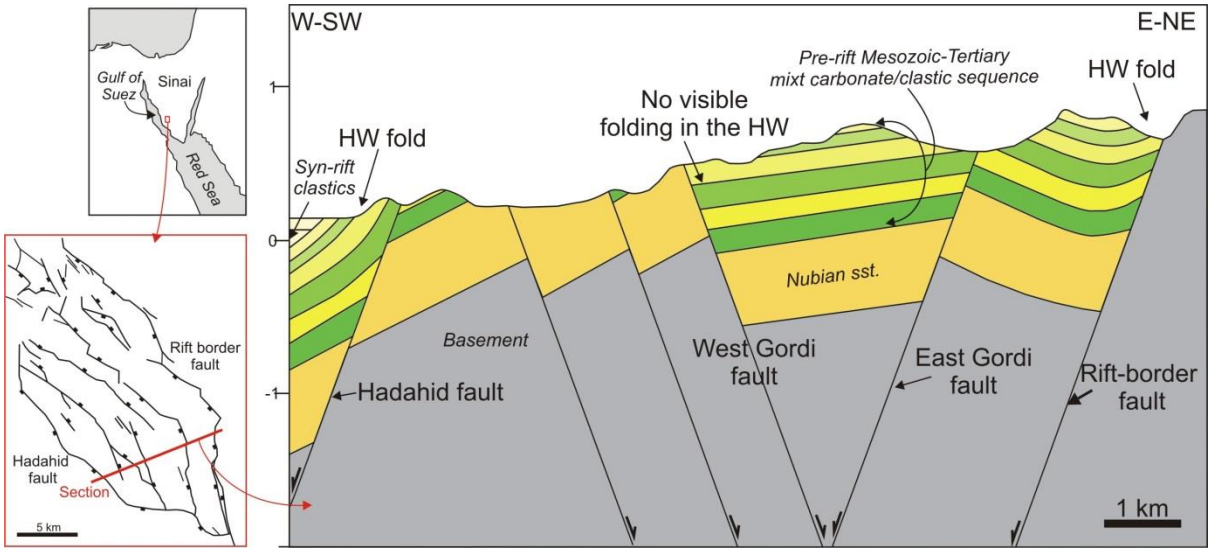

Figure 4.16 *Geological cross-section from Suez Rift (modified from Whipp, 2011). Note the large amplitude hangingwall folds associated with the simple normal faults (Hadahid fault, the rift-border fault). The conjugate West and East Gordi faults display little or no folding in their hangingwalls.*

Our findings show that the development of normal fault-propagation folds can vary significantly within a sedimentary basin and will depend not only on the presence of incompetent layers capable of inhibiting fault propagation and causing vertical fault segmentation, but also on the distribution of stress perturbations caused by mechanically interacting normal faults (***Figure 4.15***). We hypothesise similar relationships should exist between faults and folds in other extensional basins. Seismic data from the Wytch Farm oil field in the Wessex Basin (southern England) reveal similar, vertically segmented normal faults (Kattenhorn and Pollard, 2001). Displacement maxima are shifted towards the upper fault tips (within the Middle Jurassic Top Cornbrash sandstones) for conjugate faults, compared with the more symmetrical throw distribution for simple normal faults, which have displacement maxima within the Lower Jurassic Bridport and Triassic Sherwood sandstones (see figures 17 and 18 E in Kattenhorn and Pollard, 2001). The same mechanism can potentially explain the variable development of the normal fault propagation-folds seen in other rift settings, such as the Suez Rift, NW Egypt (***Figure 4.16***, from Whipp, 2011). Here, folds are poorly-developed adjacent to the conjugate West Gordi and East Gordi normal faults. In contrast, large amplitude breached

monoclines are developed adjacent to the "simple" Hadahid fault or the rift-border fault (***Figure 4.16***, from Whipp, 2011). The section in ***Figure 4.16*** is overly-simplified, but Whipp (2011) showed that the faults dip at ca. 80° within the basement and overlying Nubian sandstone. In the overlying, interbedded sequence, fault dips decrease to 60-70°, and the faults are vertically segmented. It is likely that translation of the hangingwall monoclines (such as that associated with the Hadahid Fault) across the irregular fault surface contributed to the amplification of the fold amplitude, similar to the example presented from IMF and synthesized in the model shown in ***Figure 4.15***.

4.7. Conclusions

Our observations from the Inner Moray Firth basin show that:

(i) The development of a normal fault-related fold can be explained by the contribution of several mechanisms, the relative importance of which change during the growth of the normal fault system. The mechanisms evolve from fault-propagation folding, vertical and horizontal segment linkage to fault bend folding (***Figure 4.15***).

(ii) The heterogeneous mechanical properties of the host rocks control the fault segmentation and amplitude of fault propagation folding. Shale-rich incompetent layers inhibit fault propagation generating larger amplitude unbreached monoclines. The larger fold amplitudes observed in the shale-rich, syn-rift sequence (mechanical unit 3) compared with the underlying, interbedded pre-rift sequence of similar thickness (mechanical unit 2), demonstrate the importance of the ratio of incompetent to competent strata (net-to-gross ratio) in arresting upward fault propagation and controlling the magnitude of ductile deformation.

(iii) The occurrence and development of the normal fault-related folds is influenced not only by the mechanical stratigraphy and fault geometry, but also by the mechanical interaction between fault segments of a normal fault system. Although incompetent stratigraphic units, dominated by weak lithologies can inhibit vertical propagation of the faults, generating vertical segmentation or development of monoclines above the fault vertical tip-lines, we showed that some faults can breach

the free surface very early without developing fault-tip monoclines. The variability of normal fault-related folding can be explained by the enhanced vertical propagation due to mechanical interactions between opposite dipping normal faults.

Acknowledgments

We are grateful to Ithaca Energy and Dave Brett for releasing proprietary seismic data for publication. We are thankful to Badley Geoscience Ltd. and Dave Quinn for providing license and training for TrapTester software. We also thank Schlumberger for providing academic license for Petrel, Midland Valley for providing license for Move software and Foster Findlay Associates Ltd. for providing access to GeoTeric software. We thank Al Lacazette, Paul Whipp and Scott Young for the permission to use their figures in this manuscript. Jonathan Imber acknowledges a Royal Society Industry Fellowship with Badley Geoscience Ltd. and Geospatial Research Ltd. Christopher Jackson, Douglas Paton and Tom Manzocchi provided constructive reviews that significantly improved the clarity of this manuscript.

| Chapter 5 |

Breaching of relay ramps bounded by surface-breaking normal faults

Abstract

The accumulation of strain and eventual breaching of relay ramps are fundamental to the growth of normal faults. Data obtained from breached relays in various geological settings, and spanning > 6 orders of magnitude in length scale, demonstrate that relay ramps on surface-breaking normal faults breach preferentially by propagation of the rear fault across the upper section of the ramp. There is a positive relationship between the fault-parallel relay ramp shear strain at the time of breaching and increasing displacement on the relay-bounding faults. Ramps that fail by propagation of the rear fault tend to breach at higher ramp strains and later in the growth history of the bounding fault array than ramps which fail by propagation of the front (hangingwall) fault. Where hangingwall breaching does occur, it tends to happen at an early stage in the growth of the bounding faults. The likelihood of ramp breaching on surface-breaking normal faults depends not only on ramp shear strain and the throw / separation (*T/S*) ratio of the relay-bounding faults, but also on how the throw is partitioned between the bounding faults. For *T/S* ratios between 0.3 and 0.9, the probability of ramp breaching increases if the throw on the front fault, T_{FF}, is less than ca. 1.3 times greater than the throw on the rear fault (T_{RF}). These data are consistent with the results of mechanical models, which predict larger shear stress drops within the hangingwalls (compared with the footwalls) of surface-breaking normal faults, favouring propagation of the rear fault. In the cases where $T_{FF} >> T_{RF}$, breaching requires accumulation of high shear strains and *T/S* ratios. Our results demonstrate that the mechanical interaction between the relay-bounding faults and the Earth's free surface is a first-order control on ramp breaching and hence growth of surface-breaking normal faults.

5.1. Introduction

Fault relays are ubiquitous structures in the Earth's crust, observed over a wide range of scales (Long and Imber, 2011). Relay structures occur where displacement is transferred between two or more faults that strike sub-parallel to one another and dip in the same direction (Larsen, 1988; Peacock and Sanderson, 1991; Peacock and Sanderson, 1994; Trudgill and Cartwright, 1995; Childs et al, 1995; Huggins et al., 1995; Fossen and Rotevatn, 2016). The volume of rock between the fault segments across which displacement is transferred becomes strained, and is referred to as a *relay zone*. Where steeply-dipping, normal faults cut and offset sub-horizontal strata, the beds within the relay zone are rotated, giving rise to *relay ramps* (***Figure 5.1***). The fault segments can branch at depth from a single fault or can be completely separated (Walsh et al., 2003), but in many cases appear to act in a geometrically and kinematically coherent manner (Walsh and Watterson, 1991). As fault segments grow by accumulating slip (Walsh and Watterson, 1988; Dawers and Anders, 1995; Walsh et al., 2002; Jackson et al., 2016), their stress fields overlap and interact (Pollard and Segall, 1980; Aydin and Schultz, 1990; Willemse, 1997; Crider and Pollard, 1998; Gupta and Scholz, 2000). As a result, propagation of the fault tips is impeded, leading to high displacement gradients on the relay-bounding faults, and strain accumulation within the relay zone. A relay ramp becomes breached when a *breaching fault* propagates across the ramp, linking the relay-bounding faults and, in some cases, causing the ramp and/or the tip of one or both relay-bounding faults to become inactive (Peacock and Sanderson, 1994; Ferrill et al., 2001; Imber et al, 2004; Soliva and Benedicto, 2004; Fossen and Rotevatn, 2016) (***Figure 5.2***). Relay breaching can occur by: (1) propagation of the rear fault within the upper (footwall) side of the ramp (***Figure 5.2a***); (2) propagation of the frontal fault within the lower (hangingwall) side of the relay ramp (***Figure 5.2b***); (3) approximately synchronous propagation of both rear and front faults, forming a double breached relay ramp; or (4) propagation of a mid-ramp fault, which is also commonly observed (***Figure 5.2c***). As shown below, breaching can involve a combination of styles, particularly where large, non-plane strains develop within a relay zone. As such, relay growth and breaching is integral to the growth of normal faults in the Earth's crust (Cartwright et al., 1996).

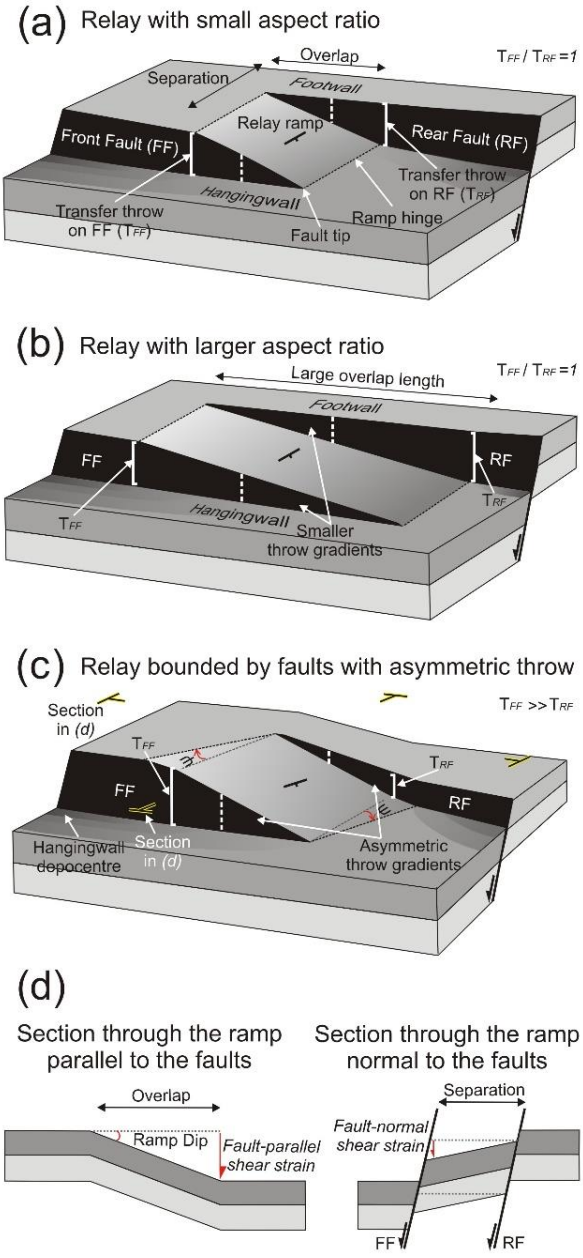

Figure 5.1 *– Schematic illustrations of intact (unbreached) relay ramps highlighting some of the terminology used within the chapter. All the illustrated relay ramps display identical throw/separation ratios if measured in the middle of the relay (white stippled lines represent the measured throw location), but with variations in overlap length in* ***(a)*** *and* ***(b)*** *and asymmetric throw distribution in* ***(c)****. Increase in the overlap length for the same value of transfer throw measured in the middle of the relay, results in smaller displacement gradients on the bounding faults* ***(b)****, and smaller ramp parallel shear strains* ***(d)****;* ***(d)*** *Sections through the relay ramp from* ***(c)*** *in a direction parallel to (left) and normal to (right) the overlapping faults.*

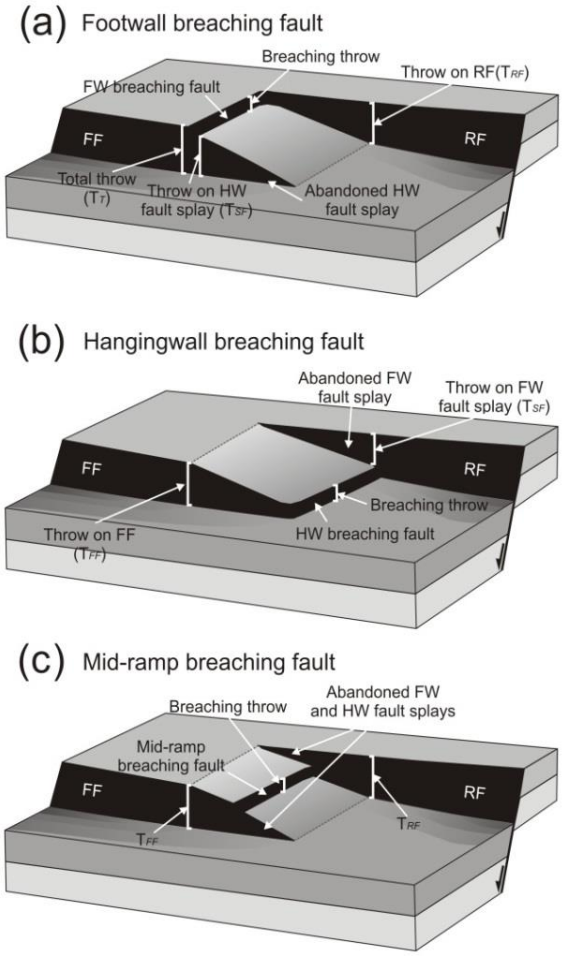

Figure 5.2 *Schematic illustrations of the styles of breaching of relay ramps:* ***(a)*** *ramp breached by the rear (footwall) fault;* ***(b)*** *breached by the front (hangingwall) fault; and* ***(c)*** *breached by a fault developed within the middle of the ramp. In some cases the breaching occurs by a combination of these styles.*

In this study we focus on the breaching of relay ramps associated with *surface-breaking* faults. If sedimentation occurs coeval with displacement on the surface-breaking faults, the faults are also called *syn-sedimentary*. The study of syn-sedimentary faults is pertinent for several reasons. (1) Where the sedimentation rate is equal to or exceeds the throw rate on the faults, offset of each syn-fault horizon records the throw subsequent to its deposition, allowing successive growth stages of each fault to be determined (Childs et al., 2003). (2) Seismogenic normal faults that interact with the Earth's free surface are likely to pose a greater seismic hazard than deeply buried faults, hence understanding *when* and *how* relay ramps become completely breached can be critical for assessing

the propagation of earthquake ruptures along segmented normal faults (Zhang et al., 1999; DuRoss et al., 2016). (3) Syn-sedimentary normal faults are commonly observed to trap, or compartmentalize, hydrocarbon accumulations in rift- and passive margin basins (Hardman and Booth, 1991). The state of relay breaching controls the closure of normal fault-bounded hydrocarbon traps, which is important when evaluating the risk and volume uncertainty of the traps (Richards et al., 2016), the subsurface fluid migration pathways (Rotevatn et al., 2007), and/or the dispersal of syn-rift sediments which can host potential reservoirs (Athmer and Luthi, 2011).

Previous studies have employed two distinct approaches to evaluate the nature and mechanism of ramp breaching (Fossen and Rotevatn, 2016 and reference therein), in many cases treated somewhat separately:

(1) Empirical observations of intact and breached relays have been used to estimate the probability of relay ramp breaching based on analysis of: (a) the measured finite strains within ramps, specifically the amount of *fault-parallel shear strain* a ramp can support prior to being completely breached (i.e. *critical ramp dip*; Fossen and Rotevatn, 2016); and/or (b) the ratio between the transferred *throw* across the relay and the *separation distance* between the overlapping segments (Imber et al., 2004; Soliva and Benedicto, 2004) (***Figure 5.1***). The probability of breaching increases as the fault-parallel shear strain and throw / separation ratio increase. Nevertheless, both parameters are one-dimensional measures that do not account for commonly observed variations in relay ramp geometry (***Figure 5.1a, b*** and ***Figure 5.3***).

(2) Mechanical models have been used to investigate the stress and/or strain under which relay ramps are breached. Three-dimensional (3-D) boundary-element models predict the static stress changes around the interacting, relay-bounding faults, and predict that breaching of relays on normal faults is most likely to occur at the centre to upper part of the relay ramp (Crider and Pollard, 1998) (***Figure 5.2***). 3-D distinct element models reproduce the kinematics of fault propagation, ramp rotation and breaching. These models show that breaching fault location is influenced by mechanical heterogeneities in the host material, and that breaching fault propagation is not instantaneous: the ramp continues to rotate, and

therefore transfer displacement between the relay-bounding faults, until they are fully linked (Imber et al., 2004).

Although there is a significant volume of published literature on how normal faults grow, we believe that a holistic approach is still needed to better understand the processes and mechanisms that govern the linkage of normal fault segments. The aim of this study is to integrate empirical observations of breached and intact relay zones with kinematic and mechanical models to explain the differences in geometry (***Figure 5.2***), timing (relative to fault growth; Cartwright et al., 1996) and likelihood of relay ramp breaching along surface-breaking normal fault arrays. This can be important for the assessment of seismic hazards. Relays can act either as barriers to rupture propagation or as rupture initiators, as stress tends to concentrate at segment boundaries. Understanding how relays become breached can help mitigate some of the risks associated with surface rupture propagation.

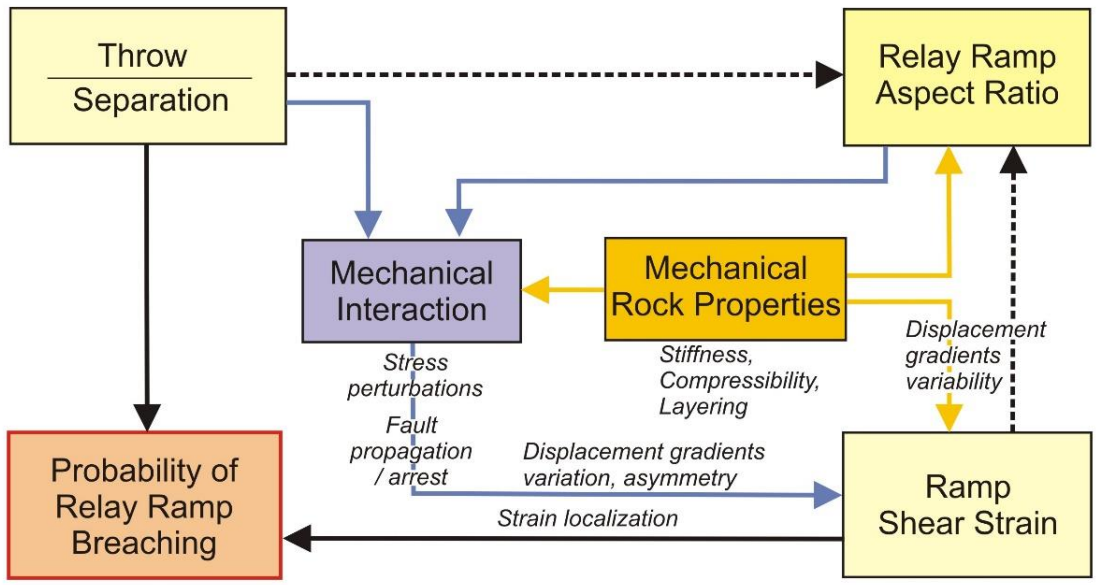

Figure 5.3 *Diagram with the main parameters used in the evaluation of relay ramp breaching. The simple criterions such as the throw/separation ratio or ramp shear strain are unidimensional and cannot reflect in entirety the complexity of the breaching process. The combined criterions offer more complete information on the internal strain and the two-dimensional geometry (aspect ratio) of the ramp, which can reflect the control of lithology (Childs et al, 2016) and influence the mechanical interaction between the bounding faults (Willemse, 1997).*

5.2. Datasets and methods

5.2.1 Datasets

The dataset used in this study comprises 128 relay ramps from high quality 3-D seismic surveys, high resolution topographic data, outcrops and published literature (digital appendix) (***Figure 5.4***). The compiled datasets cover a wide range of scales (nearly 6 orders of magnitude in terms of fault throw and separation distance), and different host rock lithologies (clastic and carbonate sedimentary rocks; volcanic rocks). We conduct a systematic, quantitative analysis of a subset of the total data (*Section 5.2.2*) obtained from two populations of seismically-imaged relay zones from the Inner Moray Firth Basin (IMF), offshore UK, and the Laminaria High, offshore NW Australia. The IMF and Laminaria High 3-D seismic surveys provide the largest number of relay zones among the various study areas, and include fault arrays that cut and offset sedimentary successions with well-characterised mechanical stratigraphy. In this way, we can (at least in part) document the influences of host-rock variability and pre-existing structural heterogeneities within these two populations – factors that are known to impact relay breaching (Fossen and Rotevatn, 2016) – which would be problematic using the complete dataset from all study sites. The 3-D seismic datasets, geological setting and mechanical stratigraphy of the IMF and Laminaria High areas have been summarised, respectively, by Lăpădat et al. (2016) and Long (2011).

The sampling interval of the seismic data analysed in this study is 2 ms. This means that the measurement errors due to the limitations in vertical seismic resolution are negligible (below 2 ms). The throws measured on seismic reflection profiles were converted from two-way-time (TWT) to depth using time-depth relations from nearby wells (see Lăpădat et al., 2016 for the IMF dataset and Long, 2011 for the Laminaria dataset), in order to generate accurate measurements of fault throws and ramp shear strains (***Figure 5.1d***). The vertical resolution of these datasets depends on depth and acquisition parameters, and varies in general from 10 to 30 m, depending on the dominant frequency of the seismic data. The analysed seismic volume covering the Parihaka fault from the Taranaki Basin, offshore New Zealand (Giba et al., 2012) has a higher frequency content (60-70 Hz), resulting in a vertical seismic resolution (i.e. tuning thickness) of < 10 m. We used this example to illustrate the

Figure 5.4 *Location map of the datasets and the type of data used in this paper (from this study and from published literature).*

style and distribution of small-scale faults at the tips of relay-bounding faults that cut and offset a succession of unconsolidated, syn-fault sediments.

The component of seismic-scale lateral fault tip-folding (i.e. ductile deformation; Walsh and Watterson, 1991) is included within the throw measurement in order to limit some of the uncertainties associated with the sub-seismic fault throw resolution (Long and Imber, 2012). In all cases, whether or not strain within the relay ramp is interpreted as being accommodated by brittle (discontinuous) or ductile (continuous) deformation is dependent on the scale of observation and the seismic resolution (Walsh and Watterson, 1991; Walsh et al., 1996). We therefore use a conservative definition of relay ramp breaching in which the faults are physically linked at the scale of observation and, in many cases, where at least one of the bounding faults is inactive.

5.2.2 Breaching parameters

We now define the quantitative parameters used to describe the ramp strains, and the nature and timing of breaching within the studied populations of relay ramps:

Fault-parallel ramp shear strain is the ratio between the transfer throw and the fault overlap length (***Figure 5.1a, d***), and has been previously used to investigate the breaching strains of relay ramps

(Imber et al, 2004; Soliva and Benedicto, 2004). In this study, we re-define the transferred throw as the average of the maximum throw on the front fault (T_{FF} in ***Figure 5.1***), measured in a direction normal to the fault from the tip of the rear segment, and the maximum throw on the rear fault, measured normal to the fault from the tip of the front fault (T_{RF} in ***Figure 5.1***).

Throw / separation ratio (T/S) is a parameter used to evaluate the probability of ramp breaching (Soliva and Benedicto, 2004; Imber et al, 2004). In these former studies, throw (or displacement) was defined as the sum of displacements on each fault segment measured on a line normal to the strike of the relay-bounding faults at the centre of the overlap. Here, we define the transferred throw as described in the previous paragraph and separation as shown in ***Figure 5.1a***, an approach that allows us to introduce the new *throw asymmetry* parameter.

Throw asymmetry is the ratio between the maximum throw of the front fault (T_{FF} in ***Figure 5.1***) and the maximum throw of the rear fault (T_{RF} in ***Figure 5.1***), measured within the overlap region, i.e. T_{FF} / T_{RF} (***Figure 5.1c***). As shown below, such asymmetry can influence the style, timing and likelihood of ramp breaching.

Breaching index (BI) measures the timing of relay ramp breaching relative to the growth (displacement history) of the host fault array (Cartwright et al., 1996). BI is defined as the ratio between the maximum throw on the inactive splay fault (T_{SF}) and the total throw of the linked fault (T_T) measured at the point of breaching, i.e. BI = (T_{SF}/T_T) * 100 (***Figure 5.2***). A low BI value indicates early ramp breaching; a high BI indicates late breaching.

We first describe relay ramps and breaching fault geometries along pre-historical surface-breaking normal faults from Inner Moray Firth (IMF) and Taranaki Basins imaged by high quality seismic reflection data. We compare them with a well exposed active relay ramp from the Basin and Range extensional province, which ruptured at the surface during a past seismic event (Wallace, 1984). We then investigate the quantitative characteristics of two populations of breached relays from the IMF and Laminaria High, making comparisons with data from other areas, including data from relays associated with strata-bound, post-depositional normal faults (*Section 5.3*). In the final section, we use

Poly3D software (Thomas, 1993) to compare the predicted stress fields around overlapping, surface-breaking and deeply-buried normal faults with our observations of natural relays (e.g. Crider and Pollard, 1998; Crider, 2001) (*Section 5.4*). Poly3D is a boundary element method which calculates the stress tensor and displacements on discontinuities (faults) subject to an applied regional load (or strain) within a homogeneous and isotropic elastic whole- or half space.

5.3. Analysis of relay breaching on surface-breaking fault arrays

5.3.1 Breaching characteristics of relay ramps

Segmented normal faults that cut and offset the Late Jurassic, syn-fault succession in the Inner Moray Firth Basin (IMF), offshore UK display seismic-scale relay ramps (***Figure 5.5***). The majority of the ramps in the IMF are breached by the footwall fault for either left-stepping or right stepping segments (***Figure 5.5a***). ***Figure 5.5b*** shows the TWT structure map for the Top Triassic horizon, which lies within the interbedded sandstones and shales of the uppermost pre-rift unit (Stevens, 1991). Here, the relay ramp is at an incipient stage of breaching in the upper and mid-ramp sections. These faults probably breach the ramp completely at a sub-seismic scale, given the limited resolution of the dataset (tuning thickness of ~20 m). However, there is no evidence that either of the bounding faults developed into an inactive splay. The fault-parallel and fault-normal shear strains within the ramp (***Figure 5.1d***) are large – even compared with other relay ramps in the IMF (***Figure 5.5a***) – and the hinges of the ramp are oriented ca. 45° from a direction normal to the faults strike. Seismic sections through the relay ramp (***Figure 5.5c*** and ***5.5d***) show the ramp dipping in a direction both parallel and normal to the strike of the bounding faults (average dip of ca. 25°).

The throw gradients on the bounding faults are large and highly asymmetric. The gradient on the front fault (ca. 0.70) is more than twice that on the rear fault (ca. 0.30) (***Figure 5.6a***). This throw asymmetry is reflected by the difference in width of the heaves on the two faults (the black polygons from ***Figure 5.5b***). Interestingly the front fault curves away from the rear segment whilst the rear fault curves towards the front fault, highlighting the propensity for upper ramp breaching.

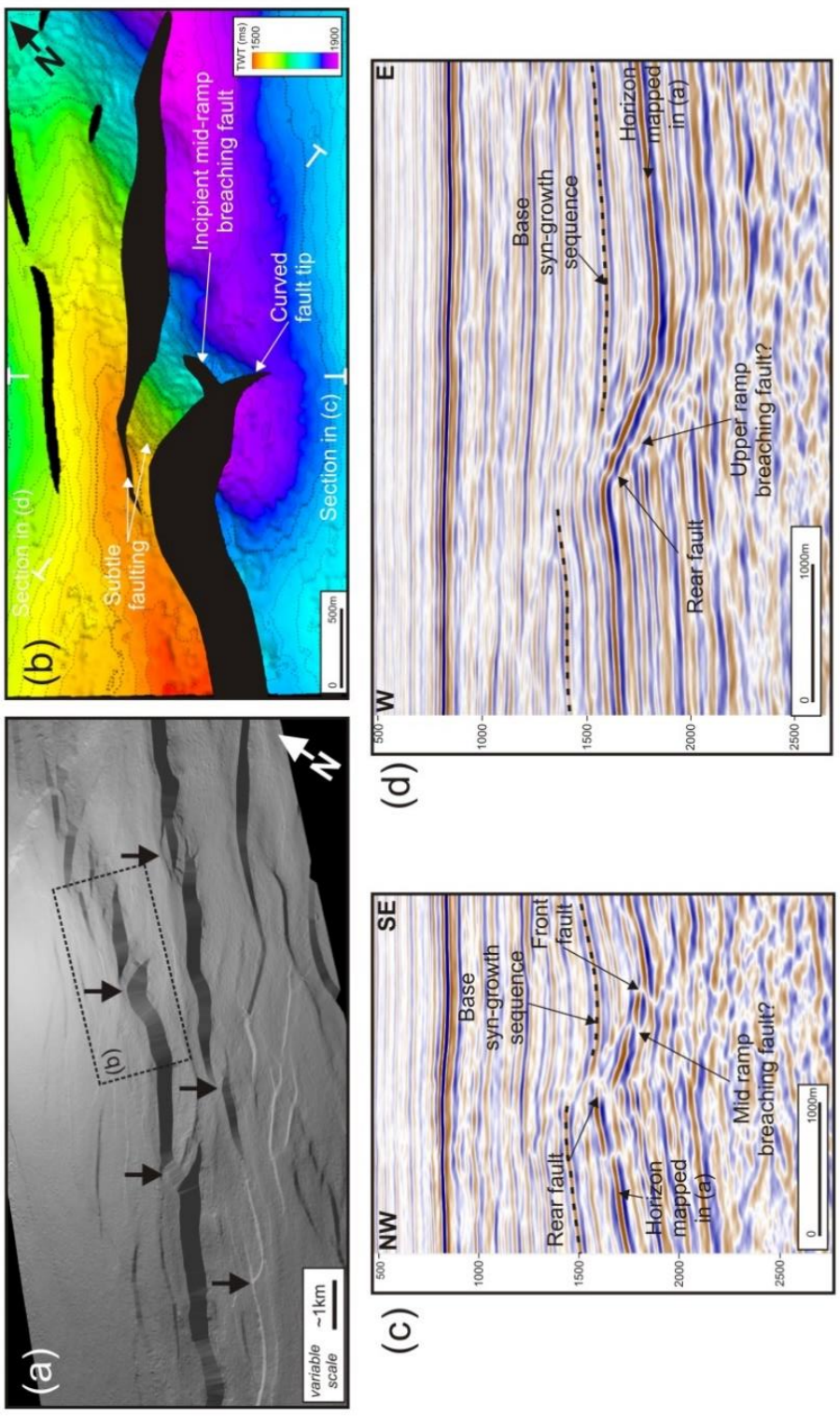
(a)
(b)
variable scale
~1km
N
(b)
Incipient mid-ramp breaching fault
Curved fault tip
Subtle faulting
Section in (d)
Section in (c)
TWT (ms)
1500
1900
0
500m
(c)
NW
SE
Base syn-growth sequence
Front fault
Rear fault
Horizon mapped in (a)
Mid ramp breaching fault?
0
1000m
(d)
W
E
Base syn-growth sequence
Horizon mapped in (a)
Rear fault
Upper ramp breaching fault?
0
1000m

Figure 5.5 – previous page (a) *3D view of Top Triassic pre-rift horizon illustrating a segmented normal fault-system from Inner Moray Firth (IMF), northern North Sea. Black arrows indicate some of the other investigated relay ramps from the IMF. Note that all ramps are at different stages of breaching and the ramp dips and internal deformation vary significantly from case to case. The rectangle delineates the relay ramp imaged in (b).* ***(b)*** *TWT structural map of a relay ramp in an incipient stage of breaching. Note the asymmetry of the fault heaves, with large heaves and curved geometry associated with the front fault. This relay ramp is characterized by particularly high shear strains in the directions parallel and normal to the bounding faults, indicated by the rhombohedral geometry, with ramp hinges oriented obliquely (45°) to the bounding faults.* ***(c)*** *Seismic section normal to the strike of the faults.* ***(d)*** *Seismic section along the dip direction of the relay; note the large dips of the ramp (~25°) are accommodated by subtle faulting.*

The segmented Parihaka fault system and associated relay ramps develop within a shale-dominated growth sequence with sandstone interbeds from the Taranaki Basin, offshore New Zealand (***Figure 5.7a***). High sedimentation rates within the basin during the Plio-Pleistocene have resulted in syn-fault strata that preserve the fault displacement histories and allow the kinematic evolution of the faults and relay ramp to be interpreted (Giba et al., 2012). The fault throw increases systematically downwards within the syn-fault interval, hence the relay ramp, which is at an incipient stage of breaching at shallow depths (***Figure 5.7a***), is completely breached at greater depth by a fault cutting through the middle of the ramp (Giba et al., 2012, their figure 9). The transfer throw at the syn-fault horizon mapped in ***Figure 5.7a*** is approximately 150 m.

The variance seismic attribute (Chopra and Marfurt, 2007) has been extracted and draped over the horizon mapped in ***Figure 5.7a***, in order to enhance visualization of small-scale faults with throws of approximately 7 m. Secondary faults splay out from a zone of intense deformation at the termination of the rear fault, and cut obliquely through the relay ramp. Secondary faults are also developed in the mid-ramp region. The spatial distribution of all these structures suggests that they formed due to interaction, and rotation of the ramp, between the two main fault segments. The overlapping part of the rear segment has an overall strike that is rotated ca. 20° clockwise from the 020° striking rear

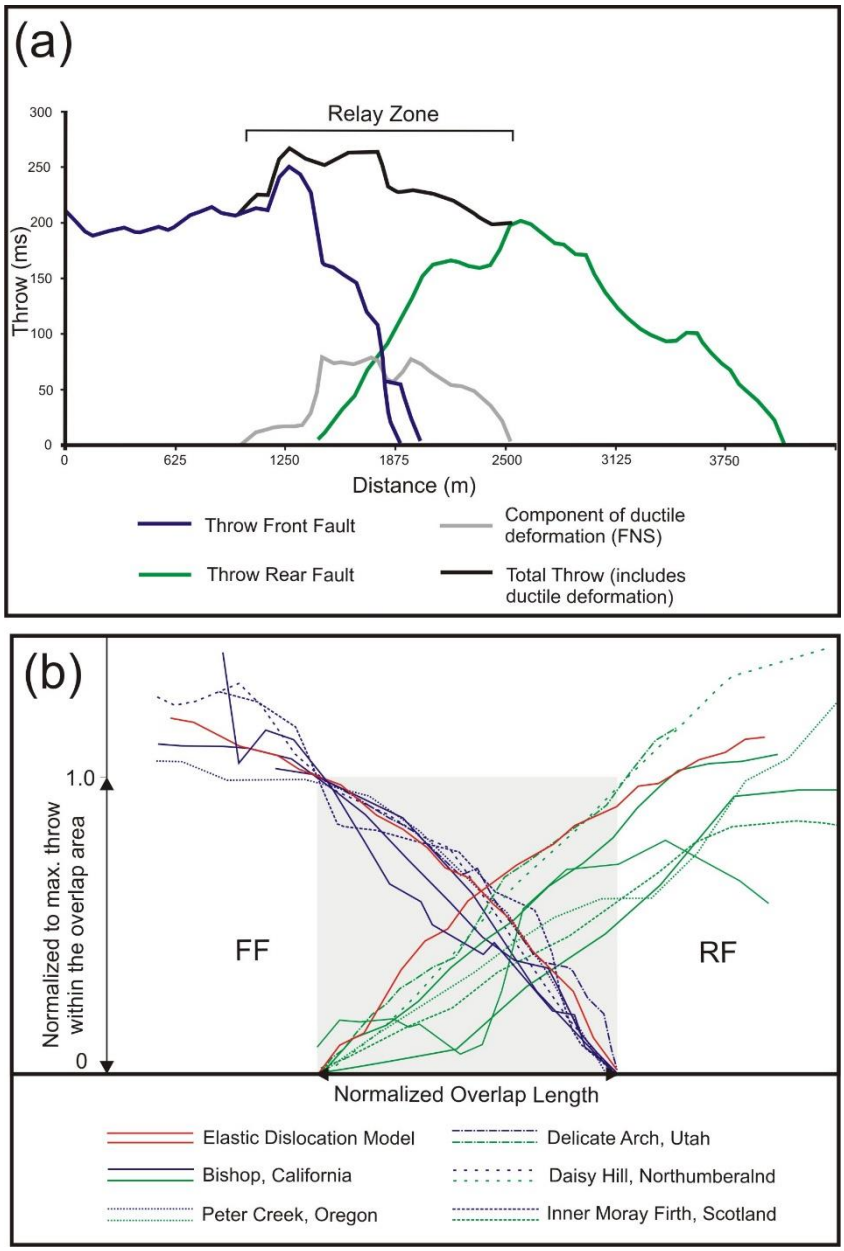

Figure 5.6 (a) *Throw-distance profile along strike of the relay bounding faults; FNS is fault-normal shear strain;* ***(b)*** *Normalized throw profiles along the strike of overlapping normal faults from the IMF and natural examples from published literature (Crider and Pollard, 1998; Huggins et al, 1995; Rotevatn et al, 2007; Hopkins and Dawers, 2016) and from a boundary-element model (Crider and Pollard, 1998).*

fault, i.e. in a direction away from the front fault. This part of the rear fault is composed of a series of right-stepping, en-échelon segments which have an approximate N-S orientation and strike at an angle of ca. 30-40° from the general trend of the overlapping part of the rear fault. The overall effect is that tip of the rear fault curves towards the front fault. In contrast, the tip of the frontal fault is characterized by splay segments that curve and step in the opposite direction, away from the rear fault (***Figure 5.7a***), similar with the IMF example presented earlier (***Figure 5.5***).

TWT structure contours in the vicinity of the Parihaka fault show that most of the displacement was accommodated by hangingwall subsidence, with just 1/6 of the displacement being accommodated by footwall uplift. This ratio is in accordance with published data for coseismic deformation associated with crustal-scale, surface breaching normal faults (Stein and Barrientos, 1985). Displacement on the syn-depositional normal faults in the IMF is also accommodated mainly by hangingwall subsidence, with a smaller component of footwall uplift as a result of block rotation according to a soft domino fault model (Walsh and Watterson, 1991; Yielding, 1990).

Figure 5.7 – next page (a) *Relay ramp from Taranaki Basin, offshore New Zealand. The variance seismic attribute is draped on the mapped surface, highlighting the secondary faults within the relay zone (plotted as planes on the stereographic projection). Note the rotation of the en-échelon segments at the tip of the rear fault (RF) toward the front fault (FF), forming an incipient breaching location at the upper hinge of the ramp, while segments splaying from the front fault curve away, in a direction opposite from the rear fault. The sketch in the upper part of the figure illustrates the main deformation pattern associated with a potential component of sinistral slip on the rear fault and the curved propagation of these segments (stippled lined) as the interaction with the frontal fault increases. Seismic data courtesy of New Zealand Petroleum and Minerals.* ***(b)*** *Relay ramp bounded by active normal faults along the Pleasant Valley fault system from the Basin and Range extensional province. The faults ruptured the surface during the 1915 M 7.6 earthquake. Data on surface displacement and localized strike-slip component is taken from Wallace (1984). Note that both faults are characterized by localized oblique slip in opposite directions, toward their hangingwall depocentres*

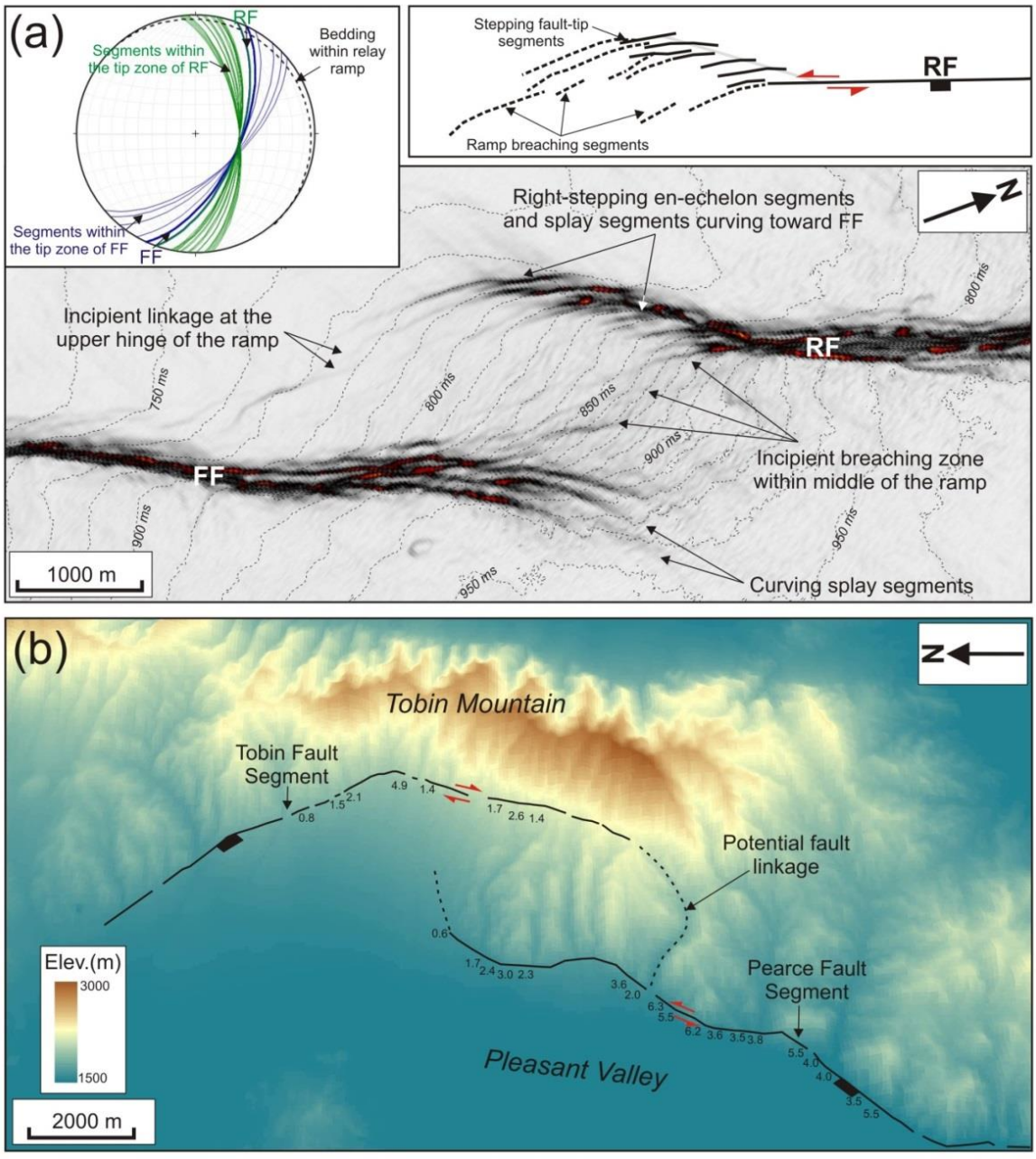
(a)
RF
Segments within the tip zone of RF
Bedding within relay ramp
Segments within the tip zone of FF
FF
Stepping fault-tip segments
RF
Ramp breaching segments
Right-stepping en-echelon segments and splay segments curving toward FF
N
Incipient linkage at the upper hinge of the ramp
RF
FF
750 ms
800 ms
850 ms
900 ms
950 ms
Incipient breaching zone within middle of the ramp
Curving splay segments
1000 m
(b)
N
Tobin Mountain
Tobin Fault Segment
Potential fault linkage
Pearce Fault Segment
Pleasant Valley
Elev.(m)
3000
1500
2000 m

Previous studies have shown that displacements on active, surface-breaching normal faults are characterised by an oblique slip component in the vicinity of the lateral tips, which is directed towards the hangingwall depocentre (Morewood and Roberts, 2000). ***Figure 5.7b*** illustrates a relay ramp bounded by two active normal fault segments which ruptured the surface during the 1915 M. 7.6 Pleasant Valley, Nevada earthquake (Wallace, 1984; DePolo, 1991). Although there was no direct evidence for continuous surface rupture across the relay (Wallace, 1984), the topography suggest that the relay ramp is in incipient stage of breaching through the rear segment (Tobin segment). The surface displacement associated with the 1915 seismic event was mainly dip-slip with some localized oblique-slip surface displacement (Wallace, 1984). Interestingly, the sense of this strike-slip component is different for the Tobin and Pierce segments in the vicinity of their overlapping area, with kinematic indicators showing a direction of slip toward their hangingwall depocentre (Wallace, 1984; ***Figure 5.7b***). This type of obliquity excludes a regional strike-slip component and can be interpreted as a consequence of the asymmetry between the larger hangingwall subsidence compared with the smaller footwall uplift (Ma and Kusznir, 1993; Morewood and Roberts, 2000; Roberts, 2007).

We consider that the stepping and overall sense of concave-to-hangingwall curvature of the relay bounding faults in the Taranaki and IMF basins can be similarly explained by a component of oblique slip at the tips of relay-bounding faults. The en-échelon fault segments in the upper part of the Parihaka relay ramp are compatible with a left-lateral component of slip near the tip of the rear fault (***Figure 5.7a***). In contrast, the tip of the front fault experienced a component of right-lateral slip, similar to the active interacting faults from Pleasant Valley, Nevada (***Figure 5.7b*)**. The intensely curved geometry of the front fault in the IMF relay ramp was probably enhanced by the very large displacement gradient toward the relay zone (***Figure 5.6a***). The asymmetric displacement gradients and curvature of the front fault induced a torsional component of strain within the ramp, manifested by its rotation about a vertical axis and a large component of fault-normal shear strain (***Figure 5.1c*** and ***5.1d***). The development of a breaching fault through the middle of the ramp may have been

promoted by the large displacements on the curving tip of the front fault causing enhanced elongation of the ramp in direction both parallel and normal to the relay-bounding faults (Stewart, 2001).

Figure 5.6b shows the normalized throw profiles of overlapping faults bounding the relay ramp from IMF, together with several other examples from relay ramps along surface-breaching normal faults, all of which are in an incipient stage of breaching through their rear fault. The profiles also include the normalized throw on two overlapping normal faults within a boundary-element model (from Crider and Pollard, 1998) for comparison. The model predicts larger throw gradients on the rear fault, causing the modelled ramp to dip back toward the footwall (Crider and Pollard, 1998). In contrast, the displayed natural relay examples typically have larger displacement gradients on the front fault than on the rear fault (***Figure 5.6b***) and tend to dip toward the hangingwall (***Figure 5.5*** and ***Figure 5.7a***).

Asymmetric surface slip gradients with larger surface slip recorded along the front segment have also been observed within active relay zone, as in the case of the 1915 Pleasant Valley, Nevada earthquake (Wallace, 1984; ***Figure 5.7b***). The relay zone along the Pataycachi fault which ruptured during the M 7.5 Sonora (Mexico) earthquake was also observed to be breached by the rear fault and to have larger magnitudes of surface slip on the front segment (Suter, 2014; his figure 8). However, preferential localization of asymmetric, large surface slip can be influenced by the pre-existing structural fabric favourably oriented with respect to the existing principal stress directions, as in the case of slip on the overlapping Hebgen and Red Canyon faults during the M 7.5 Hebgen Lake earthquake (US Geological Survey, 1964).

In the next section, we analyse the quantitative characteristics of two populations of relay ramps along historical surface-breaking normal faults in order to: 1) provide statistical evidence to support the hypothesis that relays ramps tend to breach in the upper to mid-ramp section; 2) evaluate the timing of breaching relative to fault growth; and 3) re-evaluate a published linkage criterion for segmented normal faults.

5.3.2 The free surface effect as a first-order control on the style of relay breaching

Our data suggest that breaching through the upper and mid-ramp sections is prevalent. We now test this hypothesis by analysing populations of breached (and intact) relay ramps from the IMF (27 sample size) and Laminaria High datasets (60 sample size), referring to other examples as appropriate. Approximately 67 % and 77 %, respectively, of the breached seismic-scale relay ramps associated with syn-sedimentary normal faults from the IMF and Laminaria High datasets are breached by their rear (footwall) fault (***Figure 5.7a*** and ***5.7b***). In both cases, there is little evidence for regional oblique extension which can impact the preferential breaching site (Crider, 2001), and previous studies considered the faults to be dominated by dip-slip displacement (e.g. Long and Imber, 2010; Long and Imber, 2012). Footwall breached relay ramps are also dominant within other basin-scale, syn-sedimentary normal fault systems from northern North Sea (McLeod et al., 2000) (***Figure 5.8a***) and offshore NW Australia (***Figure 5.8b***), and within thin-skinned, gravitational normal fault system from Gulf of Mexico (Yielding, 2016). Footwall breached relay ramps also appear to be common along surface-breaching normal fault systems from the western United States, within the Canyonlands graben system (Cartwright et al., 1996) (***Figure 5.8c***), and within the active Basin and Range extensional province (see examples in DePolo, 1991; Anders and Schlische, 1994; Crider and Pollard, 1998; Hopkins and Dawers, 2016; Ferrill et al., 2016).

The complex fault trace geometry of the Wasatch fault system, which marks the eastern boundary of the Basin and Range, is also characterized by first-order fault linkage through the footwall faults (***Figure 5.8d***). The style of breaching associated with post-depositional, strata-bound normal faults is more variable (***Figure 5.7c***). In contrast to surface-breaking faults, strata-bound faults are buried at the time of slip, and hence likely to be isolated mechanically from the Earth's free surface. The segmented, post-depositional normal faults from outcrops at Fumanyá and Nigüelas in Spain, described in detail by Soliva and Benedicto (2004), are characterized by relay ramps that are breached in approximately 50% of cases by a mid-ramp fault (sample = 18) (***Figure 5.5c***).

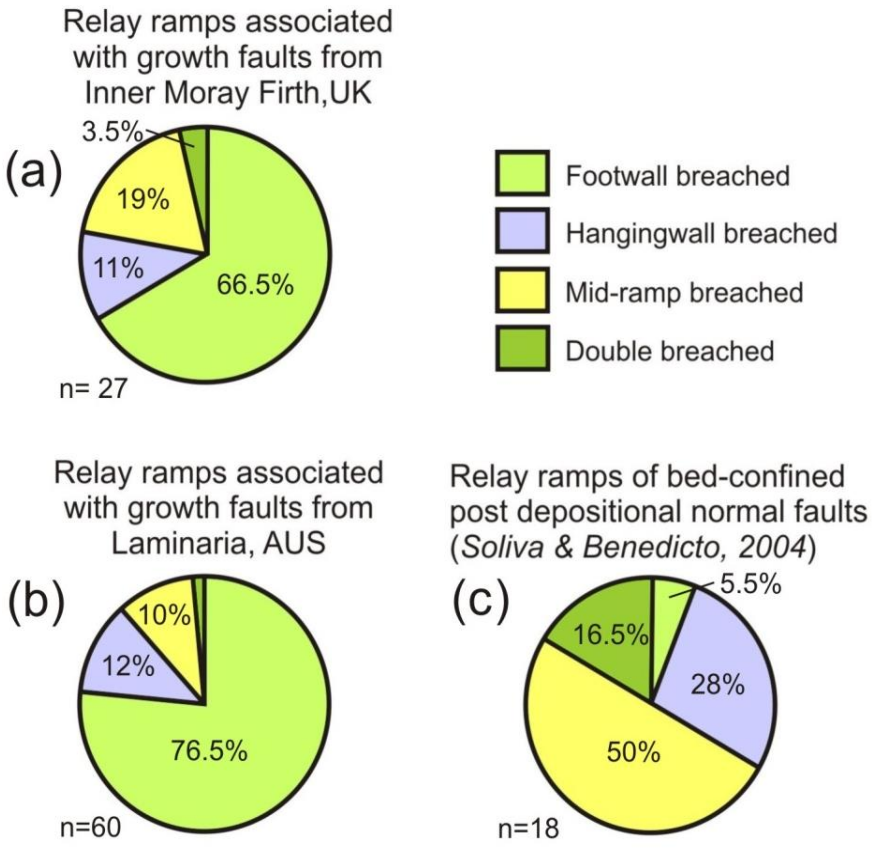

Figure 5.8 *Variability of the relay ramp breaching styles (in percentage) from: two of the analysed syn-depositional normal fault arrays from* ***(a)*** *Inner Moray Firth, offshore UK and* ***(b)*** *Laminaria High, offshore NW Australia; and* ***(c)*** *post-depositional normal faults from outcrop data, published by Soliva and Benedicto (2004).*

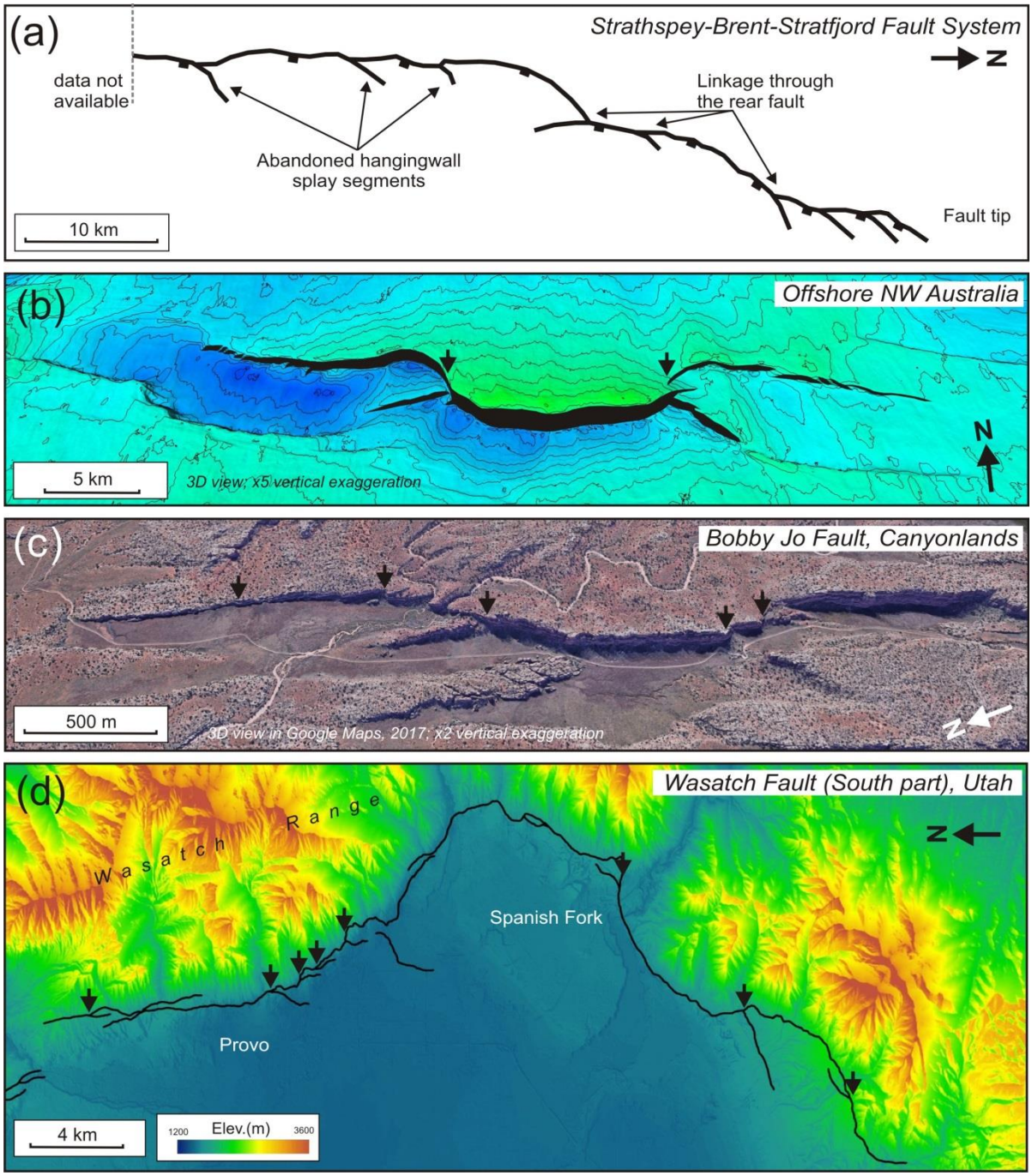
(a)
Strathspey-Brent-Stratfjord Fault System
N
data not available
Linkage through the rear fault
Abandoned hangingwall splay segments
Fault tip
10 km
(b)
Offshore NW Australia
N
5 km
3D view; x5 vertical exaggeration
(c)
Bobby Jo Fault, Canyonlands
500 m
3D view in Google Maps, 2017; x2 vertical exaggeration
N
(d)
Wasatch Range
Wasatch
Range
Wasatch Fault (South part), Utah
N
Spanish Fork
Provo
4 km
1200
Elev.(m)
3600

Figure 5.9 – previous page (a) *Traces of a linked normal fault array from Strathspey-Brent-Statfjord, northern North Sea (modified from McLeod et al., 2000);* ***(b)*** *3D view of a normal fault system from offshore NW Australia, displaying curved fault trace geometries especially in the zones of fault interaction (black arrows);* ***(c)*** *Satellite image of Bobby Jo fault, from Canyonlands, Utah (image courtesy of Google Maps). The black arrows indicate the fault branching locations, with breached relays located in the hangingwall of the fault system (Cartwright et al., 1996);* ***(d)*** *Elevation map of the southern part of the Wasatch fault system (eastern Basin and Range province). Note the highly curved map geometry of the system, with the majority of the splays located in the hangingwall. Arrows indicate footwall branch-points. Fault traces are from U.S. Geological Survey.*

A heterogeneous style of breaching appears to be common in other examples of relay ramps associated with post-depositional normal faults from outcrops in Somerset (Peacock and Sanderson, 1994) and Northumberland (Long, 2011).

The data are consistent with the hypothesis that mechanical interaction with, or isolation from the Earth's free surface is a first-order control on the style of relay breaching, an idea explored further in *section 5.5*. We now investigate how the style of breaching impacts on strain within the relay ramp, and the timing of breaching with respect to the displacement history of the fault array.

5.3.3 The relationship between the style of breaching, ramp strain and breaching index

The breaching of relay ramps is not an instantaneous process. The ramps continue to tilt as the bounding segments accommodate displacement until they finally become fully linked (Imber et al., 2004). Relay zones associated with syn-sedimentary faults on the Laminaria High indicate that there is a broadly positive relationship between breaching index (BI) and the fault-parallel ramp shear strain at the time of breaching (***Figure 5.9a***). In other words, high ramp strains are more likely to develop the later in the growth history of a fault array that a ramp is breached. Interestingly, we observe that the shear strain at which a ramp becomes breached varies by up to a factor of 9 (***Figure 5.9a***), despite

the presumably limited variability in mechanical stratigraphy and regional stress conditions across the Laminaria High study area (Long and Imber, 2012).

The data also show that relay ramps that are breached by the hangingwall fault typically display low BI, and breach at lower fault-parallel shear strains than footwall and mid-ramp breached relays (***Figure 5.9a***). This relationship suggests that breaching by propagation of the hangingwall fault – if it occurs at all – is more likely to occur at an early stage in the growth of the bounding faults. This relationship is illustrated in ***Figure 5.9b***, where we observe that the footwall breached ramp (R1) has significantly larger dips than the hangingwall breached ramp (R2). In addition, in relay ramps where the bounding faults are non-parallel (R3; ***Figure 5.9c***), breaching can occur rapidly and without the ramp accumulating large shear strains.

To summarize, our observations indicate that relays on surface-breaking normal faults tend to breach in the upper (or mid-) ramp region; however, lower ramp breaching, when it occurs, is more likely to happen at an early stage during fault growth. In the light of these findings, we now explore the likelihood of relay ramp breaching for two populations of surface-breaking normal faults and we use additional observations from the literature to develop a conceptual model of breaching fault behaviour.

Figure 5.10 – next page (a) *Ramp breaching index vs fault-parallel ramp shear stain, for relay ramps from the Laminaria High, offshore Australia. The breaching index (BI, Cartwright et al., 1996) is defined by the relation* $BI = (T_{SF} / T_T) * 100$ *where* T_{SF} *is the maximum throw on the abandoned splay and* T_T *is the cumulative throw, of the throw on the abandoned splay and the breaching throw. Note that the relay ramps which are breached by the rear fault are predominant and are characterized by larger shear strains and breaching index values than the hangingwall breached relay ramps;* ***(b)*** *3D view of a footwall-breached (R1) and a hangingwall-breached (R2) relay ramp along a linked fault system from Laminaria High. Note the larger dips (i.e. larger ramp shear strain) of the footwall breached ramp;* ***(c)- previous page*** *3D view of a relay ramp (R3) bounded by slightly non-parallel overlapping faults, which enhances the early breaching (i.e. low shear strains).*

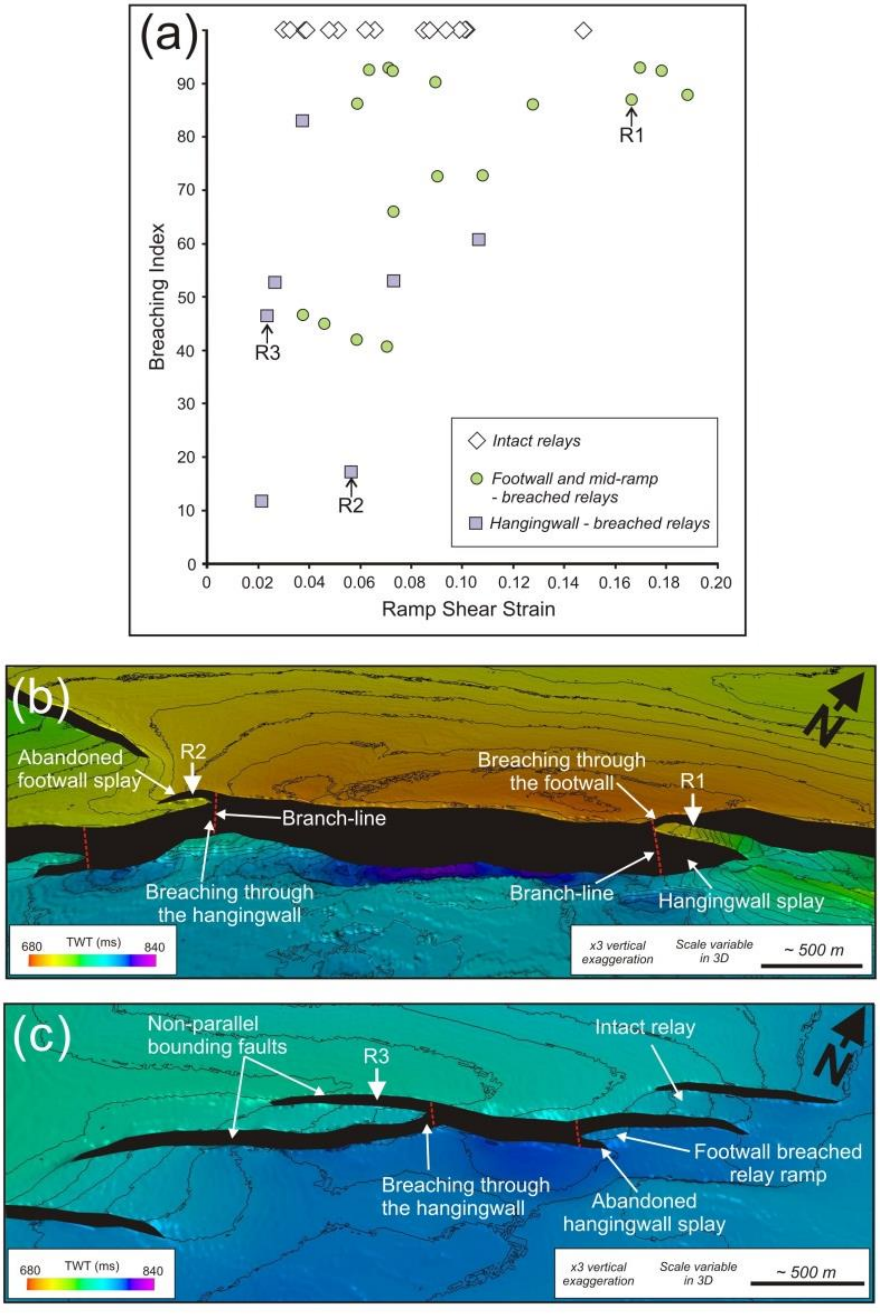
(a)
Breaching Index
Ramp Shear Strain
R1
R2
R3
Intact relays
Footwall and mid-ramp - breached relays
Hangingwall - breached relays
(b)
Abandoned footwall splay
R2
Branch-line
Breaching through the hangingwall
Breaching through the footwall
R1
Branch-line
Hangingwall splay
TWT (ms)
680
840
x3 vertical exaggeration
Scale variable in 3D
~ 500 m
(c)
Non-parallel bounding faults
R3
Intact relay
Footwall breached relay ramp
Breaching through the hangingwall
Abandoned hangingwall splay
TWT (ms)
680
840
x3 vertical exaggeration
Scale variable in 3D
~ 500 m

5.3.4 Influence of throw asymmetry on ramp breaching

Soliva and Benedicto (2004) and Imber et al. (2004) demonstrated that the likelihood of a relay ramp to be breached increases with increasing throw/separation (T/S) ratio (***Figure 5.1*** and *Section 5.2.2*). According to data published by Soliva and Benedicto (2004), ramps are intact if T/S < 0.27 and fully breached if T/S > 1.0. The dashed lines on the separation *vs* throw plots (***Figure 5.10a, b***) illustrate these limits, with ramps that fall between the limiting values likely to be in an incipient stage of breaching (Soliva and Benedicto 2004). Nevertheless, the T/S at which a ramp becomes breached appears to vary with lithology. For example, relays developed within interbedded shale and coal beds (Huggins et al., 1995) can remain intact for T/S > 1.0, because weaker, interbedded lithologies can accommodate ramp rotation by bed-parallel slip (Walsh et al., 1999), favouring high shear strains prior to ramp breaching (Imber et al., 2004). But even within the same dataset (i.e. Laminaria), where geological and regional stress conditions are assumed not to vary significantly, there is a significant scattering of the data within the mixed (i.e. linking stage) domain (T/S between 0.3-0.9). Hence, breaching likelihood cannot be explained solely by the relation between throw and separation.

The three right-stepping normal fault segments from the Laminaria High, shown in ***Figure 5.11***, illustrate this point. The fault segments are separated by two relay ramps, R4 and R5. R4 (between faults F1 and F2) appears to be intact, whilst R5 (between faults F2 and F3) is breached (***Figure 5.11b***). The average fault-parallel ramp shear strains for R4 and R5 are very similar, 0.087 and 0.090, respectively. The throw / separation (T/S) ratios are 0.61 for R4 and 0.35 for R5; in other words, the relay with the *greater* T/S ratio (R4) is intact. The close proximity of the two relays, and the similar character of the seismic reflections, suggest that deca- to hectometre-scale lithological variations are unlikely explain why R5 was breached at a lower T/S ratio than R4. It is, however, apparent that the front fault to R4 (F1; ***Figure 5.11a***) has a significantly larger maximum throw (52 m) and transfer throw (43 m) than the rear fault (23 m) (***Figure 5.11c, d)***. In contrast, the rear fault to the breached ramp, R5 (F3; ***Figure 5.10a***), has a slightly larger throw than the front fault (F2) (***Figure 5.11c***, ***d***). The intact relay ramp from the IMF described in *Section 3.1* (***Figure 5.5***) is also characterized by a

large asymmetry in throw, with the transfer throw on the front fault being much larger than transfer throw on the rear fault. This relay is not completely breached even though it has the largest T/S ratio from the IMF dataset. Thus, the throw asymmetry, in addition to throw / separation ratio, appears to be an important linkage criterion.

Figure 5.10c shows the throw/separation ratio, fault-parallel ramp shear strain and throw asymmetry (T_{FF} / T_{RF}) at the time of breaching, plotted by increasing T/S ratio, for 34 relay ramps from the Laminaria High and 7 relays from the IMF. We exclude breached relays characterised by very low breaching indices, because of the difficulty backstripping large breaching fault throws to estimate throw asymmetry and T/S at the time of breaching. The relay ramps are all intact for T/S < 0.3 (apart from R3; ***Figure 5.10***) and, for the Laminaria High dataset, all ramps are breached for T/S > 0.9. There are no ramps, breached or intact, with a T/S ratio larger than 0.74 in the IMF dataset. Also, there is an overall increase in shear strains with increasing T/S, but no direct correlation between the two parameters: relay ramps become breached at very variable shear strains.

The throw asymmetry parameter (***Figure 5.10c***) shows that the transfer throw on the relay-bounding faults can be very asymmetrical. Interestingly, relay ramps that are bounded by faults with a large throw asymmetry (i.e. $T_{FF} >> T_{RF}$) are more likely to be intact even for higher T/S ratios. ***Figure 5.10d*** shows a graph of T/S *vs* throw asymmetry for the relay ramps from Laminaria and IMF. The stippled horizontal lines mark the lower (0.3) and upper limit (0.9) of the T/S transition zones between the domains of intact and the breached relays (cf. Soliva and Benedicto, 2004). Relays with large throw asymmetry (T_{FF} / T_{RF} > 1.3 to 2.3; ***Figure 5.10d***) are more likely to be intact, whilst relays with bounding faults characterised by symmetric throws or larger throws on the rear fault (i.e. T_{FF} / $T_{RF} \leq$ 1.0), are more likely to be breached.

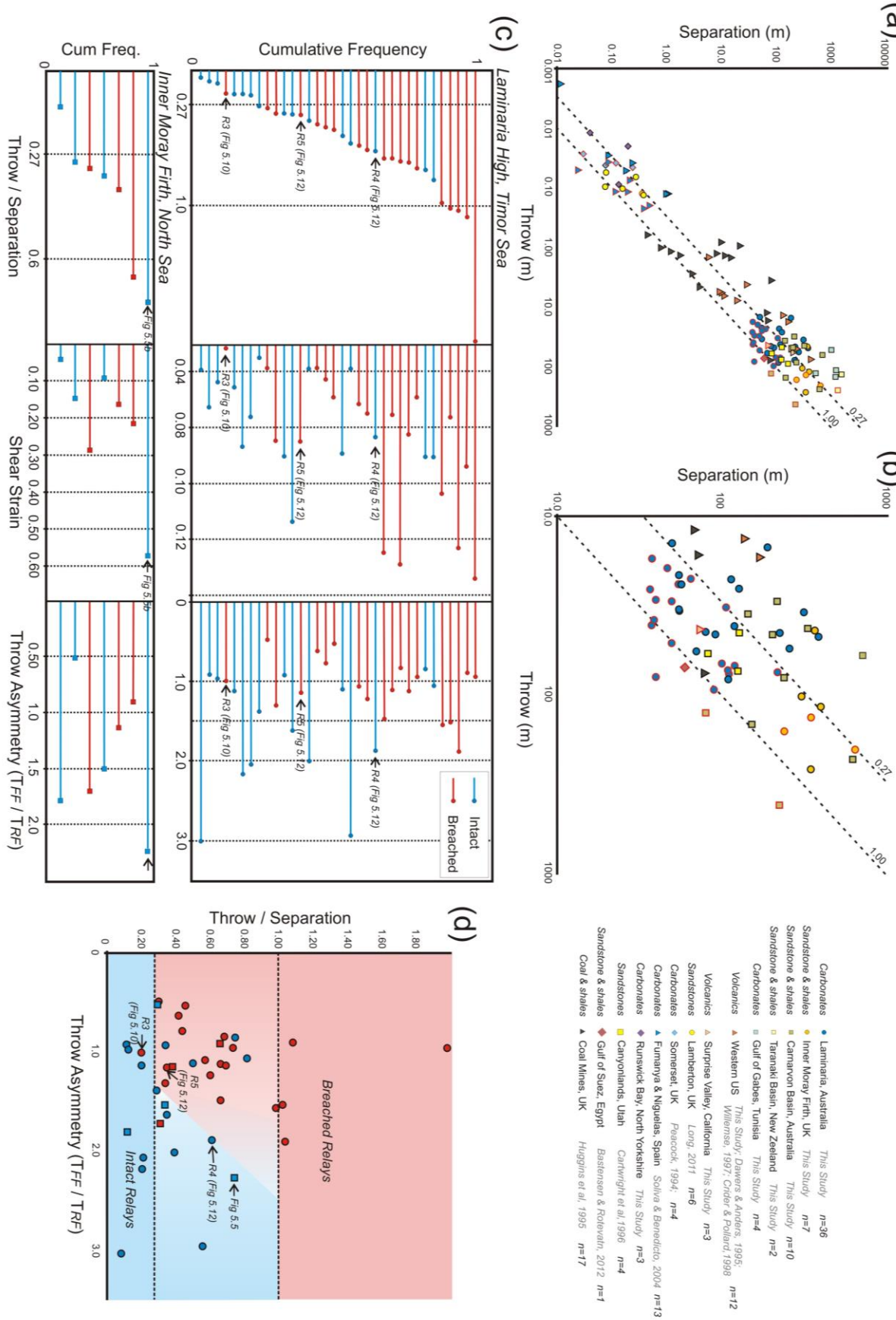
(a)
Separation (m)
Throw (m)
0.27
1.00
(b)
Separation (m)
Throw (m)
0.27
1.00
Carbonates
Sandstone & shales
Sandstone & shales
Carbonates
Volcanics
Volcanics
Sandstones
Carbonates
Carbonates
Sandstones
Sandstone & shales
Coal & shales
Laminaria, Australia This Study n=36
Inner Moray Firth, UK This Study n=7
Carnarvon Basin, Australia This Study n=10
Taranaki Basin, New Zealand This Study n=2
Gulf of Gabes, Tunisia This Study n=4
Western US This Study; Dawers & Anders, 1995; Willemse, 1997; Crider & Pollard,1998 n=12
Surprise Valley, California This Study n=3
Lamberton, UK Long, 2011 n=6
Somerset, UK Peacock, 1994; n=4
Fumanya & Niguelas, Spain Soliva & Benedicto, 2004 n=13
Runswick Bay, North Yorkshire This Study n=3
Canyonlands, Utah Cartwright et al,1996 n=4
Gulf of Suez, Egypt Bastensen & Rotevath, 2012 n=1
Coal Mines, UK Huggins et al, 1995 n=17
(c)
Laminaria High, Timor Sea
Inner Moray Firth, North Sea
Cumulative Frequency
Cum Freq.
Intact
Breached
R3 (Fig 5.10)
R4 (Fig 5.12)
R5 (Fig 5.12)
Fig 5.5
Fig 5.6
Throw / Separation
Shear Strain
Throw Asymmetry (TFF / TRF)
(d)
Throw / Separation
Breached Relays
Intact Relays
R3 (Fig 5.10)
R4 (Fig 5.12)
R5 (Fig 5.12)
Fig 5.5
Throw Asymmetry (TFF / TRF)

Figure 5.11 – previous page (a) *Logarithmic diagram of throw vs separation for intact (black outline) and breached relay ramps (red outline) from this study and previous studies;* ***(b)*** *Part of the diagram from* ***(a)*** *showing in more detail the plot area covered by the seismic-scale relay ramps;* ***(c)*** *Graph with normalized cumulative number vs throw/separation, fault parallel ramp shear strain and throw asymmetry for breached and intact relay ramps from Laminaria High and Inner Moray Firth;* ***(d)*** *Plot with throw/separation vs throw asymmetry for relay ramps from the Laminaria High (circles) and the IMF (squares).*

To our knowledge, there is no evidence, in either the Laminaria High or the Inner Moray Firth, for pre-existing structures which might favour early breaching of some of the relay ramps. Additionally, there is no suggestion that the lithology of the host rocks and, by inference, their mechanical properties vary significantly over deca- to hectometre scales within the same stratigraphic intervals (Long and Imber, 2012; Lăpădat et al., 2016). Therefore, we hypothesise that the variable breaching strains and the ramp breaching likelihood are influenced by the way in which the overlapping faults interact, specifically the way in which asymmetric transfer throw affects or is influenced by the mechanical interaction. We discuss this point in the next section of the paper.

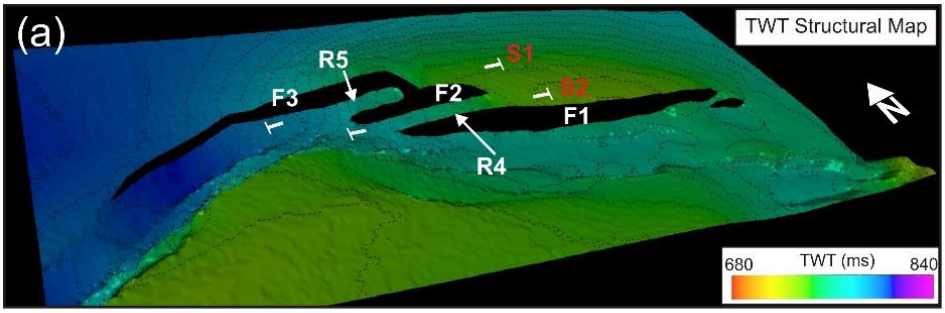

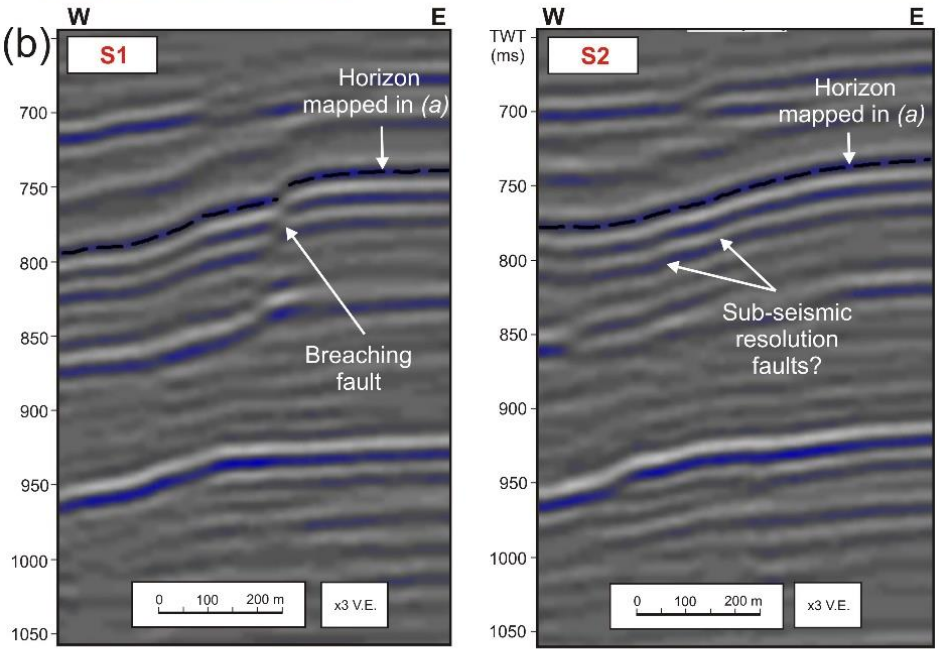

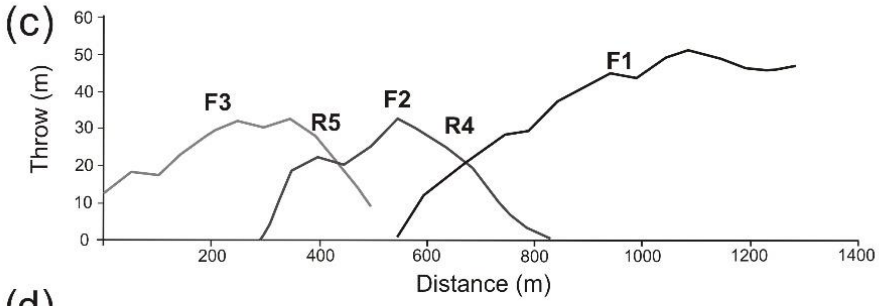

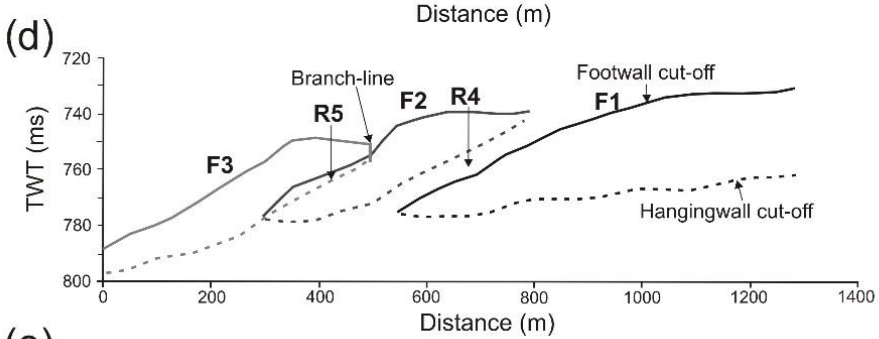

(e)

	R4	R5		R4	R5
Transfer throw (m)	33.4	22.5	Throw / Separation	0.61	0.35
Separation (m)	55	65	Ramp Strain	0.087	0.090

Figure 5.12 (a) *3D view of normal fault segments separated by two relay ramps, one intact and one breached from Laminaria High, Bonaparte Basin (offshore Australia);* ***(b)*** *Seismic sections through the relay ramps parallel with the strike of the faults. Rotation of the ramp is very likely to be accommodated by sub-seismic scale faults (throw < 10 m), indicated by subtle flexure of the reflectors in S2;* ***(c)*** *Throw-distance profiles along the strike of the three mapped segments;* ***(d)*** *Projection of the horizon cut-offs on a vertical plane parallel with the faults strike;* ***(e)*** *The main relay ramp parameters. Seismic data courtesy of Geoscience Australia.*

5.4. Mechanical models and discussions on breaching styles

Evidence from the spatial and temporal occurrence of earthquakes suggests that faults interact mechanically through their slip-induced stress fields (Stein, 1999). Crider and Pollard (1998) and Crider (2001) used elastic boundary-element method models to analyse the mechanical interaction between overlapping normal faults and the breaching of relay ramps, assuming that the breaching fault location can be predicted from the distribution of Coulomb shear stress perturbations after a single, modelled slip event. We follow their approach to investigate the distribution of Coulomb shear stress around two overlapping, interacting normal faults. The aim is to understand how mechanical interaction between the relay-bounding faults and the Earth's free surface influences relay breaching.

The boundary-element model comprises two discontinuities (i.e. fault surfaces) located within a homogeneous elastic medium, on which we apply a remote driving stress consistent with an extensional failure regime, where maximum principal stress ($\sigma 1$) is vertical and the minimum compressive horizontal stress ($\sigma 3$) is oriented normal to the fault strike. The faults dip at ~60° and converge slightly downwards (see model insets in ***Figure 5.12***). This model geometry is in accordance with the concept that normal faults grow in a coherent manner, usually by upward fault bifurcation from a deeper fault structure (Childs et al., 1995). In one of the models the faults are located within an elastic whole space and in the other one the faults reach the free surface. In this way

we can analyse how Earth's free surface influences the stress interaction between surface-breaking overlapping faults. The model has certain simplifications and limitations. It does not allow spatial heterogeneities in the elastic properties of the material, such as rock layering encountered in nature (the medium is completely homogenous). Also, when subject to deviatoric stresses the faults slip freely, hence the model does not consider any friction on the fault surfaces. Incorporation of friction on the fault planes would only decrease the magnitude of the stress perturbations, but not their distribution. The slip on faults generates changes in the stress within the surrounding elastic medium. Similarly, by changing the stiffness of the material (i.e. Young's modulus), the distribution of the perturbed stresses does not change, only its magnitude (i.e for same deviatoric stress, the induced slip decreases in materials with larger Young's modulus, hence the stress perturbations are smaller). Previous work by Willemse (1997) showed that the effect of Poisson's ratio is moderate, more compressible rocks showing a larger degree of interaction. In the experiments presented in this chapter we used a Poisson's ratio of 0.25 and a Young's modulus of 20 GPa. However, variations of these elastic parameters do not alter the final conclusions of the modeling.

Coulomb failure stress (CFS) is a measure of the likelihood of failure of potential surfaces located within that medium (Crider and Pollard, 1998). Specifically, CFS describes a relationship between the normal and shear stresses by considering also a frictional resistance to slip on those surfaces. Changes in CFS have been calculated based on the formula:

$$CFS = ((\sigma_1 - \sigma_3)/2-(\sigma'_1 - \sigma'_3)/2)-0.2*((\sigma_1 + \sigma_3)/2-(\sigma'_1 + \sigma'_3)/2)$$

where σ'_1 and σ'_3 are the values of the initial maximum and minimum principal compressive stresses and σ_1 and σ_3 are the post-deformation principal stresses. We consider a coefficient of friction of 0.2 which is appropriate for less consolidated sedimentary rocks in the proximity of the Earth's surface (Behnsen and Faulkner, 2012). Also, because the model does not consider pore fluid pressure, a lower coefficient of friction accounts for any potential pore fluid pressure effect. Variation in the coefficient of friction does not modify the main outcome of the results, however a more complete investigation is

required to investigate the variability of the friction coefficient on the distribution and magnitude of stress perturbations.

Figure 5.12a shows the distribution of Coulomb failure shear stress (CFS) perturbations draped on the deformed surface of an originally horizontal plane located in the centre of two overlapping normal faults. The faults have elliptical upper tip-lines and are located within an elastic whole space. This configuration can be used to approximate the stress distribution associated with slip on buried, post-depositional normal faults (Willemse, 1997). The shear stress increases at the tip of the faults, but decreases along the strike of the fault traces, delineating a near-symmetric, elliptical stress drop zone (or "stress shadow") within both the footwall and the hangingwall (***Figure 5.12a***). Willemse (1997) showed that the spatial distribution and size of the stress drop zone depends on the size (height) of the fault and the magnitude of slip. This stress drop zone inhibits the propagation of an overlapping fault, requiring large displacement gradients near the tips of the bounding faults in order to overcome the decrease in shear stress (Gupta and Scholz, 2000). The model suggests that the ratio of stress increase at the fault tips *vs* stress drop is identical in both the hangingwall and the footwall sides of the relay. This result is consistent with the lack of preferred upper or lower ramp breaching for relays on buried, post-depositional normal faults (***Figure 5.7c***)

Figure 5.12b shows the distribution of Coulomb failure shear stress perturbations on a displaced surface located 600 m below the free surface, due to slip on two sub-parallel, overlapping normal faults that dip ~60° within an elastic half-space. The fault tip-lines are elliptical, having the uppermost tip-lines located immediately below the free surface. The observation location, within the upper half of the faults, was chosen based on the fact that surface-breaching faults have displacement maxima skewed toward the free surface (Rudniki and Wu, 1995; Childs et al., 2003), and therefore lateral fault propagation would be likely to occur first within this upper section of the faults (Aydin and Schultz, 1990). The separation between the overlapping segments decreases towards depth, as in the previous model from ***Figure 5.12a,*** simulating an upward splay from a main fault located below 4000m**,** which is not included in the model. In contrast to Crider's and Pollard's (1998) model, we do not include opening mode deformation. The modelled joint planes (***Figure 5.12***, right-hand side) are used for the

purpose of illustrating the reorientation of maximum horizontal compressive stress (σ_2), along which the interacting faults are likely to propagate in relation with the zones of modified Coulomb shear stress. The locus of increased Coulomb failure shear stress within the region of overlap (***Figure 5.12b***) favours upper ramp breaching, a finding consistent with Crider and Pollard (1998), and consistent with data from the Laminaria High and IMF (***Figure 5.5c, d***). The stress drop zone is highly asymmetrical, with a larger stress decrease in the hangingwall. Propagation of the front fault is likely to be impeded by the stress drop zone in the hangingwall of the rear fault. As a result, large displacement gradients can potentially accumulate on the front fault, an inference that is consistent with observations of natural relay zones (e.g. ***Figure 5.6f***), and with the large throw asymmetry associated with many intact relays (***Figure 5.10***). Conversely, the zone of increased Coulomb shear stress within the footwall of the front fault favours rapid propagation of the rear fault, which will probably lead to breaching of the relay ramp. This may explain why many of the relay ramps associated with surface-breaking normal faults are breached through the footwall side. Asymmetry in the horizontal component of displacement, with larger heaves on the front faults, will introduce a component of fault-normal shear (Peacock and Sanderson, 1994), causing the relay to twist and dip toward the mutual hangingwall. This asymmetry can potentially explain why relay ramps usually dip toward the hangingwall and offers an explanation for the differences between the geometry of the natural example and the elastic dislocation models of a single slip event described by Crider and Pollard (1998). An alternative explanation for this is that relay ramps develop where the ramp-bounding faults grow upwards through a syn-fault sequence, breaching a previously-developed fault propagation fold (Lăpădat et al., 2016). Our elastic models replicate successfully the geometry of many natural relays which have a dipping component toward the mutual hangingwall (***Figure 5.12***). This geometry was obtained only when the separation length between the overlapping segments is significantly smaller than the size of the bounding faults, an outcome that is consistent with the coherent fault growth model (Childs et al., 1995).

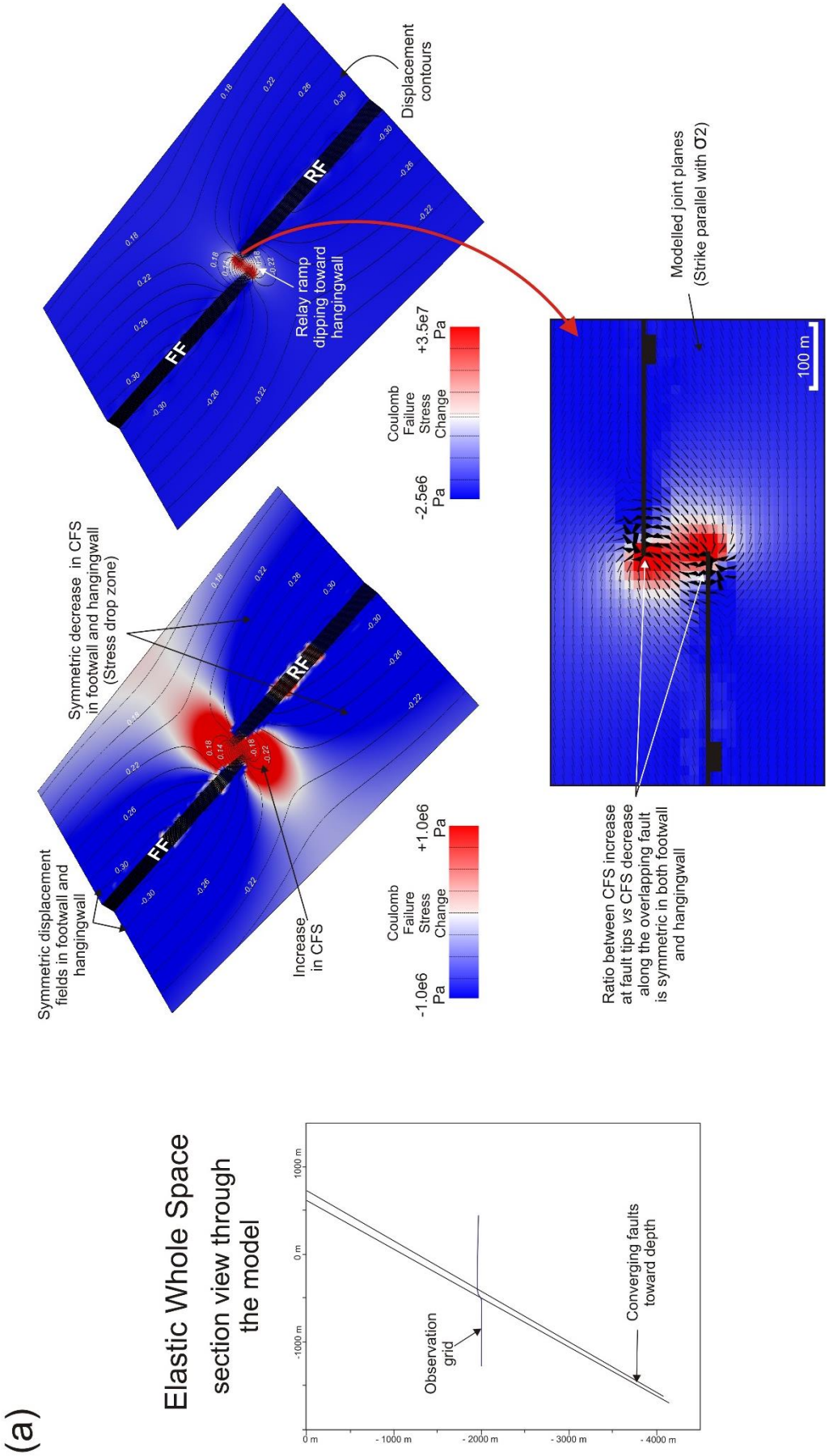
(a)
Elastic Whole Space
section view through
the model
1000 m
0 m
-1000 m
0 m
- 1000 m
- 2000 m
- 3000 m
- 4000 m
Observation
grid
Converging faults
toward depth
Symmetric displacement
fields in footwall and
hangingwall
Symmetric decrease in CFS
in footwall and hangingwall
(Stress drop zone)
Increase
in CFS
Coulomb
Failure
Stress
Change
+1.0e6
Pa
-1.0e6
Pa
FF
RF
Displacement
contours
Relay ramp
dipping toward
hangingwall
Coulomb
Failure
Stress
Change
+3.5e7
Pa
-2.5e6
Pa
Modelled joint planes
(Strike parallel with σ2)
100 m
Ratio between CFS increase
at fault tips vs CFS decrease
along the overlapping fault
is symmetric in both footwall
and hangingwall

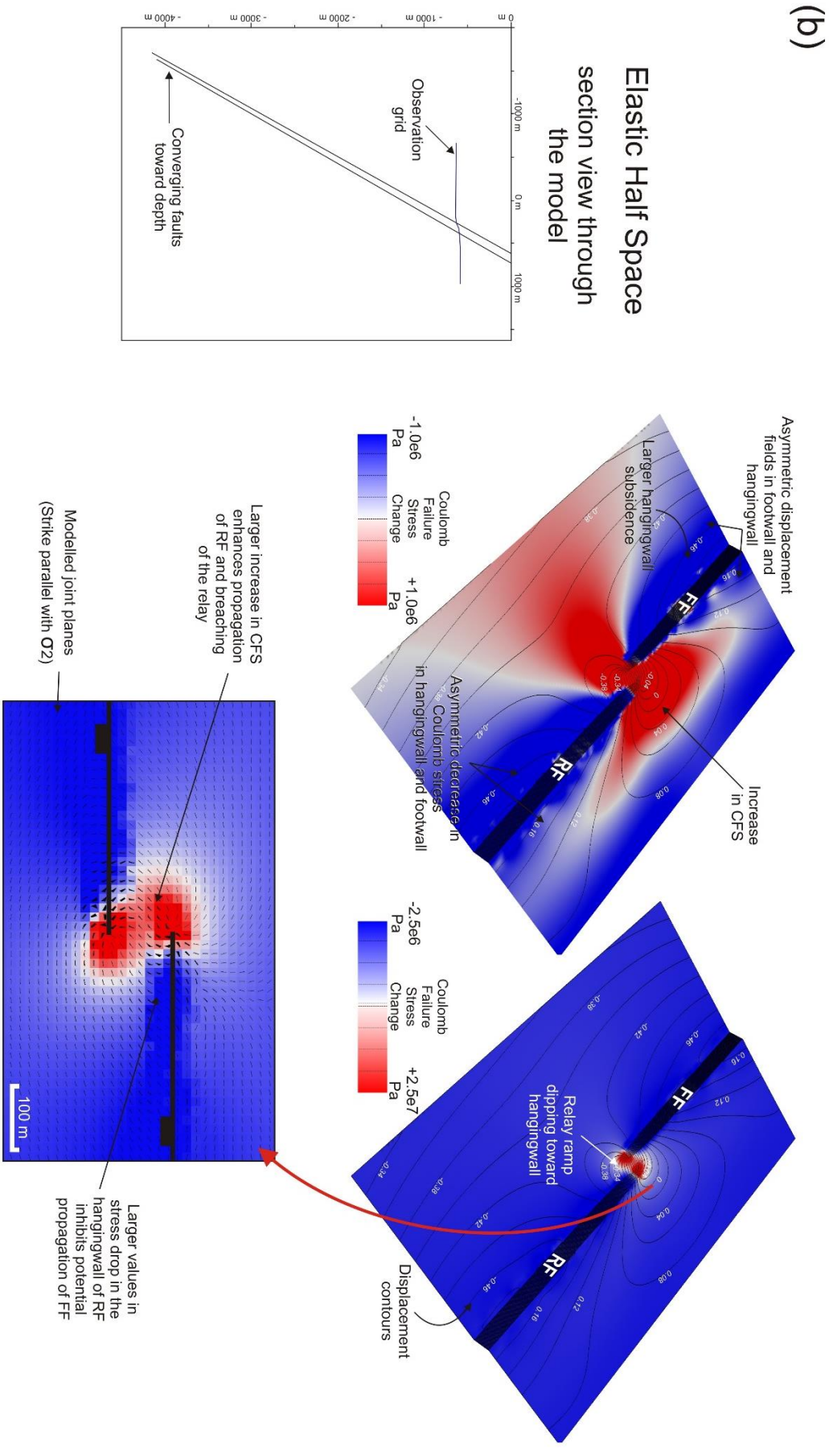
(b)
Elastic Half Space
section view through
the model
Observation
grid
Converging faults
toward depth
Asymmetric displacement
fields in footwall and
hangingwall
Larger hangingwall
subsidence
Increase
in CFS
Asymmetric decrease in
Coulomb stress
in hangingwall and footwall
Coulomb
Failure
Stress
Change
-1.0e6
Pa
+1.0e6
Pa
Relay ramp
dipping toward
hangingwall
Displacement
contours
-2.5e6
+2.5e7
FF
RF
Larger increase in CFS
enhances propagation
of RF and breaching
of the relay
Modelled joint planes
(Strike parallel with σ2)
Larger values in
stress drop in the
hangingwall of RF
inhibits potential
propagation of FF
100 m

Figure 5.13 – previous page (a) *Distribution of changes in Coulomb failure shear stress (CFS) associated with imposed remote stress on two overlapping normal faults, which dip at ~60° and converge slightly downwards. The faults are located within an elastic whole-space (see inset of a cross-section through the model). The analysed grid is situated in the centre of the faults. Black contours represent displacement isolines; colours represent changes in CFS; tick marks from the detailed grid (right-hand side) represent the orientations of potential failure planes, parallel to σ2, which can describe trajectories of later fault propagation* ***(b)*** *CFS changes associated with displacement on two overlapping normal faults, which dip at ~60° and converge slightly downwards. The faults are embedded within an elastic half-space. The horizontal plane of observation is located 600 m below the free surface. Note the asymmetry in both displacement fields and changes in CFS in comparison with the model from* ***(a)***.

Throw asymmetry across a relay zone is not necessarily the result of mechanical interaction between the overlapping faults: asymmetry can arise simply because one fault is larger than the other (i.e. has a larger displacement and/or length). Because there is a direct relationship between the size of the fault and the displacement it can accrue (Walsh and Watterson, 1988), the increased Coulomb shear stress perturbations at the tips of the rear fault should be smaller than those associated with the front fault. Similarly, the shear stress drop zone related with slip on the frontal fault is significantly larger. According to Gupta and Scholz (2000), the magnitude of the stress drop is always larger than the increase in shear stress at the fault tips. Therefore, a significantly larger throw on the front fault and hence larger associated stress drop would be more likely to inhibit the propagation of a smaller (in terms of displacement and length) rear fault, similar with the example from Laminaria from ***Figure 5.11***. Also, it would probably require larger strains before being completely breached, as in the example from IMF (***Figure 5.5***).

The data presented in ***Figure 5.9a*** suggest that breaching by the hangingwall fault, if it happens, takes place at an earlier stage in the evolution of a surface-breaking normal fault array than upper ramp breaching. It is possible that the propagation of the front fault is mechanically easier if the faults begin to interact and overlap at an early stage during their growth, when the displacement-dependent stress

shadow zones are not well developed. Irregularities in fault geometry, non-parallelism of the relay-bounding faults or local lithological heterogeneities could induce stress concentrations that are large with respect to the incipient stress shadows, giving rise to early breaching of the relay ramps, by either front or rear faults. Also, during the early stages of fault growth, the component of oblique slip associated with the asymmetric accommodation of displacement between hangingwall subsidence and footwall uplift (Roberts, 2007) is likely to be small, again favouring propagation toward the rear fault. Segmentation along the Wasatch fault system (DuRoss, 2016) or along the East African Rift (Morley, 2002) indicate similar patterns of relay breaching, with first-order linkage occurring predominantly through the rear fault.

Observations on natural examples and mechanical analysis indicate that surface-breaking, segmented normal faults arrays tend to link by propagation of the rear segment through the upper part of relay ramp. Hence, from a seismic hazard point of view, surface ruptures across relay zones are more likely to occur through the rear fault. However, it needs to be considered that fault growth and linkage is a three-dimensional process. Earthquakes nucleate in the lower part of the crust, usually at depths below 5 km and seismic slip induced fault propagation and linkage can be influenced by changes with depth in stress conditions and rheology, which can result in further complexities of fault linkage. Long and Imber (2012) also described complex 3D geometries of relay zones, which influenced by the heterogeneous mechanical layering of rocks, displayed variable breaching characteristics at different levels, but with the shallower, near-surface part of the relay being breached by the rear fault.

5.5. Conclusions

1) Breaching of relay ramps associated with syn-sedimentary normal fault arrays on the Laminaria High and in the Inner Moray Firth (IMF) Basin occurs preferentially within the upper to mid-ramp section, typically by propagation of the footwall fault. Relay ramps associated with strata-bound, post-depositional normal faults show a larger variation in breaching styles compared with relays on syn-sedimentary faults.

2) The breaching indices and fault-parallel ramp shear strains at breaching tend to be larger for footwall breached relay ramps than for hangingwall breached relay ramps, although there is variability within this overall trend. Thus, breaching by propagation of the hangingwall fault, when it does happen, tends to occur early in the evolution of a surface-breaking normal fault array.
3) Relay ramps on the Laminaria High and in the IMF tend to be intact when the throw / separation (T/S) ratio is < 0.3, and breached when T/S > 0.9. This result is consistent with a previously published criterion for segment linkage. Relays with T/S ratios between these limiting values are likely to remain intact if the throw on the front fault is greater than 1.3 to 2.3 times the throw on the rear fault the relay ramp.
4) The qualitative and quantitative characteristics relay breaching along surface-breaking normal fault arrays can be explained by the asymmetric partitioning of slip, and associated stress drop or stress enhancement zones, caused by mechanical interaction of the relay-bounding faults with the Earth's free surface.

Acknowledgments

We thank Mark Allen for his comments and suggestions on an earlier version of this manuscript.

| Chapter 6 |

Geological controls on the geometries and strain variability within relay ramps

Abstract

The geometries and kinematic evolution of relay ramps are inherently related to the growth and the interaction processes of neighbouring normal faults. It is generally accepted that the relay ramp aspect ratio (the ratio between fault overlap length and separation distance between bounding faults) is controlled by the mechanical interaction between the faults and that the host rock lithology also plays an important role. In this study, by including the displacement component within the fault dip- and fault strike-parallel domains, we can investigate both the effects of lithology and fault interaction on the three-dimensional geometry and strain characteristics within relay ramps. We show that normal fault-bounded ramps within mechanically competent rocks tend to develop a larger spectrum of aspect ratios, with a mean aspect ratio larger than those developed in incompetent rocks. Ramps with high aspect ratio developed in competent rocks usually have tabular geometries and smaller fault-parallel shear strains. Incompetent lithologies have relay ramps with lower aspect ratio, higher fault parallel-shear strains and a significant component of fault normal shear, which results in rhomboidal relay ramp geometry. Faults propagation is more easily impeded within incompetent lithologies, resulting in higher stress interactions and development of higher displacement gradients, which in many cases are highly asymmetrical. The dip direction of the relay ramp toward the mutual hangingwall can be both the result of fault-propagation folding during the underlapping stage of the relay and by shearing in the plane normal to the faults, as a result of larger displacement gradients on the front faults. Mechanical models indicate asymmetric shear stress drop for surface breaching normal faults, which can inhibit propagation of the front fault and accumulation of asymmetrically larger displacement gradients.

6.1. Introduction

The transfer of displacement across two or more normal faults that cut sub-horizontal beds occurs through zones of ductile deformation, called *relay zones* (Larsen, 1988; Peacock and Sanderson, 1991; Peacock and Sanderson, 1994; Trudgill and Cartwright, 1995; Childs et al., 1996). Within a relay zone, the beds are continuously rotated and strained as slip accumulates on the bounding faults (Ferrill and Morris, 2001; Imber et al., 2004) forming a relay ramp. With increasing displacement the faults propagate until they become physically linked and the relay is breached (Crider and Pollard, 1998; Imber et al., 2004) (previously discussed in *Chapter 5*). Hence, relay ramps are dynamic structures with geometries that evolve through time as faults propagate, interact and link (Peacock and Sanderson, 1994).

The two-dimensional, map-view geometry of the relay ramps is defined by the *relay aspect ratio* (Huggins et al., 1995; Acocella et al., 2000; Long and Imber, 2011), which is the ratio between the fault overlap length and the separation distance between the bounding faults (***Figure 6.1a***). Previous studies showed that the relationship between overlap and separation follows a power-law scaling trend over 8 orders of magnitude, with a mean aspect ratio value of 4.2 (Long and Imber, 2011). The main controlling factor on the variability of relay aspect ratio is thought to be the stress interaction between the neighbouring faults (Gupta and Scholz, 2000; Long and Imber, 2011). However, Willemse (1997) showed that the degree of mechanical interaction between neighbouring segments varies itself with the initial spatial arrangements of the fault segments. Hence, the geometrical evolution of the ramp is controlled by the spatial configuration of the overlapping/underlapping segments at the time when faults start to interact. Long and Imber (2011) showed that normal faults confined to mechanical layering and those formed by reactivation of pre-existing structures are mechanically favoured to develop high aspect ratio relay ramps (with an average aspect ratio > 8). Although any obvious correlation between lithology and relay aspect ratio was not observed, Long and Imber (2011) argued that any possible relationship could have been hindered by the large scale of observation of their relay data (over 8 orders of magnitude).

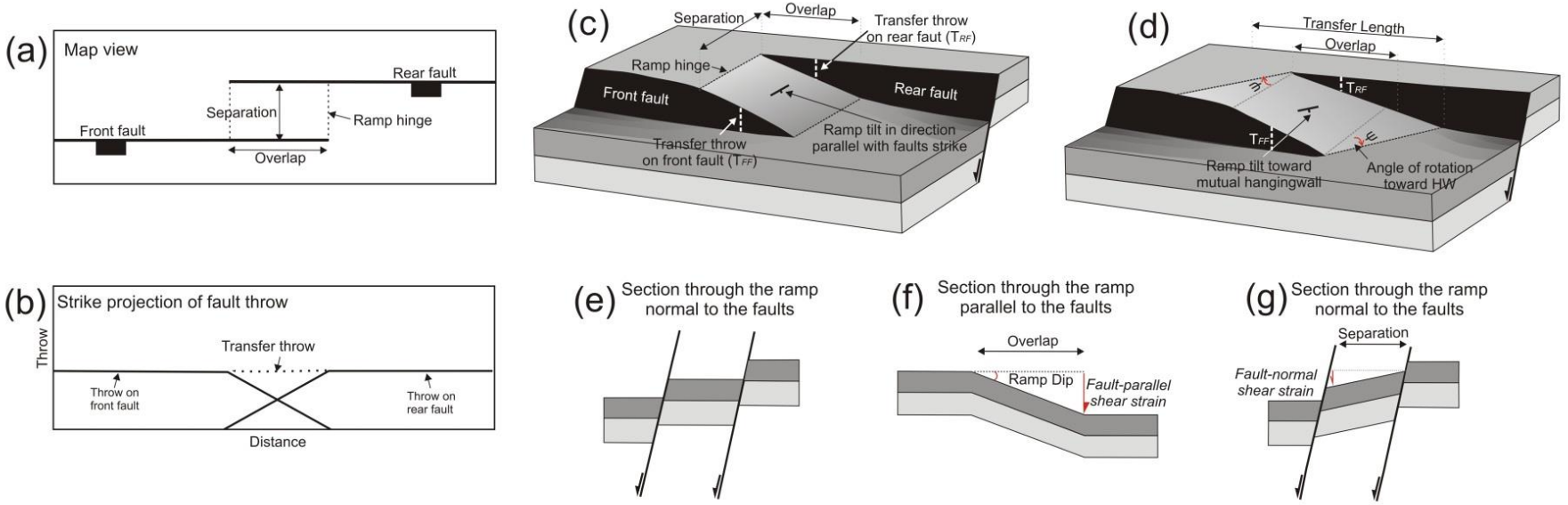

Figure 6.1 (a) *Sketch of two overlapping normal fault segments in horizontal plane view. The two-dimensional geometry of a relay ramp is described by the overlap length and the separation distance between the segments.* ***(b)*** *Strike projection on a vertical plane of the throw distribution on the two segments from (a) showing throw thrasfer within the relay zone.* ***(c)*** *3D sketch of a relay ramp with tabular geometry;* ***(d)*** *3D sketch of a rhombohedral relay ramp; the relay throw transfer is measured in the centre of relay on both faulst and includes the component of bed rotation within the fault-normal plane if present (see (g));* ***(e)*** *Section through a tabular ramp in a direction orthogonal to the faults;* ***(f)*** *Section through a relay ramp in a direction parallel the overlapping faults;* ***(g)*** *Section in a direction orthogonal to the faults through a rhombohedral ramp which dips toward the hangingwall.*

However, the mechanical properties of the host rocks influence how fault segments interact through their elastic stress fields (Willemse, 1997; Gupta and Scholz, 2000) and hence, lithology is expected to indirectly control the relay aspect ratio (Long and Imber, 2011). Also, Childs et al. (2016) suggested that the relay ramp aspect ratio is controlled by the mechanical properties of the host rocks at the time of deformation and by the reactivation of pre-existing basement structures. Specifically, their findings indicate that relay ramps developed within competent lithologies, such as the massive sandstones from SE Utah (Entrada, Navajo or Wingate sandstones) have aspect ratios larger than the global mean (Long and Imber, 2011), typically larger than 5, or even larger than 10. Furthermore, Childs et al. (2016) identified the reactivation of pre-existing structures as the cause for high aspect ratio relay ramps.

In this chapter we go a step further by investigating the three-dimensional geometry of relay ramps (***Figure 6.1c*** and ***6.1d***) by adding to the map-view aspect ratio the third dimension given by the displacement component on the bounding faults (***Figure 6.1b***). In this way we can investigate better the effects of both fault interaction and mechanical properties of the host rocks on the relay ramp geometry, and also on the variability of strain. Specifically, we analyse the variability of *fault-parallel shear strain* (***Figure 6.1e***) and *fault-normal shear strain* components (***Figure 6.1f***) within relay ramps in relation to the relay aspect ratio and the dominant lithology of the host rocks. Surprisingly, previous research work has not focused much attention on the relationship between the two- dimensional ramp geometry and the strain characteristics. To our knowledge, only Childs et al. (2016) investigated the relationship between the relay aspect ratio, lithology and the shape of the relays (rectangular *vs* rhomboidal). However, their maximum aspect ratio data was limited to around 6 (their figure 8). The compiled data, from our own analysis and previously published literature, indicate that lithology critically influences the three-dimensional geometry and the strain characteristics within relay zones. Also, we show that the fault-normal shear strain component within relay ramps bounded by surface breaching normal faults is not only a consequence of the monoclinal folding during the underlapping stage of the relay (Childs et al., 2016), but can be explained by the mechanical interaction between the overlapping segments.

Better understanding of the relay ramp geometries and associated strain variability can be important during the exploration of rift basins and passive margins and the appraisal or development of normal fault-bounded prospects, since relay ramps can act as trapping structures or leaking pathways for hydrocarbons (Rotevatn et al., 2007). Also, the analysis of finite strain relay ramps can offer potential important insights into how normal faults grow in different mechanical stratigraphic settings (Cartwright et al., 1995; Jackson et al., 2016).

6.2. Datasets and methods

6.2.1. Datasets

The datasets within this study comprises 118 relay ramps from high quality 3-D seismic surveys, high resolution topographic data, outcrops and published literature (see digital appendix), which have provided good quality or enough information to measure with confidence the main parameters that were used in the analysis. The compiled datasets cover a wide range of scales and different lithologies with various mechanical properties, from competent carbonate or sandstone layers to incompetent coals and unconsolidated clastic sediments.

Accurate measurement of the parameters that define the ramp geometry and strain is critical for the quantitative analysis used in this study. The sampling interval of the seismic data used in this study is 2 ms, meaning that the measurement errors due to the limitations in vertical seismic resolution are negligible (below 2 ms). The overlap length is defined in map view as the distance measured parallel to the strike of the faults, between the neighbouring fault tips (***Figure 6.1***). There can be a certain degree of uncertainty related to the accurate identification of the fault tips (i.e. locations of zero displacement on the fault) based on interpretation of seismic data, which has limited vertical (ranging in general from 10 to 30 m) and lateral resolution. We included in our measurements the component of seismic-scale lateral fault tip-folding (i.e. ductile deformation; Walsh and Watterson, 1991) in order to limit some of the uncertainties associated with the sub-seismic fault throw resolution (Long and Imber, 2012). The fault throws measured on seismic reflection profiles were converted from two-way-time (TWT) to depth using time-depth relations from nearby wells (see Lăpădat et al., (2016) for

the IMF dataset and Long (2011) for the Laminaria dataset), in order to produce reliable measurements of fault throws and associated ramp shear strains (***Figure 6.1***).

6.2.2. Parameters

Fault-parallel ramp shear strain is the ratio between the average throw measured on the bounding faults (measured in a direction normal to the fault from the tip of the other overlapping segment) and the fault overlap length (***Figure 6.1 e***). The fault-parallel ramp shear strain is directly related to the dip of the ramp measured in a direction parallel to the strike of the faults. Previously, it has been used to evaluate the strains of the relay ramps prior to breaching (Imber et al., 2004; Soliva and Benedicto, 2004). The fault-parallel ramp shear strain is controlled by the displacement gradients on the bounding faults (Ferrill and Morris, 2001), hence it is a direct measurement of the interaction between the overlapping faults segments and the critical amount of strain a ramp can support before being breached.

Fault-normal shear strain (***Figure 6.1 f***) is the shear strain measured in the centre of the relays, in the plane normal to the overlapping faults. It represents the ratio between the vertical component of displacement accommodated by bed rotation in the direction orthogonal to the bounding faults and the separation distance. The data used in this study are at different scales and from various sources, outcrops and 3D seismic reflection data. To minimize the errors related to time-depth conversion for the seismic data, we utilize as a proxy for fault-normal shear strain the amount of ductile deformation as a percentage of the total throw in the fault-normal direction measured in the centre of the relay ramp. Relay ramps with perfect tabular geometries will have no bed rotation in the direction perpendicular to the overlapping faults, hence the fault-normal shear strain will be zero.

In the following section we present the results of the analysis of the ramp strain and its relationship to the relay ramp geometries and the lithologies of the host rocks. Then, we describe in more detail several examples of relay ramps from contrasting lithological sequences and we provide a mechanical model for explaining the variability of strain within relay ramps bounded by syn-sedimentary (surface breaking) normal faults.

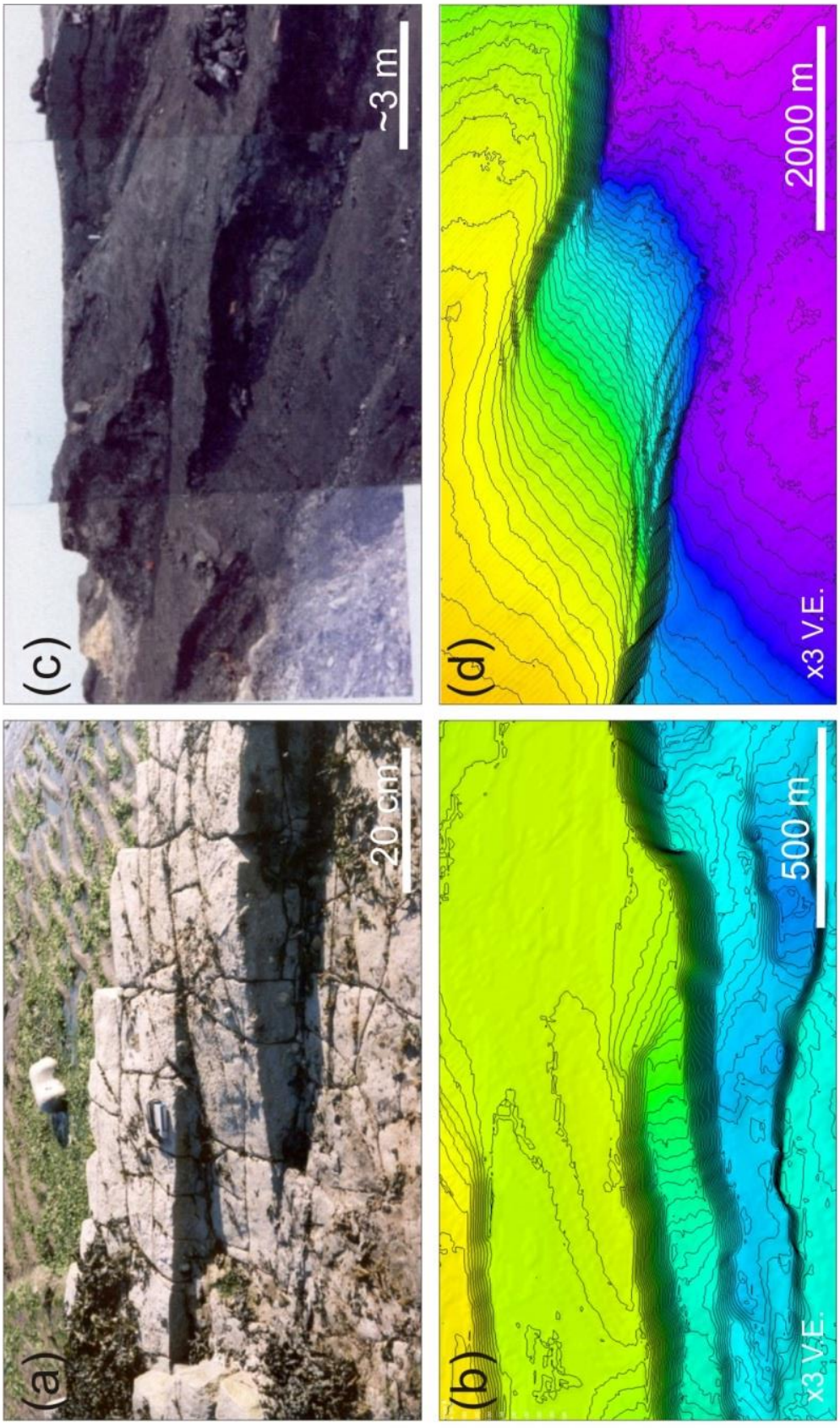
(a)
20 cm
(b)
500 m
x3 V.E.
(c)
~3 m
(d)
2000 m
x3 V.E.

Figure 6.2 – previous page *Examples of relay ramps at different scales and within different type of lithologies.* ***(a)*** *Relay ramp in carbonates from Kilve, Somerset (image from https://www.fault-analysis-group.ucd.ie/gallery/relay.htm, courtesy of Fault Analysis Group, University College Dublin);* ***(b)*** *relay ramp in carbonates mapped on 3D seismic reflection data from Laminaria High, offshore NW Australia; warm colours represent zones of higher elevation and cold colours are associated with areas of lower elevation;* ***(c)*** *relay ramps in a coal seam at Plenmellor open cast, Northumberland (from Huggins, 1995, image from https://www.fault-analysis-group.ucd.ie/gallery/relay.htm, courtesy of Fault Analysis Group, University College Dublin);* ***(d)*** *relay ramp imaged by 3D seismic data, developed within a syn-growth sand-shale sequence from the Taranaki basin, offshore New Zealand. Warm colours represent zones of higher elevation and cold colours are associated with areas of lower elevation.*

6.3. Data analysis and results

Ductile strains within relay ramps are often thought to be relatively simple because the ramps accommodate deformation predominantly in the direction parallel to the slip direction on the bounding faults (hence, the term "neutral" relay zones from Walsh et al, 1999). However, the strains within ramps are very often more complex (Rotevatn et al., 2007) and they cannot be entirely characterized by simple-shear deformation. ***Figure 6.2*** shows several illustrative relay ramp examples from this work and from previously published data. The relay ramps shown here have different sizes, from outcrop bed-scale relay ramps to large seismic-scale ones. Also, they are developed within lithologies with very different mechanical properties, such as stiff carbonates or ductile coals and shales (the mechanical properties of rocks and the mechanical stratigraphy were discussed in *Section 2* from *Chapter 3*). ***Figure 6.2a*** shows a decametric-scale relay ramp from Kilve, Somerset, developed in a mechanically competent carbonate layer, within an interbedded Liassic limestone-shale sequence (Peacock and Sanderson, 1994). ***Figure 6.2b*** is a relay ramp also developed within a carbonate sequence, but at seismic scale, with overlap lengths of several hundreds of meters, within the Laminaria High, offshore Australia. The structural contour lines (in two-way travel time) from ***Figure 6.2b*** indicate that the beds in the relays are dipping approximately parallel to the strike of the bounding faults. Hence, the relay ramp has a simple tabular geometry, similar to the smaller scale

relay from Kilve, where much of the strain is accommodated in the fault strike-parallel plane by simple shear deformation (***Figure 6.1e***). ***Figure 6.2c*** shows relay ramps within a Carboniferous coal seam from Plenmellor opencast in Northumberland which accommodates transfer throw of several meters on the surrounding normal faults (from Huggins et al., 1995). ***Figure 6.2d*** illustrates a much larger, kilometre scale relay ramp bounded by normal faults with tens to hundreds of meters of throw and developed within a shale-dominated sand-shale growth interval from the Taranaki basin, offshore New Zealand. These last two relay ramps developed within mechanically incompetent lithologies (coals and unconsolidated shales and sands) and are characterized by beds/horizons which have a pronounced component of dip toward the mutual hangingwall of the bounding faults. In these cases, the ramp deformation is more complex, because the ramp tilting is in the direction parallel to the faults and is accompanied by a variable component of shear in the fault-normal direction, generating a rhombohedral ramp geometry (Huggins et al., 1995; Walsh et al., 1996). The variations in shear in both strike-parallel and dip-parallel directions lead to complex deformation patterns, characteristic for a triclinic strain geometry (Lin et al., 1998) (***Figure 6.1d***).

In the next section, we investigate the relationship between the two-dimensional arrangement of the overlapping fault segments (i.e. aspect ratio), the lithology of the host rocks and the fault-parallel and fault-normal shear strain components within the ramp, which essentially define the three-dimensional geometry of relay ramps.

6.3.1. Lithological control on relay aspect ratio

Figure 6.3a shows a logarithmic plot between the fault overlap length and the separation distance for relay ramps from this study and from published literature (from Long and Imber, 2012), within various lithologies and on a range of scales over 7 orders of magnitude. We observe a significant degree of scattering within individual datasets and within the same lithologies. Data overlapping between different lithologies from various localities suggest, at a first inspection, no obvious relationship between lithology and aspect ratio (Long and Imber, 2011).

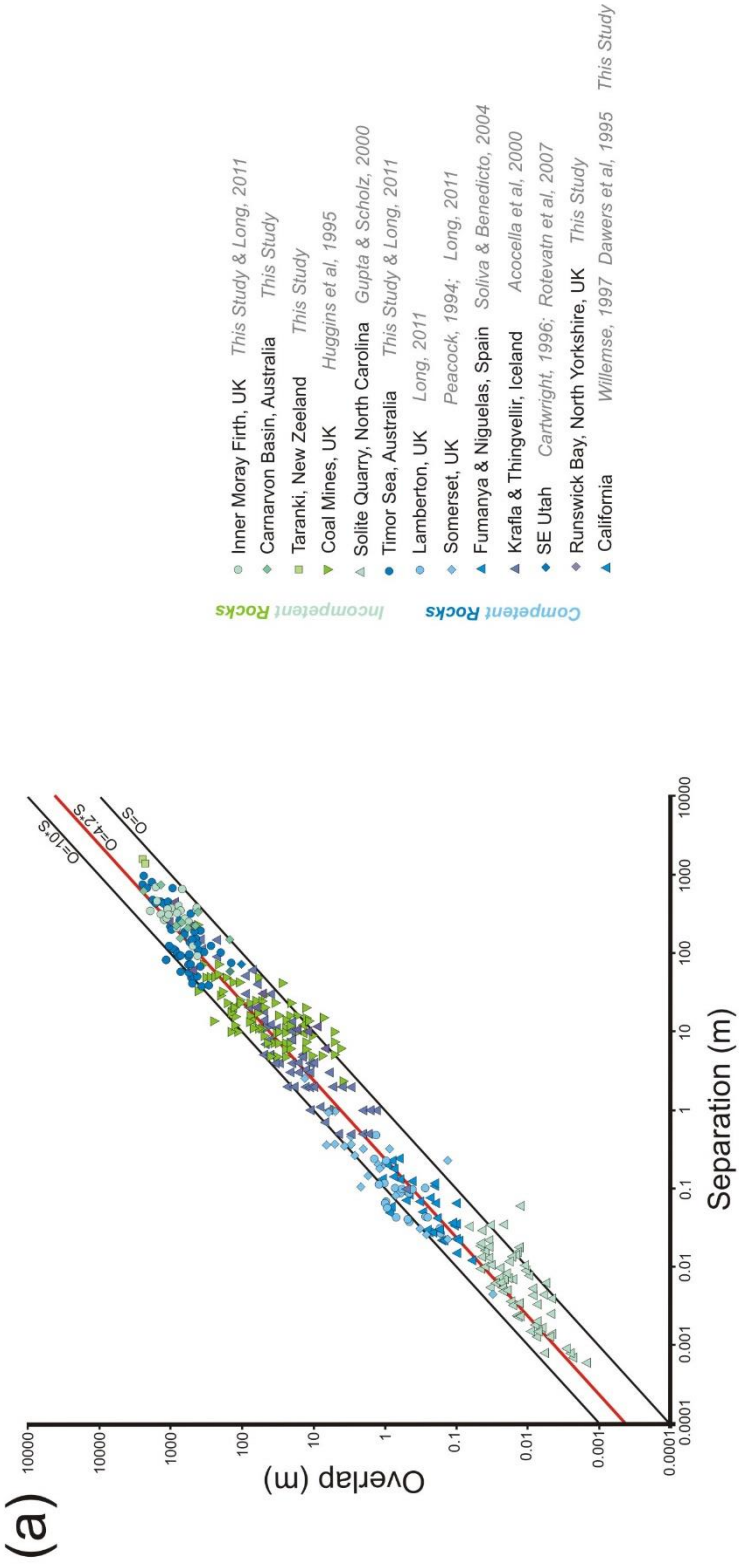
(a)
Overlap (m)
Separation (m)
10000
1000
100
10
1
0.1
0.01
0.001
0.0001
O=10*S
O=4.2*S
O=S
Competent Rocks
Incompetent Rocks
Inner Moray Firth, UK This Study & Long, 2011
Carnarvon Basin, Australia This Study
Taranki, New Zeeland This Study
Coal Mines, UK Huggins et al, 1995
Solite Quarry, North Carolina Gupta & Scholz, 2000
Timor Sea, Australia This Study & Long, 2011
Lamberton, UK Long, 2011
Somerset, UK Peacock, 1994; Long, 2011
Fumanya & Niguelas, Spain Soliva & Benedicto, 2004
Krafla & Thingvellir, Iceland Acocella et al, 2000
SE Utah Cartwright, 1996; Rotevatn et al, 2007
Runswick Bay, North Yorkshire, UK This Study
California Willemse, 1997 Dawers et al, 1995 This Study

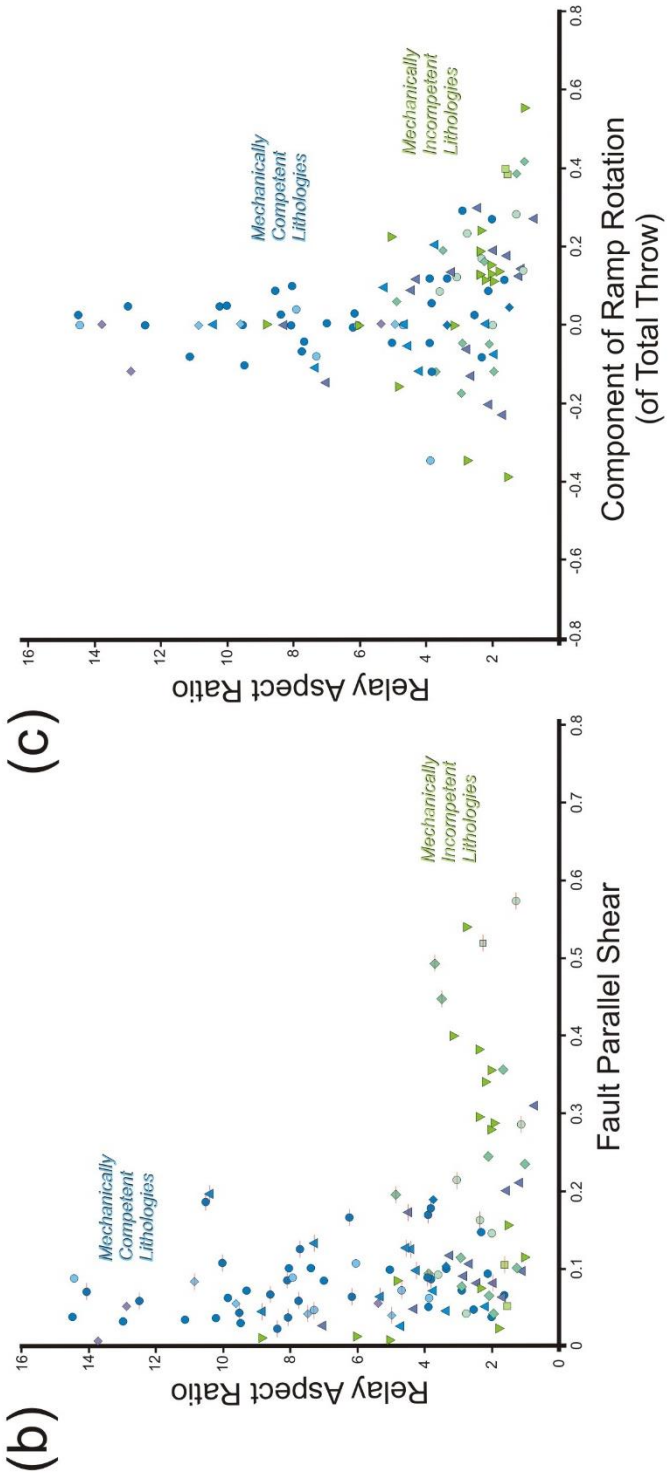
(b)
Relay Aspect Ratio
Fault Parallel Shear
Mechanically Competent Lithologies
Mechanically Incompetent Lithologies
(c)
Relay Aspect Ratio
Component of Ramp Rotation (of Total Throw)
Mechanically Competent Lithologies
Mechanically Incompetent Lithologies

Figure 6.3 (a) *Bi-logarithmic diagram of overlap vs separation for relay ramps from this study and published literature;* ***(b)*** *Fault parallel-shear vs relay ramp aspect ratio;* ***(c)*** *Amount of bed rotation in the fault normal direction as percentage of total fault displacement vs relay ramp aspect ratio.*

However, if we take the average aspect ratio for each particular data-set, we notice that the relay ramps developed in mechanically competent lithologies (carbonates, sandstones) tend to develop higher average aspect ratios than the ramps developed in softer lithologies (coals, silts, unconsolidated sands and shales) (***Table 6.1, Figure 6.3a***). Hence, lithology seems to control at least in part the two-dimensional geometry of the relay ramps. Nevertheless, even in this case, we cannot exclude other local geological factors influencing the mean aspect ratio of each data-set (Long and Imber, 2012). For example, the highest values of relay aspect ratios (>7) are from outcrops where normal faults are confined to mechanical layering (Long and Imber, 2012) (e.g. Kilve, Lamberton data-sets in ***Figure 6.4***). Meanwhile, relay ramps developed in unconsolidated growth strata, from Inner Moray Firth (UK) or Chandon (offshore NW Australia), or outcrop-scale examples of relay ramps developed in siltstones (from Gupta and Scholz, 2000) plot mostly below the global average (red axis in ***Figure 6.3a***).

6.3.2. Relay aspect ratio vs shear strain components

In order to assess better the control of lithology on the three-dimensional geometry of relay ramps we now analyse the relationship between the aspect ratio of relay ramps and the fault-parallel and fault-normal shear strain components within the ramp. From the relay aspect ratio *vs* fault-parallel shear strain displayed on the graph from ***Figure 6.3b***, two main points can be drawn:

Data	Source	Origin	Data Type	Lithology	No.	Mean Aspect Ratio
Runswick Bay, North Yorkshire	This Study	This Study	Outcrop	Carbonates	3	10.6
Lamberton, Berwickshire	Long, 2011	Long, 2011	Outcrop and lidar	Sandstones	21	8.6
Kilve, Somerset	Long, 2011	Long, 2011	Outcrop	Carbonates	49	8.2
SE Utah, USA	Childs et al, 2016	Childs et al, 2016	Outcrop	Sandstones	-	>5
Laminaria, offshore NW Australia	This Study and Long, 2011	This Study and Long, 2011	3D Seismic	Carbonates	90	4.9
SW Iceland	Acocella, 2000	Long, 2011	Outcrops	Basalts	56	4.3
Volcanic Tablelands, Surprise Valley, California	Willemse, 1996; Dawers, 1995; This Study	Willemse, 1996; Dawers, 1995; This Study	Outcrops and high resolution topographic data	Volcanics	15	3.1
Yorkshire and Northumberland coal mines	Huggins et al, 1995	Long, 2011	Mine plans and open casts	Coals	17	3.1
Solite Quarry, Virginia, USA	Gupta and Scholz, 2000	Long, 2011	Outcrop	Siltstone	64	2.9
Inner Moray Firth, offshore UK	This Study and Long, 2011	This Study and Long, 2011	3D Seismic	Sandstones-shales	28	2.9
Chandon, offshore NW Australia	This Study	This Study	3D Seismic	Sandstones-shales	10	2.8

Table 6.1. *Data showing average values of relay ramp aspect ratio from different geological settings and within different host rock lithologies.*

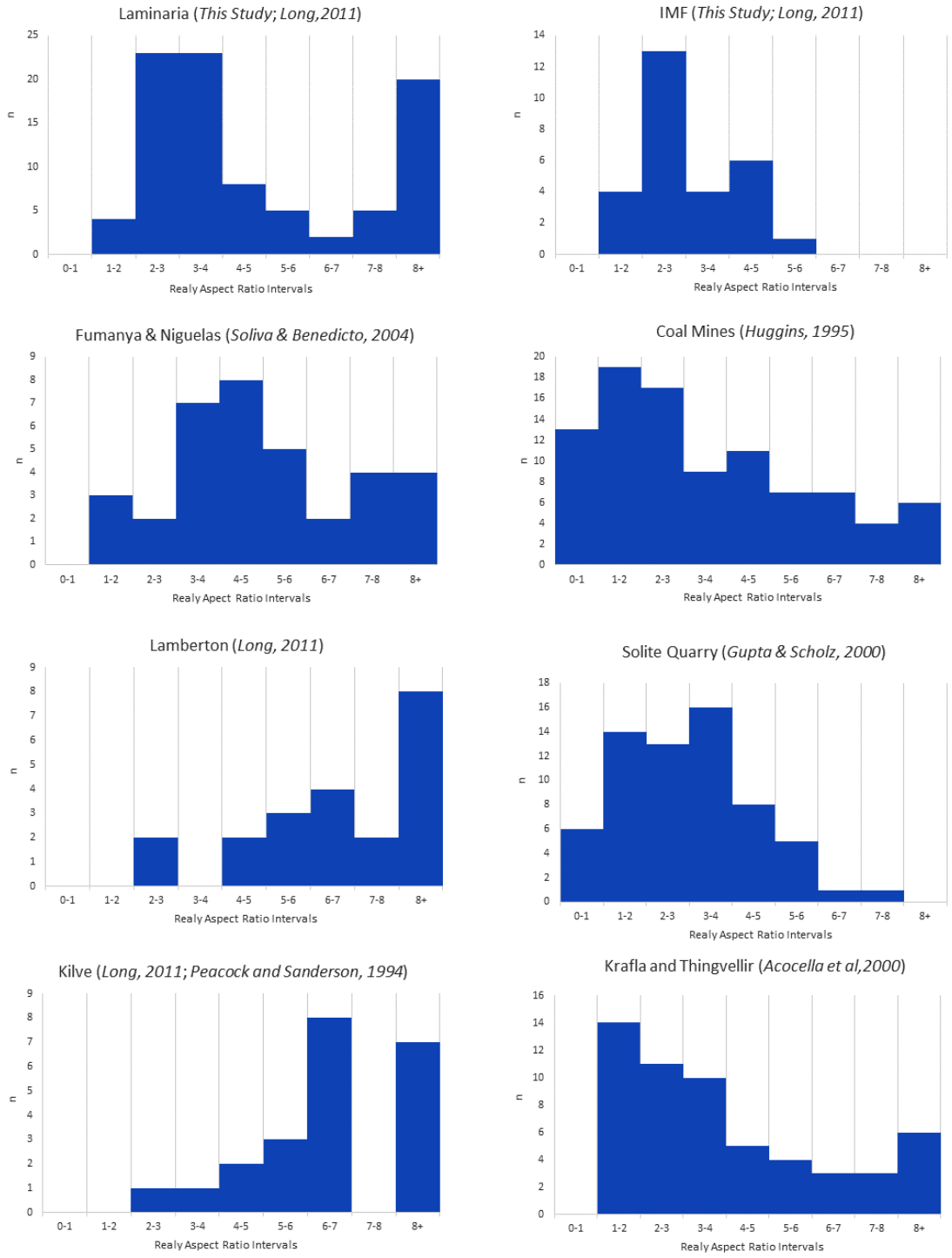

Figure 6.4 *Histograms showing the distribution of relay ramps aspect ratio (AR) data from this study and from published literature. Note that the larger numbers of high AR ramps are associated with more competent lithologies (left side column). The distribution is highly skewed toward high AR for the ramps associated to strata-bound normal faults, e.g. Lamberton, Kilve (Long, 2011). Low AR ramps are characteristic for more incompetent rocks (e.g. IMF, Coal Mines, Solite Quarry) but also for the competent basalts from Iceland (Acocella et al, 2000).*

(i) the relay ramps associated with normal faults within mechanically weaker lithologies (coals, interbedded shales and sandstones) develop, as one would expect, larger fault-parallel shear strains than the ramps formed within more competent rocks (limestones, sandstones) (Walsh et al., 1999; Imber et al., 2004);

(ii) fault-parallel shear strain increases with decreasing relay aspect ratio. However, the distribution of data suggest that this second point is the effect of different lithologies, with the relay ramps developed within mechanically weaker rocks, such as the syn-sedimentary normal faults from Inner Moray Firth or the relay ramps associated with normal faults within the British Coal Measures (Huggins et al., 1995), having a smaller spectrum of aspect ratios than the ramps within lithologies with a higher mechanical strength. Again, this last observation supports the hypothesis of Childs et al. (2016) that relay ramps formed in competent lithologies have higher aspect ratios than the ones developed within softer rocks.

Figure 6.3c shows a plot of relay ramp aspect ratio *vs* the amount of bed rotation in the fault normal plane as proportion of the total transfer throw, measured within the middle of the overlap length. Relay ramps with perfect tabular geometries will have no bed rotation in the direction normal to the overlapping faults and hence will have zero fault-normal shear strains. Therefore, this parameter is a direct indicator of the shear component within the relay in the fault normal plane. Negative values indicate that the ramp has a component of dip toward the mutual footwall. The incompetent lithologies, characterized by lower shear moduli, are able, as in the case of fault-parallel shear strain, to accommodate a larger amount of shearing in the fault-normal direction than the competent lithologies. The relay ramps developed within mechanically competent rocks and which have a high aspect ratio have a smaller component of fault-normal bed rotation (Long and Imber, 2010). The large overlap lengths would create strain compatibility issues for accommodating any shearing components in the fault-normal direction for rocks with large shear modulus.

A segmented normal fault array from the Laminaria High in the Northern Bonaparte basin, offshore NW Australia illustrates this latter case (***Figure 6.5a*** and ***6.6***). These WSW-ENE oriented normal

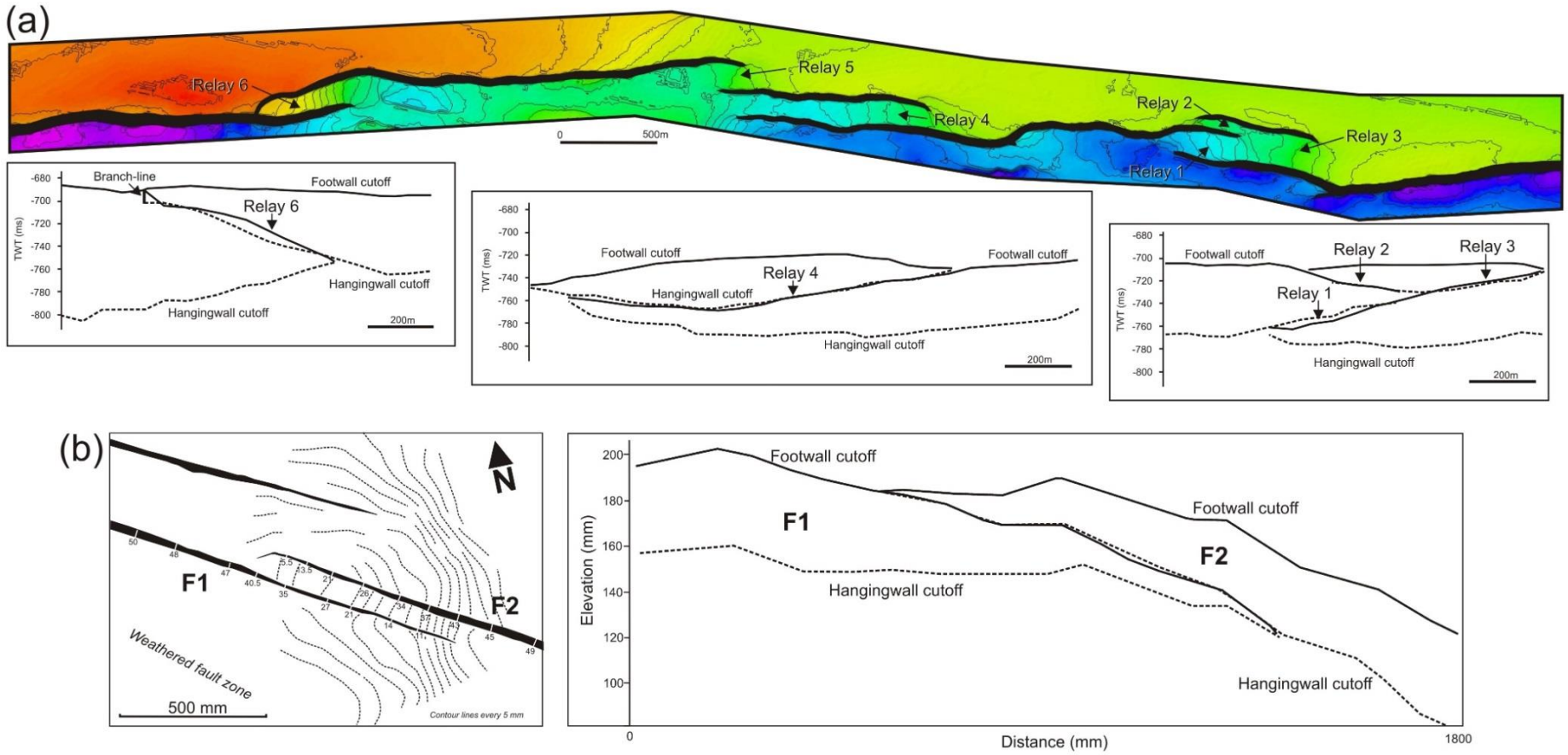

Figure 6.5 (a) *Segmented normal fault array and associated relay ramps developed within limestones from Laminaria High, Bonaparte Basin (offshore NW Australia). The relay ramps have tabular geometries with a minimal component of shear in the fault normal direction. The projections of the horizon cut-offs on a vertical plane parallel with the strike of the faults show complementary distribution of throw.* ***(b)*** *Tabular relay ramp with high aspect ratio in limestones from Kilve (from Peacock and Sanderson, 1994). Note the similarity with the relay ramps from (a).*

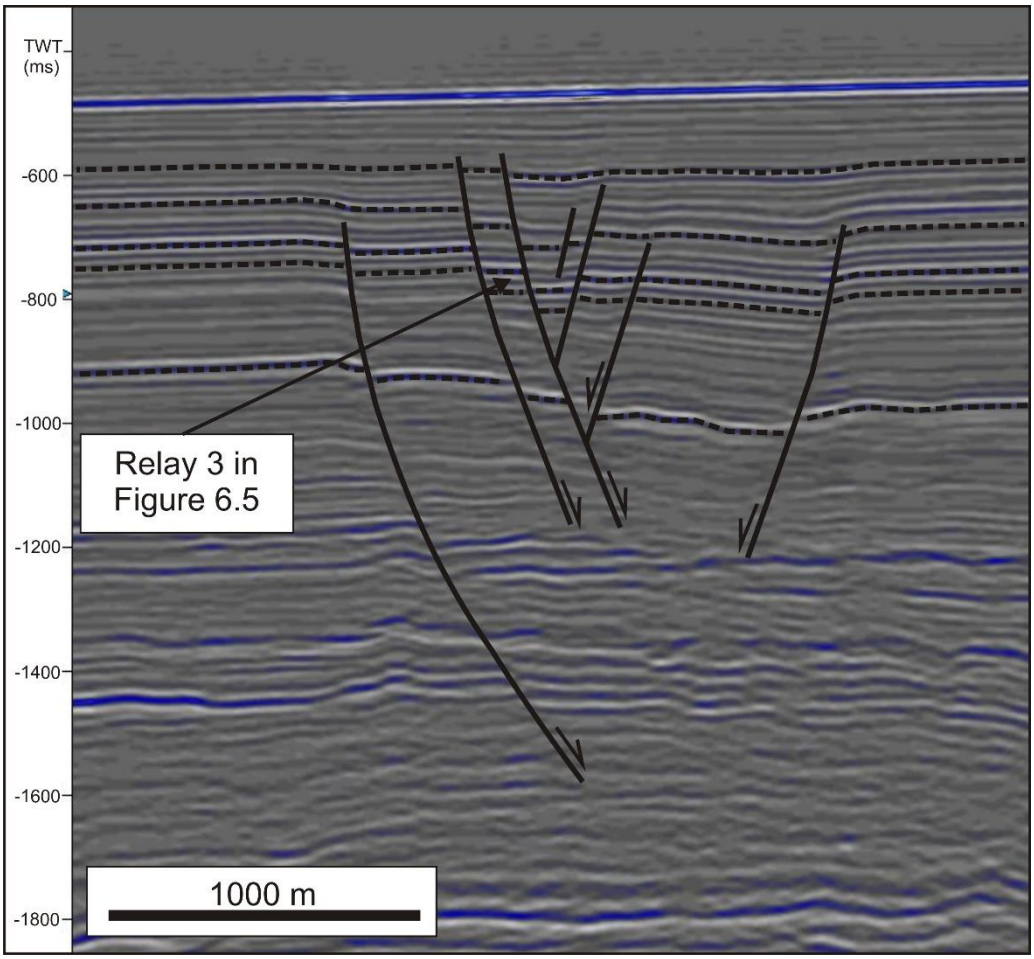

Figure 6.6 *Seismic section orthogonal to the normal faults and relay ramp no. 3 from Laminaria (from Figure 6.5a)*

faults formed by reactivation of pre-existing E-W oriented Mesozoic structures as a result of the flexure of the Australian margin during collision with the SE Asian microplates (DeRuig et al., 2000).

The horizon mapped in ***Figure 6.5a*** is located within the pre-growth interval, consisting of a homogeneous carbonate sequence of Mio-Pliocene age (Long and Imber, 2012). The faults have relatively steep dips within the analysed interval (75-80°) and become shallower dipping at depth (***Figure 6.6***), where the stratigraphy becomes more mud-rich (Long and Imber, 2012) and where some of them link with the older structures. The high strength of the rocks within the analysed interval can potentially explain the steep dips of the faults within this stratigraphic section (Peacock and

Sanderson, 1992). The fault displacement varies within the analysed sequence from tens meters up to 200 m. The displacement along these segmented normal faults is transferred through relay ramps, which have relatively simple tabular geometries (***Figure 6.5a***). The horizon separation diagram from ***Figure 6.5a*** shows the projection of the mapped horizon cut-offs on a section parallel to the strike of the faults. The complementarity of the discontinuous throw within the overlapping region indicates the kinematic coherency of the fault system. The relay ramps are usually characterized by smaller fault-parallel shear strains than other analysed relays, with values below 0.2, most of them below 0.1 (***Figure 6.3***). The map geometry of the relays can be quite variable, but overall, they have an above average relay aspect ratio of 4.9.

Similar to the relay ramps described from Laminaria, the ramps from Kilve, Somerset have also tabular geometries, high aspect ratios and small displacement gradients (***Figure 6.5b***; from Peacock and Sanderson, 1994). As discussed by previous workers (Peacock and Sanderson, 1994; Long and Imber, 2011), the two-dimensional geometries of the relays from Kilve can be the result of several factors, such as: (i) confinement of the faults to mechanical layering; (ii) reactivation of pre-existing structures which enhance rapid propagation of the faults and development of large overlap lengths and (iii) the mechanical properties of the material (Gudmundsson, 2011).

In the case of confinement of the faults to mechanical layering, the propagation of the upper/lower fault tips is vertically restricted by the presence of overlaying and underlying mechanically weaker layers (usually plastic shales) which absorb the strain energy and impede fault propagation (Wilkins and Gross, 2002; Soliva and Benedicto, 2005; Ferrill et al., 2007). Hence, the faults propagate preferentially laterally, where they tend to develop larger than normal overlap lengths, as we can observe on the plot from ***Figure 6.3a*** and the histograms from ***Figure 6.4***.

Similarly, the relay ramps with high aspect ratio can be associated with normal faults formed by reactivation of pre-existing structures. Relatively rapid strain localization associated with reactivation favours propagation and development of larger overlap lengths (Childs et al., 2016). This can potentially be the case for the development of the relay ramps from Laminaria, which formed by re-

activation of pre-existing, deeper faults; or the case of the relays associated with normal faults from Kilve, that reactivated of pre-existing veins (Long and Imber, 2012).

Another controlling factor for the development of relay ramps with high aspect ratios is the mechanical properties of the rocks (Childs et al, 2016). The relative high mechanical strength and brittleness of the host rock (carbonates, sandstones) enhances rapid strain energy release, fast propagation of the faults and development of larger than normal overlap lengths at smaller strain values.

In all these cases the result is that that the faults do not accumulate significant displacement during the rapid achievement of their near-final trace length (Jackson et al., 2016). Hence the associated stress shadow zones are not well developed, and the faults can achieve large overlap lengths (Gupta and Scholz, 2000). Also, that means that the overlapping segments start to interact when the high aspect ratio is already well developed. Previous mechanical models of overlapping normal faults indicated that the degree of mechanical interaction decreases with increasing the overlap length (Willemse et al., 1996; Crider and Pollard, 1998). Hence, this can potentially explain the tapering and the symmetry of the displacement profiles toward the interacting tips for the normal faults with high aspect ratio relay ramps from Laminaria or Kilve (***Figure 6.5***).

6.3.3. Fault-normal shear strain within relay ramps

A generally accepted hypothesis is that the amount of bed rotation in the fault-normal plane within relays is related to monoclinal folding occurring during the underlapping stage (Childs et al., 2016). However, previous research has shown many relay ramps develop their near-final overlap configuration quite rapidly (Giba et al., 2012; Jackson et al., 2016), hence the amount of bed rotation toward the hangingwall should be limited (Childs et al., 2016).

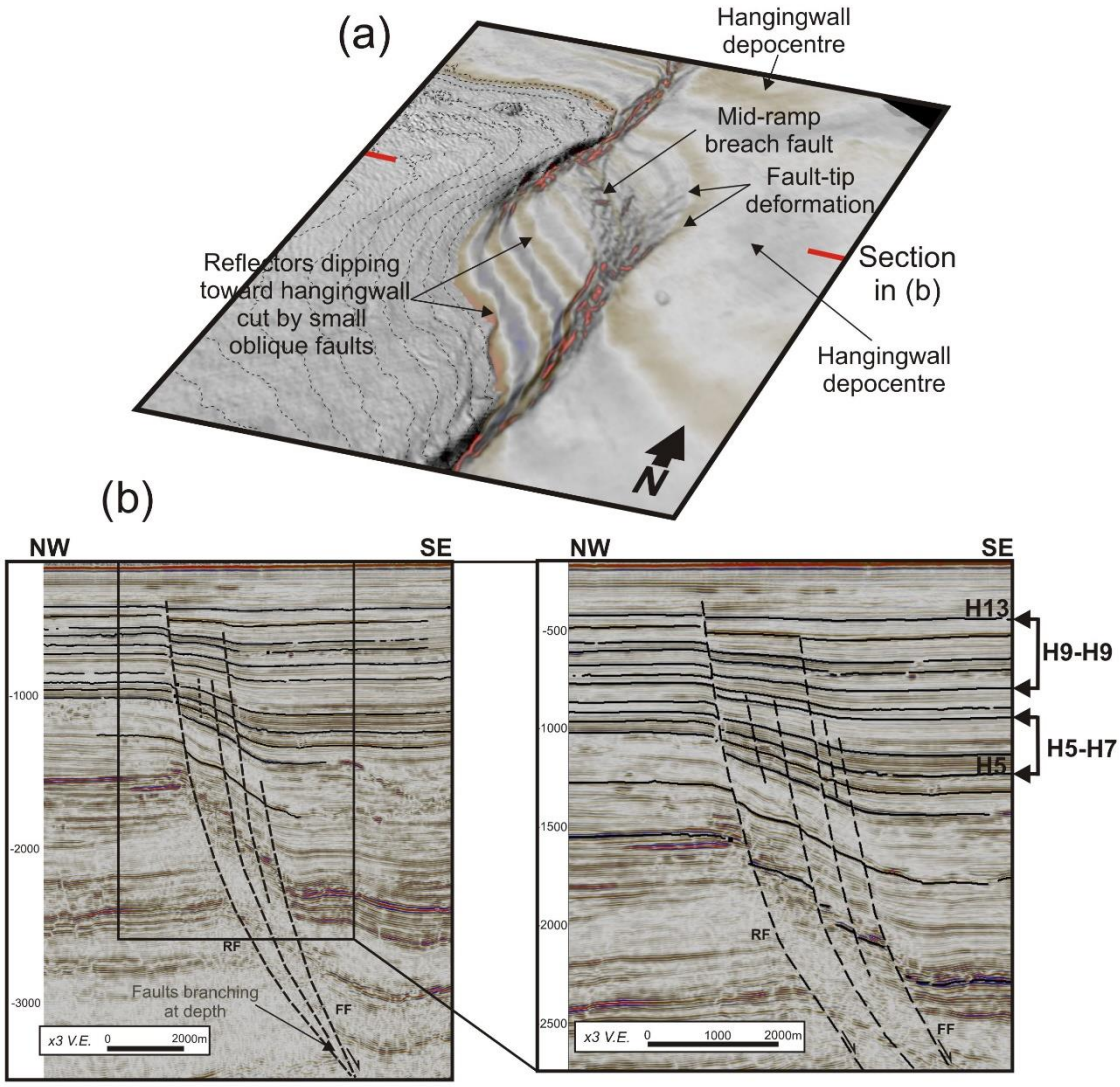
(a)
Hangingwall depocentre
Mid-ramp breach fault
Fault-tip deformation
Reflectors dipping toward hangingwall cut by small oblique faults
Section in (b)
Hangingwall depocentre
N
(b)
NW
SE
NW
SE
H13
H9-H9
H5-H7
H5
-500
1000
1500
2000
2500
-1000
-2000
-3000
RF
FF
Faults branching at depth
x3 V.E. 0 1000 2000m
x3 V.E. 0 2000m

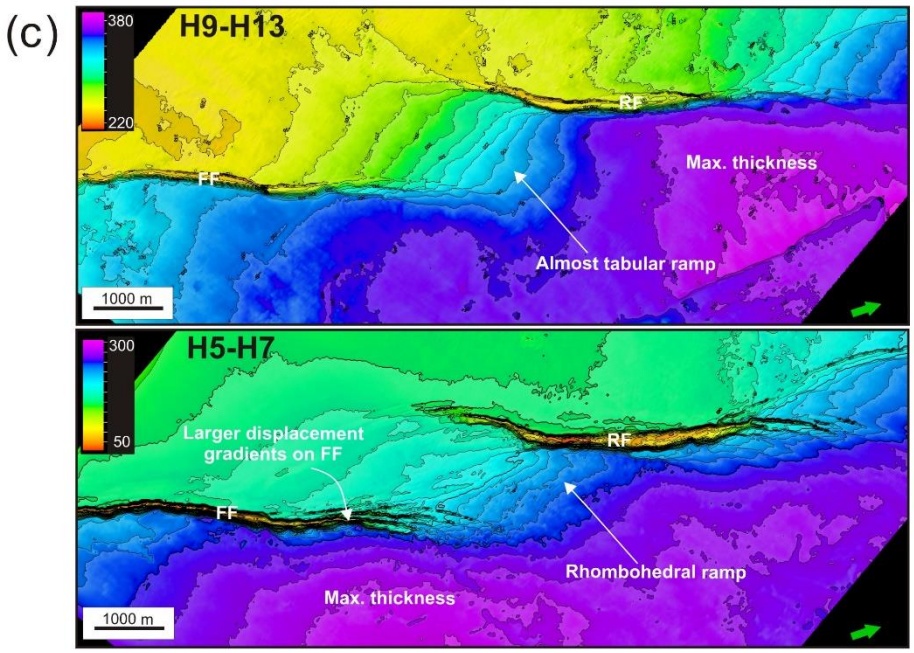
(c)
H9-H13
380
220
RF
FF
Max. thickness
Almost tabular ramp
1000 m
H5-H7
300
50
Larger displacement gradients on FF
RF
FF
Rhombohedral ramp
Max. thickness
1000 m

Figure 6.7 – previous page (a) *Horizontal combined slice section (reflectivity and variance) through a relay ramp from Taranaki basin, offshore New Zealand. Note the rhombohedral shape of the relay with a component of dip toward the hangingwall.* ***(b)*** *The fault-normal shear component of the relay is clearly visible on the seismic section through the middle of the relay, and normal to the bounding fault;* ***(c)*** *Isopach maps within two different intervals highlighted in section from (b). The maps show the thickness of sediments deposited synchronous with displacement on the two overlapping faults, front fault (FF) and rear fault (RF). Colder colours represent areas of larger thicknesses.*

For example, ***Figure 6.7*** illustrates a relay ramp along the Parihaka fault system, from the Taranaki Basin, offshore New Zealand. The relay ramp is associated with growth normal faults within a shale-dominated sequence with sandstone interbeds.

Figure 6.7a displays a time slice view through the relay ramp, showing the seismic reflection slice combined with the variance attribute (Chopra and Marfurt, 2007). This enhances the visualization of both the map-view structural trend of the reflectors and the smaller scale secondary faulting within the ramp. Secondary faults are developed obliquely, at an angle of 20-30° to the strike of the beds within the relay (***Figure 6.7a***). The strike of the horizons is also highly oblique to the strike of the faults, indicating a component of dip within the relay toward the mutual hangingwall, clearly seen in section from ***Figure 6.7b***. Interestingly, the uppermost growth packages within the relay zone indicate that the ramp reached the present overlap with very small displacement accrued on the bounding faults, hence the amount of folding during the underlapping stage is insignificant. The cross-section shows steeper dips of the ramp at deeper levels and evidence from isopach maps suggests that rotation occurred synchronously with displacement on the faults when the faults were already in the overlapping stage (***Figure 6.7c***). Moreover, the kinematic analysis of Giba et al. (2012) indicated that the Parihaka relay ramp established its geometry relatively early during the geologic evolution, hence significant monoclinal folding during the underlapping stage is not sufficient to explain rotation of the relay toward the common hangingwall.

Isopach maps of syn-growth strata indicate that depocenters (maximum thickness areas) are situated adjacent to the interacting tip of the front fault implying larger throw gradients on the front fault during deposition of the H5-H7 interval (***Figure 6.7c***). Because of the syn-sedimentary nature of the faults, the displacement decreases upwards within the syn-growth interval (e.g. H9-H13), hence the interaction between the faults is expected to be smaller (Peacock and Sanderson, 1994; Willemse, 1997). Although the depocenter migrates northwards toward the hangingwall of the rear fault (***Figure 6.7c***), the hangingwall subsidence within the proximity of the relay zone is more symmetrically distributed within H9-H13 interval and the lower ramp hinge is almost orthogonal to the strike of the bounding faults (***Figure 6.7c***). Supported by smaller secondary deformation within the ramp, this suggests a smaller degree of fault interaction at this level, where most of the strain is accommodated by fault-parallel shear. This relay ramp from the Taranaki basin illustrates that the rotation of the ramp toward the common hangingwall occurs during the overlapping stage of syn-sedimentary normal faults and it is not necessarily only the result of monoclinal folding during the underlapping stage (Childs et al., 2016).

The Peter Creek ramp (Oregon) is a relay ramp associated with normal faults which cut through basalts within the northern part of Basin and Range and it was described in detail by Crider and Pollard (1998) (***Figure 6.8***). The relay ramp shows similar geometrical characteristics, having a component of dip toward the hangingwall and larger throw gradients on the front fault (***Figure 6.8b***). Crider and Pollard (1998) tried to model numerically the geometry of a relay ramp however, their elastic solutions predicted larger throw gradients on the rear fault in a single slip event (***Figure 6.8b***), causing the ramp to dip back toward the footwall. Their explanation was that the difference in the ramp geometry between nature and model was probably the result of more complex fault geometries at depth or changes in the friction coefficient. However, we believe that the inconsistencies between model and field observations can be explained through a simple model comprising a sequence of slip-events, which is more appropriate for how slip and associated strain accumulates on natural normal faults. In the following section we propose a mechanical model to explain the preferential dip of the relay ramps toward the hangingwall side.

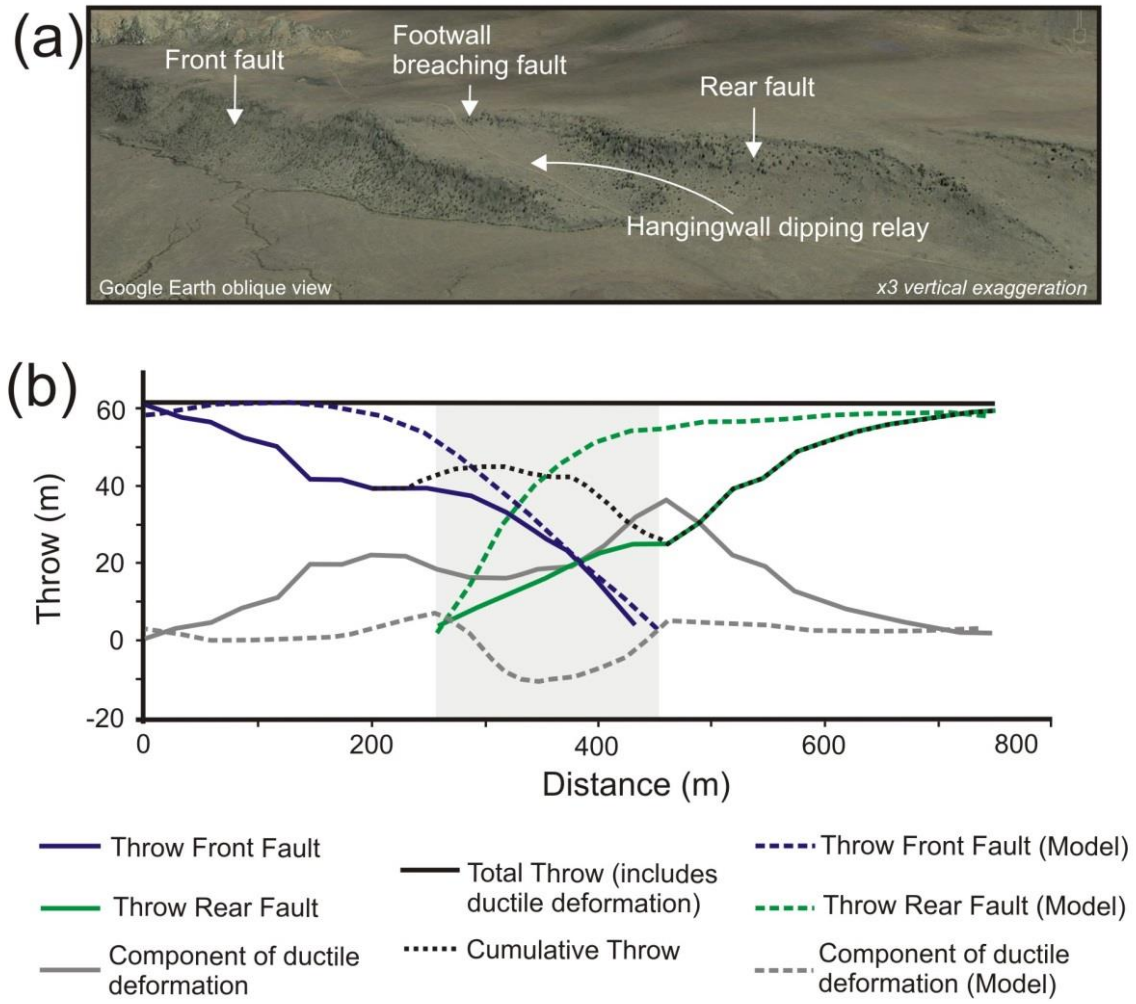

Figure 6.8 (a) *Google Earth view of a relay ramp within volcanic rocks from Peter Creek, Oregon. The throw profile from* ***(b)*** *shows the asymmetric throw distribution on the two faults, with larger throw gradients on the front fault (0.22). However, the relay is breached through the upper part by the rear fault which has smaller throw gradients (0.14) Throw data taken from Crider and Pollard (1998).*

In ***Figure 6.9*** we plot the proportion of the fault-normal ramp rotation to the total transfer throw measured within the middle of the relay ramp (***Figure 6.1***) *versus* the ratio between the throw gradients on the front fault and the throw gradients on the rear fault. The ratio between the throw gradients on the bounding faults emphasizes any potential throw asymmetry which can influence the overall three-dimensional geometry of the ramp and its associated strains. In this graph we show relay ramps associated with syn-sedimentary normal faults from three different seismic volumes analysed. There is a positive correlation between throw asymmetry and the amount of bed rotation toward the hangingwall, especially for the IMF data (R^2=0.70). This is to be expected in a coherent fault system, where any asymmetry within the vertical and horizontal components of displacement will cause the ramp to shear in both fault-parallel and fault-normal directions and to twist along a sub-vertical axis in order to maintain the kinematic coherency of the system (Peacock and Sanderson, 1994; Tentler and Acocella, 2010).

We observe that the relay ramps which have a component of dip toward the hangingwall (positive values on the horizontal axis from ***Figure 6.9***), seem to predominate in respect over the tabular ramps (FNRR/TT = 0) and the footwall-dipping relays. This confirms observations of previous researchers, which described the hangingwall dipping relays as the most common configuration (Childs et al., 1995; Huggins et al., 1996; Childs et al., 2016). McFadzean (2002) analysed relay ramps from Bishop, California and observed that the ramps dip predominantly toward the hangingwall, and that they dip toward the footwall when the separation between segments increases above a certain threshold distance (150 m in this case). We can speculate that as the separation between overlapping faults increases, the faults are not kinematically related, hence the geometry of the ramp will be simply controlled by the hangingwall subsidence topography associated with displacement on the rear fault.

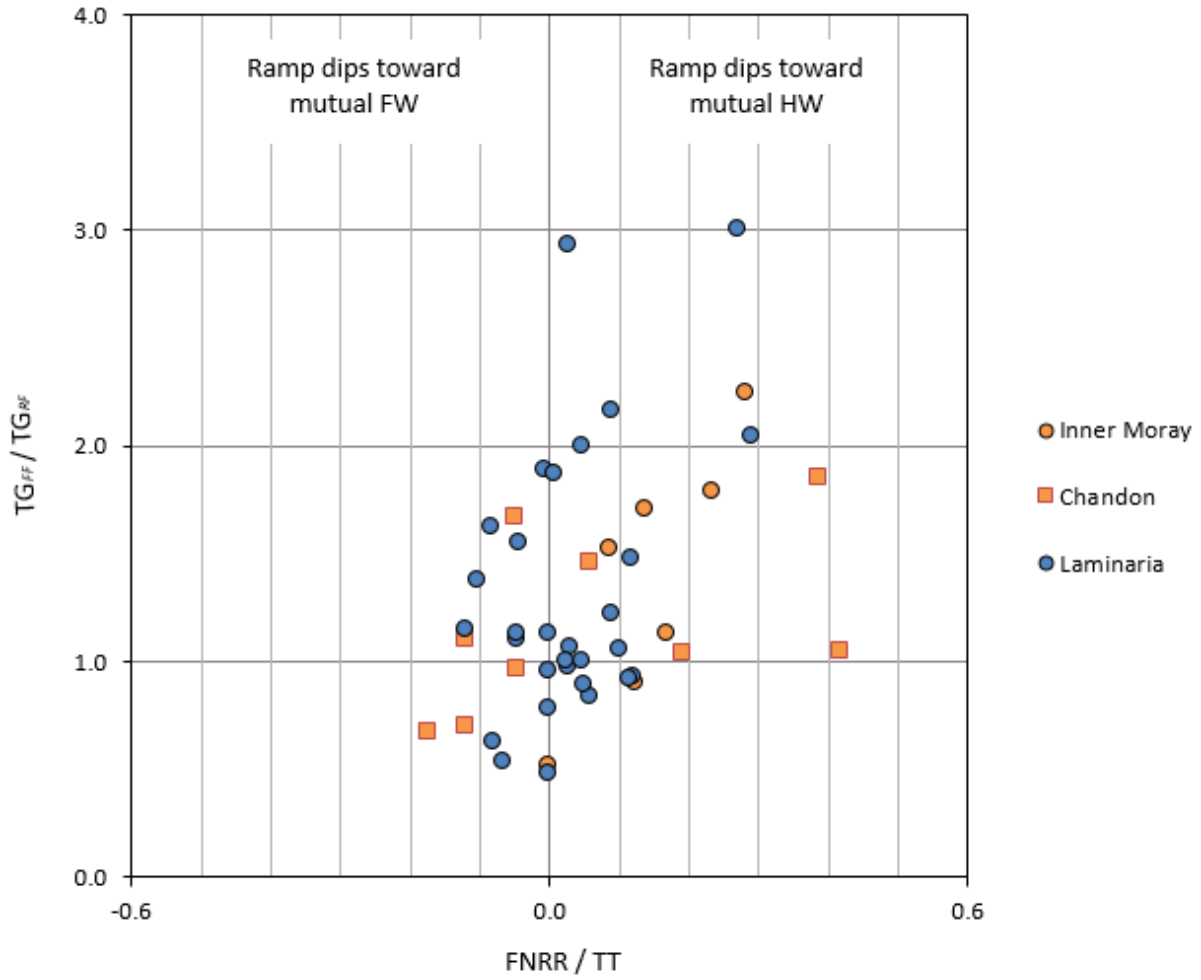

Figure 6.9 *Diagram showing the ratio between throw gradients of the front fault (TGFF) and the ones on the rear fault (TGRF) vs the amount of ductile deformation or fault-normal ramp rotation (FNRR) of the total transfer throw (TT) within the relay for syn-sedimentary normal faults mapped on seismic data. Negative values on the horizontal axis indicate that the relay dips toward the footwall / rear fault. It can be observed a positive correlation, as asymmetry increases with larger gradients on the front fault, the amount of relay rotation toward mutual hangingwall increases.*

6.4. Discussion

Geomechanical models of overlapping normal faults showed that the degree of interaction between segments decreases with increasing the overlap length (Willemse, 1996). This can potentially explain smaller displacement gradients and the symmetry of the displacement profiles of the normal faults bounding high aspect ratio relay ramps (***Figure 6.5***). However, ***Figure 6.3c*** shows that relay ramps within both mechanically incompetent and competent lithologies are characterized by a variable amount of fault-normal shear if they have average or below average relay aspect ratios. We hypothesize that not only the lithology controls the fault-normal shear strain but also the mechanical interaction and the geometrical configuration of the overlap and separation distance between segments.

In the mechanical models described in the previous chapter (*Chapter 5*), we have shown that displacement on overlapping normal faults embedded within a homogeneous elastic half-space (consistent with surface-breaking syn-sedimentary normal faults) generate an asymmetric distribution of the decrease in Coulomb shear stress zones, larger and better developed within the hangingwall side of the faults (***Figure 6.10a***). Gupta and Scholz (2000) assumed that in order for a fault to propagate it needs to overcome the yield strength of the surrounding rocks and the shear stress drop associated with the slip on the interacting fault. The asymmetrically larger shear stress shadow zone within the hangingwall side will make the propagation of the front fault more likely to be impeded, leading to accumulation of larger displacement gradients on the frontal segment. Equally, the zone of increased Coulomb shear stress within the footwall of the front fault will enhance more rapid propagation of the rear fault, which will probably lead to breaching of the relay ramp. This may explain why many of the relay ramps associated with surface-breaking normal faults are breached through the footwall side (discussed in *Chapter 5*). Asymmetry in the components of displacement will generate a component of fault-normal shear causing the relay to twist and dip toward the mutual hangingwall (Peacock and Sanderson, 1994). This asymmetry can potentially explain why relay ramps usually dip toward the hangingwall (***Figure 6.8b*** and ***Figure 6.9***).

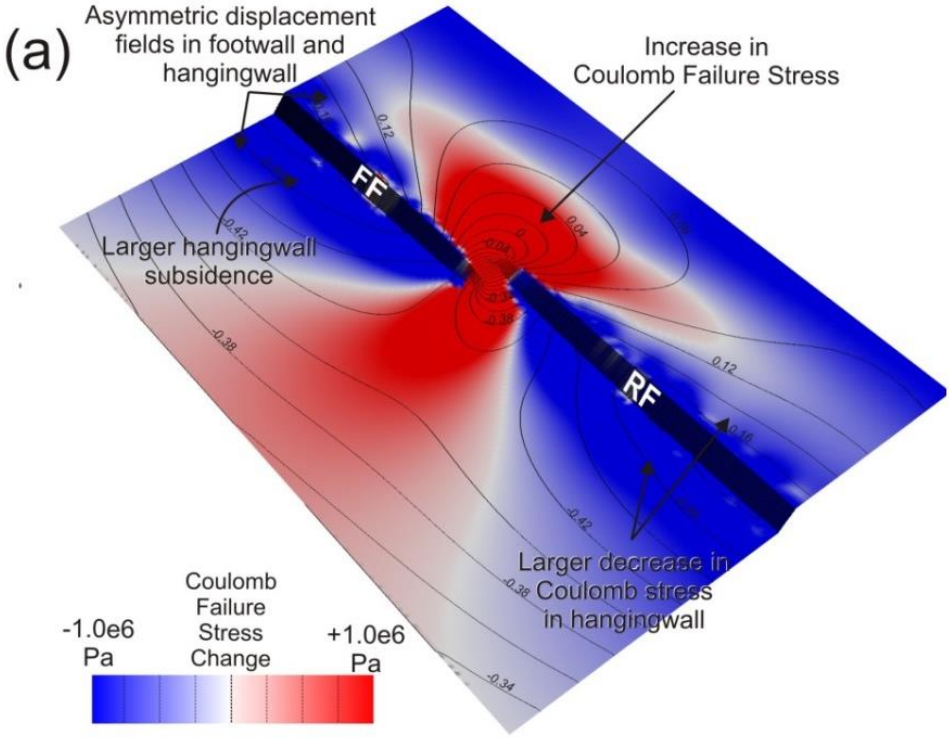
(a)
Asymmetric displacement fields in footwall and hangingwall
Increase in Coulomb Failure Stress
FF
RF
Larger hangingwall subsidence
Larger decrease in Coulomb stress in hangingwall
Coulomb Failure Stress Change
-1.0e6 Pa
+1.0e6 Pa

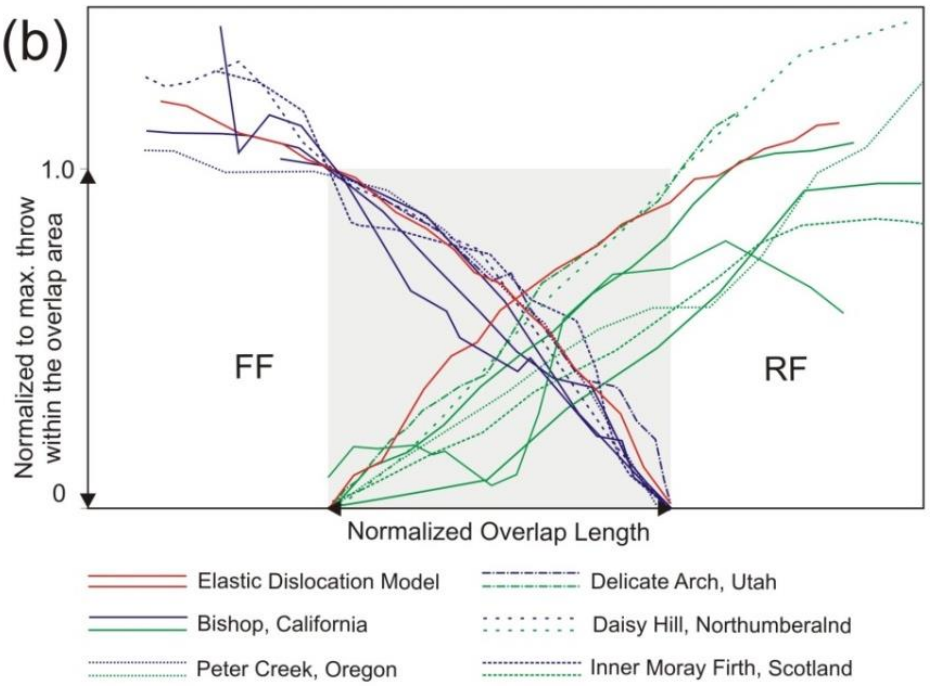
(b)
1.0
0
Normalized to max. throw within the overlap area
FF
RF
Normalized Overlap Length
Elastic Dislocation Model
Bishop, California
Peter Creek, Oregon
Delicate Arch, Utah
Daisy Hill, Northumberalnd
Inner Moray Firth, Scotland

Figure 6.10 – previous page (a) *Distribution of Coulomb Failure Stress associated with displacement on two overlapping normal faults located within an elastic half-space. Contours represent change in elevation. Note the asymmetric stress drop zone, with larger distribution and magnitude within the hangingwall. As a result, the frontal fault would require larger displacement gradients to propagate, in order to overcome the larger shear stress decrease in the hangingwall of the rear fault. Meanwhile, the rear fault accrues smaller displacement gradients, because it propagates more rapidly. The asymmetry in throw distribution, with larger displacement gradients on the front fault twists the relay toward hangingwall.* ***(b)*** *Examples of throw profiles in the overlapping region with relay ramps having a component of dip toward hangingwall, which display generally larger throw gradients on the front fault.*

6.5. Conclusions

In this chapter we showed that by including the fault-parallel and fault-normal shear strain components in the analysis of the map-view geometry of the relay ramps we gain better insights into the influence that lithology and fault interaction have on the three-dimensional geometry and variability of strain within the relay ramps. We showed that normal faults within competent rocks (limestones, massive sandstones) tend to develop relay ramps with higher aspect ratios, with smaller fault-parallel shear strains and which usually display tabular geometries, indicating a low component of fault-normal shear strain. Meanwhile, lower aspect ratio relay ramps are more likely to be developed in incompetent or less consolidated sediments, and usually display higher fault parallel-shear strains and a significant component of fault normal shear, which results in rhomboidal relay ramp geometry. The propagation of the faults is more easily impeded within incompetent lithologies, which generates higher stress interactions, resulting in development of higher displacement gradients. The dip of the relay ramp toward the mutual hangingwall can be both the result of fault-propagation folding during the underlapping stage of the relay and by shearing in the plane normal to the faults, as a result of asymmetric displacement gradient on the interacting faults.

| Chapter 7 |

Discussion and future work

7.1. Variability of ductile strain along strike of a single fault-array

Within this thesis we described the variability of continuous (ductile) deformation associated with the growth of normal faults in sedimentary stratigraphic sequences with various mechanical properties. The mechanical heterogeneity of the sedimentary layers plays an essential role in controlling the geometry of the faults and the distribution of ductile strain within the volume of rock surrounding the normal faults. The study of seismic-scale folds associated with normal faults in the Inner Moray Firth basin (*Chapter 4*) shows that vertical variations in mechanical stratigraphy causes along dip segmentation of the normal fault array. Vertical segmentation and linkage varies significantly along the fault strike, which may generate localized bends in the fault surface. As a result, the displacement of the hangingwall over these irregular fault plane geometries can generate ductile folding, with amplitudes that vary depending on displacement, geometry of the bend and pre-existing evolution of the fault. The geometries of the folds supported by growth strata indicators suggested that prior to fault-bend folding, some of the faults developed folds as a result of upper fault-tip propagation. Hence, in some areas the final fold amplitude is the result of both fault-propagation and fault-bend folding processes, which may have variable contributions along the strike of a single fault array. It is very likely that the zones within the finite folded structure that suffered two separate folding events have an increased distribution and intensity of secondary faulting and fracturing, similar to what has been described in fault-bend folds within compressional regimes (Cosgrove, 2015). Further field studies can potentially reveal if these different events of folding can be distinguished based on structural mapping and fracture analysis in the field. Folds associated with normal faults within the Suez Rift are a possible surface analogue of the folds from the northern North Sea. Although very well known for the surface exposures of normal-fault propagation folds (Khalil and McClay, 2002),

the extensional faults from Sinai (Suez Rift) display changes in fault dip similar to the faults from Inner Moray Firth, with steeper fault geometry within the competent units at depth and shallower dips within the overlaying clastic-carbonate interbedded sequence (Whipp, 2011). Variable displacement across these irregular, and laterally variable convex-toward-the-hangingwall bends in the fault plane may explain some of the along strike-variations in the amplitude of folding within the Suez Rift basin.

7.2. Mechanical stratigraphic control on normal fault-related deformation

7.2.1. Implications for fractured reservoirs

Mechanical stratigraphy also has an important role in influencing the characteristics and distribution of secondary deformation accommodating larger seismic-scale normal fault-related ductile deformation. The studies of the strain characteristics associated with normal fault-related folds within various mechanical stratigraphic conditions (*Chapter 2* and *Chapter 3*) have shown that the competence contrast is a key factor in controlling the partitioning of strain and the patterns of small-scale brittle deformation within the competent layers. High mechanical competence contrast favours strain partitioning. The incompetent layers deform plastically, while the brittle deformation within the competent beds is predominantly dominated by antithetic faults or rotated tensile fractures which were reactivated in shear. The flexure of beds with similar mechanical properties (e.g. rigidity and stiffness) will determine a component of slip parallel to the bedding surface (Higgs et al, 1991; Sanz et al, 2008), as in the case of the Buda limestone layers (Ferill et al, 2007) or the Cedar Mountain sandstone and conglomerates layers along the Moab fault. We have seen that the depositional geometries of the bed interfaces can significantly influence the intensity of the deformation within the competent layers, thus impacting the fracture density within potential reservoirs. Geometrically smooth, planar bed interfaces such as the Buda limestone layers from the Big Brushy Canyon monocline (Ferrill et al., 2007) will accommodate a large part of the strain by bed-parallel shear (Smart et al., 2011), with a relatively low intensity of through-going fractures within the competent layers. Meanwhile, if the bed boundaries are non-planar, such as the down-cutting sandstone channels of the Cedar Mountain

Formation within the hangingwall fold of Moab fault (*Chapter 3*), slip on these irregular bed interfaces will favour localized stress concentrations at bed asperities which will result in localized development of fractures and faults or reactivation in shear of pre-existing fractures. Therefore, apart from the mechanical properties of the rocks, the mechanical thicknesses and the mechanical competence contrast between layers, the geometry of the layer boundaries within the mechanical stratigraphy has a significant role in controlling the intensity and distribution of fracturing. Further investigations through mechanical modelling (i.e. discrete element modelling) can offer important insights for a better understanding of the influence of the bed geometries (e.g. with variations in the incision of the channel) on the frictional slip behaviour along lenticular surfaces and their effect on the distribution of brittle strain within channelized sandstone systems. Such studies would be relevant for reservoir modelling and evaluation of dynamic flow properties within folded and fractured channel sandstones reservoirs.

7.2.2. Implications for shale smear distribution and fault seal

The geometries and the strain patterns within folds associated with normal faults are strongly controlled by the mechanical properties of the layered stratigraphy. Evolution of the deformation processes and structures that relate to folding development will invariably influence the geometry, internal composition and permeability properties of the fault zones (Caine et al., 1996) and consequently will impact the trapping of hydrocarbons.

In a recent comprehensive review on clay smears, Vrolijk et al. (2016) argued that it is necessary to better understand the kinematics of secondary faulting and folding associated with normal faulting to improve our current knowledge of the distribution and, especially, the termination of shale smears. Development of shale smears along normal faults is an important element that can impede the lateral flow of hydrocarbons within normal faulted reservoirs (Smith, 1980; Webber et al., 1987; Lehner and Pilaar, 1997). Shale smears form by various mechanisms, such as shearing, injection or abrasion, depending on the rheological properties of the host lithologies and the depth of deformation (Lindsay

et al., 1993; Lehner and Pilaar, 1997; Vrolijk et al., 2016). In this discussion we exclude shale smears formed by abrasion of mechanically strong, deeply buried shales (Lindsay et al., 1993) and we focus on shale smears formed by ductile deformation processes and, in many cases, are associated with folding (Vrolijk at al., 2016). Therefore, it is reasonable to hypothesize that, since both shale smearing and folding are the result of ductile deformation, the evolution of shales smears is controlled by the very same factors that control the development of folding.

Evaluation of the occurrence of shale smears or the sealing potential of normal faults in the subsurface is performed through the use of deterministic or stochastic techniques (Dee et al., 2010). The stochastic methods do not necessarily consider the composition of a fault zone as contributing to its sealing capacity, but rather consider multiple possibilities of bed juxtaposition on multiple faults, with the premise that all sand-to-sand juxtaposition allows leakage of hydrocarbons (James et al., 2004). The different deterministic (or empirical) methods (Shale Gouge Ratio, Clay Smear Potential, Shale Smear Factor) are variations based on two geologic parameters: the thickness of the displaced shale layers and the fault throw (Yielding et al., 2010). The algorithms are based on empirical data which indicates that shale smears thin with increasing throw on the fault, becoming discontinuous if the throw is ca. 5 times larger than the overall thickness of the displaced shales (Yielding et al., 2012). Expressed by the deterministic fault models, the shale smear becomes discontinuous at a Shale Gouge Ratio (Yielding et al., 1997) of 0.2 (shale thickness / throw) or a Shale Smear Factor (Lindsay et al., 1993) of 5 (throw / shale thickness). Data indicate that the critical Shale Smear Factor can vary substantially with confining pressure and ductility (or clay content within the shale beds) (Grant, 2016). However, the algorithms assume that shale smears thin with increasing displacement, for which reason the probability of a continuous shale smear (and the sealing potential) decreases with increasing distance from the source bed.

Nevertheless, Childs et al. (2007), analysing a normal faulted, poorly consolidated turbidite sequence from Taranaki Basin, observed a high variability in the thickness distribution of the shale smear and that holes within smear can occur almost everywhere along the main fault plane, even in the immediate vicinity of the shale source layer (***Figure 7.1a, b***). Childs et al., (2007) noticed that

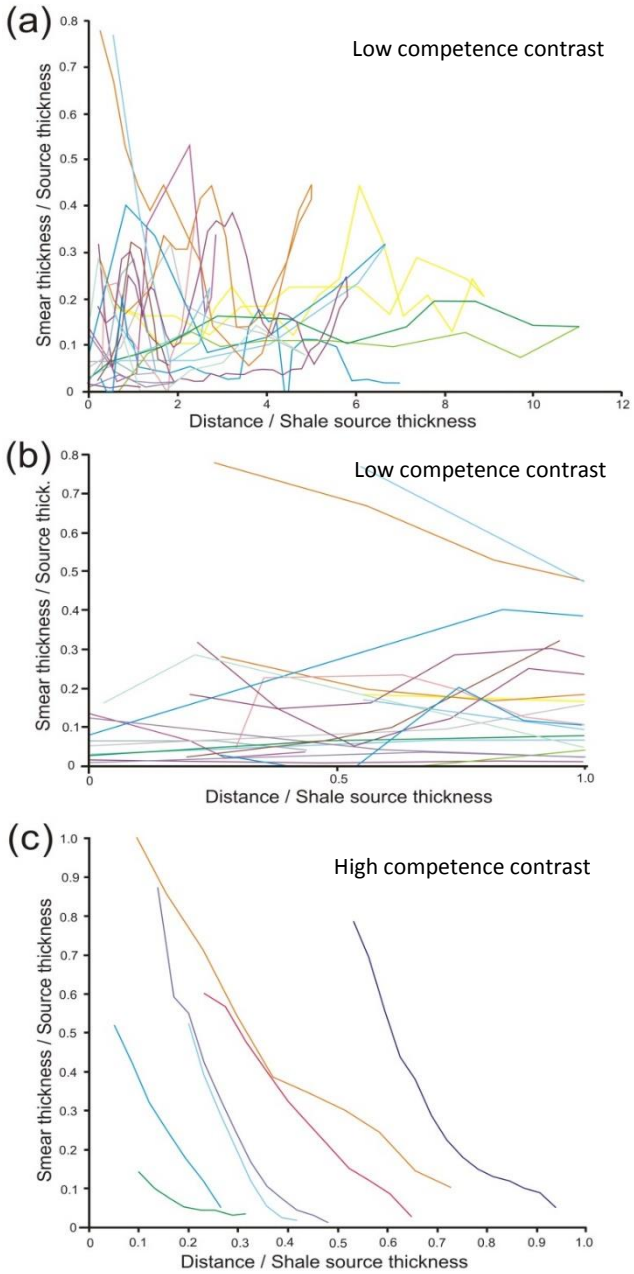

Figure 7.1. *Clay smear thickness vs distance from the source shale layer for* ***(a)*** *several profiles through faults within the Taranaki Basin, New Zealand (from Childs et al, 2007);* ***(b)*** *detail of the same Taranaki fault data (from Childs et al, 2007) with smear thickness distribution along a distance/ source thickness < 1.0;* ***(c)***. *profiles with smear thickness distribution along the Moab fault, Utah (data from Davatzes and Aydin, 2005). Note that in the case of the faults from Taranaki Basin there is no relationship between distances from the source and smear thickness, while in the case of Moab fault thinning of the smear corresponds with increasing distance from the source shale layer*

the disruption of shale smears is controlled by the distribution of strain within the fault zone, particularly by the synthetic Riedel shears. Vrolijk et al. (2016) argued that the current fault seal methods have limitations by failing to incorporate model parameters that take into consideration the deformation processes and the mechanical properties of the rocks at the time of deformation. They propose a mechanical framework that predicts the deformation processes responsible for generating shle smear, based on the relative mechanical properties of the sands and shales (Vrolijk et al., 2016; their figure 27). We consider that a similar approach can be taken in describing the main deformational processes that control the strain variability within folds, and which in turn influence the thickness and distribution of shale smears.

Figure 7.2 shows a schematic diagram for a hypothetical sand-shale interbedded sequence, in which the content of shale varies along the vertical axis (the percentage of shale forming the sequence increases downwards) and the mechanical competence contrast between sands and shales changes by increasing the competence of the sands, along the horizontal axis (from homogeneous mechanical behaviour in the left-hand side toward highly anisotropic mechanical layering toward right). The reason for using these two parameters is that, as we have previously seen in *Chapter 3* and *Chapter 4*, the style of folding, the deformation mechanisms and partitioning of strain are highly dependent on mechanical anisotropy and the percentage of shale (or other incompetent lithologies) within the sequence. The scheme presented here is very simplified and shows typical end-member cases of the deformation styles encountered within an interbedded sand-shale sequence with different ratios of shale and different consolidation (competency) of the sands. Hence, it is important to point out that that there will be a gradual transition and mixing between the deformation processes described here, as the two parameters change. In this conceptual model we hypothesize that the deformation structures that accommodated folding are the same ones responsible for entraining, thinning and disrupting the shale smears into the fault zone. Therefore, we consider that the evolution of shale smears can significantly differ depending on the variability of strain associated with folding within a mechanically heterogeneous stratigraphic sequence (***Figure 7.2***). For example, fault-propagation folds developed in stratigraphic sequences with high competence contrast are characterized by progressive

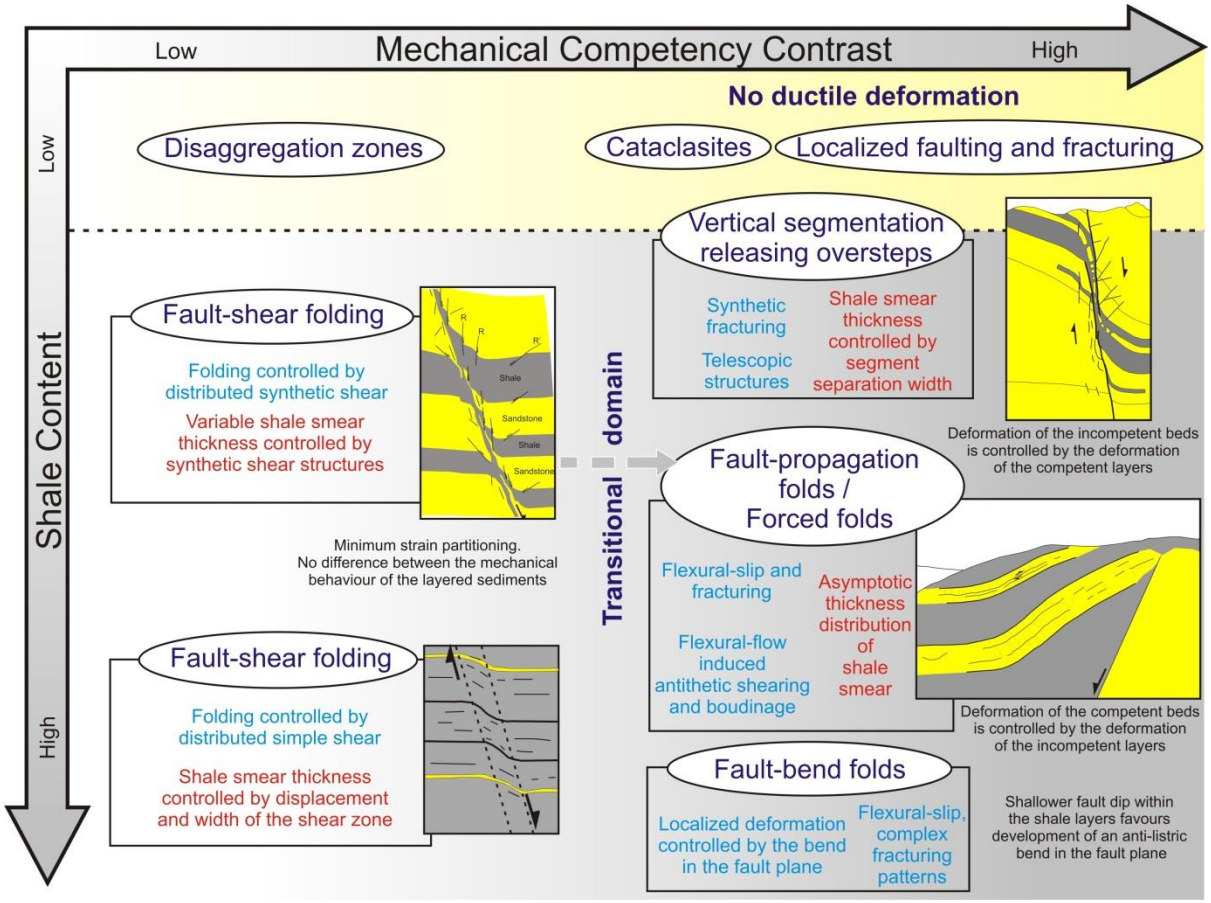

Figure 7.2 *Diagram showing the main normal-fault related folding deformation patterns within a sand-shale interbedded sequence, in which the content of shale increases downwards along the vertical axis and the mechanical competence contrast between sands and shales increases to the right along the horizontal axis. Hence, on the left-hand side we have deformation characteristic for poorly consolidated sediments, while on the right-hand side the degree of consolidation increases but only for the lithologies that we defined as competent, so that some folding can occur. Note that this sketch is a representation of the end-members of the deformation styles, and a significant overlapping transitional domain can be encountered in natural examples.*

thinning of the shale smear as the folds increase in amplitude (e.g. Moab). ***Figure 7.1c*** shows a plot of the normalized smear width *vs* normalized distance from the shale source in the hangingwall from several locations along the Moab fault (Davatzes and Aydin, 2005). We observe that the shale smear is defined by an asymptotic shape, thinning progressively with increasing displacement but maintaining a smaller smear thickness for a larger distance from the source bed. These shapes are consistent with the geometries of the normal drag folds developed in the hangingwall of the Moab

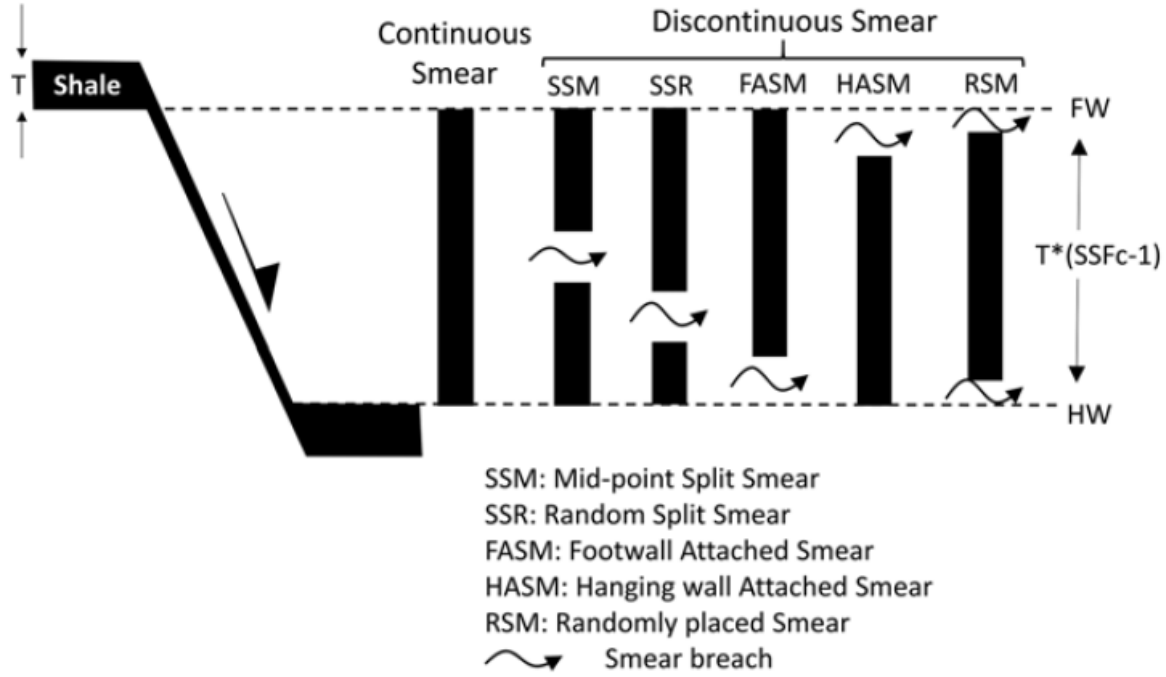

Figure 7.3 *Diagram showing possible locations for shale smear to be breached relative to the shale source layer (from Grant, 2016). The Mid-point Split Smear Model (SSM) is the standard model contained within the Shale Smear Factor or Shale Gouge Ratio methods. Our observations indicate that SSM and together with HASM (Hangingwall Attached Smear Model) seem to correspond for stratigraphic sequences with high mechanical competency contrast. A more random breaching of the sale smear can occur in sequences with low mechanical competence contrast.*

fault (*Chapter 4*). The antithetic-dominated style of secondary faulting is confined to the competent layers and does not contribute to the abrupt termination of the shale smears during the fault-propagation fold stage. The antithetic sense of slip can contribute to the process of shale injection into the fault zone, by increasing the horizontal compressive stresses, within the shale source interval adjacent to the main deformation zone, in a similar manner with the one described by Lehner and Pilaar (1997). This style of progressive thinning of the shale smear with increasing displacement indicates that in this case the deterministic fault seal methods, such as Shale Smear Factor or Shale Gouge Ratio appropriately describe the possibility of shale smear continuity (***Figure 7.3***). In the case where folding and shale smearing develop in stratigraphic sequences with lower mechanical

competence contrast (e.g. Gullfaks Field, from Hesthammer and Fossen, 1998) the deformation and thinning of the shales is accommodated by multiple synthetic slip surfaces, similar to the examples described by Childs et al (2007) and Doughty (2003). In this situation the distributed secondary shear faulting can create potential breaches within the shale smear at any point along the fault (***Figure 7.3***). In this case, a stochastic approach for evaluating the likelihood of sealing is probably considered as more appropriate (Childs et al, 2007). Hence, applying the appropriate fault seal evaluation method can be determined based on understanding the responsible mechanisms contributing to the development of the shale smear.

Our hypothesis is that the mechanical stratigraphy and especially the mechanical competency contrast are responsible for controlling the distribution of strain, and hence the disruption of the shale smear. Further studies from other localities or experiments are necessary to test the validity of our hypothesis. A comparative study between different field examples, to demonstrate any relationship between the smear breaching locations described by Grant (2016) and the mechanical stratigraphic conditions of the host sedimentary sequence at the time of deformation would be interesting to investigate in more detail. Potentially, a new workflow can be established within fault sealing methodologies, one that integrates the relative mechanical competence contrast at the time of deformation, as well as shale content.

7.3. The control of mechanical interaction between faults on distribution of strain within the volume surrounding normal faults

In *Chapters 4, 5 and 6* we investigated the effects of the mechanical interaction between normal faults on the distribution of deformation within a volume of rock (or an elastic material) surrounding the normal faults.

It is generally accepted that active segments within the same fault system interact mechanically through their slip-induced stress fields (Stein, 1999). In *Chapter 4* we explained the variability in the occurrence and magnitude of normal fault-propagation folds through the interaction between opposite

dipping normal faults. Mechanical models indicate that conjugate normal faults that intersect within layers with low compressibility display geomechanical characteristics favourable for migration of stress concentrations near the upper fault tips (Young, 2001). We hypothesize that these stress perturbations enhance upward propagation of the faults, by generating higher propagation/slip ratios and the development of low amplitude folds, or no folding. Further investigations in other areas with similar mechanical stratigraphic conditions (i.e. intersecting tips in competent rocks) would be required to investigate the stratigraphic conditions under which these effects would occur or when would be inhibited (increase in thickness or ductility of the weak layers which contributed to the initial development of the fault-propagation folds). Seismological evidence indicates sequential slip events on opposite dipping normal faults as a result of the stress transfer and interaction between the conjugate pairs. Payne et al (2004) described the events associated with the Devil Canyon 1984 earthquake, which triggered sequential movement on a conjugate normal fault pair, comprising the Challis segment and the Lone Pine faults from northern Basin and Range. The sequence was characterized by an initial deeper main seismic event followed by a sequential movement at a shallower depth on the conjugate pair (Payne et al, 2004). Mechanical models suggest that slip on conjugate normal faults that intersect within a material with low compressibility enhances the migration of the maximum slip toward the upper fault tip (Maerten et al, 1999; Young, 2001). Remote sensing techniques such as InSAR have been proven to be extremely useful in imaging the characteristics of surface deformation and slip distribution associated with seismic slip events (Walters et al, 2009). They can potentially provide further insights on surface deformation associated to sequential slip events on active conjugate normal fault pairs. Specifically, how does the surface rupture and subsidence patterns vary within the faulted area as a result of successive slip events on opposite dipping normal faults?

A better understanding of the processes and mechanisms that control the evolution of normal fault segment boundaries can be extremely important for the assessment of seismic hazards. Segmented seismogenic faults can display diverse and complex behaviours during seismic slip events. Relay zones can act either as barriers to rupture propagation or as rupture initiators along seismogenic

normal faults (Zhang et al., 1999; Spina et al., 2008; Biasi and Wesnousky, 2016). Understanding how normal faults interact and how relays zones become breached can help mitigate some of the risks associated with rupture propagation during normal slip events.

In *Chapter 5* we have shown that the style of breaching of relay ramps associated with syn-sedimentary (surface breaking) normal faults is influenced by the interaction between overlapping normal faults and the free surface of the earth. Quantitative and qualitative analysis indicated that the ramps associated with surface breaking normal faults are breached preferentially through the rear fault. Employed mechanical simulations predict in the proximity of the free surface asymmetrically larger decrease in shear stress within the hangingwall side and zones of increased shear stress within the footwall side of the ramp which favour breaching through the rear fault. Kinematic evidence from active surface breaching normal faults from the Apennines and Basin and Range support the mechanical solution and display localized components of strike slip at the fault tips toward the hangingwall depocenter (Wallace et al., 1984; Morewood and Roberts, 2000), which enhances the curved propagation toward the hangingwall of the overlapping faults and breaching through the rear fault.

Biasi and Wesnousky (2016) showed that relay zones bounded by normal faults are less effective on stopping rupture propagation than relay zones associated with strike-slip or reverse-slip fault segments. This indicates that the fault segments are likely to be physically linked at depth and they bifurcate upwards toward the surface of the earth, where, observed in map-view, they appear discontinuous (Walsh et al., 2003). Long and Imber (2012) showed that breaching of relay zones associated with normal faults developed within mechanically heterogeneous layered rocks can vary substantially in three dimensions, resulting in segmented fault branch-lines. Further studies are required to investigate the geometrical complexities associated to the three-dimensional variability of relay zone breaching along segmented seismically active normal faults.

Our study shows the benefit of studying syn-sedimentary normal faults for understanding the behaviour of seismogenically active, surface-breaking normal faults. We consider that it is essential to

integrate structural analysis of past geological structures that benefit from high quality seismic reflection imaging with the analysis and interpretation of seismological and geodetic data from currently active normal faults. In this way we can better understand the processes of fault growth in four-dimensions (including the time component at different scales) and potentially we can better mitigate some of the risks associated with seismic ruptures on interacting segment boundaries. For future research, it would be ideal to be able to monitor seismically active overlapping normal fault segments that are also imaged by high resolution 3D seismic reflection data (in active extensional areas such as the Gulf of Corinth). In this way we can investigate the short-term behaviour of the relay zones and the geometrical and mechanical conditions under which these structures can act as barrier to seismic rupture or when they act as rupture initiators. Active seismic monitoring combined with InSAR data can compensate for the limited resolution of conventional seismic datasets and can potentially offer insights into the sequential evolution of relay ramps, given that current evidence from seismic data suggests that relay zones develop their near-final geometry almost instantaneously at geologic-time scale (Jackson et al., 2016).

| References |

Acocella, V., Gudmundsson, A., Funiciello, R., 2000. Interaction and linkage of extension fractures and normal faults: examples from the rift zones of Iceland. *Journal of Structural Geology* 22, 1233-1246.

Allmendinger, R. W., 1998. Inverse and forward numerical modelling of trishear fault propagation folds. *Tectonics* 17, 640-656.

Anders, M. H. and Schlische, R. W., 1994. Overlapping faults, intrabasin highs, and the growth of normal faults. The Journal of Geology 102, 165-179.

Anderson, E. M., 1951. The dynamics of faulting and dyke formation with application to Britain. *Oliver and Boyd, Edinburgh,* 206 p.

Athmer, W. and Luthi, S. M., 2011. The effect of relay ramps on sediment routes and deposition: A review. *Sedimentary Geology* 242, 1-17.

Aydin, A. and Schultz, R. A., 1990. Effect of mechanical interaction on the development of strike-slip faults with echelon patterns. *Journal of Structural Geology* 12, 123-129.

Aydin, A. and Eyal, Y., 2002. Anatomy of a normal fault with shale smear: Implications for fault seal. *American Association of Petroleum Geologists Bulletin* 86, 1367-1381.

Barnett, J. M., Mortimer, J., Rippon, J. H., Walsh, J. J., Watterson, J. J., 1987. Displacement geometry in the volume containing a single normal fault. *American Association of Petroleum Geologists* 8, 925-937.

Bastensen, E. and Rotevatn, A. 2012. Evolution and structural style of relay zones in layered limestone-shale sequences: insights from the Hammam Faraun Fault Block, Suez rift, Egypt. *Journal of the Geological Society, London* 169, 477-488.

Baudon, C. and Cartwright, J., 2008. Early stage evolution of growth faults: 3D seismic insights from the Levant Basin, Eastern Mediterranean. *Journal of Structural Geology* 30, 888-898.

Behnsen, J. and Faulkner, D. R., 2012. The effect of mineralogy and effective normal stress on frictional strength of sheet silicates. *Journal of Structural Geology* 42, 49-61.

Berg, S. S. and Skar, T., 2005. Control on damage zone asymmetry of a normal fault zone: outcrop analysis of a segment of the Moab Fault, SE Utah. *Journal of Structural Geology* 27, 1803-1822.

Biasi, G. P. and Wesnousky, S. G., 2016. Steps and gaps in ground ruptures: empirical bounds on rupture propagation. *Bulletin of the Seismological Society of America* 106, 1110–1124.

Bonini, L, Basili, R., Toscani, G., Burrato, P., Seno, S., Valensise, G., 2015. The role of pre-existing discontinuities in the development of extensional faults: An analogue modeling perspective. *Journal of Structural Geology* 74, 148-158.

Bradshaw, G. A. and Zoback, M. D., 1988. Listric normal faulting, stress refraction and the state of stress in the Gulf Coast basin. *Geology* 16, 271-274.

Burhannudinnur, M. and Morley C. K., 1997. Anatomy of growth fault zones in poorely lithified sandstones and shales: implications for reservoir studies and seismic interpretation: part 1, outcrop study. *Petroleum Geoscience* 3, 221-224.

Caine, J. S., Evans, J. P., Forster, C. B., 1996. Fault zone architecture and permeability structure. *Geology* 24, 1025-1028

Cardozo, N., Bhalla, K., Zehnder, A. T., Allmendinger, R. W., 2003. Mechanical models of fault propagation folds and comparison to the trishear kinematic model. *Journal of Structural Geology* 25, 1-18.

Cartwright, J. A., Trudgill, B. D., Mansfield, C. S., 1995. Fault growth by segment linkage: an explanation for scatter in maximum displacement and trace length data from the Canyonlands Grabens of SE Utah. *Journal of Structural Geology* 17, 1319-1326.

Cartwright, J. A., Mansfield, C., Trudgill, B., 1996. The growth of normal faults by segment linkage. *In*: Buchanan, P. G. and Nieuwland, D. A. (Eds) *Modern Developments in Structural Interpretation, Validation and Modelling. Geological Society of London Special Publications* 99, 163-177.

Cartwright, J. A. and Husse, M., 2005. 3D seismic technology: the geological 'Hubble'. *Basin Research* 17, 1-20.

Childs, C., Watterson, J., Walsh, J. J., 1995. Fault overlap zones within developing normal fault systems. *Journal of the Geological Society of London* 152, 535-549.

Childs, C., Nicol, A., Walsh, J.J., Watterson, J., 1996. Growth of vertically segmented normal faults. *Journal of Structural Geology* 18, 1839-1397.

Childs, C., Nicol, A., Walsh, J. J., Watterson, J., 2003. The growth and propagation of synsedimentary faults. *Journal of Structural Geology* 25, 633-648.

Childs, C., Walsh, J. J., Manzocchi, T., Strand, J., Nicol, A., Tomasso, M., Schopfer, M. P. J., Aplin, A., 2007. Definition of a Fault Permeability Predictor from Outcrop Studies of a Faulted Turbidite Sequence, Taranaki, New Zealand. *In:* Jolley, S. J., Barr, D., Walsh, J. J., Knipe, R. J. (Eds.). *Structurally Complex Reservoirs. Geological Society of London Special Publications* 292, 235-258.

Childs, C., Manzocchi, T., Walsh, J. J., Bonson, C. G., Nicol, A., Schöpfer, M. P. J., 2009. A geometric model of fault zone and fault rock thickness variations. *Journal of Structural Geology* 31, 117-126.

Childs, C., Manzocchi, A., Nicol, A., Walsh, J. J., Conneally, J. C., Delogkos, E., 2016. The relationship between normal drag, relay ramp aspect ratio and fault zone structure. *In*: Childs, C., Holdsworth, R.E., Jackson, C. A.- L., Manzocchi, T., Walsh, J. J. & Yielding, G. (Eds). *The Geometry and Growth of Normal Faults*. *Geological Society of London Special Publications* 439, 355-372.

Chopra, S. and Marfurt, K. J., 2007. Seismic attributes for prospect identification and reservoir characterization. *Geophysical Developments Series. SEG/EAGE Publisher*, 481p.

Cooke, M. L., and Pollard, D. D., 1997. Bedding-plane slip in initial stages of fault-related folding. *Journal of Structural Geology* 19, 567-581.

Corfield, S. and Sharp, I. R., 2000. Structural style and stratigraphic architecture of fault propagation folding in extensional settings: a seismic example from the Smørbukk area, Halten Terrace, Mid-Norway. *Basin Research* 12, 329–341.

Cosgrove, J. W., 2015. The association of folds and fractures and the link between folding, fracturing and fluid flow during the evolution of a fold-thrust belt: a brief review. *In:* Richards, F. L., Richardson, N. J., Rippington, S. J., Wilson, R. W. and Bond C. E., (Eds). *Industrial Structural Geology: Principles, Techniques and Integration*. *Geological Society of London Special Publications* 421, 41-68.

Couples, G. D., Lewis, H., Tanner, P. W. G., 1998. Strain partitioning during flexural-slip folding. *In:* Coward, M. P., Daltaban, T. S. and Johnson, H. (Eds). *Structural Geology in Reservoir Characterization. Geological Society of London Special Publications* 127, 149-165.

Cowie, P. A., 1998. A healing-reloading feedback control on the growth rate of seismogenic faults. *Journal of Structural Geology* 20, 1075-1087.

Crider, J. G. and Pollard, D. D., 1998. Fault linkage: Three-dimensional mechanical interaction between echelon normal faults. *Journal of Geophysical Research* 103, 24373-24391.

Crider, J. G., 2001, Oblique slip and the geometry of normal fault linkage: mechanics and a case study from the Basin and Range in Oregon. *Journal of Structural Geology* 23, 1997-2009.

Davatzes, N. C. and Aydin, A., 2005. Distribution and nature of fault architecture in a layered sandstone and shale sequence: An example from the Moab fault, Utah. *In:* Sorkhabi, R. and Tsuji, Y. (Eds) *Faults, fluid flow, and petroleum traps: American Association of Petroleum Geologists Memoir* 85, 153 – 180.

Davies R. J., Turner J. D., Underhill, J. R., 2001. Sequential dip-slip movement during rifting: a new model for the evolution of the Jurassic trilete North Sea rift system. *Petroleum Geoscience* 7, 371-388.

Davis, G. H., 1984. Structural Geology of Rocks and Regions. *John Wiley & Sons, New York*. 492 p.

Davis, G. H. and Reynolds, S., 1996. Structural Geology of Rocks and Regions. 2nd Edition. *Wiley & Sons, New York,* 776 p.

Dawers, N. H. and Anders, M. H., 1995. Displacement - length scaling and fault linkage. *Journal of Structural Geology* 5, 607-614.

Dee, S. J., Yielding, G., Freeman, B., Bretan, P., 2007. A Comparison between Deterministic and Stochastic Fault Seal Techniques. *In*: Jolley, S. J., Barr, D., Walsh, J. J., Knipe, R. J. (Eds). *Structurally Complex Reservoirs. Geological Society of London Special Publications* 292, 259-270.

DePolo, C. M., Clark, D. G., Slemmons, D. B., Ramelli, A. R. 1991. Historical surface faulting in the Basin and Range province, western North America: implications for fault segmentation. *Journal of Structural Geology* 13, 123-136.

De Ruig, M., Trupp, M., Bishop, D., Kuek, D., Castilo, D., 2000. Fault arhitecture and the mechanics of fault reactivation in the Nancar Trough/Laminaria area of the Timor Sea, northern Australia. APPEA Jouranl, 40174-40193.

Doelling, H. H., 1988, Geology of Salt Valley Anticline and Arches National Park, Grand County, Utah. *Utah Geological and Mineral Survey Bulletin* 122, 1-58.

Doelling, H.H., Ross, M.J., and Mulvey, W.E, 2002, Geologic Map of the Moab 7.5' Quadrangle, Grand County, Utah. *Utah Geological Survey Map* 181.

Donath, F. A., 1970. Some information squeezed out of rock. *American Scientist* 58, 54– 72.

Doughty, P.T., 2003. Clay smear seals and fault sealing potential of an exhumed growth fault, Rio Grande rift, New Mexico. *American Association of Petroleum Geologists Bulletin,* 87, 427-444.

Dula, W. D., 1991. Geometric models of listric normal faults and rollover folds. *American Association of Petroleum Geologists Bulletin* 75, 1609-1625.

DuRoss, C. B., Personius, S. F., Crone, A. J., Olig, S. S., Hylland, M. D., Lund, W. R., Schwartz, D. P., 2016. Fault segmentation: New concepts from the Wasatch Fault Zone, Utah, USA. *Journal of Geophysical Research: Solid Earth* 121, 1131-1157.

Ellis, P. G. and McClay, K. R., 1988. Listric extensional fault systems - results of analogue model experiments. *Basin Research* 1, 55-70.

Erslev, E. A., 1991. Trishear fault – propagation folding. *Geology* 19, 617-620.

Færseth, R. B., 2006. Shale smear along large faults: continuity of smear and fault seal capacity. *Journal of the Geological Society of London* 163, 741-751.

Ferrill, D. A., Stamatakos, J. A., Sims, D., 1999. Normal fault corrugation: implications for growth and seismicity of active normal faults. *Journal of Structural Geology* 21, 1027–1038.

Ferrill, D. A. and Morris, A. P., 2001. Displacement gradient and deformation in normal fault systems. *Journal of Structural Geology* 23, 619-638.

Ferrill, D. A., Morris, A. P., Sims, D. W., Waiting, D. J., Hasegawa, S. 2005. Development of synthetic layer dip adjacent to normal faults, *In:* Sorkhabi, R. and Tsuji, Y. (Eds). *Faults, fluid flow, and petroleum traps. American Association of Petroleum Geologists Memoir* 85, 125– 138.

Ferrill, D. A., Morris, A. P., Smart, K. J., 2007. Stratigraphic control on extensional fault propagation folding: Big Brushy Canyon Monocline, Sierra Del Carmen, Texas. *In:* Jolley, S. J., Barr, D., Walsh,

J. J., Knipe, R. J. (Eds). *Structurally complex reservoirs. Geological Society of London Special Publications* 292, 203–217.

Ferrill, D. A. and Morris, A. P., 2008. Fault zone deformation controlled by mechanical stratigraphy, Balcones fault system, Texas. *American Association of Petroleum Geologists Bulletin* 92, 359-380.

Ferrill, D. A., Morris, A. P., McGinnis, R. N., Smart, K. J., Ward, W. C., 2011. Fault zone deformation and displacement partitioning in mechanically layered carbonates: The Hidden Valley fault, central Texas. *American Association of Petroleum Geologists Bulletin* 95, 1383–1397.

Ferrill, D. A., Morris, A. P., McGinnis, R. N., 2012. Extensional fault-propagation folding in mechanically layered rocks: The case against the frictional drag mechanism. *Tectonophysics* 576-577, 78-85.

Ferrill, D. A., Morris, A. P., McGinnis, R. N., Smart, K. J., 2016. Myths about normal faulting. *In*: Childs, C., Holdsworth, R. E., Jackson, C. A. -L., Manzocchi, T., Walsh, J. J., Yielding, G. (Eds). *The Geometry and Growth of Normal Faults. Geological Society of London Special Publications* 439, 41-56.

Ferrill, D. A., Morris, A. P., McGinnis, R. N., Smart, K. J., Watson-Morris, M. J., Wigginton, S. S., 2016. Observations on normal-fault scarp morphology and system evolution of the Bishop Tuff in the Volcanic Tableland, Owens Valley, California, U.S.A. *Lithosphere* 8, 238-253.

Ferrill, D. A., Morris, A. P., McGinnis, R. N., Smart, K. J., Wigginton, S. S., Hill, N. J., 2017. Mechanical stratigraphy and normal faulting. *Journal of Structural Geology* 94, 275-302.

Fodor, L., Turki, S. M. Dalub, H., Al Gerbi, A., 2005. Fault-related folds and along-dip segmentation of breaching faults: syn-diagenetic deformation in the south-western Sirt basin, Libya. *Terra Nova* 17, 121-128.

Fossen, H. and Hesthammer, J., 1998. Structural geology of the Gullfaks Field, northern North Sea. *In:* Coward, M. P., Daltban, T. S. and Johnson, H. (Eds). *Structural Geology in Reservoir Characterization. Geological Society of London Special Publications* 127, 231-261.

Fossen, H., Johansen, T. E. S., Hesthammer, J., Rotevatn, A., 2005. Fault interaction in porous sandstone and implications for reservoir management; examples from southern Utah. *American Association of Petroleum Geologists Bulletin* 89, 1593-1606.

Fossen, H. and Rotevatn, A., 2016. Fault linkage and relay structures in extensional settings – A review. *Earth-Science Reviews* 154, 14-28.

Foxford, K. A., Garden, I. R., Guscott, S. C., Burley, S. D., Lewis, J. J. M., Walsh, J. J., Waterson, J., 1996. The field geology of the Moab fault. *In:* A. C. Huffman, W. R. Lund, and L. H. Goodwin (Eds). *Geology and resources of the Paradox basin: Salt Lake City, Utah, Utah Geological Association Guidebook* 25, 265– 283.

Foxford, K. A., Walsh, J. J., Watterson, J., Garden, I. R., Guscott, S. C., Burley, S. D., Fisher, Q. J., Knipe, R. J., 1998. Structure and content of the Moab fault zone, Utah, U.S.A. and its implications for fault seal prediction. *In*: G. K. Jones, Q. J. Fisher, and R. J. Knipe (Eds). *Faulting, fault sealing and fluid flow in hydrocarbon reservoirs. Geological Society of London Special Publications* 147, 87–103.

Fraser, S. I., Fraser, A. J., Lentini, M. R., Gawthorpe, R. L., 2007. Return to rifts – the next wave: fresh insights into the petroleum geology of global rift basins. *Petroleum Geoscience* 13, 99-104.

Garden, I. R., Guscott, S. C., Burley, S. D., Foxford, K. A., Walsh, J. J., Marshall, J., 2001. An exhumed palaeo-hydrocarbon migration fairway in the Entrada sandstone of SE Utah, U.S.A. Geofluids, 1, 195-213.

Geikie, J., 1912. Structural and Field Geology. *Oliver and Boyd, London*, 626 p.

Giba, M., Walsh, J. J., Nicol, A., 2012. Segmentation and growth of an obliquely reactivated normal fault. *Journal of Structural Geology* 39, 253-267.

Glennie, K., Higham, J., Stemmerik, L., 2003. Permian. 91-103. *In:* Evans, D., Graham, C., Armour, A. and Bathurst, P. (Eds). *The Millenium Atlas: Petroleum geology of the Central and Northern North Sea*. The Geological Society of London.

Goldsmith, P.J., Hudson, G., Van Veen, P., 2003. Triassic. 105-27. *In:* Evans, D., Graham, C., Armour, A. and Bathurst, P. (Eds). *The Millenium Atlas: Petroleum geology of the Central and Northern North Sea*. The Geological Society of London.

Grant, J. V. and Kattenhorn, S. A., 2004. Evolution of vertical faults at an extensional plate boundary, southwest Iceland. *Journal of Structural Geology* 26, 537-557.

Grant, N. T., 2016. A geometrical model for shale smear: implications for upscaling in faulted geomodels. *Petroleum Geoscience* 23, 39-55.

Grasemann, B., Martel, S., Passchier, C., 2005. Reverse and normal drag along a fault. *Journal of Structural Geology* 27, 999-1010.

Groshong, R. H., 1989. Half-graben structures: Balanced models of extensional fault-bend folds. *Geological Society of America Bulletin* 101, 96-105.

Gross, M. R., 1995. Fracture partitioning: Failure mode as a function of lithology in the Monterey Formation of coastal California. *Geological Society of America Bulletin* 107, 779-792.

Gudmundsson, A., 1987. Tectonics of the Thingvellir fissure swarm, SW Iceland. *Journal of Structural Geology* 9, 61-69.

Gudmundsson, A., 2004. Effects of Young's modulus on fault displacement. *C.R. Geoscience* 336, 85-92.

Gupta, A., Cowie, P. A., Dawers, N. H., Underhill, J. R., 1998. A mechanism to explain rift basin subsidence and stratigraphic patterns through fault-array evolution. Geology 26, 595-598.

Gupta, A. and Scholz, C. H., 2000. A model of normal fault interaction based on observations and theory. *Journal of Structural Geology* 22, 865-879.

Hardman, R. F. P. and Booth, J. E., 1991. The significance of normal faults in the exploration and production of North Sea hydrocarbons. *In:* Roberts A. M., Yielding, G., Freeman, B. (Eds). *The Geometry of Normal Faults. Geological Society of London Special Publications* 56, 1-13.

Hardy, S. and McClay, K. R., 1999. Kinematic modeling of extensional fault propagation folding. *Journal of Structural Geology* 21, 695–702.

Hardy, S. and Allmendinger, R., 2011. Trishear. A review of kinematics, mechanics, and applications. *In* K. McClay, J. Shaw and J. Suppe, (Eds). *Thrust fault-related folding. American Association of Petroleum Geologists Memoir* 94, 95-119.

Henderson, J., 2012. Geological Expression: data driven-interpreter guided approach to seismic interpretation. *First Brake* 30, 73-78.

Hesthammer, J. and Fossen, H., 1998. The use of dipmeter data to constrain the structural geology of the Gullfaks Field, northern North Sea. *Marine and Petroleum Geology* 15, 549-573.

Hesthammer, J. and Fossen, H., 2001. Structural core analysis from the Gullfaks area, northern North Sea. *Marine and Petroleum Geology* 18, 411-439.

Higgs, W. G., Williams, G. D., Powell, C. M., 1991. Evidence for flexural shear folding associated with extensional faults *Geological Society of America Bulletin* 103, 710-717.

Homberg, C., Schnyder, J., Roche, V., Leonardi, V., Benzaggagh, M. 2017. The brittle and ductile components of displacement along fault zones. *In*: Childs, C., Holdsworth, R. E., Jackson, C. A.-L., Manzocchi, T., Walsh, J.J. and Yielding, G. (Eds). *The Geometry and Growth of Normal Faults. Geological Society of London, Special Publications* 439, 395-412.

Hongxing, G. and Anderson, J. K., 2007. Fault throw profile and kinematics of normal fault: conceptual models and geologic examples. *Geological Journal of China Universities* 13, 1, 75-88.

Hopkins, M. C. and Dawers, N. H., 2016. Vertical deformation of lacustrine shorelines along breached relay ramps, Catlow Valley fault, southeastern Oregon, USA. *Tectonophysics* 674, 89-100.

Huggins, P., Watterson, Walsh, J. J., Childs, C., 1995. Relay zone geometry and displacement transfer between normal faults recorded in coal-mine plans. *Journal of Structural Geology* 12, 1741-1755.

Hughes, A. N. and Shaw, J. H, 2015. Insights into the mechanics of fault-propagation folding styles. *Geological Society of America Bulletin* 127, 1752-1765.

Iacopini, D. and Butler, R. W. H., 2011. Imaging deformation in submarine thrust belts using seismic attributes. *Earth and Planetary Science Letters*, 302, 414-422.

Imber, J., Tuckwell, G. W., Childs, C., Walsh, J. J., Manzocchi, T., Heath, A. E., Bonson, C. G., Strand, J., 2004. Three-dimensional distinct element modelling of relay growth and breaching along normal faults. *Journal of Structural Geology* 26, 1897-1911

Imber, J., Perry, T., Jones, R.R., Wightman, R.H., 2012. Do cataclastic deformation bands form parallel to lines of no finite elongation (LNFE) or zero extension direction? *Journal of Structural Geology* 45, 158-172.

Jackson, C. A -L., Gawthorpe, R. L., Sharp, I. R., 2006. Style and sequence of deformation during extensional fault-propagation folding: examples from the Hammam Faraun and El-Qaa fault blocks, Suez Rift, Egypt. *Journal of Structural Geology* 28, 519-535.

Jackson, C. A -L. and Rotevatn, A., 2013. 3D seismic analysis of the structure and evolution of a salt-influenced normal fault zone: A test of competing fault growth models. *Journal of Structural Geology* 54, 215–234.

Jackson, C. A. -L., Bell, R. E., Rotevatn, A., Tvedt, A. B. M., 2017. Techniques to determine the kinematics of synsedimentary normal faults and implications for fault growth models. *In:* Childs, C., Holdsworth, R. E., Jackson, C. A.-L., Manzocchi, T., Walsh, J. J., Yielding, G. (Eds). *The Geometry and Growth of Normal Faults, Geological Society of London Special Publications* 439, 187-217.

James, W. R., Fairchild, L. H., Nakayama, G. P., Hippler, S. J., Vrolijk, P. J., 2004. Fault-seal analysis using a stochastic multifault approach. *American Association of Petroleum Geologists Bulletin* 88, 885-904.

Janecke, S. U., Vandenburg, C. J., Blankenau, J. J., 1998. Geometry, mechanisms and significance of extensional folds from examples in the Rocky Mountain Basin and Range province, U.S.A. *Journal of Structural Geology* 20, 841–856.

Jin, G., Groshong, Jr., R. G., Pashin, J. C., 1999. Relationship between drag fold geometry and fracture production in the Selma chalk, Gilbertown oil field, southwest Alabama. *Gulf Coast Association of the Geological Societies Transaction* 49, 148-149.

Jin, G. and Groshong Jr., R. H., 2006. Trishear kinematic modeling of extensional fault propagation folding. *Journal of Structural Geology* 28, 170–183.

Jin, G., Groshong, Jr., R. G., Pashin, J. C., 2009. Growth trishear model and its application to the Gilbertown graben system, southwest Alabama. *Journal of Structural Geology* 31, 926-940.

Johnson, K. M. and Johnson, A. M., 2002. Mechanical models of trishear-like folds. *Journal of Structural Geology* 25, 1-18.

Jones, R. R., Kokkalas, S. McCaffrey, K. J. W., 2009. Quantitative analysis and visualisation of nonplanar fault surfaces using terrestrial laser scanning (LIDAR) – The Arkitsa fault, central Greece, as a case study. *Geosphere* 5, 465-482.

Kanninen, M. F. and Poppelar, C. H., 1985. Advanced Fracture Mechanics. *Oxford Science Publications*, 584 p.

Kattenhorn, S. A. and Pollard, D. D., 2001. Integrating 3-D seismic data, field analogues and mechanical models in the analysis of segmented normal faults in the Wytch Farm oil field, southern England, United Kingdom. *American Association of Petroleum Geologists Bulletin* 85, 1183-1210.

Khalil, S. M. and McClay, K. R., 2002. Extensional fault-related folding, northwestern Red Sea, Egypt. *Journal of Structural Geology* 24, 743-762.

Kim, Y. - S. and Sanderson, D. G., 2005. The relationship between displacement and length of faults: a review. *Earth Science Reviews* 68, 317-334.

Lacazette, A., 2001. Extensional fault bend folding: implications for localized fracturing. www.naturalfractures.com/1.3.2.htm.

Larsen, P. - H., 1988. Relay structures in a Lower Permian basement-involved extension system, East Greenland. *Journal of Structural Geology* 10, 3-8.

Lăpădat, A., Imber, J., Yielding, G., Iacopini, D., McCaffrey K. J. W., Long, J. J., Jones, R. R., 2016. Occurrence and development of folding related to normal faulting within a mechanically heterogeneous sedimentary sequence: a case study from Inner Moray Firth, UK. *In:* Childs, C., Holdsworth, R. E., Jackson, C. A. -L., Manzocchi, T., Walsh, J. J., Yielding, G. (Eds). *The Geometry and Growth of Normal Faults, Geological Society of London Special Publications* 439, 373-394.

Lehner, F. K. and Pilaar, W. F., 1997. The emplacement of clay smears in synsedimentary normal faults: inferences from field observations near Frechen, Germany. *In*: Møller-Pedersen, P., Koestler, A. G. (Eds). *Norwegian Petroleum Society Special Publications. Hydrocarbon Seals: Importance for Exploration and Production*. Elsevier Science, 39-50.

Lindsay, N. G., Walsh, J. J., Watterson, J., Murphy, F. C., 1993. Outcrop studies of shale smears on fault surfaces. *In*: Flint, S. S. and Bryant, I. D. (Eds). *The Geological Modelling of Hydrocarbon Reservoirs and Outcrop Analogues. Blackwell Scientific Publications*, Oxford, 113-123.

Linsley, P. N., Potter, H.C., McNab, G., Racher, D., 1980. The Beatrice Field, Inner Moray Firth, UK North Sea. In: *Halbouty, M. T.* (Ed). *Giant Oil and Gas Fields of the decade 1968-1978. American Association of Petroleum Geologists Memoir* 30, 117-129.

Long, J. J. and Imber, J., 2010. Geometrically coherent continuous deformation in the volume surrounding a seismically imaged normal fault-array. *Journal of Structural Geology* 32, 222-234.

Long, J. J. and Imber, J., 2011. Geological controls on fault relay zone scaling. *Journal of Structural Geology* 33, 1790-1800.

Long, J. J. and Imber, J., 2012. Strain compatibility and fault linkage in relay zones on normal faults. *Journal of Structural Geology* 36, 16-26.

Long, J. J., 2011. Geometry, evolution and scaling of fault relay zones in 3D using detailed observations from outcrops and 3D seismic data. *Unpublished Thesis,* Durham University, 221p.

Ma, X. Q. and Kusznir, N. J., 1993. Modelling near-field subsurface displacements for generalized faults and fault arrays. *Journal of Structural Geology* 15, 1471-1484.

Maerten, L., Willemse, E.J.M., Pollard, D.D., Rawnsley, K., 1999. Slip distributions on intersecting normal faults. *Journal of Structural Geology* 21, 259–271

Mandl, G., 1988. Mechanics of Tectonic Faulting. *Elsevier,* New York, 407 p.

Mansfield, C. S. and Cartwright, J. A., 1996. High resolution fault displacement mapping from three-dimensional seismic data: evidence for dip linkage during fault growth. *Journal of Structural Geology* 18, 249-263.

Marchal, D., Guiraud, M., Rives, T., 2003. Geometric and morphologic evolution of normal fault planes and traces from 2D to 4D data. *Journal of Structural Geology* 25, 135-158.

McClay K. R. and Scott, A. D., 1991 Experimental models of hangingwall deformation in ramp–flat listric extensional fault systems. T*ectonophysics*, 188, 85–96

McFadzean, P. J. 2002. Normal fault interaction and relay ramp development on the Volcanic Tableland, E. California. *Unpublished PhD Thesis,* University of Edinburgh, 190 p.

McGinnis, R. N., Ferrill, D. A., Morris, A. P., Smart, K. J., 2016. Insight on mechanical stratigraphy and subsurface interpretation. *In:* B. Krantz, C. Ormand, and B. Freeman (Eds). *3-D structural interpretation: Earth, mind, and machine*. *American Association of Petroleum Geologists Memoir* 111, 111–120.

McLeod, A. E., Dawers, N. H., Underhill, J. R., 2000. The propagation and linkage of normalfaults: insights from the Strathspey–Brent–Statfjord fault array, northern North Sea. *Basin Research* 12, 263–284.

Morley, C. K., 2002. Evolution of large normal faults: Evidence from seismic reflection data. *American Association of Petroleum Geologists Bulletin* 86, 961-978.

Morewood, N., C. and Roberts, G. P., 2000. The geometry, kinematics and rates of deformation within an en échelon normal fault segment boundary, central Italy. *Journal of Structural Geology* 22, 1027-1047.

Morris, A. P., Ferrill, D. A., Henderson, D. B., 1996. Slip-tendency analysis and fault reactivation. *Geology* 24, 275-278.

Nicol, A., Walsh, J. J., Watterson, J., Bretan, P. G., 1996. Three-dimensional geometry and growth of conjugate normal faults: *Journal of Structural Geology* 17, 847–862

Nicol, A., Walsh, J. J., Watterson, J., Underhill, J. R., 1997. Displacement rates of normal faults. *Nature*, 390, 157-159.

Ole Kaven, J. and Martel S. J., 2007. Growth of surface-breaching normal faults as a three-dimensional fracturing process. *Journal of Structural Geology* 29, 1463-1476.

Pashin, J. C., Groshong, R. H., Jin, G., 1998. Structural modeling of a fractured chalk reservoir: toward revitalizing Gilbertown Field, Choctaw County, Alabama. *Gulf Coast Association of Geological Societies Transactions*, 48, 335-348.

Payne S. J., Zollweg, J. E., Rodgers D. W., 2004. Stress Triggering of Conjugate Normal Faulting: Late Aftershocks of the 1983 Ms 7.3 Borah Peak, Idaho, Earthquake. *Bulletin of the Seismological Society of America* 94, 3828–844.

Peacock, D. C. P. and Sanderson, D. G., 1991. Displacements, segments linkage and relay ramps in normal fault zones. *Journal of Structural Geology* 13, 721-733.

Peacock, D. C. P and Sanderson, D. J., 1992. Effects of layering and anisotropy on fault geometry. *Journal of the Geological Society of London* 179, 793-802.

Peacock, D. C. P. and Sanderson, D. G., 1994. Geometry and development of relay ramps in normal fault systems. *American Association of Petroleum Geologists Bulletin* 78, 147-165.

Peacock, D. C. P. and Sanderson, D. J., 1999. Deformation history and basin-controlling faults in the Mesozoic sedimentary rocks of the Somerset coast. *Proceedings of the Geologists' Association* 110, 41-52.

Pollard, D. D. and Fletcher, R. C. 2005. Fundamentals of Structural Geology, *Cambridge University Press*, 500 p.

Powell, J. W., 1875. Exploration of the Colorado River of the West and its Tributaries. *Government Printing Office*, Washington D.C., 291 p.

Price, N. J. and Cosgrove, J. W., 1990. Analysis of geological structures. *Cambridge University Press*, 502 p.

Putz - Perrier, M. W., and Sanderson, D. J., 2008. Spatial distribution of brittle strain in layered sequences. *Journal of Structural Geology* 30, 50-64.

Putz - Perrier, M. W. and Sanderson, D. J., 2011. Distribution of faults and extensional strain in fractured carbonates of the North Malta Graben. *American Association of Petroleum Geologists Bulletin* 94, 435-456.

Putz - Perrier, M. W., 2008. Distribution and scaling of extensional strain in sedimentary rocks. *Unpublished PhD Thesis*, Imperial College, London, 219p.

Ramsay, J. G., 1967. Folding and fracturing of rocks. *The Blackburn Press*, *New Jersey* 568 p.

Ramsay, J. G., 1974. Development of chevron folds. *Geological Society of America Bulletin* 85, 1741-1754.

Richards, F. L., Richardson, N. J., Bond, C. E., Cowgill, M., 2015. Interpretational variability of structural traps: implications for exploration risk and volume uncertainty. *In:* Richards, F. L., Richardson, N. J., Rippington, S. J., Wilson, R. W. and Bond, C. E. (Eds). *Industrial Structural Geology: Principles, Techniques and Integration. Geological Society of London Special Publications* 421, 7-27.

Roberts, A. M., Badley, M. E., Price, J. D., Huck, W., 1990. The structural history of a transtensional basin: Inner Moray Firth, NE Scotland. *Journal of Geological Society* 147, 87-103.

Roberts, D. G., and Bally, A. 2012. Regional geology and tectonics. Vol. 1B Phanerozoic Rift Systems and Sedimentary Basins. *Elsevier*, 500p.

Roberts, G. 2007. Fault orientation variations along the strike of active normal fault systems in Italy and Greece: Implications for predicting the orientations of subseismic-resolution faults in hydrocarbon reservoirs. *American Association of Petroleum Geologists Bulletin* 91, 1-20.

Roche, V., Homberg, C., Rocher, M., 2012. Fault displacement profiles in multilayer system: from fault restriction to fault propagation. *Terra Nova* 24, 499-504.

Rotevatn, A., Fossen, H., Hesthammer, J., Aas, T. E., Howell, J. A., 2007. Are relay ramps conduit for fluid flow? Structural analysis of a relay ramp in Arches National Park, Utah. *In:* Lonergan, L., Jolly, R. J. H., Rawnsley, K., Sanderson D. J. (Eds). *Fractured Reservoirs. Geological Society of London Special Publications* 270, 55-71.

Rotevatn, A. and Jackson, C. A. -L. 2014. 3D structure and evolution of folds during normal fault dip linkage. *Journal of Geological Society* 171, 821-829.

Rudnicki, J.W. and Wu, M., 1995. Mechanics of dip-slip faulting in an elastic half-space. *Journal of Geophysical Research* 100, 22173-22186.

Rykkelid, E. and Fossen, H., 2002. Layer rotation around vertical fault overlap zones: observations from seismic data, field examples, and physical experiments. *Marine and Petroleum Geology* 19, 181-192.

Saltzer, D. and Pollard, D. D. 1992. Distinct element modelling of structures formed in sedimentary overburden by extensional reactivation of basement normal faults. *Tectonics*, 11, 165-174.

Sanz, P. F., Pollard, D. D., Allwardt, P. F., Borja, R. I., 2008 Mechanical models of fracture reactivation and slip on bedding surfaces during folding of the asymmetric anticline at Sheep Mountain. *Journal of Structural Geology* 30, 1177-1191.

Schlische, R. W. 1995. Geometry and origin of fault-related folds in extensional settings. *American Association of Petroleum Geologists Bulletin* 79, 1661-1678.

Schöpfer, M. P. J., Childs, C., Walsh, J. J., 2007. Two-dimensional distinct element modeling of the structure and growth of normal faults in multilayer sequences: 2. Impact of confining pressure and strength contrast on fault zone geometry and growth. *Journal of Geophysical Research*, 112, B10404.

Schueller, S., Braathen, A., Fossen, H., Tveranger, J., 2013. Spatial distribution of deformation bands in damage zones of extensiona faults in porous sandstones: Statistical analyisis of field data. *Journal of Structural Geology* 52, 148-162.

Segall, P. and Pollard, D. D., 1980. Mechanics of discontinuous faults. *Journal of Geophysical Research* 85, 4337-4350.

Sharp, I., Gawthorpe, R., Underhill, J., Gupta, S., 2000. Fault-propagation folding in extensional settings: examples of structural style and synrift sedimentary response from the Suez rift, Sinai, Egypt. *Geological Society of America Bulletin* 112, 12, 1877-1899.

Sibson, R. H., 2000. Fluid involvement in normal faulting. *Journal of Geodynamics* 29, 469-499.

Skuce, A. G., 1996. Forward modelling of compaction above normal faults: an example from the Sirte Basin, Libya. *Geological Society of London Special Publications* 99, 135-146.

Smart, K. J., Ferrill, D. A., Morris, A. P., 2009. Impact of interlayer slip on fracture prediction from geomechanical models of fault-related folds. *American Association of Petroleum Geologists Bulletin* 93, 1447-1458.

Smart, K. J., Ferrill, D. A., Morris, A. P., Bichon, B. J., Riha, D. S., Huyse, L., 2010. Geomechanical modeling of an extensional fault-propagation fold: Big Brushy Canyon monocline, Sierra del Carmen, Texas. *American Association of Petroleum Geologists Bulletin* 94, 221-240.

Smith, D. A. 1980. Sealing and nonsealing faults in Louisiana Gulf Coast Salt Basin. *American Association of Petroleum Geologists Bulletin* 64, 145-172.

Soliva, R. and Benedicto, A., 2004. A linkage criterion for segmented normal faults. *Journal of Structural Geology* 26, 2251-2267.

Spina, V., Tondi, E., Galli, P., Mazzoli, S., Cello, G., 2008. Quaternary fault segmentation and interaction in the epicentral area of the 1561 earthquake (Mw = 6.4), Vallo di Diano, southern Apennines, Italy. *Tectonophysics* 453, 233-245.

Stearns, D. W. 1978. Faulting and forced folding in the Rocky Mountains foreland. *Geological Society of America Memoir* 151, 1-38.

Steen, O., Sverdrup, E., Hanssen, T. H., 1998. Predicting the distribution of small faults in a hydrocarbon reservoir by combining outcrop, seismic and well data. *In*: Jones, G., Fisher, Q., J., Knipe, R. J. (Eds) *Faulting, fault sealing and fluid flow in hydrocarbon reservoirs. Geological Society of London Special Publications* 147, 27-50.

Stein, R. S. and Barrientos S. E., 1985. Planar high-angle faulting in the Basin and Range: Geodetic analysis of the 1983 Borah Peak, Idaho, earthquake. *Journal of Geophysical Research* 90, 11355-11366.

Stein, R. S., 1999. The role of stress transfer in earthquake occurrence. *Nature* 402, 605-608.

Stevens, V., 1991. The Beatrice Field, Block 11/30a, UK North Sea. *In Abbots, I.L. (Ed) United Kingdom Oil and Gas Fields, Geological Society of London, Memoirs*, 14, 245-252.

Stewart, S. A., 2001. Displacement distributions on extensional faults: Implications for fault stretch, linkage, and seal. *American Association of Petroleum Geologists Bulletin* 85, 587-599.

Suter, M., 2014. Rupture of the Pitáycachi Fault in the 1887 Mx 7.5 Sonora, Mexico earthquake (southern Basin and Range Province): rupture kinematics and epicentre inferred from rupture branching patterns. *Journal of Geophysical Research: Solid Earth* 120, 617 - 641.

Tavani, S. and Granado, P., 2015. Along-strike evolution of folding, stretching and breaching of supra-salt strata in the Platforma Burgalesa extensional forced fold system (northern Spain). *Basin Research* 27, 573-585.

Tentler, T. and Acocella, V., 2010. How does the initial configuration of oceanic ridge segments affect their interaction? Insights from analogue models. *Journal of Geophysical Research* 115, B01401.

Thomas, A. L., 1993. Poly3D: A three-dimensional polygonal element displacement discontinuity boundary element computer program with applications to fractures, faults and cavities in the Earth's crust. *M.S. Thesis,* Stanford University, 58p.

Thomson, K. and Underhill, J. R., 1993. Controls on the development and evolution of structural styles in the Inner Moray Firth Basin. *In:* Parker, J. R. (Ed). *Petroleum Geology of Northwest Europe: Proceedings of the fourth Conference. The Geological Society of London*, 1167–1178

Thorsen, C. E., 1963. Age of growth faulting in southeast Louisiana. *Gulf Coast Association of Geological Societies* 13, 103-110.

Townsend, C., Firth, I. R., Westerman, R., Kirkevollen, L., Harde, M., Andersen., T., 1998. Small seismic-scale fault identification and mapping. *In:* Jones, G., Fisher, Q. J., Knipe, R. J. (Eds) *Faulting, Fault Sealing and Fluid Flow in Hydrocarbon Reservoirs*. *Geological Society of London Special Publications* 147, 1-25.

Treagus, S. H., 1973. Buckling stability of viscous single-layer system oblique to the principal compression. *Tectonophysics* 19, 271-289.

Trudgill, B. and Cartwright, J., 1995. Relay-ramp forms and normal-fault linkages, Canyonlands National Park, Utah. *Geological Society of America Bulletin* 106, 1143-1157.

Trudgill, B., 2010. Evolution of salt structures in the northern Paradox Basin: Controls on evaporite deposition, salt wall growth and supra-salt stratigraphic architecture: Evolution of salt structures in the northern Paradox Basin. *Basin Research* 23, 208 - 238.

Tvedt, A. B. M., Rotevatn, A., Jackson, C. A -L., Fossen, H., Gawthorpe, R. L., 2013. Growth of normal faults in multilayer sequences: A 3D seismic case study from the Egersund Basin, Norwegian North Sea. *Journal of Structural Geology* 55, 1-20.

Twiss, R. J. and Moores, E. M., 1992. Structural Geology. *W.H. Freeman and Company, New York*. 532 p.

Underhill, J. R., 1991. Implications of Mesozoic-Recent basin development in the western Inner Moray Firth, UK. *Marine and Petroleum Geology* 8, 359–369.

Vrolijk, P. J., Urai, J. L., Ketterman, M., 2016. Clay smear: Review of mechanisms and applications. *Journal of Structural Geology* 86, 95-152.

Wallace, R. E., 1984. Faulting related to the 1915 earthquakes in Pleasant Valley, Nevada. *U.S. Geological Survey Professional Paper* 1274 – A.

Walsh, J. J. and Watterson, J., 1987. Distributions of cumulative and seismic slip on a single normal fault surface. *Journal of Structural Geology* 9, 1039-1046.

Walsh, J. J. and Watterson, J., 1988. Analysis of the relationship between displacements and dimensions of faults. *Journal of Structural Geology* 10, 239-247.

Walsh, J. J. and Watterson, J., 1991. Geometric and kinematic coherence and scale effects in normal fault systems. *In:* Roberts, A., M. Yielding, G., Freeman, B. (Eds). *The Geometry of Normal Faults. Geological Society of London Special Publications* 56, 193-203.

Walsh, J. J., Watterson, J., Childs, C., Nicol, A., 1996. Ductile strain effects in the analysis of seismic interpretations of normal fault systems. *In:* Buchanan, P. G. and Nieuwland, D. (Eds). *Modern development in structural interpretation, validation and modelling*. *Geological Society of London Special Publications* 99, 27-40.

Walsh J. J., Watterson, J., Bailey, W. R., Childs, C., 1999. Fault relays, bends and branch-lines. *Journal of Structural Geology* 21, 1019-1026.

Walsh, J. J., Nicol, A., Childs, C., 2002. An alternative model for the growth of normal faults. *Journal of Structural Geology* 24, 1669-1675.

Walsh, J. J., Bailey, W. R., Childs, C., Nicol, A., Bonson, C. G., 2003. Formation of segmented normal faults: a 3-D perspective. *Journal of Structural Geology* 25, 1251-1262.

Walsh, J. J., Childs, C., Imber, J., Manzocchi, T., Watterson, J., Nell, P. A. R., 2003. Strain localisation and population changes during fault system growth within the Inner Moray Firth, Northern North Sea. *Journal of Structural Geology* 25, 307-315.

Walters, R. J., Elliott, J. R., D'Agostino, N., England, P. C., Hunstad, I., Jackson, J. A., Parsons. B., Phillips, R. J., Roberts, G., 2009. The 2009 L'Aquila earthquake 9central Italy): A source mechanism and implications for seismic hazard. *Geophysical Research Letters* 36, L17312.

Watterson, J., Childs, C., Walsh, J. J., 1998. Widening of fault zones by erosion of asperities formed by bed-parallel slip. *Geology* 26, 71-74.

Watterson, J., Nicol, A., Walsh, J. J, Meier, D., 1998. Strains at the intersection of synchronous conjugate normal faults. *Journal of Structural Geology* 20, 363-370.

Weber, K. J., Mandl, G., Pilaar, W. F., Lehner, F., Precious, R. G., 1978. The role of faults in hydrocarbon migration and trapping in Nigerian growth fault structures. *In: Offshore Technology Conference*, Dallas, Texas, United States, 2643-2653.

Whipp, P. S., 2011. Fault-propagation folding and the growth of normal faults. *Unpublished Thesis*, Imperial College, London, 518 p.

White, I. R. and Crider, J. G., 2006. Extensional fault-propagation folds: mechanical models and observations from the Modoc Plateau, northern California. *Journal of Structural Geology*, 28, 1352-1370.

Wibberley, C. A. J., Yielding, G., DiToro, G. 2008. Recent advances in the understanding of fault zone internal structure: a review. *In*: Wibberley, C. A. J., Kurz, W., Imber, J., Holdsworth, R. E. and Collettini, C. (Eds). *The Internal Structure of Fault Zones: Implications for Mechanical and Fluid-Flow Properties Geological Society of London Special Publications* 299, 5–33.

Wilkins, S. J. and Gross, M. R., 2002. Normal fault growth in layered rocks at Split Mountain, Utah: influence of mechanical stratigraphy on dip linkage, fault restriction and fault scaling. *Journal of Structural Geology* 24, 1413-1429.

Willemse, E. J. M., Pollard, D. D., Aydin, A., 1996. Three-dimensional analyses of slip distributions on normal fault arrays with consequences for fault scaling. *Journal of Structural Geology* 18, 295–309.

Willemse, E. J. M., 1997. Segmented normal faults: Correspondence between three-dimensional mechanical models and field data. *Journal of Geophysical Research* 102, 675–692.

Willemse, E. J. M. and Pollard, D. D., 2000. Normal fault growth: evolution of tipline shapes and slip distribution. *In:* Lehner F. K., and Urai, J L. (Eds). *Aspects of Tectonic Faulting*. *Springer-Verlag, Berlin*, 193-226.

Withjack, M. O., Olson, J., Peterson, E., 1990. Experimental models of extensional forced folds. *American Association of Petroleum Geologists Bulletin* 74, 1038–1054.

Withjack, M. O. and Callaway, S., 2000. Active normal faulting beneath a salt layer: an experimental study of deformation patterns in the cover sequence. *American Association of Petroleum Geologists Bulletin* 84, 627-651.

Xiao, H. and Suppe, J., 1992. Origin of rollovers. *American Association of Petroleum Geologists Bulletin* 76, 509-529.

Yielding, G., 1990. Footwall uplift associated with Late Jurassic normal faulting in the northern North Sea. Journal of the *Geological Society, London,* 147, 219-222.

Yielding, G., Freeman, B., Needham, D. T., 1997. Quantitative fault seal prediction. *American Association of Petroleum Geologists Bulletin* 81, 897-917.

Yielding, G., Bretan, P., Freeman, B., 2010. Fault seal calibration: a brief review. *In:* Jolley, Fisher, Ainsworth, Vrolijk, Delisle, S. (Eds). *Reservoir Compartmentalization. Geological Society of London Special Publications* 347, 243-255.

Yielding, G., 2012. Using probabilistic shale smear modelling to relate SGR predictions of column height to fault-zone heterogeneity. *Petroleum Geoscience* 18, 33-42.

Yielding, G., 2016. The geometry of branchlines. *In:* Childs, C., Holdsworth, R. E., Jackson, C. A. -L., Manzocchi, T., Walsh, J. J., Yielding, G. (Eds). *The Geometry and Growth of Normal Faults*, *Geological Society of London Special Publications* 439, 11-22.

Young, M. J., Gawthorpe, R. L., Hardy, S., 2001. Growth and linkage of a segmented normal fault zone; the Late Jurassic Murchison-Statfjord North Fault, northern North Sea. *Journal of Structural Geology* 23, 1933-1952.

Young, S. S., 2001. Geometry and mechanics of normal faults with emphasis on 3D seismic data, conjugate faults, and the effects of sedimentary layering. *Unpublished Thesis.* Stanford University, 167 p.

Zhang, P, Mao, F., Slemmons, D. B., 1999. Rupture terminations and size of segment boundaries from historical earthquake ruptures in the Basin and Range Province. *Tectonophysics* 308, 37-52.

Ziegler, P. A., 1990. Geological atlas of Western and Central Europe. *Shell Internationale Petroleum Maatschappij*, 554 p.

Ziesch, J., Aruffo, C. M., Tanner, D. C., Beilecke, T., Dance, T., Henk, A., Weber, B., Tenthorey, E., Lippman, A. and Krawczyk, C. M. 2015. Geological structure and kinematics of normal faults in the Otway Basin, Australia, based on quantitative analysis of 3-D seismic reflection data. *Basin Research*, 1-20.